Crosshole seismic processing of physical model and coal measures data

Miles Leggett

Crosshole Seismic Processing of Physical Model and Coal Measures Data

by

Miles Leggett

A thesis submitted in partial fulfilment
of the requirements for the degree of
Doctor of Philosophy

Department of Geological Sciences

University of Durham
1992

Acknowledgements

Firstly, I would like to thank my supervisor Dr. Neil Goulty for all his help and encouragement throughout my research work, and my parents for all their support throughout.

Thanks also to all those in the department who have helped make this work possible, in particular Ed Kragh, Mike Findlay, Peter Rowbotham and Salim Al-Rawahy for all the help with computing and fieldwork and the moments of hilarity. Thanks go also to British Coal Opencast for providing the boreholes, and to its staff for all the help they provided. Also the drillers, without whom we might still be stuck in the mud somewhere in deepest Cumbria.

I acknowledge the N.E.R.C. for my postgraduate award.

I have to thank all those other people who have made my stay in Durham bearable; Dave, Chris, Angus, Peter, Salim, Neville, Trish, Dan, Richard, Paul, Jane, Nilpf, Tim and everybody else who I have forgotten to mention. Finally, huge thanks go to Audrey for keeping me sane.

Abstract

Crosshole seismic techniques can be used to gain a large amount of information about the properties of the rock mass between two or more boreholes. The bulk of this thesis is concerned with two crosshole seismic processing techniques and their application to real data.

The first part of this thesis describes the application of traveltime and amplitude tomographic processing in the monitoring of a simulated EOR project. Two physical models were made, designed to simulate 'pre-flood' and 'post-flood' stages in an EOR project.

The results of the tomography work indicate that it is beneficial to perform amplitude tomographic processing of cross-well data, as a complement to traveltime inversion, because of the different response of velocity and absorption to changes in liquid/gas saturations for real reservoir rocks. The velocity tomograms image the flood zone quite accurately. Amplitude tomography shows the flood zone as an area of higher absorption but does not image its boundaries as precisely, because multi-pathing and diffraction effects are not accounted for by the ray-based techniques used.

Part two is concerned with the crosshole seismic reflection technique, using data acquired from a site in northern England. The processing of these data is complex and includes deconvolution, wavefield separation and migration to a depth section. The two surveys fail to pin-point accurately the position of a large fault; the disappointing results, compared to earlier work in Yorkshire, are attributed to poorer generation of compressional body waves in harder Coal Measures strata.

The final part of this thesis describes the results from a pilot seismic reflection test over the Tertiary igneous centre on the Isle of Skye, Scotland. The results indicate that the base of a large granite body consists of interlayered granites and basic rocks between 2.1 and 2.4km below mean sea level.

Table of contents

Chapter I

Introduction

1.1 Synopsis

The research described in this thesis falls into three distinct parts of which the first two, larger parts are concerned with crosshole seismology, while the third, smaller part consists of a pilot experiment for a conventional seismic reflection survey.

The first part deals with the traveltime and amplitude tomographic processing of data collected using two physical models to simulate the pre-flood and post-flood stages in an enhanced oil recovery (EOR) project. The prime objective was to determine the suitability of such processing methods for monitoring of EOR projects.

The second part is concerned with the processing of crosshole seismic reflection data with some results from crosshole surveys conducted in Coal Measures rocks in the north of England. This part is an extension of previous work, and the aim was to try and enhance the processing sequence and obtain depth-migrated sections from planned opencast coal mine sites.

Part three describes the acquisition, processing and interpretation of a seismic reflection test dataset collected on the Isle of Skye, Scotland. The pilot experiment was intended to investigate the seismic reflection response from the base of a granitic intrusion, part of the Skye Tertiary central intrusive complex.

1.2 Borehole seismic methods

Various borehole techniques are used in the oil exploration industry (e.g. Hardage, 1992; Balch et al., 1982; Fitch, 1984). Check shot surveys have been used for many years to calibrate borehole sonic logs. More recently the check shot survey has been extended as a vertical seismic profile (VSP), in which the

seismic reflection response of the strata is obtained at the borehole. The VSP is recorded by firing a source close to the top of the borehole at the rig while a geophone is positioned in the borehole over a range of depths at 10-20m intervals. VSPs are helpful for correlation of surface seismic reflection sections with well-log information. The VSP data generally have broader bandwidth than surface seismic data. The VSP method has been further developed to include offset VSPs, where the source is fired at a constant offset from the rig, and walkaway VSPs, where the source is fired at several different locations (offsets) while the geophone location is kept constant. If a VSP is recorded with a deviated well, then a seismic traverse along the course of the well is obtained. VSPs provide information that help tie in well data with a high degree of confidence. From the results one can determine the detectability of certain horizons, and also the amplitude and character of the reflections. VSPs also aid in prediction ahead of the bit and are used for deconvolution of surface seismic surveys using the downgoing wavefield.

1.3 Crosshole tomography

In a crosshole, or cross-well, seismic survey, the source is positioned over a range of depths in one borehole with receivers in the other. The seismic crosshole technique offers a means to investigate the rock mass between two or more boreholes. First applications of this technique only made use of the direct wave arrival times which were inverted to produce a velocity tomogram of the subsurface between the boreholes (see e.g. Worthington, 1984). This is known as traveltime tomography.

In amplitude tomography, the amplitudes of the same direct wave arrivals are inverted to estimate the absorption field between the boreholes. Attenuation effects include elastic transmission loss of energy from the direct waves due to reflection and diffraction. Geometric spreading and source/receiver directivity functions and coupling factors also need to be considered. In so far as these effects are taken into account, the anelastic absorption field is estimated by amplitude tomographic processing.

Inversion methods for traveltime tomography were reviewed by Worthington (1984) and in greater detail by Ivansson (1987). The most widely used method is the simultaneous iterative reconstruction technique (SIRT), first developed by Gilbert (1972) for medical applications and introduced into

geophysics by Dines and Lytle (1979). Krajewski et al. (1989) clearly describe a variation of SIRT which they used on physical model data.

The use of amplitude tomography is common in medical applications (e.g. Brooks and di Chiro, 1976) but is rare in seismic experiments, although Bregman et al. (1989a) succeeded in imaging a fracture zone in a granitic rock mass on an absorption tomogram. The same matrix inversion methods may be used as in traveltime tomography, but working with the logarithms of observed amplitudes. However, an estimate of the velocity field between the boreholes is needed before amplitude inversion can begin, in order to trace raypaths between source and receiver locations. As a rule of thumb, straight raypaths should not be assumed if velocity variations exceed 15%.

1.4 Crosshole seismic reflection surveys

Other crosshole imaging methods use also the scattered arrivals that are present after the direct wave arrival: e.g diffraction tomography (Devaney, 1984), wave equation imaging (Pratt & Worthington, 1988), and reflection processing (Findlay et al., 1991). Other arrivals present in the data are reflections from interfaces between the boreholes. The crosshole dataset can be thought of a set of several offset VSPs where the source and receivers are all below ground level. Data processing of the survey is similar to that of a set of offset VSPs, but is necessarily more complicated. This technique has been investigated in this thesis using data from opencast coal exploration sites in the U.K.

1.5 Opencast coal mining

Opencast coal mining was first carried in the U.K. in 1942, as a wartime measure. Mines were shallow, with depths of only a few metres. Now, a typical opencast site is mined to around 100m. This is small by world standards, due to the urban environment of the U.K. Site boundaries are restricted by main roads, railways and towns. Site reserves are usually in the region of 5 million tonnes, with some small private mines having reserves of only 50,000 tonnes. Current annual production from opencast coal mining is approximately 15 million tonnes, which accounts for at least 15% of the U.K.

total coal production. Coal produced from opencast mining is generally of higher quality and is cheaper than coal from deep mines.

In England and Wales, most of the opencast sites are supervised by British Coal Opencast (BCO), and are worked by civil engineering companies who tender for each site on the basis of a detailed specification provided by the BCO. After a site has been worked, BCO are obliged to restore the land for agricultural, industrial or leisure purposes.

1.5.1 Site exploration

The usual exploration method used in the opencast coal industry in the U.K. is to drill a dense grid of boreholes to determine the site reserves and overburden ratio. The overburden ratio (ratio of overburden thickness to coal thickness) is a primary controlling factor in opencast mining and rarely exceeds 25:1. Seams as thin as 0.15 or 0.1m may be mined in the U.K. The initial grid of boreholes is drilled on 120m centres to the deepest seam of interest, and this may be reduced to 60m if the site proves attractive. This is sufficient for undisturbed ground, but in the presence of faulting and old workings, further boreholes may be drilled on 30m centres.

Most boreholes are geophysically logged using natural gamma, density and sonic tools, and cores may be taken to check coal quality and rock properties. The Coal Measures in Northern England consist mainly of interbedded sandstones and mudstones with seat earths and coal seams less than 2m thick. The "diggability" of the rocks is an important engineering consideration and determines the possible need for blasting.

All the data from the boreholes are combined to provide information about the structure, drift thickness and coal seam depths and thicknesses. An estimate of the site reserves is made on the basis of this information, and civil engineering companies are invited to tender for the contract to extract at least this tonnage, quoting a price per tonne. Site exploration has to be thorough and accurate as the company which wins the contract for the site may make financial claims on BCO if site reserves turn out to be less than predicted. Claims may also be made if there are unanticipated geological difficulties for extraction which were not specified when tenders were invited. No geophysical surveying technique is routinely used to aid exploration.

Small faults (i.e. with a throw of 2m or less) are extremely difficult to detect from borehole information, so there is potential for a geophysical technique which is able to image such small features. Old workings are also present at most sites, usually of the pillar and stall type where pillars of coal are left behind to prevent collapse of the mineworkings. Up to 70% of the coal can be left behind in this case and this may make up the bulk of economically viable reserves in a site. The presence of old workings makes estimation of reserves more difficult. Old plans may exist but are rarely accurate.

1.5.2 Geophysical exploration methods used

Surface seismic reflection surveys have been used as an exploration tool for deep mines for many years, with target depths of hundreds of metres, but poor imaging is obtained in the top 100m of sections (see Ziolkowski, 1979). Shallow seismic sections suffer from interference from ground roll and refracted waves, which is very dependent on the shallow geology (e.g. Bredewout and Goulty, 1986).

In-seam seismic methods have also been employed successfully in deep mines to map seam continuity (e.g. Jackson, 1985) using seam waves. A geological fault of throw greater than, or equal to, seam thickness can disrupt the mining process. This has not been successful in shallow seams. Crosshole reflection techniques were investigated by Goulty et al. (1990), and proved successful in imaging coal seams.

It is hoped that the crosshole seismic reflection technique will be a valuable tool in opencast coal exploration in imaging faults accurately and fill in information where boreholes cannot be drilled.

PART 1

Chapter II

Tomography

2.1 Applications of tomography

There has been much interest in using cross-well traveltime tomography to observe the progress of fluids injected into reservoir rocks during enhanced oil recovery (EOR) processes. If repeated surveys were carried out, then EOR processes could be monitored over a period of time, a technique that has been called "time-lapse tomography". There is a need to determine the spatial distribution of the changes of reservoir properties with time. Of particular importance is the need to know the direction of propagation and rate of movement of steam or fire-flood fronts. The relationship between the seismic properties of the reservoir rocks and their production qualities needs to be established and understood. The seismic properties (i.e, velocity and absorption) of the reservoir rocks can be used to provide information about the porosity, saturation, hydrocarbon type, temperature and other related parameters.

The dependence of seismic velocity and absorption on oil reservoir rock properties was reviewed by Nur (1987). For compressional waves, there is a significant drop in velocity between water saturations of 1.0 and 0.9 (see Fig. 2.1), the rest of the pore space being filled with gas, but little further change as the water saturation is reduced to zero at constant pore pressure (Domenico, 1976; Murphy, 1982). However, absorption peaks at some water saturation between 0.6 and 0.9, at approximately double its value at total saturation (1.0) or at saturations less than 0.5 (Winkler and Nur, 1982; Murphy, 1984). There is also a large temperature effect on compressional wave velocity in heavy oil or tar sands, with velocity decreasing as temperature increases, especially around the melting temperatures of the heavy hydrocarbons (Marion and Nur, 1991). A rapid increase in temperature also causes partial gas saturation and thermal fracturing, which can further decrease seismic velocity. Between 25-150°C there is nearly a 40% decrease in compressional velocity (Nur, 1987).

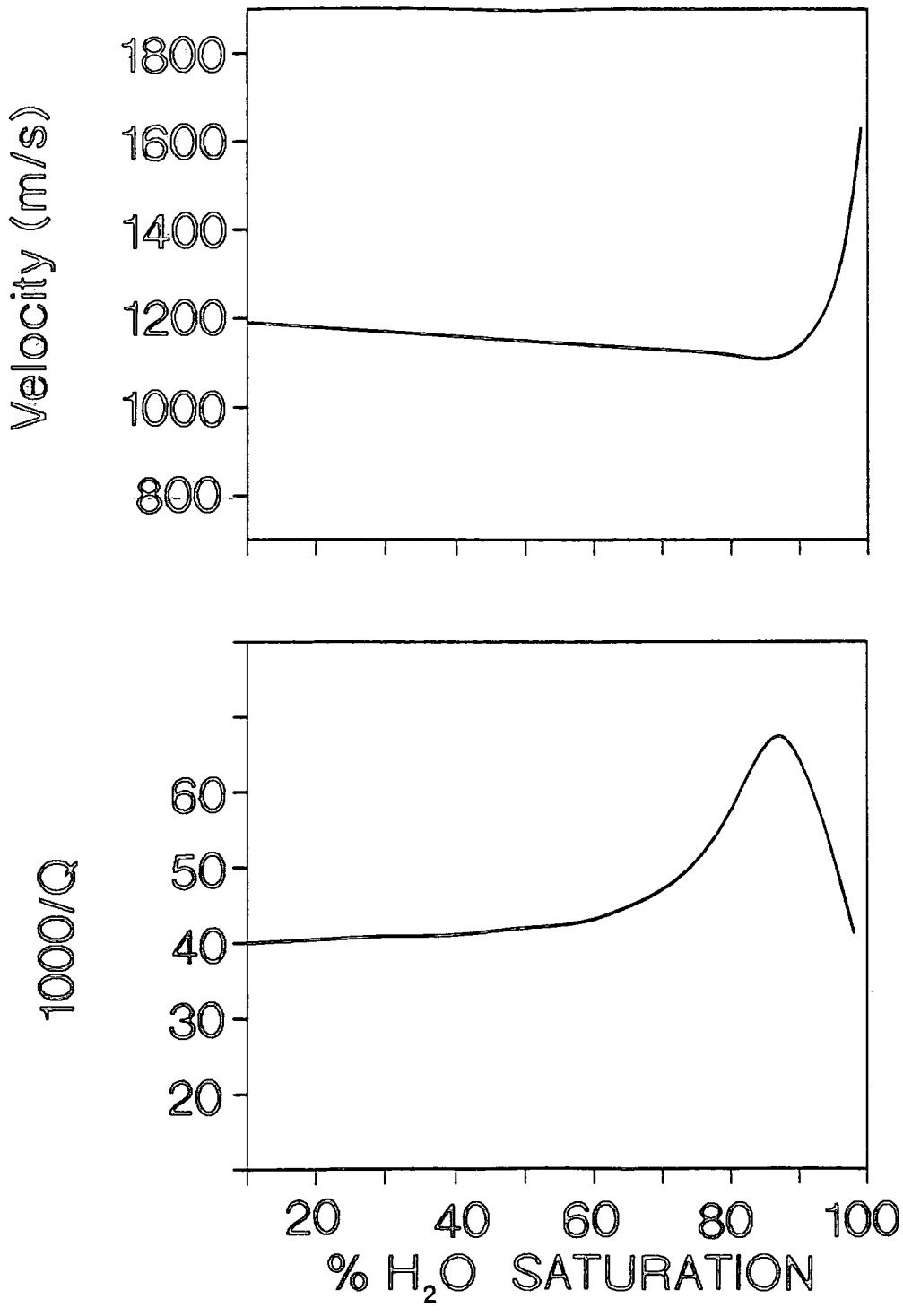

Figure 2.1 Variation of absorption and compressional velocity with water saturation in rocks (after Murphy, 1982).

Suitable applications of time-lapse tomography include:

○ Tracking movement of the gas cap to an oil reservoir during production. In particular, it would be advantageous to delay gas breakthrough to the production wells for as long as possible.

○ Tracking the flood front during enhanced oil recovery (EOR) by water flooding. Breakthrough, by water channelling through the more permeable beds, should be avoided.

○ Tracking thermal fronts during EOR by fire or steam flooding. Real examples of these applications have been published by Macrides et al. (1988), Bregman et al. (1989b) and Justice et al. (1989).

Monitoring applications for seismic tomography are not limited to hydrocarbon production. Carabelli (1988) reported a programme of sonic velocity tomography surveys for checking the integrity of concrete and earth dams in Italy. A long term monitoring programme would simply involve repeated surveys at appropriate intervals, and computing the difference tomograms. Similarly, repeated monitoring surveys could be carried out around underground engineering installations to check the stability of the rock mass. Time-lapse tomography could also be used in geothermal energy exploration to locate fracture zones for water flow after explosive stimulation or hydro-fracturing. Tomography surveys have been conducted successfully in deep mines to follow changes in stress as mining progresses (Körmendi et al., 1986), and used to locate a magnetite ore body between boreholes approximately 165m apart (Gustavsson et al., 1986).

Numerical modelling, to generate synthetic seismograms, is a versatile way of demonstrating the potential of tomographic inversion schemes. Physical modelling, using ultrasonic frequencies on a scaled model, provides an even more realistic simulation of field data, as all types of elastic waves are necessarily present. Furthermore, source directivity effects, noise, and source and receiver positioning errors are also included. It takes more effort, and involves more expense, to make changes to a physical model than to vary the parameters of a numerical model. Consequently, physical models are used sparingly, but note that it can be useful to evaluate the limitations of numerical modelling schemes against a physical model dataset in applications where a number of model datasets need to be generated.

2.2 SIRT

The SIRT method can cope with any source and receiver geometry and can be used with curved-raytracing algorithms. The observed traveltime can be expressed as the following line integral

$$t_k = \int_{raypath\ k} s(x,z)\, dl \qquad (2.1)$$

where t_k is the traveltime of the ray k, dl is an element of length and s(x,z) is the slowness (reciprocal of velocity) at a position (x,z) in the survey area. The area to be imaged is divided into Cartesian cells assigning a uniform velocity s_j to each cell. In the discretized case of cells, the above integral can then be approximated by

$$t_k = \sum_j d_{kj} s_j \qquad (2.2)$$

where d_{kj} is the path length in cell j for raypath k.

Equation (2.2) may be written in matrix form as

$$\mathbb{T} = \mathbb{D}\mathbb{S} \qquad (2.3)$$

where $\mathbb{T}$ is the vector of traveltimes, $\mathbb{S}$ is the vector of slowness values (reciprocal of velocity) in each cell, and each element d_{kj} of matrix $\mathbb{D}$ is the length of the segment of the raypath k which lies within cell j. For an initial assumed velocity field, which defines $\mathbb{S}$, one calculates $\mathbb{D}$ and $\mathbb{T}$ by raytracing. Then the calculated traveltimes are compared with the observed traveltimes and a new estimate of the velocity field is made. This procedure is repeated iteratively until the variance between calculated and observed traveltimes reaches a minimum. Starting with equation (2.2) we have

$$t_k^n = \sum_j s_j^n x_{kj}$$

where t_k^n is the estimated traveltime for the estimated slowness field s_j^n at the start of iteration n. The true slowness field which fits the observed traveltimes t_k can then be represented as a perturbation of this:

$$t_k = \sum_j d_{kj} (s_j^n + \Delta s_{jk}^n)$$

where Δs_{jk}^n represents the error in the slowness for cell j estimated from raypath k during iteration n.

The traveltime error is then

$$\Delta t_k^n = t_k - t_k^n = \sum_j d_{kj} \Delta s_{jk}^n \qquad (2.4)$$

Dines and Lytle (1979) proposed minimising the arbitrary criterion

$$c = \sum_j \Delta s_{jk}^{n\,2}$$

subject to (2.4) to obtain the update to each cell estimated from each raypath

$$\Delta s_{jk}^n = \frac{\Delta t_k^n d_{kj}}{\sum_j d_{kj}^2} \qquad (2.5)$$

After all rays have been traced through the region of interest, the update applied to the slowness in cell j following iteration n, Δs_j^n, is the average of the values Δs_{jk}^n for all the rays which pass through cell j. The improved estimate of the slowness field is then

$$s_j^{n+1} = s_j^n + \Delta s_j^n \qquad (2.6)$$

This forms the basis of the reconstruction algorithm. Its implementation on a computer is relatively straightforward and takes the following form:

○ The region of interest is divided into discrete cells, and each is assigned an initial uniform slowness, or velocity.

○ Raypaths are traced through the cells from all source to receiver positions to calculate the estimated traveltime of each ray, and the path length of each ray in each cell.

○ Changes in slowness are calculated for each cell according to (2.5) for all rays which pass through the cell, and are averaged.

The slowness field is then updated using equation (2.6).

The whole process is then repeated iteratively, raytracing through the current estimate of the velocity field, calculating traveltimes along those raypaths, and updating the velocity field. The variance between observed and calculated traveltimes characteristically decreases to a minimum after several iterations and then starts to increase. Thus a straightforward criterion for choosing the optimum velocity field is that it should be the one for which the variance between calculated and observed traveltimes reaches a minimum. In practice this is usually complicated by the variance oscillating up and down between successive iterations around the minimum, before starting to increase monotonically. The best velocity field is usually chosen when the variance starts to show only small changes after each iteration, and before large artifacts appear in the velocity field.

The initial velocity field may also be estimated by a simple back-projection of the traveltime data (Wong et al., 1983). Back-projection is carried out by assuming all straight raypaths, and taking the slowness of each cell to be the average slowness of those raypaths passing through that cell (in proportion to the length of the raypath segment in the cell). A computer program written by Dyer (1988) was used to invert the traveltime data. This was implemented on the Northumbrian Universities Multiple Access Computer Mainframe computer by Wye (1986), and a curved-raytracing algorithm, Raysyn (Cassel, 1982), was modified for use with crosshole geometry. These programs have been further modified and implemented on the Sun UNIX system in the Department.

2.2.1 SIRT inversion of amplitudes

For amplitude tomographic reconstruction the same relationship as for the traveltime tomography applies, for the appropriate variables. The amplitude of a seismic plane wave of frequency f propagating along the x-axis at velocity v in a homogeneous medium of quality factor Q is given by

$$A_x = A_o \exp(-\alpha x) \tag{2.7}$$

where A_o is the amplitude at the origin and the absorption coefficient α is given by

$$\alpha = \pi f / Q v$$

then for an inhomogeneous medium, with variations in α, (2.7) must be replaced by

$$-ln [A_k / A_o] = \int_{raypath} \alpha \, dx \tag{2.8}$$

The field to be imaged is divided into square cells as in the traveltime tomography, so the discretized form of (2.8) must be used :

$$- ln [A_k / A_o] = \sum_j \alpha_j d_{kj} \tag{2.9}$$

A_o is now the reference amplitude at unit distance from the source, A_k is the measured amplitude after traversing raypath k, α_j is the absorption coefficient in cell j, and d_{kj} is the length of raypath k within cell j. This equation may be used in the same way as in traveltime tomography to form the basis of the SIRT method, provided that the measured amplitudes in a real experiment are adjusted for geometrical spreading, elastic transmission losses, source/receiver directivity functions and coupling factors, where they are necessary. Referring to (2.3), $\mathbb{T}$ is now the vector of negative logarithms of amplitude ratios and $\mathbb{S}$ is the vector containing cell values of absorption coefficients to be found. The raypaths are traced through the final velocity model from the traveltime tomographic inversion, and are not changed between iterations in the amplitude inversion.

2.2.2 Geometrical spreading corrections

Separate calculations were made to calculate geometric spreading factors in the plane of the section and out of the plane.

The in-plane correction was calculated by incrementing the in-plane take-off angle at the source by a small amount $\delta\theta$, and raytracing to find the perpendicular shift in raypath position, $r_\theta\delta\theta$, at the receiver.

The velocity structure is invariant in the out-of-plane direction, so the out-of-plane correction factor is quite readily calculated from the raypath geometry (see Fig. 2.2). The out-of-plane shift of the raypath at the receiver $r_\phi\delta\phi$ corresponding to a very small take-off angle $\delta\phi$ in the out-of-plane direction has to be calculated. (The out-of-plane take-off angle is always zero for rays traced within the plane of the section).

Consider two media having velocities V_1 and V_2, respectively, separated by a vertical boundary (see Fig. 2.2). For an in-plane raypath impinging on this vertical interface let the angle of incidence be θ_1 and the angle of refraction be θ_2. Now, letting the out-of-plane angle increment to the small value $\delta\phi_1$, the angles of incidence and refraction are; $cos^{-1}[\ cos\theta_1 cos\delta\phi_1\ ]$ and $cos^{-1}[\ cos\theta_2\ cos\delta\phi_2\ ]$, respectively. Using Snell's Law,

$$\frac{V_1}{V_2} = \frac{\sqrt{1 - cos^2\theta_1 cos^2\delta\phi_1}}{\sqrt{1 - cos^2\theta_2 cos^2\delta\phi_2}} = \frac{sin\ \theta_1}{sin\ \theta_2}$$

This can be written as

$$(1 - cos^2\theta_1 cos^2\delta\phi_1)\ sin^2\ \theta_2 = (1 - cos^2\theta_2 cos^2\delta\phi_2)\ sin^2\ \theta_1$$

As $\delta\phi_1$, $\delta\phi_2$ are infinitesimal, the following relations hold

$$cos^2\delta\phi_1 = (1 - \delta\phi_1^2)/2$$

$$cos^2\delta\phi_2 = (1 - \delta\phi_2^2)/2$$

Substitution and simplification leads to the relation, for a vertical boundary

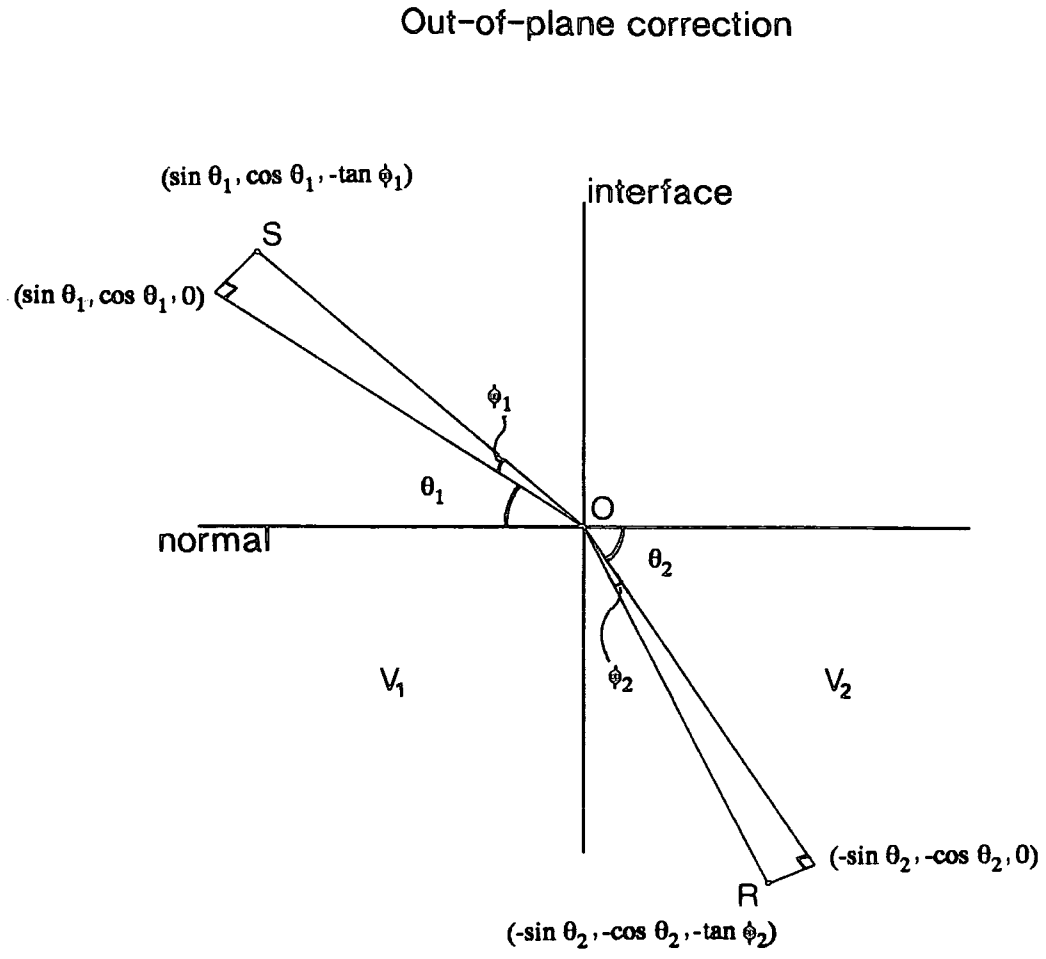

Figure 2.2 Raypath geometry for calculation of the out-of-plane geometrical spreading correction.

$$\delta\phi_2 = \frac{tan\theta_2}{tan\theta_1}\,\delta\phi_1 \qquad (2.10)$$

For a horizontal interface, the angle of incidence becomes $90\text{-}\theta_1$ and the relation is

$$\delta\phi_2 = \frac{tan\theta_1}{tan\theta_2}\,\delta\phi_1 \qquad (2.11)$$

These relations can be generalised to give the out-of-plane angle of the raypath in each cell, $\delta\phi_{kj}$, in terms of an initial infinitesimal out-of-plane angle $\delta\phi$ at the source. In order to calculate the out-of-plane shift $r_\phi\delta\phi$, the raypath length segment d_{kj} in each cell must be multiplied by $\delta\phi_{kj}$ and the results summed:

$$r_\phi\delta\phi = \sum_j d_{kj}\delta\phi_{kj} \qquad (2.12)$$

This quantity is readily calculated from the in-plane angles and raypath length segments in each cell, known from raytracing. For each seismogram the geometric-spreading amplitude correction factor is $\sqrt{r_\theta r_\phi}$.

2.2.3 Corrections for transmission losses at interfaces

The corrections used for elastic transmission losses at interfaces are Zoeppritz coefficients calculated using the formulae given by Cerveny et al. (1977) and Bortfeld (1962). These corrections are equivalent to source and receiver coupling factors in a field experiment. The Zoeppritz coefficients were calculated for the water/model interfaces only, as the velocity and density contrasts within the model itself are small enough to be ignored. For a ray impinging on an interface between two homogeneous, isotropic media, having P-wave velocities α_1 and α_2, S-wave velocities β_1 and β_2 and densities ρ_1 and ρ_2, respectively, the transmission coefficient depends only upon the angle of incidence and on the velocities and densities at both sides of the interface. Instead of the angle of incidence θ, the ray parameter p is used. The Zoeppritz coefficient R_p for a transmitted compressional wave is given by

$$R_p = 2\alpha_1\rho_1 P_1 D^{-1} \{ \beta_2 P_2 X + \beta_1 P_4 Y \}$$

where

$$D = \{ q^2 p^2 P_1 P_2 P_3 P_4 + \rho_1 \rho_2 (\beta_1\alpha_2 P_1 P_4 + \alpha_1\beta_2 P_2 P_3) +$$

$$\alpha_1\beta_1 P_3 P_4 Y^2 + \alpha_2\beta_2 P_1 P_2 X^2 + \alpha_1\alpha_2\beta_1\beta_2 p^2 Z^2 \}$$

and

$$q = 2(\rho_2\beta_2^2 - \rho_1\beta_1^2), \qquad X = \rho_2 - qp^2$$

$$Y = \rho_1 + qp^2, \qquad Z = \rho_2 - \rho_1 - qp^2$$

$$P_1 = (1 - \alpha_1^2 p^2)^{1/2}, \qquad P_2 = (1 - \beta_1^2 p^2)^{1/2}$$

$$P_3 = (1 - \alpha_2^2 p^2)^{1/2}, \qquad P_4 = (1 - \beta_2^2 p^2)^{1/2}.$$

$$p = \sin\theta / \alpha_1$$

2.4 Factors influencing image quality

The effects of varying the size of cells, smoothing and other options on the performance of the SIRT algorithm have been investigated extensively by Wye (1986), and in lesser detail by Lendzionowski (1986) and Findlay (1987). The main criterion for an accurate tomographic inversion is to have a wide angular coverage of rays. The ideal situation occurs when the target to be imaged can be examined from all sides, as in medical tomography. Limited directional coverage will result in a smearing of the image in the direction of the raypaths, with associated loss in horizontal resolution. It can be difficult to obtain detailed velocity images because of gaps in obtainable ray coverage (Dyer & Worthington, 1988), and if an anomaly is not both crossed and bordered by raypaths, identification of the shape and location of the anomaly is necessarily less precise (Krajewski et al., 1989). Small variations in seismic velocity that are found in real rocks produce small time shifts which can be of the order of standard errors in the data.

2.4.1 Influence of cell size on inversion

With a small cell size, the result is more likely to contain artifacts of the inversion, especially around the edges of the area of interest. As cell size decreases, the number of rays within cells also decreases, which leads to a reduction in the stability of the reconstruction. Larger cells lead to a smoother

inversion, but some loss of resolution will result from increasing the cell size, so the actual size chosen is a compromise. It appears from experiments carried out by Lendzionowski (1986) that the optimum cell dimension is (close to) the source/receiver separation. Krajewski et al. (1989) suggest that the smallest pixel, or cell, size should be 1-1.5 times the maximum anomaly dimension that one expects to resolve. Higher resolution (smaller cells sizes) will be offset by the build up of artifacts, but very large cell sizes will give smoothing of anomalies to an unacceptable level.

2.4.2 Effect of over and under-iteration

In general, the lower the number of iterations, the lower the contrast and, correspondingly, resolution of the inversion. With more iterations of the SIRT inversion method, the resolution and contrast of anomalies will increase, but there is a corresponding increase in the number and size of artefacts, and the iteration process may even begin to diverge. The convergence of the iteration process is measured by calculating the variance between observed and calculated traveltimes. Fig. 2.3 shows the variance measured over ten iterations for the physical model data to be described in more detail in Chapter III.

2.4.3 Effect of noise on the reconstruction

Noise can be described as being the accumulated error on the traveltime data, including picking errors on the direct-wave arrival times, random errors in the acquisition and errors in source/receiver positions. Wye (1986) added a Gaussian distribution of errors to the data. For errors in the traveltimes having a standard deviation of only 1%, the results show little difference; with 2% error, parts of the reconstruction become less well defined; and with 5% error any resolution in the image has been lost due to the anomalies introduced by the errors. Bois et al. (1972) have shown that random errors of up to ±5ms in traveltimes did not affect large-scale structure in their inversion to a significant degree.

The greater the errors in the data then the greater the loss in resolution of in the image, because each ray will "see" a different slowness field in the common cells that they traverse. This results in the reconstruction being only one of many different solutions that will fit the data.

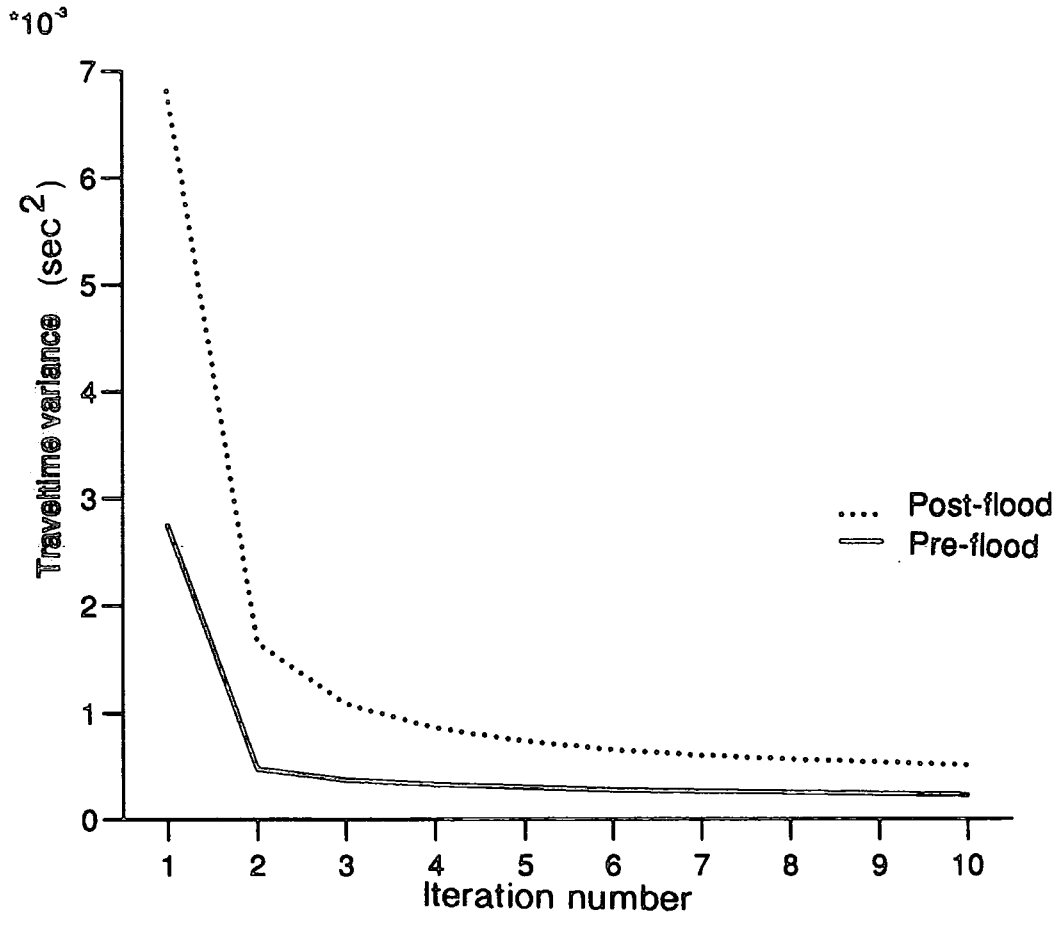

Figure 2.3 Variances calculated from tomographic inversion of traveltime data from physical model datasets.

2.4.4 Smoothing of the reconstructed field

If smoothing of the reconstructed field is carried out after each iteration, the results show much improvement and the stability of the reconstruction is also increased. Smoothing may be of more use where there are errors in the traveltime data. For example, if there is a lot of noise in the recorded traces, the accuracy of picking the direct-wave arrival time is much reduced, which could lead to poor results from the inversion process.

It is sometimes beneficial to perform smoothing on the current guess of the reconstructed field, to ensure a stable convergence of the iteration process. There are numerous smoothing procedures to be found in the literature, but the algorithm suggested by Krajewski et al. (1989) is useful for suppressing statistical pseudo-anomalies without blurring the actual anomalies required. The algorithm is a combination of the "selective smoothing" of Radcliff et al. (1984) combined with weighting factors suggested by Dines and Lytle (1979). Each slowness (or absorption coefficient) s_{ij} in cell ij is replaced by $\overline{s_{ij}}$, given by

$$\overline{s_{ij}} = \frac{4s_{ij} + s_{i-1,j} + s_{i+1,j} + s_{i,j-1} + s_{i,j+1}}{8}$$

At the edge of the grid the neighbouring cell outside is assumed to have the same slowness or absorption as the edge cell itself. To avoid smoothing of actual anomalies, a maximum difference or constraint can be chosen. Cells are only included in the smoothing algorithm if the difference between these cells and the cell under consideration is smaller than the chosen maximum slowness or absorption difference (measured as a percentage).

2.4.5 Borehole deviation

Accurate positioning of source and receiver arrays is important in tomography. A deviation of 1m laterally of each borehole with a borehole spacing of 50m would give errors of up to 4% in source-receiver spacing, and these will inevitably affect the estimated velocity field. Borehole deviation should be measured when the boreholes are geophysically logged.

Chapter III

Tomographic reconstruction of physical model data

3.1 Introduction

This chapter presents the results of traveltime and amplitude tomographic processing, including difference tomograms, from a physical model dataset designed to represent 'pre-flood' and 'post-flood' stages in an EOR process. The model was built in two halves, with and without a flood zone of a known geometry in a reservoir layer, so that both pre-flood and post-flood datasets could be generated. The purpose of the experiment was to demonstrate the potential of these relatively straightforward tomographic techniques for routine use in monitoring applications.

3.2 Model and data acquisition

The physical models were comprised of seven layers made of five different epoxy resin mixtures (Fig. 3.1). There is an overall increase in velocity with depth, the deepest interface is faulted, and one layer contains a channel feature. Pre-flood and post-flood models were made together in one solid block, in the same mould, and the upper surface of each layer was machined off before pouring the next layer. After the fifth, reservoir layer had been poured and set, it was machined to cut out the 'flood zone' over the half of the block which was to form the post-flood model, but left intact for the other half. A different epoxy mixture was then poured in to represent the flood, and two further layers added on top across both halves of the block. The complete block was then cut in two (Fig. 3.2), separating the pre-flood and post-flood models. As each layer of the block was made in a single batch, the pre-flood and post-flood models should be identical, apart from the flood zone, to within the tolerance of the milling machine (0.025mm).

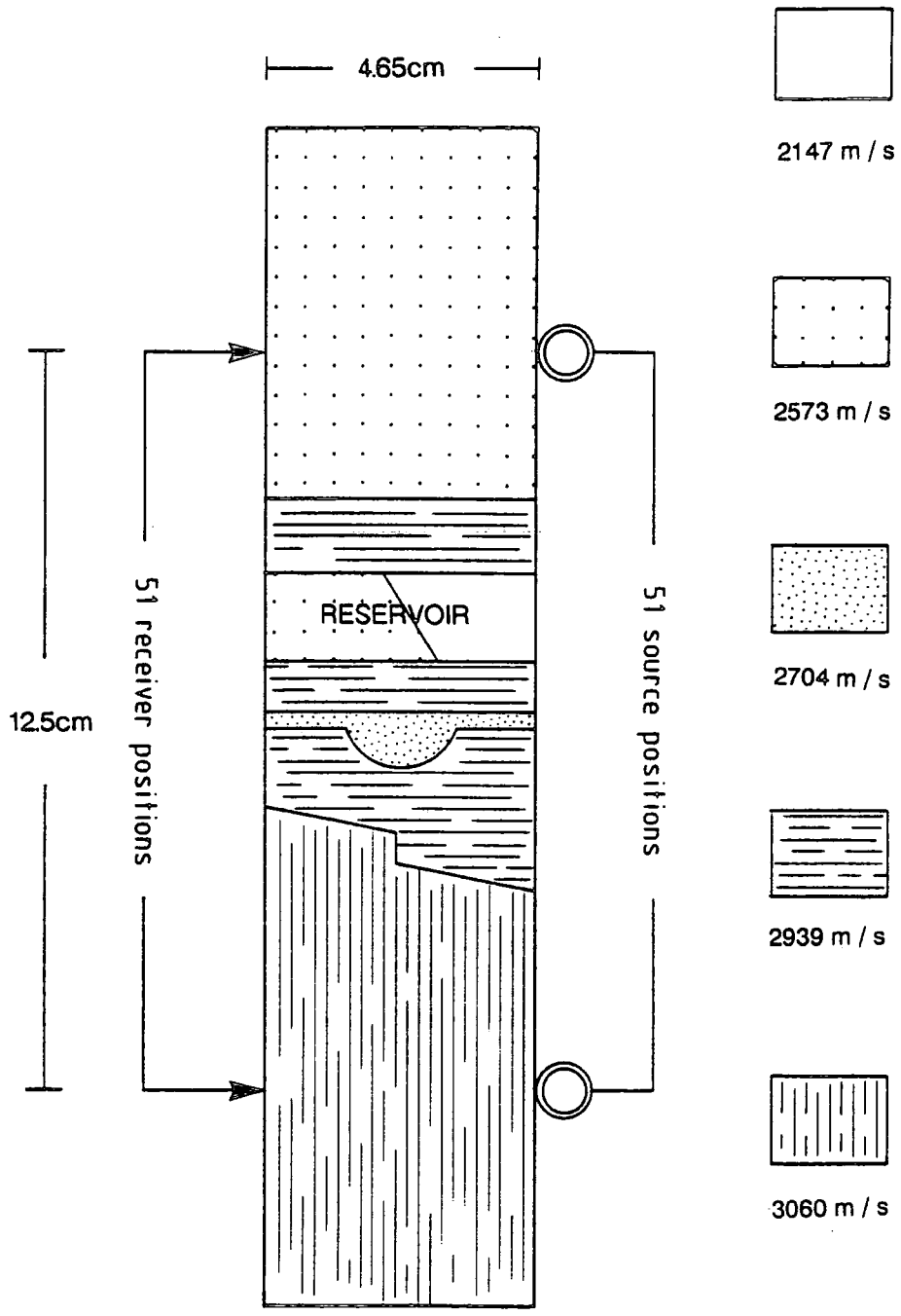

Figure 3.1 Cross-section of model showing source and receiver positions. The P-wave velocities of the various layers are indicated to the right. The right-hand part of the reservoir layer was replaced by material with P-wave velocity 2147m/s in the post-flood model.

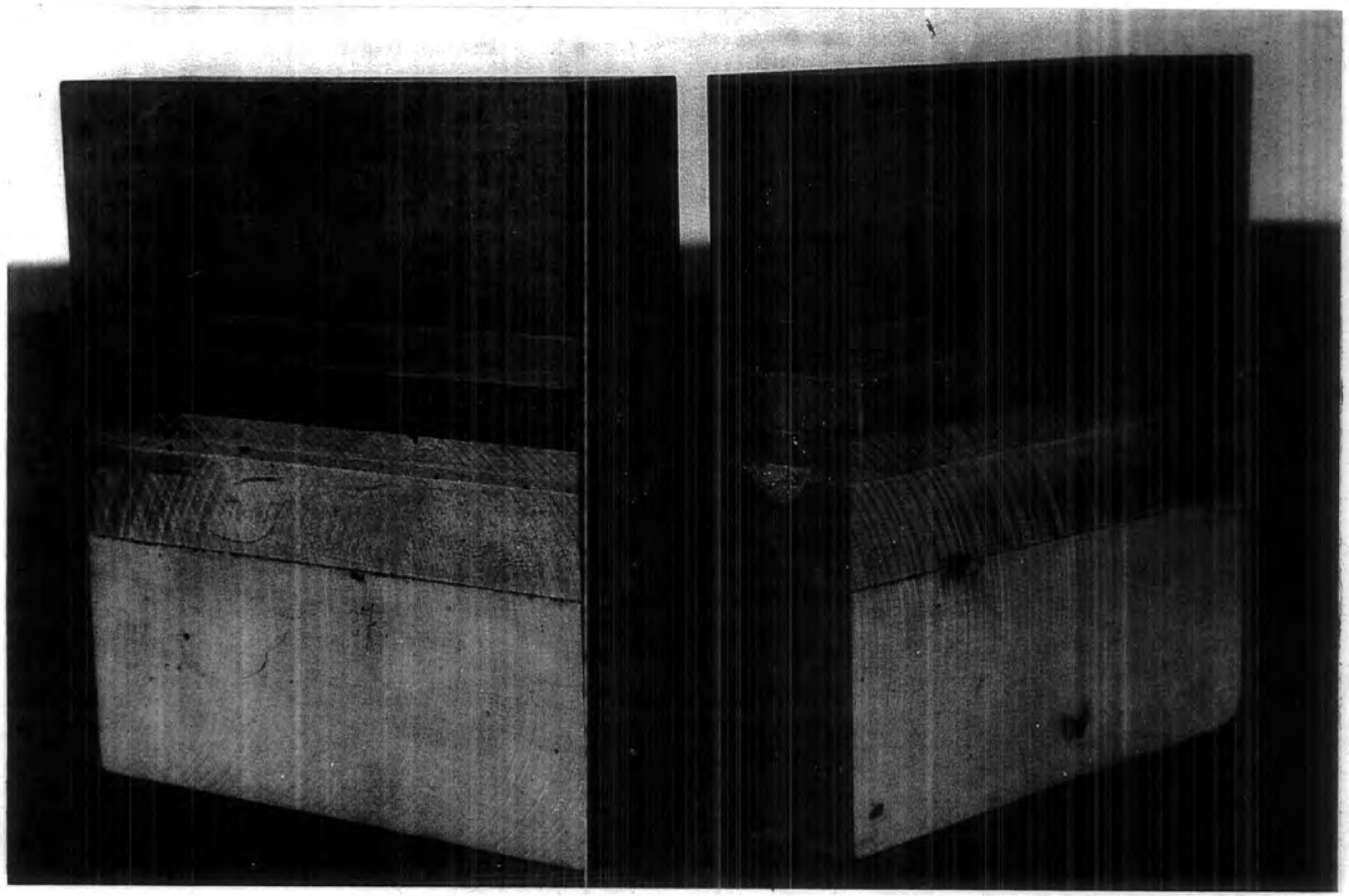

Figure 3.2 The pre-flood and post-flood models were moulded in a single block which was subsequently cut in half. The pre-flood model is on the right.

The crosshole seismic survey was simulated in the ultrasonic seismic modelling laboratory at the University of Durham (Sharp et al., 1985). Each model was submerged in a water tank, and ultrasonic transducers were positioned at each side, as shown in Fig. 3.1. The cylindrical source transducer is 7mm in diameter, and is 5mm long in the axial direction which is perpendicular to the plane of the section. The receiver transducer has an active element of 1mm diameter. Both transducers were positioned so that there was some clearance between them and the sides of the model.

Seismograms were recorded at 51 receiver locations from 51 source locations with source and receiver spacings of 2.5mm, giving a total of 2601 traces for each model. The ultrasonic bandwidth was approximately 200-500kHz, which meant that the crosshole separation was around seven wavelengths. In evaluating the results it is convenient to scale lengths and frequencies in the experiment by a factor of 1000 in order to simulate realistic dimensions for a cross-well survey. Thus the simulated well separation is about 55m and the simulated seismic bandwidth was approximately 200-500Hz. The experiment and results will be described henceforth in terms of scaled dimensions. Velocities remain unchanged by this scaling.

3.3 Previous work on the dataset

Previous work on this dataset (Pratt and Goulty, 1991 ; Pratt et al., 1991) has been done to demonstrate the capabilities of full waveform inversion schemes: diffraction stack migration and frequency-domain acoustic and elastic wave equation imaging. Traveltime tomography, using direct wave traveltimes, was carried out in those studies to provide an initial estimate of the velocity field for more sophisticated algorithms. However, in order that weaknesses in the traveltime inversion should not corrupt images obtained from the full wavefield schemes, rays were traced through the known geometry of the layering in the model. Here, it is merely assumed that calibrated sonic logs were run in both wells to give an initial estimate of the velocity field in the pre-flood situation by linear interpolation. Thus, as far as possible, the tomographic inversions simulate the results which could be obtained in a real crosshole experiment.

3.4 Traveltime tomography results

The direct wave arrival times for the pre-flood and the post-flood datasets were picked automatically after deconvolving the measured source signature to zero-phase. The peak of the deconvolved direct arrival wavelet was picked on each trace to give the traveltime of the direct arrival. Mis-identification of head wave first arrivals as direct arrivals can cause distortion of the tomographic image by introducing higher velocity anomalies. However, head wave first arrivals were too small in amplitude to be detected in these data. We can be confident about this because the time moveout of head waves and direct waves is different.

As the source has cylindrical symmetry and the receiver dimensions are small compared to the wavelength, little directivity of the wavelet was found. So an average source wavelet was taken for the range of take-off angles applicable in the datasets from the solid models, and this was used to calculate the deconvolution operator. The desired output was chosen to be a zero-phase wavelet with the same amplitude spectrum as the input. Results of the deconvolution process for a trace recorded through water only are shown in Fig. 3.3, with the corresponding amplitude spectra of the wavelets. It can be seen that this deconvolution process has significantly compressed the first arrival wave-train, which has a fairly reverberatory nature. A typical common-receiver gather from the data through the pre-flood solid model is shown in Fig. 3.4. Comparison with Fig. 3.3 shows that there has been some relative loss of amplitude at high frequencies.

For the preliminary results in Fig. 3.5, an initial velocity field was found by simple back-projection. Then ten iterations of SIRT were performed with raypath information obtained from raytracing through the current estimate of the velocity field. The velocity field was divided into square cells (2.5m x 2.5m) with uniform velocity in each cell, and Snell's law was obeyed at interfaces when raytracing. The compressional wave velocity in water, which is rather sensitive to temperature, was estimated as 1467m/s for the pre-flood run, and 1477m/s for the post-flood run, from recordings through the water only. The water layer velocities remained fixed throughout all iterations. Due to the size of the piezo-electric source, a static time-shift of +9 samples (≡ 2.25ms) was applied to all direct wave arrival times in order to correct source datum locations to the centre of each transducer position.

(a)

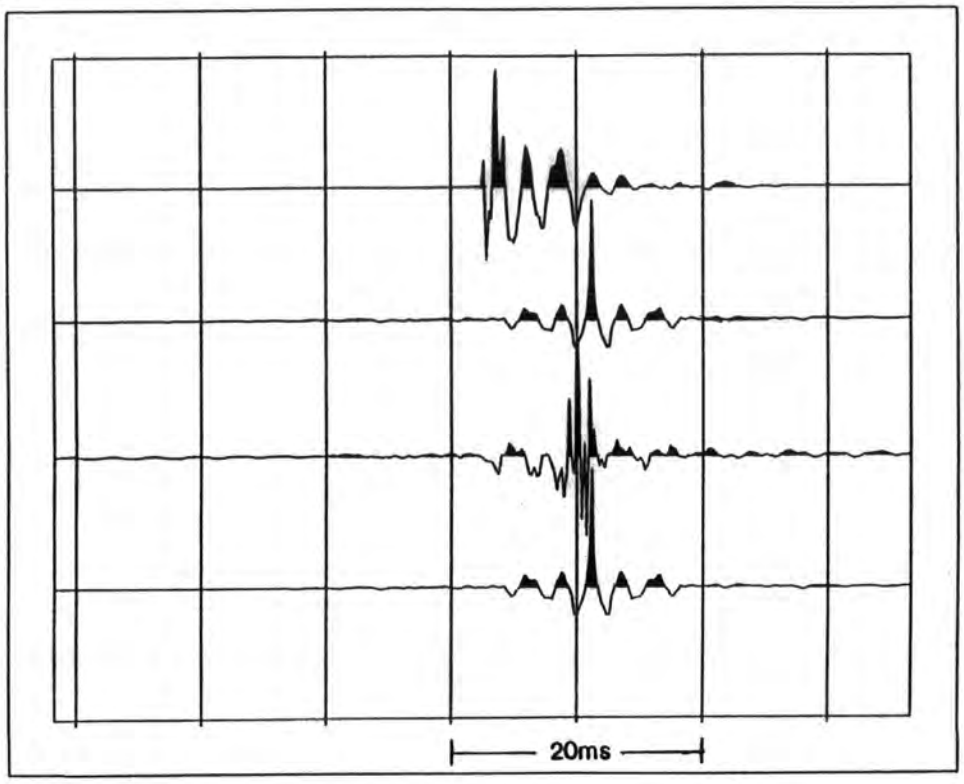

(b)

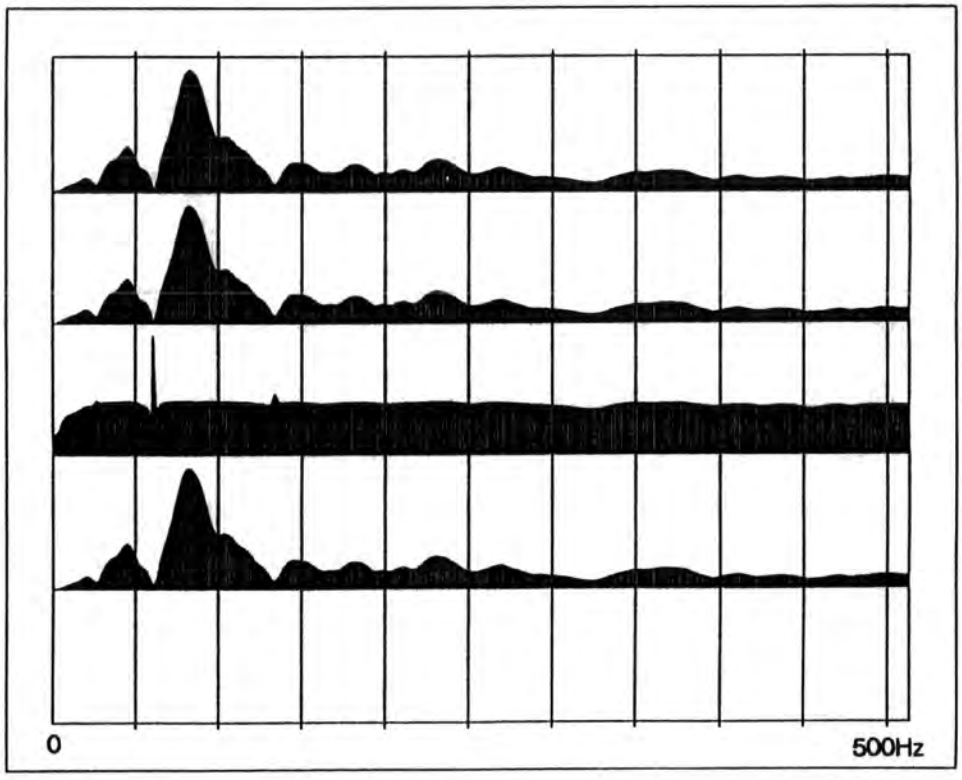

Figure 3.3 Deconvolution process : (a) From top to bottom the traces are : source wavelet measured through water with the model removed, desired output for design of the source signature deconvolution filter, the deconvolution filter, the actual output. (b) Corresponding amplitude spectra.

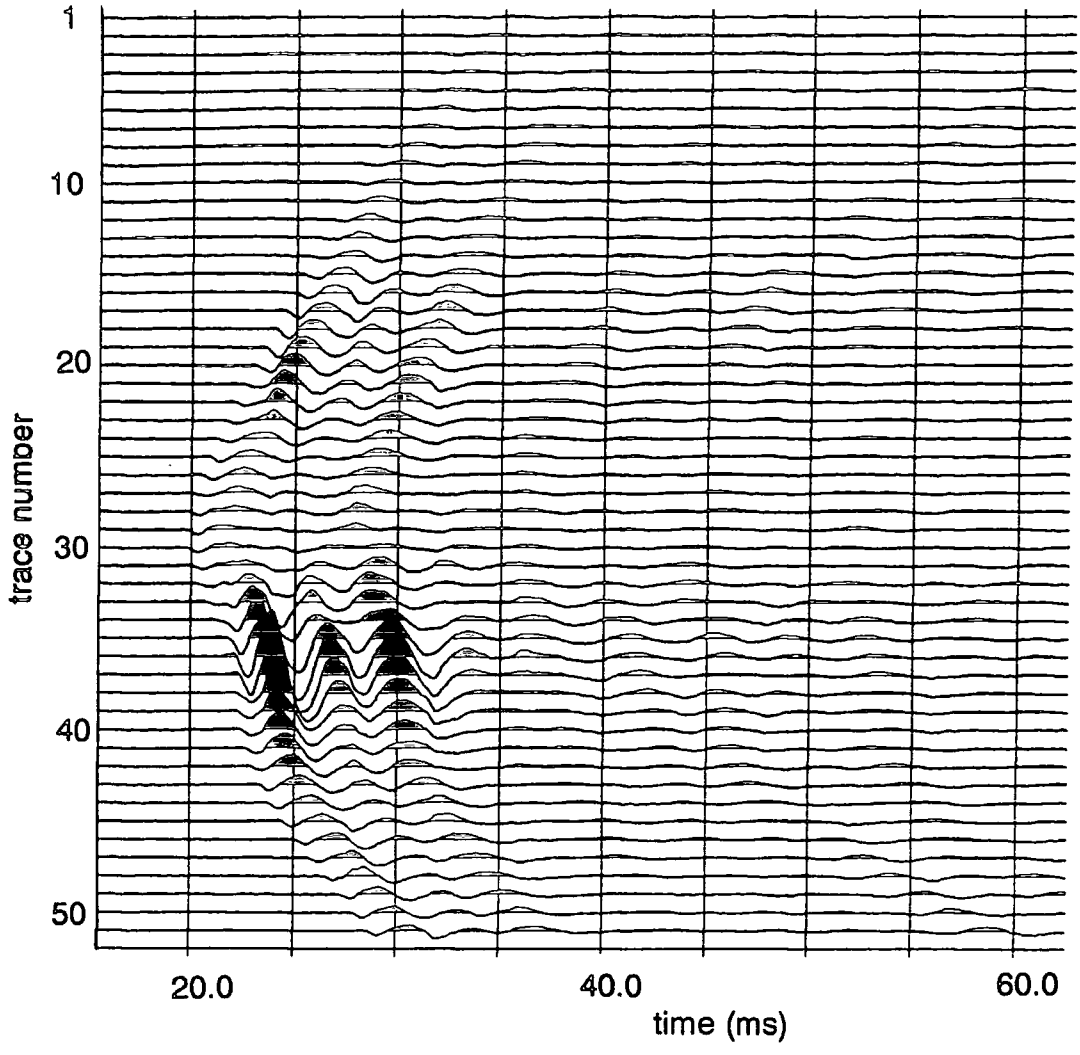

Figure 3.4 Common-receiver gather from the pre-flood dataset with the receiver at 55m depth. The top trace is from the deepest source position at 125m depth and the bottom trace from the shallowest source position, arbitrarily assigned to be at 0m depth.

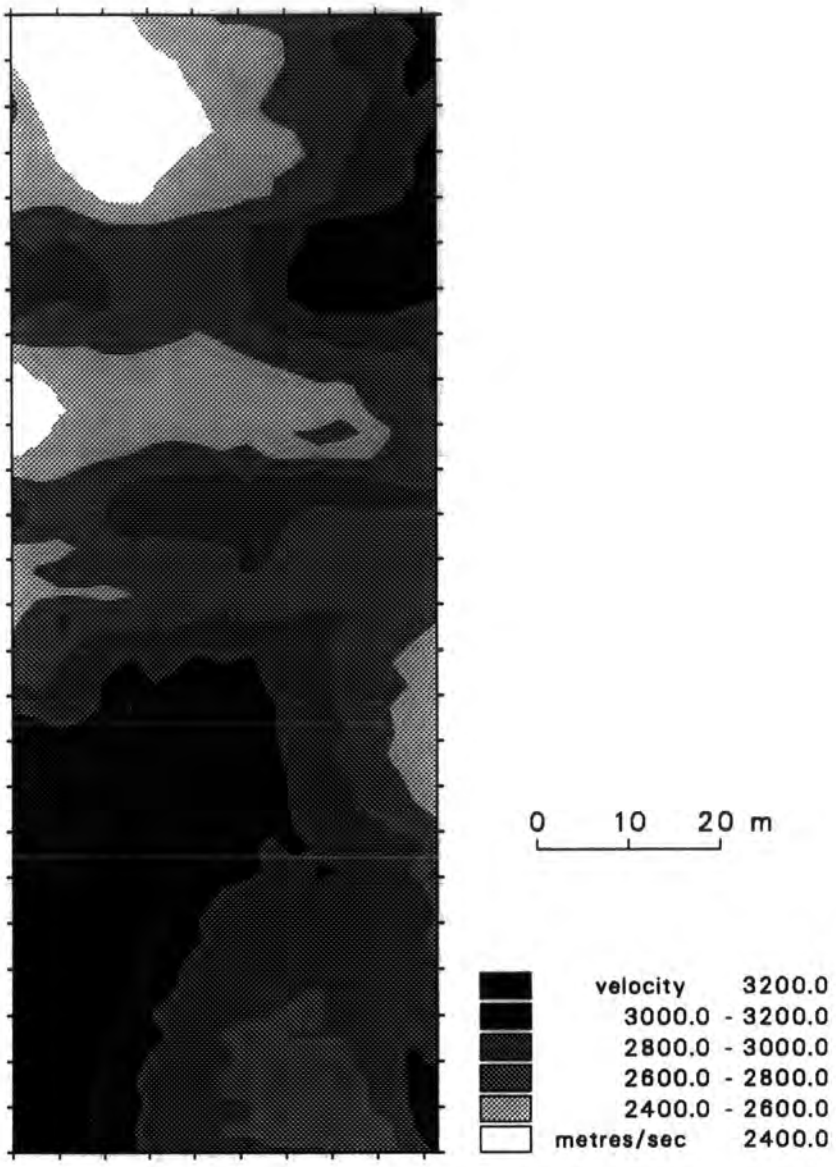

Figure 3.5 Pre-flood velocity tomogram obtained by simple back-projection and ten iterations of the SIRT algorithm.

There is an obvious asymmetry in the velocity tomogram and the boundaries are not distinct across the whole width of the tomogram. This asymmetry can be ascribed to non-parallelism of source and receiver arrays, and a small vertical relative shift between them, as described below.

3.4.1 Errors in source and receiver positioning

Although source spacing and receiver spacing were accurately maintained throughout the experiment, the relative coordinates of source and receiver positions were subject to small errors. Corrections could be calculated for this because an initial dataset was run before each physical model was placed in the tank, with only water between the source and receiver positions. From this it was determined that the horizontal spacing between each pair of source and receiver at the same nominal depth varied from 54.65m to 55.70m from top to bottom of the model, and that receiver positions were 0.5m shallower than corresponding source position. The corrections to source and receiver positions are analogous to carrying out accurate well deviation surveys in a field experiment.

3.4.2 Inversion of traveltimes with borehole deviations included

The traveltime data were inverted using ten iterations of SIRT with raypath information obtained as above. The initial velocity (see Fig. 3.6) was formed by assuming that sonic logs had been run in both boreholes to locate interfaces, which were then linearly interpolated across the survey area. The velocities used were those calculated from the horizontal direct wave arrival times (with source and receiver both at the same depth).

Raypath coverage, through the final velocity model obtained by inverting the pre-flood traveltimes, from every fifth source position is shown in Fig. 3.7. After each iteration, the selective smoothing algorithm described by Krajewski et al. (1989) was applied to the image to ensure a stable convergence of the iteration process and to suppress statistical pseudo-anomalies.

The velocity tomograms from the pre-flood data and the post-flood data are shown in Fig. 3.8. The image obtained from the pre-flood data (Fig. 3.8a) is quite satisfactory, with all the boundaries between layers clearly identifiable.

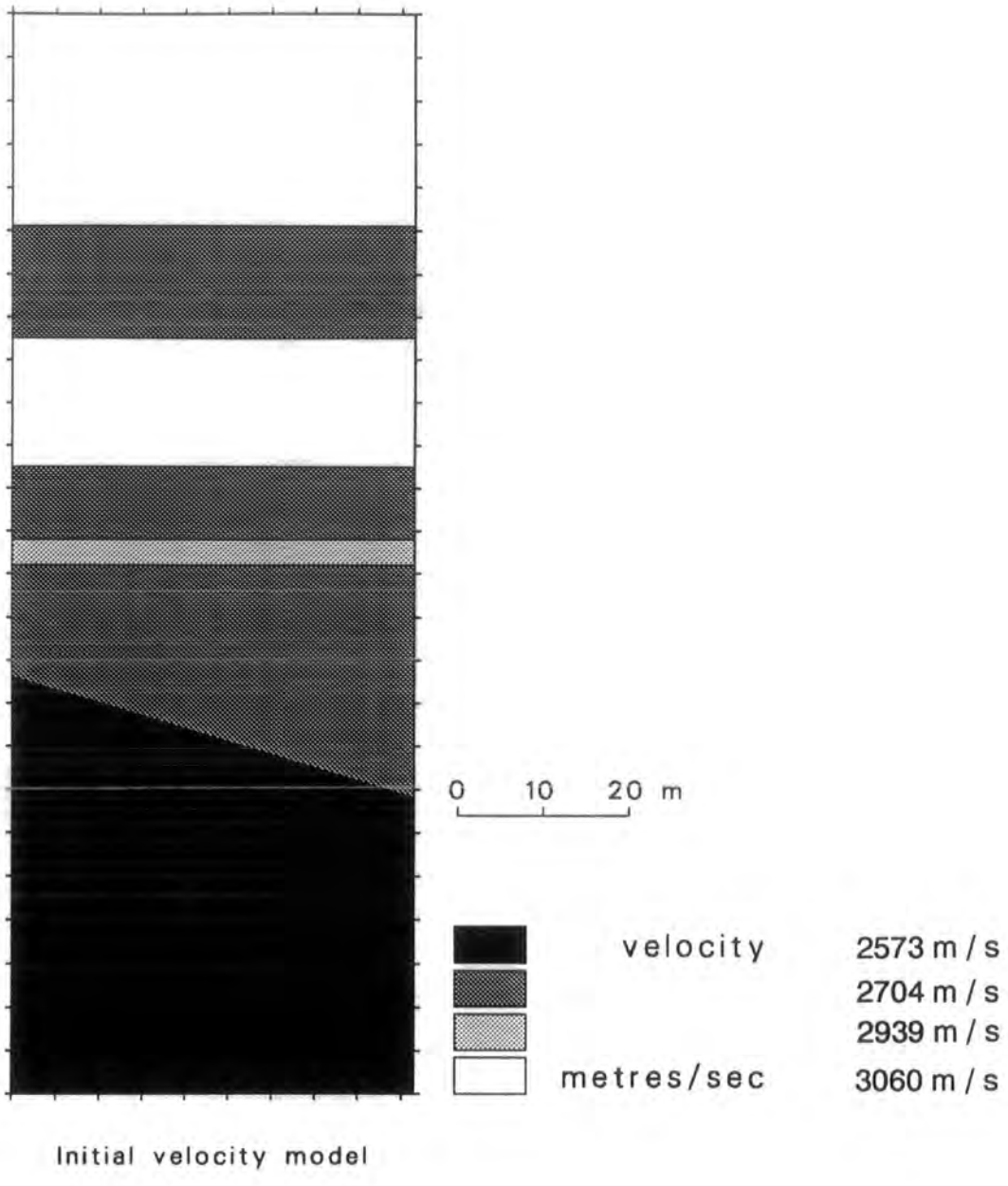

Figure 3.6 Initial velocity model used for the traveltime inversion. Tick marks around the edge of the model are at 5m intervals (scaled distance).

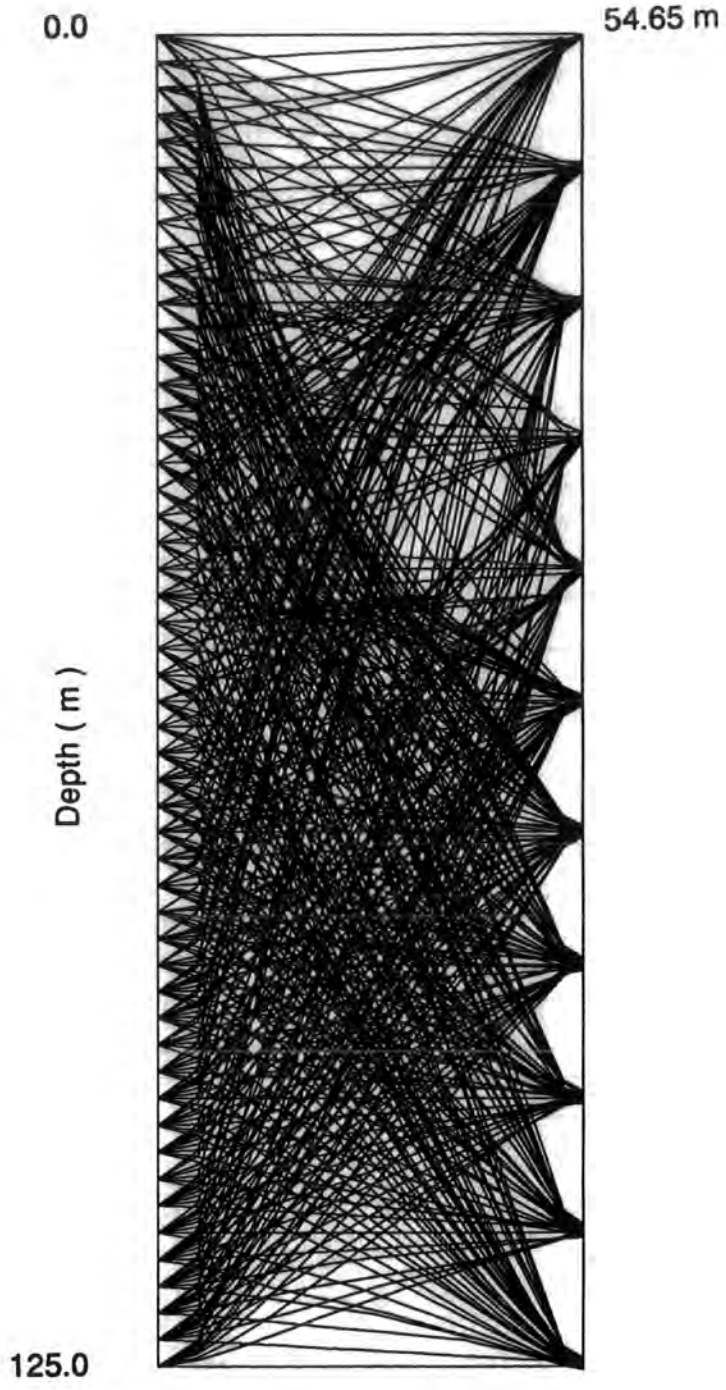

Figure 3.7 Raypath coverage through the final velocity field of the pre-flood inversion for every fifth source position.

The position of the channel can be identified and even the dipping boundary (although not the vertical discontinuity along it) is imaged. The flood zone is quite well located in Fig. 3.8b, but the interfaces are more difficult to identify in the post-flood image.

The difference between the pre-flood and the post-flood images (Fig. 3.8c) shows more clearly the position of the flood zone and that the flood front is located accurately. The magnitude of the velocity perturbation introduced by the flood zone is approximately 400m/s, corresponding to a reduction by 15%.

The velocity tomogram from the pre-flood data (Fig. 3.8a) is much better than that obtained previously (Fig. 3.5), due to the calculation and application of borehole deviations. The obvious asymmetry in Fig. 3.5 is introduced because the measured traveltime, for longer raypaths from shallower source positions to deeper receiver locations, is greater than that which would be measured without deviation. This gives rise to an asymmetric lower velocity area.

3.5 Amplitude tomography

The aim of a tomographic amplitude reconstruction is to image the absorption coefficient of the region under investigation. Traveltime inversion necessarily has to be performed initially to obtain an estimate of the velocity field and the raypath information.

3.5.1 Determination of amplitudes

Various methods of calculating the amplitude values of the direct wave arrivals were investigated using the common-receiver gather recorded in the water only, and the best one chosen on the criterion that it showed the least scatter compared to a smooth decay curve of amplitude with range. The techniques investigated were:

(1) RMS energy over a window of 20 samples starting at the direct wave arrival time.

(2) RMS energy over a window of 20 samples about the direct wave arrival time after deconvolution to zero-phase.

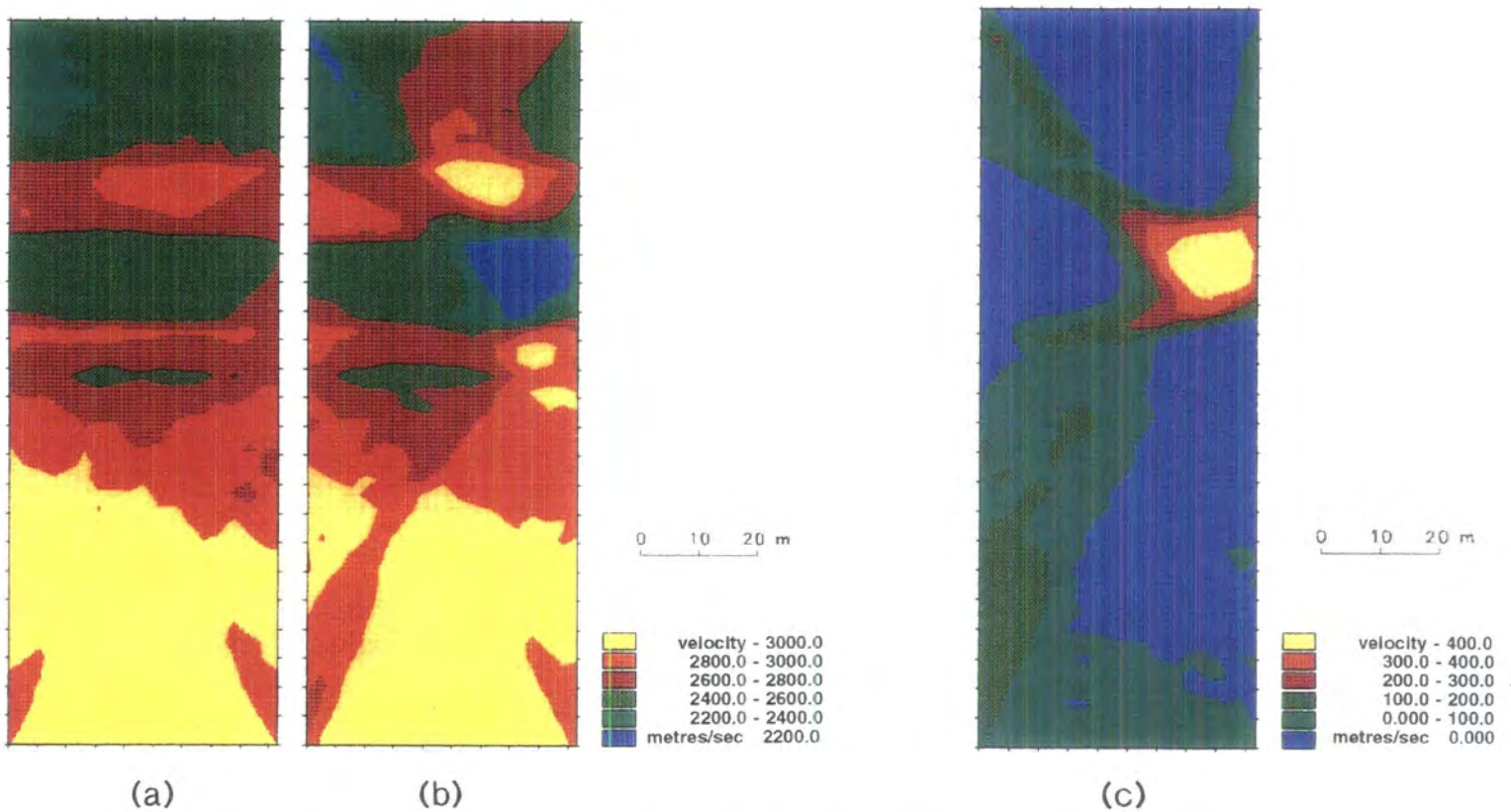

Figure 3.8 Velocity tomograms : (a) pre-flood ; (b) post-flood ; (c) difference.

(3) Peak value of direct wave arrival after deconvolution to zero-phase.

(4) Average amplitude over a window of 20 samples starting at the direct wave arrival time.

(5) Average amplitude over a window of 20 samples about the direct wave arrival time after deconvolution to zero-phase.

(6) RMS amplitude over a window of 20 samples about the direct wave arrival time after deconvolution to zero-phase and interpolation by a factor of 4 in the time domain.

(7) RMS envelope amplitude of the complex seismic trace over a window of 20 samples about the direct wave arrival time after deconvolution to zero-phase and interpolation by a factor of 4 in the time domain.

The direct-wave arrival on each trace was initially converted to a zero-phase wavelet, as described in the previous chapter. Following this process, the traces were interpolated by a factor of 4 in the time domain (by padding with zeros in the frequency domain). The complex seismic trace was then calculated using the method outlined by Taner et al. (1979), and the amplitude of the first arrival calculated to be the RMS envelope over a window of 20 samples (≡5ms) about the direct wave arrival time. (Recall that the peak of the zero-phase wavelet lies at the first break of the trace). Figure 3.9 shows a trace after deconvolution, with the corresponding quadrature trace.

3.5.2 Complex seismic trace analysis

In complex seismic trace analysis, the seismic trace $f(t)$ is treated as the real part of an analytic signal, or complex trace,

$$F(t) = f(t) + if^*(t)$$

where $f^*(t)$ is the quadrature trace.

The real seismic trace, $f(t)$, can be expressed in terms of a time-dependent amplitude $A(t)$ and a time-dependent phase $\theta(t)$ as

$$f(t) = A(t) \cos \theta(t)$$

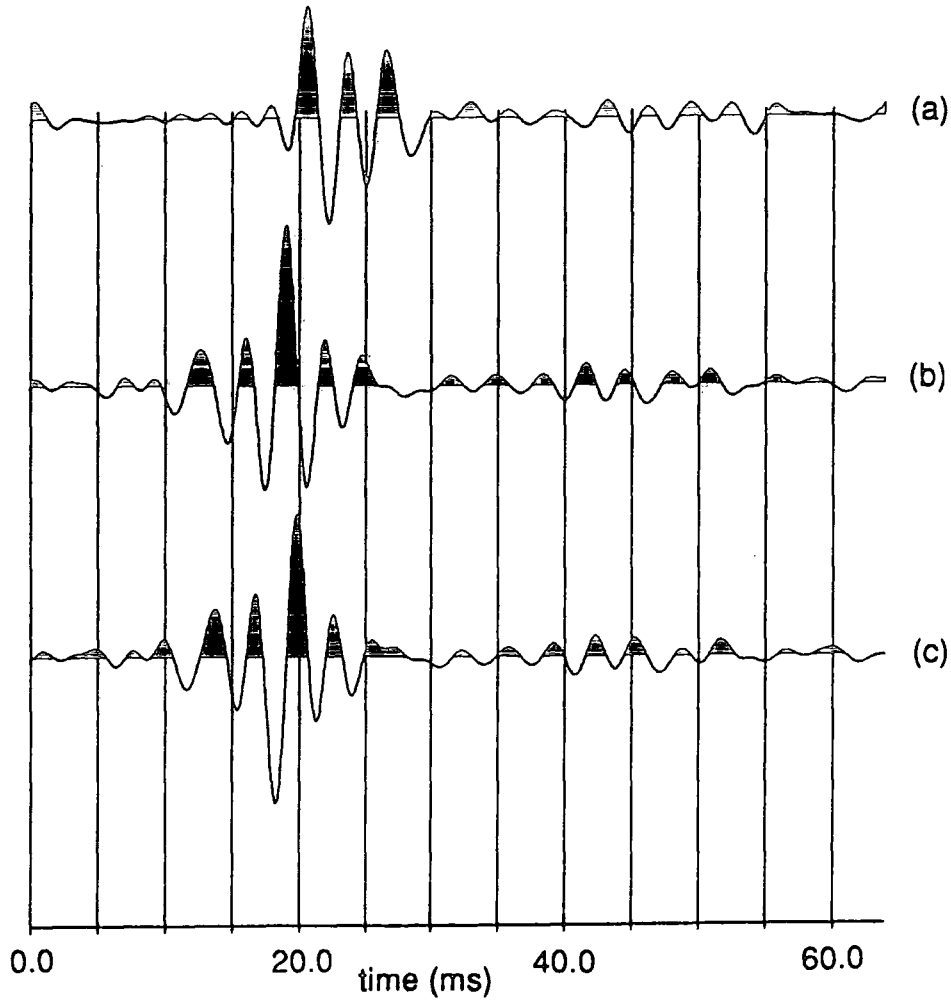

Figure 3.9 (a) A typical trace before signature deconvolution. (b) The same trace after signature deconvolution. (c) The quadrature trace corresponding to (b). The 20-sample window for RMS envelope amplitude estimation is 5ms long.

The quadrature trace $f^*(t)$ is then

$$f^*(t) = A(t) \sin \theta(t)$$

and the complex trace $F(t)$ is

$$F(t) = A(t)e^{i\theta(t)}.$$

If $f(t)$ and $f^*(t)$ are known, $A(t)$ and $\theta(t)$ can be found. The amplitude spectrum of the complex trace vanishes for negative frequencies and has twice the magnitude of the real trace for positive frequencies. The complex seismic trace can be calculated by taking the Fourier transform of the real trace, zeroing the amplitudes for negative frequencies and doubling the amplitude for positive frequencies, and then taking the inverse Fourier transform. The quadrature trace can also be calculated by simply applying a phase-shift of $\pi/2$ to the real trace in the frequency domain, and then transforming back to the time domain.

Figure 3.10 shows a comparison of pre-flood and post-flood amplitude values for a common-source gather with the source at 67.5m depth. The presence of the flood zone is indicated by the decrease seen in the post-flood amplitude values between receiver positions 30 and 45.

The next step is to apply corrections for the effects of directivity, geometrical spreading and for losses in amplitude due to reflection and transmission at water/model interfaces (equivalent to coupling factors in a real dataset).

3.5.3 Directivity in the measured reference amplitude

The reference amplitude, A_o, was calculated from recordings through the water only (with the model removed). The absorption in water at the ultrasonic frequencies used in modelling is negligible, as shown by Kaye and Laby (1973). At 10° C absorption in water is given approximately by

$$(\alpha / f^2) = 36 \times 10^{-15} \text{ neper m}^{-1} \text{ Hz}^2$$

where f is frequency in Hertz and α is absorption in nepers per metre (1 neper=8.686dB). Nevertheless, examination of these amplitudes revealed that they do not decay as 1/r. This is because the receiver transducer has some

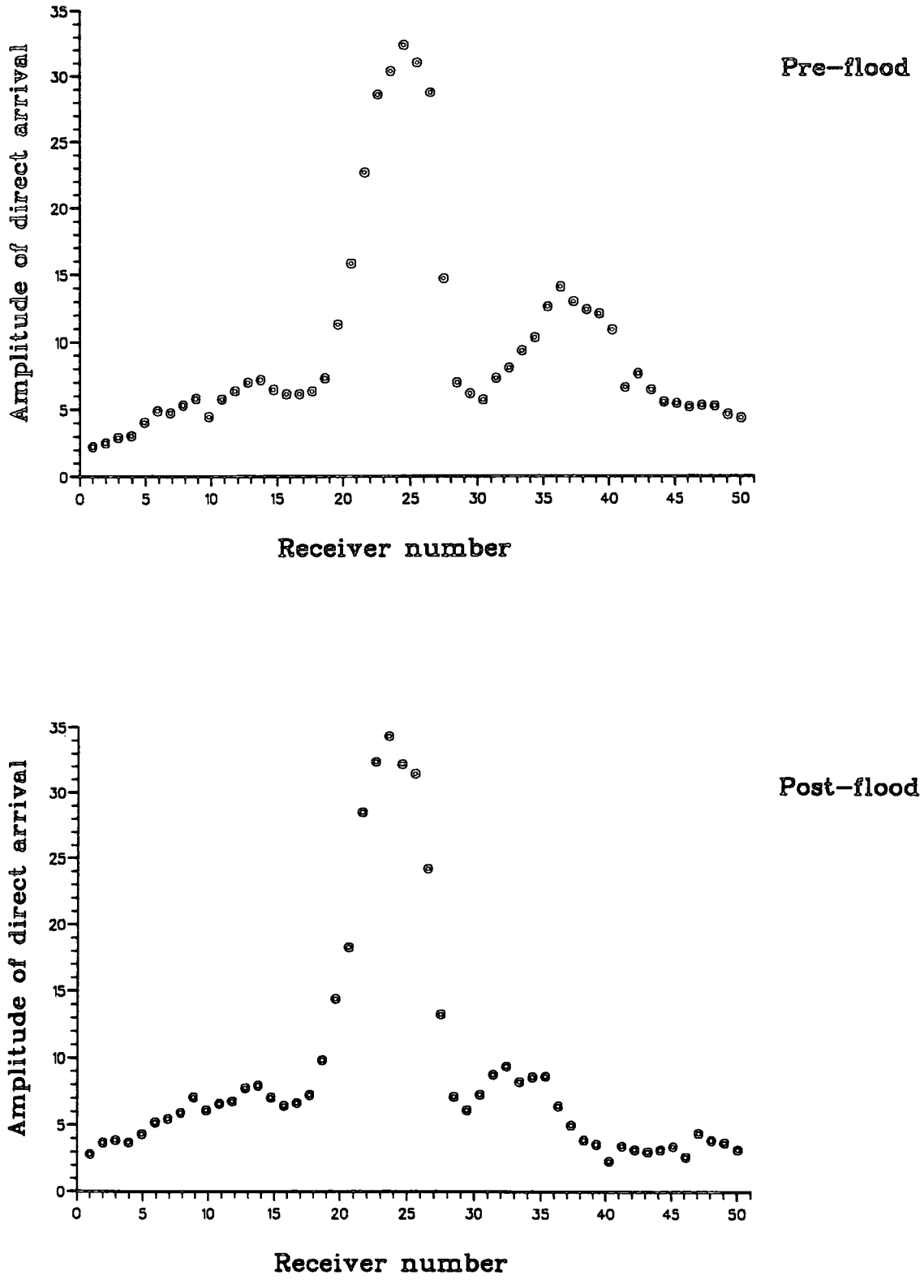

Figure 3.10 Comparison of pre-flood and post-flood direct-wave amplitudes for source position at 67.5m depth.

directivity which must be corrected for. The directivity is symmetrical (see figure 3.11), with amplitudes reduced by a factor of about 2 for the steepest raypath reaching the receiver positions. So the directivity effect was measured from recordings through the water, and correction factors applied according to the inclination of the raypaths at the receivers.

3.6 Results of the amplitude tomography

The initial results from the amplitude tomography show little of real interest. Figure 3.12a shows the absorption tomogram obtained for the pre-flood model. Boundaries between the layers are not as well defined as for the traveltime results. The channel feature and dipping interface cannot be identified. The post-flood image (Fig. 3.12b) is dominated by high absorption with no structure visible, and the flood zone cannot be identified accurately. The effect of the highly attenuating flood zone has smeared out the image. It is not surprising that these absorption tomograms are less sharp than the velocity tomograms because of diffraction effects. However, in the difference tomograms for amplitude inversion, diffraction effects should be identical for both models except where the velocity field has changed.

Difference tomograms were calculated from the data in two ways. First the log ratio of the pre-flood and the post-flood amplitude values was used as input for the SIRT inversion method, assuming that any differences in the various correction factors between the two datasets are negligible. Raypaths used were for the pre-flood velocity field. The difference tomogram in Fig. 3.12c shows the flood zone as an area of higher absorption, but the boundaries of the flood zone are not accurately imaged. Secondly, the absorption tomograms in Figs 3.12a and 3.12b, which were calculated using the respective raypath information from the pre-flood and post-flood velocity models, have been simply subtracted, to produce the difference tomogram in Fig. 3.12d. The flood zone is imaged with better continuity, but again its edges are blurred.

Using the absorption values obtained, and a peak frequency of 350Hz, the approximate value of Q in the flood zone and reservoir is estimated to be around 13 and 20 repsectively, which is in the range of values found by Murphy (1982) for the variation of quality factor with saturation in sedimentary reservoir rocks.

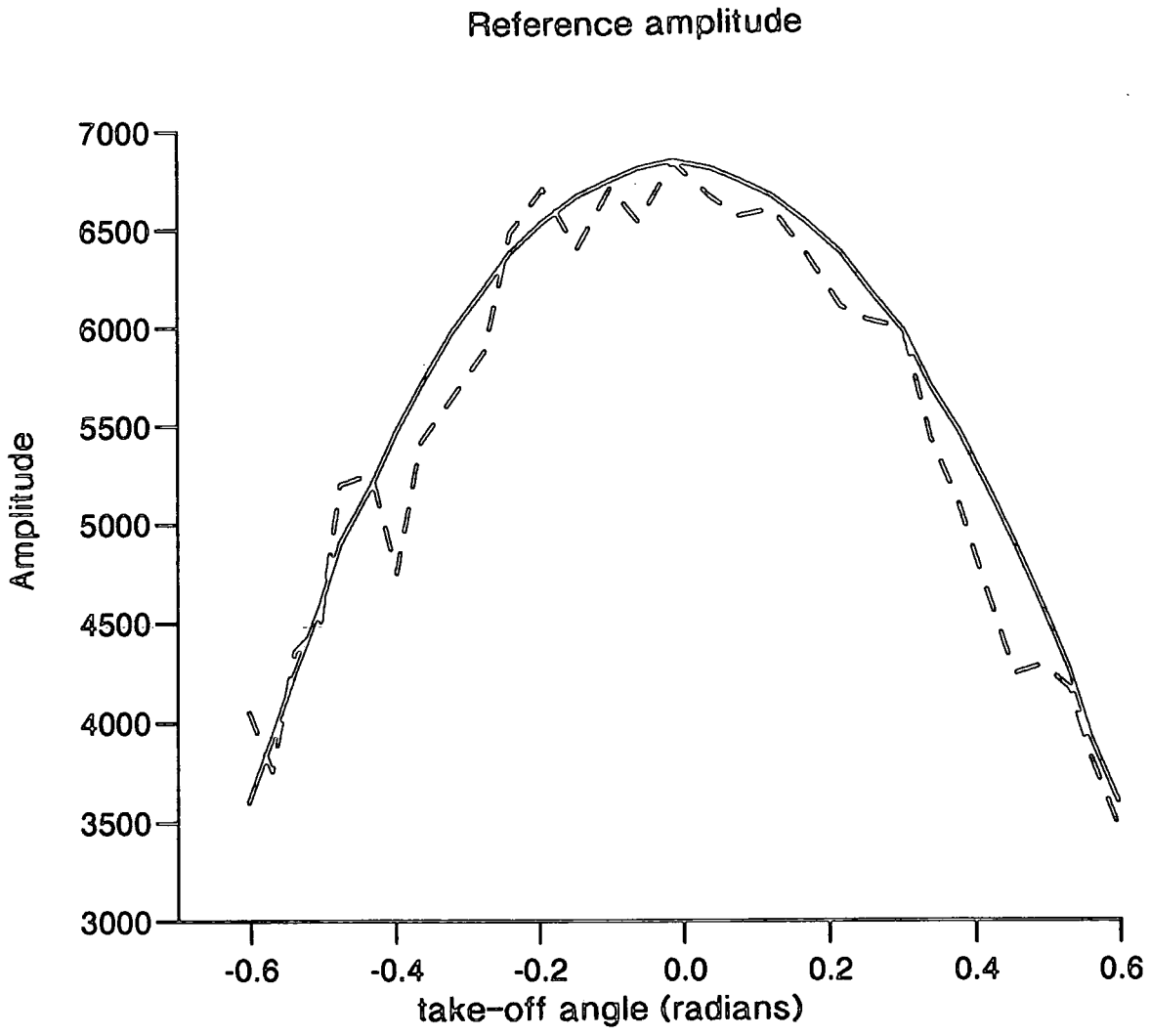

Figure 3.11 Measured amplitudes through water only with the model removed. The broken line shows the values as measured, the solid curve is the smoothed directivity function.

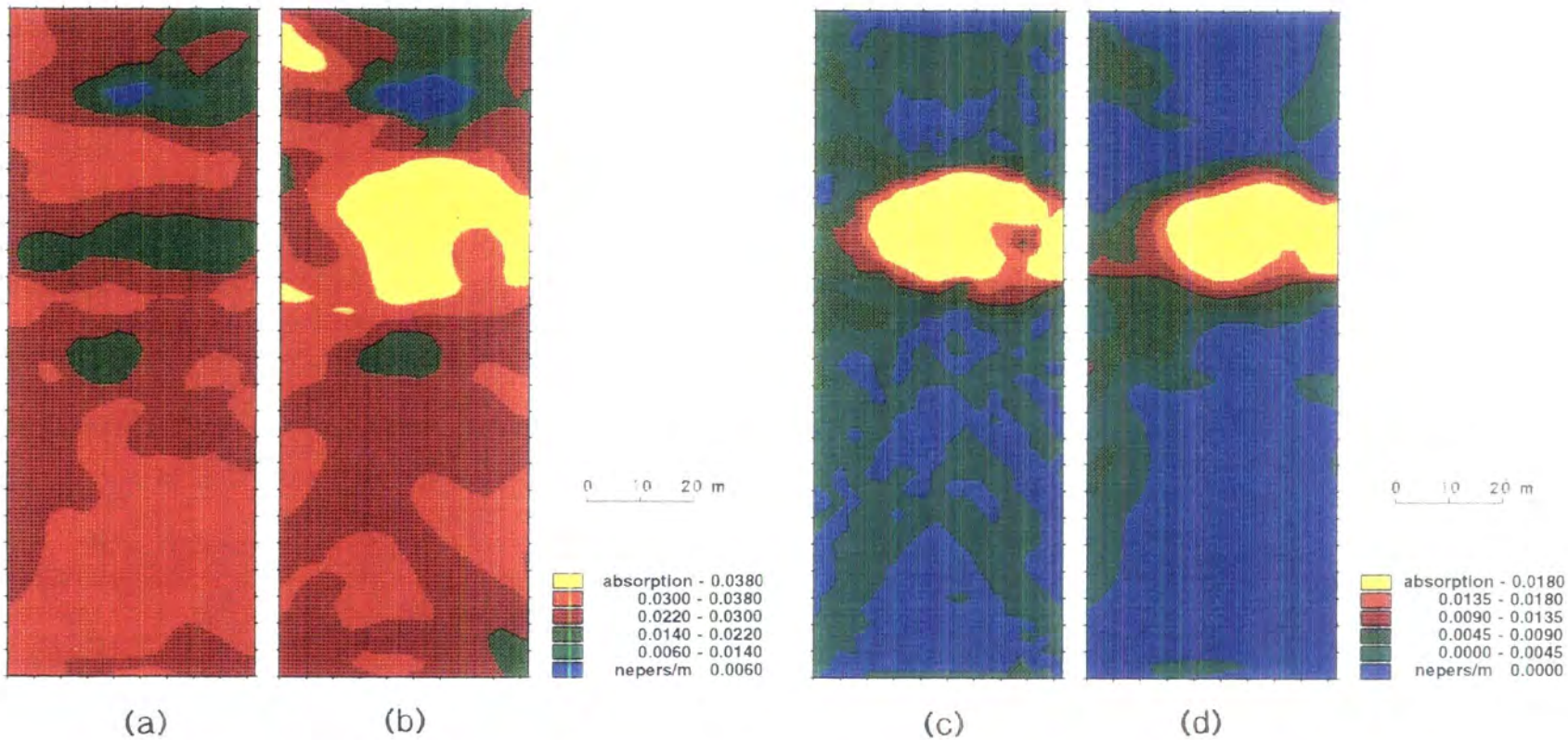

Figure 3.12 Absorption tomograms : (a) pre-flood ; (b) post-flood ; (c) difference tomogram using pre-flood/post-flood amplitude ratios and raypaths for the pre-flood velocity field ; (d) difference tomogram formed by subtracting (a) from (b).

3.6.1 Effect of corrections on the results

The effects of the corrections for geometrical spreading, transmission losses and directivity on the inversions have also been tested. Inversions have been performed as follows, and the difference field calculated as for Fig. 3.12d in each case. Five iterations were used for all inversions.

(1) No corrections applied to the data for geometrical spreading, transmission losses or directivity. Fig 3.13a shows the difference tomogram calculated assuming the reference amplitude to be the amplitude of the direct arrival recorded in the water only from a horizontal raypath.

(2) Inclusion of the corrections for losses due to transmission and reflection at the water model interfaces produces the difference tomogram shown in Fig. 3.13b. No directivity was included in the inversion.

(3) Fig. 3.13c shows the difference tomogram with the application of both the correction for transmission losses and in-plane geometrical spreading, but without the correction for directivity.

(4) Fig. 3.13d is the difference tomogram produced with the inclusion of corrections for losses due to transmission, in-plane and out-of-plane geometrical spreading, but excluding the directivity of the reference amplitude.

The application of all the calculated correction factors necessarily produces a better image than without. In the difference tomogram in Fig. 3.12d, the flood zone is better imaged with more continuity of the edges.

3.6.2 Discussion

In the amplitude reconstruction the same assumptions as for traveltime tomography have been made; i.e that the direct arrival amplitude or traveltime is considered to have been measured after travelling along a simple raypath using the theory of geometrical optics. However, the physical propagation of seismic waves involves diffraction. Thus transmission of energy from source to receiver takes place through the first Fresnel volume, whose section at any point along the raypath is the first Fresnel zone.

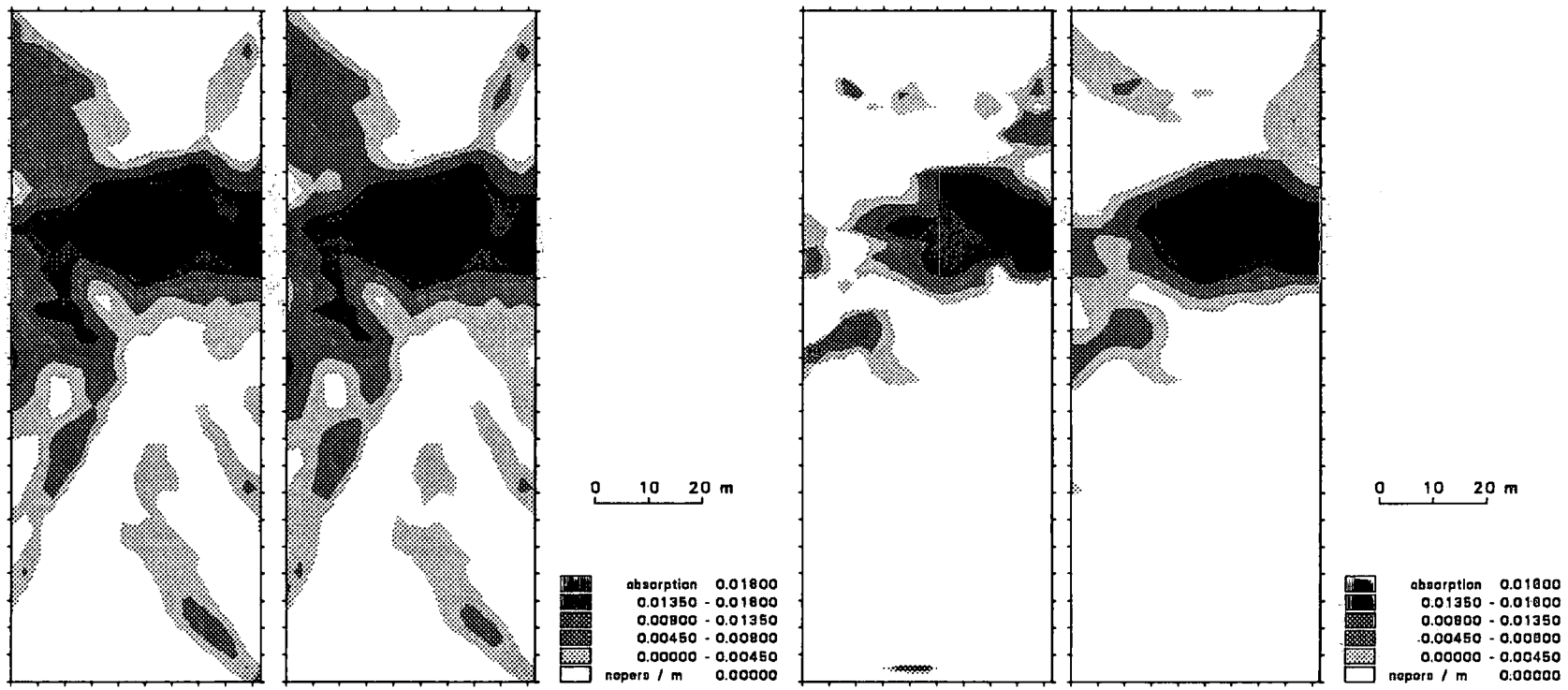

Figure 3.13 Difference tomograms formed by inverting amplitudes with different applications of corrections, but without correcting for the directivity: (a) no corrections applied; (b) corrections for transmission losses applied; (c) corrections for transmission losses and in-plane geometrical spreading applied; (d) all corrections except directivity included.

For a raypath of total length d and a seismic wave of wavelength λ, the diameter of the first Fresnel zone on a perpendicular section at the centre of the raypath is approximately $\sqrt{d\lambda}$. The mean wavelength in our dataset (using scaled dimensions) is 9m. Thus for raypath lengths of 50-130m, the mid-point diameter of the first Fresnel zone is 20-35m. These diameters are greater than the thickness of the reservoir layer in our model (15m). Thus it is not surprising that the absorption tomograms are more blurred than the velocity tomograms.

In most real situations it is likely that higher frequencies could be propagated (e.g. Harris, 1988) but that the ranges would be greater. The resolution is improved if the frequency is increased (and the sampling interval correspondingly decreased), but reduced if the range d is increased.

Another effect is multi-pathing. In Fig. 3.14 traces from the deeper source positions to the shallowest receiver position are shown, for both datasets. On the post-flood data the amplitudes show a substantial decrease as the raypaths start to cross the flood zone. As the source goes deeper, the amplitudes increase again, followed by a further decreasing trend. The larger amplitudes around source position 42 are due to multi-pathing around the bottom corner of the flood front, which has counteracted the loss in amplitude due to increased absorption in the flood zone. Multi-pathing due to sharp corners in the physical model will not be compensated by our raytracing-based method for calculating geometric spreading.

In principle, it would have been possible to attempt to correct for multipathing by tracing rays at all take-off angles from each source position through the velocity field. In practice, the sharp corners in the flood zone are not accurately imaged in the velocity tomogram, and it is doubtful whether an attempt to correct for multipathing would have resulted in significant improvement.

Both diffraction and multi-pathing effects could be taken into account by forward modelling with synthetic seismograms to calculate direct wave amplitudes through the velocity model. This is beyond the scope of the present study, but it can be noted that even if forward modelling according to wave theory were used, the amplitude tomographic reconstruction technique is based on tracing simple raypaths. Both diffraction and multipathing effects on the difference tomogram are large in this dataset because of the 15% velocity reduction and large absorption coefficient in the flood zone.

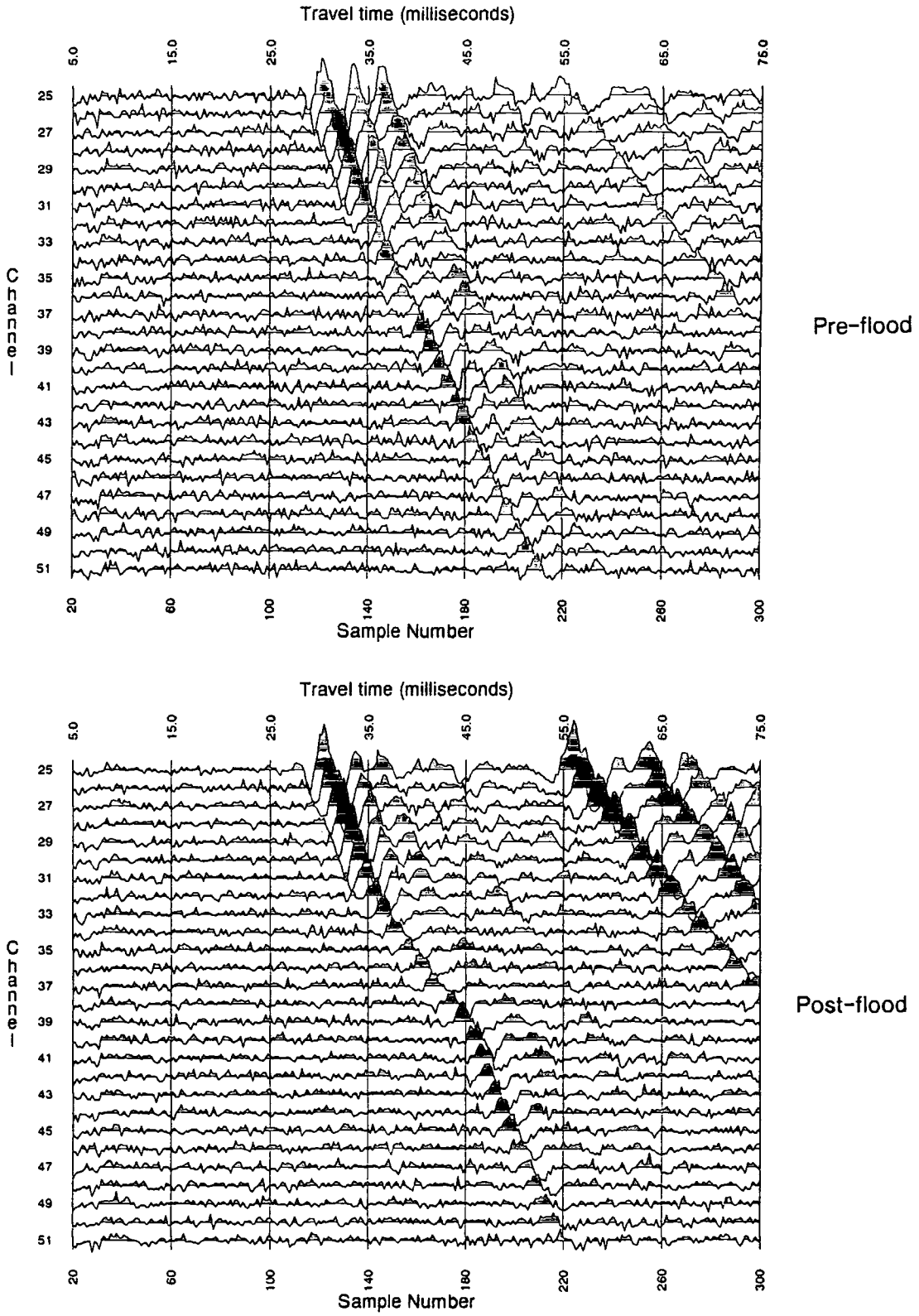

Figure 3.14 Common-receiver gathers for the shallowest receiver positions from the pre-flood and post-flood datasets (deeper source positions only).

A fundamental limit on the resolving power of tomographic imaging schemes is imposed by the angular distribution of raypaths. Wells need to be completed substantially below the reservoir horizon in order to obtain a wide angular distribution of raypaths through the reservoir and so image it satisfactorily. If the wells are terminated shortly below the reservoir, then some scheme for imaging the scattered, or reflected, wavefields would have to be used (e.g. Findlay et al., 1991; Pratt and Goulty, 1991). Not many crosshole datasets between cased wells have yet been acquired, and it remains to be seen whether reflection signals of adequate strength can be acquired for satisfactory imaging. Winbow (1991) has shown theoretically that 99% of the energy emitted by radial sources travels as tube waves, which is discouraging. However, enough cross-well datasets have been acquired for us to be confident that direct arrivals can be clearly observed, so tomographic imaging is certainly viable given suitable raypath geometry.

3.7 Conclusions on time-lapse tomography

Overall, the results are promising. Traveltime tomography has been shown to be effective in imaging a simulated EOR flood, with clear and accurate determination of the geometry of the flood zone. Amplitude tomographic reconstruction of the same datasets identified the flood zone as an area of higher absorption, but was unable to map the geometry precisely. The main failing in the amplitude tomography was dealing with the amplitudes without taking into account the effects of multipathing and diffraction thereby producing a blurred image.

From these results, it can be seen that traveltime tomography is the better candidate for the monitoring of enhanced oil recovery processes, and is well suited to this application, although the method will not sharply focus vertical discontinuities. The effectiveness of amplitude tomography is reduced where the reservoir geometry includes features which cause multi-pathing and the tomograms will be blurred by failing to account for diffraction effects.

However, real reservoir rocks are heterogeneous and there will be wide variations in liquid/gas saturations through the reservoir in response to EOR processes. Amplitude tomography may be able to complement traveltime tomography because the behaviour of absorption and velocity with varying fluid saturations is different. For example, at water saturation > 0.9, the velocity is

high and the absorption is low; at water saturations between 0.6 and 0.9, the velocity is low and the absorption is high; and at water saturations less than 0.6, the velocity is low and the absorption is low. Thus combined interpretation of velocity and absorption tomograms may be more robust.

PART 2

Chapter IV

The crosshole seismic reflection technique

4.1 Introduction

The crosshole seismic reflection technique has been investigated using boreholes on an opencast coal exploration site at Lostrigg, West Cumbria. The objective has been to determine its potential for locating old mineworkings and small-scale geological features. This chapter deals with the acquisition of the data and the data processing methods used in the crosshole seismic reflection technique, and associated problems.

4.2 Crosshole seismic reflection

A crosshole seismic survey has sources positioned over a range of depths in one borehole and receivers in another borehole to record the transmitted and scattered wavefields. In a typical survey, sources are placed at 2m intervals in the first borehole and repeated with the hydrophone receiver array at two or more levels with a common receiver position to check for any timing errors. By placing both source and receivers below the water table, the frequency content of the data is higher than that of VSPs.

A typical field set-up is shown in Fig. 4.1. The hydrophone string is lowered into borehole B and the source is positioned in borehole A. Shots are repeated at the same depth for different hydrophone levels to increase the receiver coverage. When this is done, one hydrophone position is kept in common to allow a check to be made on shot repeatability and timing.

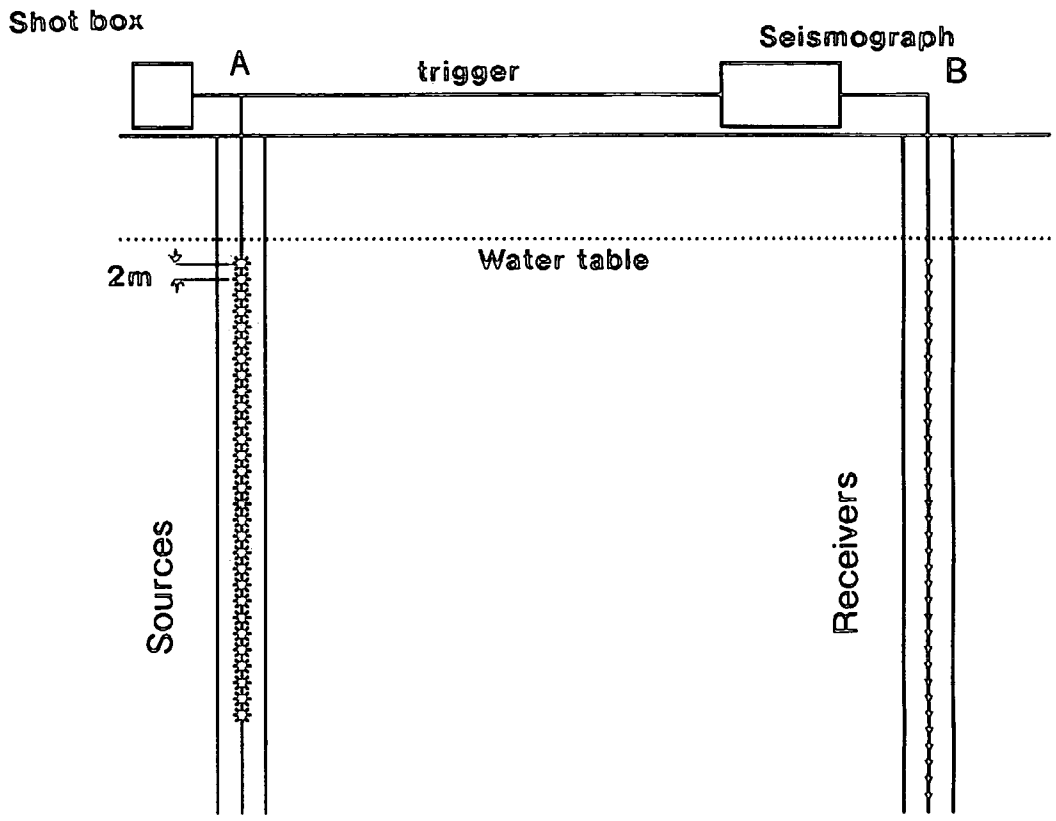

Figure 4.1 Typical field set-up for a crosshole seismic survey.

4.2.1 Source and receivers

The source used in the surveys at Lostrigg consisted of either an electrical detonator (No. 8 seismic type) or approximately 12.5g of dynamite. The charge was placed at the end of a short hollow steel tube to give the source enough weight so that it could be raised and lowered easily through the water in the borehole.

A 12-channel hydrophone string was used in all surveys, with a 2m hydrophone spacing. The hydrophones were connected to the signal cable by a pig-tail joint, and each hydrophone plus joint was encased in a plastic sleeve to prevent snagging on the borehole wall. The signal cable was fastened onto a nylon rope to make it easier to handle.

4.2.2 Recording equipment

An *EG&G Geometrics ES-2401* 24-channel enhancement seismograph was used in the field to record the data. Some in-field processing could be applied to the data (e.g. agc, bandpass filtering) for quality control, and the shot records could be plotted in the field. In the field, data were stored in SEG-DOS format on to 3.5 inch floppy discs. These data were transferred to the Sun system and reformatted for processing.

4.2.3 Field set-up

A sampling interval of 200μsec was used in all surveys and 1024 samples of data were recorded. Shots were usually fired at successive intervals of 2m and the seismograph was triggered to start recording as the detonator exploded. This was achieved by wrapping a wire around the detonator and attaching this to the trigger lead. As soon as the detonator explodes the trigger lead becomes open circuit; this is detected by the trigger circuitry and initiates recording. This method gives very accurate timing breaks, with very few timing errors detected. Occasional timing errors could be attributed to electrical pick-up between firing and triggering lines.

Limits were imposed on the range of source and receiver locations by the depth of the water table and by blockages in the boreholes. Most boreholes

were blocked above the total depth drilled. There is no response from a hydrophone if it is not immersed in water, and the coupling of the source energy to the borehole is insufficient if the source is not below the water table. Borehole collapse and blockage caused many surveys to be abandoned, as well as limiting maximum source and receiver depths. The boreholes begin to deteriorate a few days after drilling, which is unfortunate as they were often required several days after being drilled. This was the main reason for blockages encountered at Lostrigg.

4.3 Processing of crosshole reflection data

Processing of crosshole seismic reflection surveys is complex and consists of several distinct stages : data editing, deconvolution, wavefield separation, velocity field estimation and pre-stack depth migration to a depth section.

4.3.1 Data transfer and editing

Following acquisition in the field, the data were transferred from DOS-format floppy discs to the Sun computer system in the Department of Geological Sciences. The data were converted from SEG-DOS to the in-house processing format (direct-access binary files with data headers). Where different levels of the hydrophone string had been used, then the common-shot gathers had to be combined to form the final common-shot gather for processing. The common-channels (used to check for timing errors and shot repeatability) were then compared as a precautionary measure. The two (or more) different levels were then combined and the common channel(s) removed. Fig. 4.2 shows a raw common-shot record, with the shot at 38m and receivers from 16m to 82m depth, from survey 1 described in Chapter V. First breaks picked for the common-shot record are shown by a black dot on each trace (this is used in all following figures).

4.3.2 Waveshaping deconvolution

It was sometimes beneficial to suppress the lower frequencies in the data before migration, and this can be achieved by using a high pass filter. Also, there are advantages in changing the phase of the source wavelet in the data. A

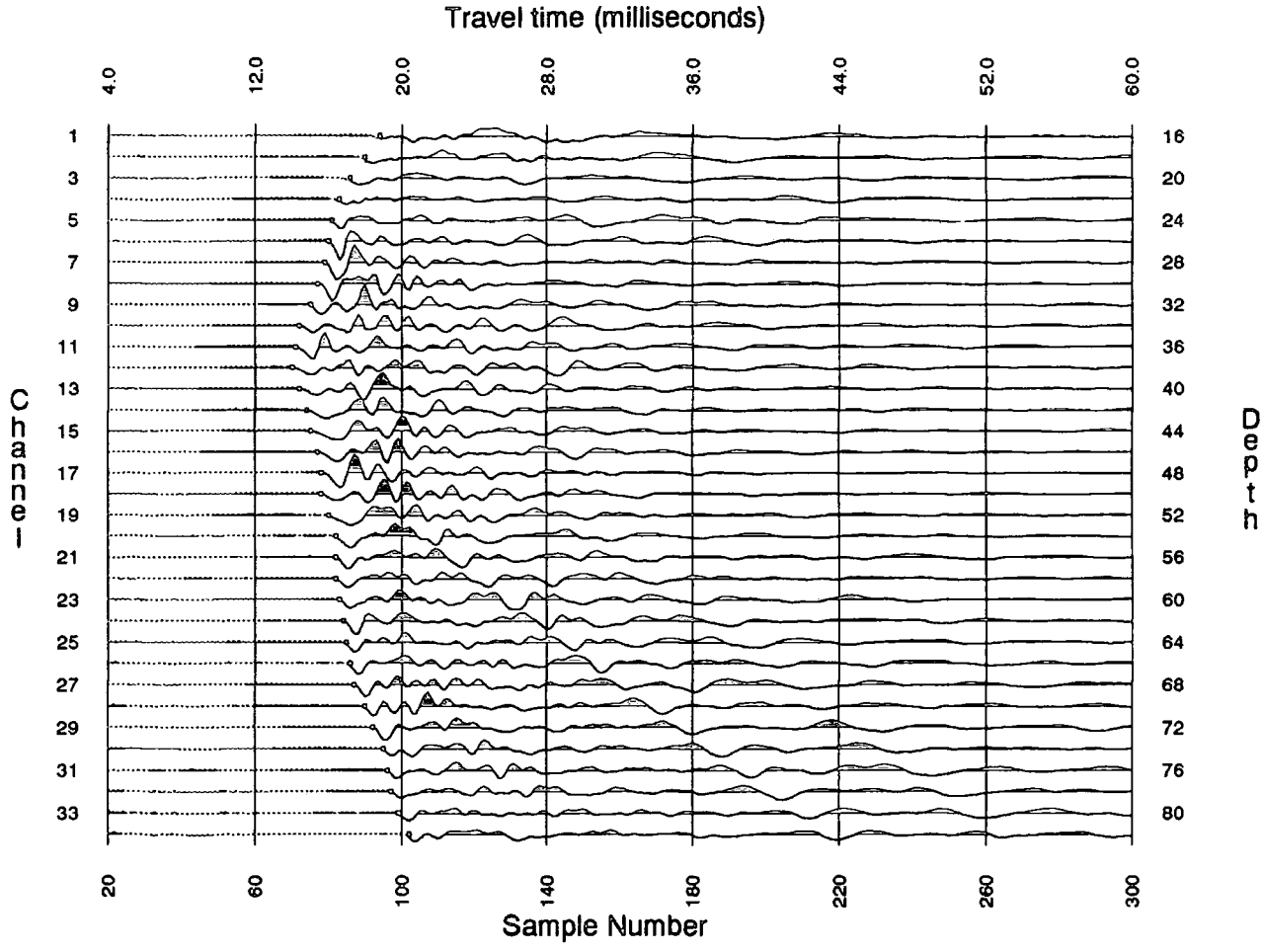

Figure 4.2 A raw common-shot record from a crosshole seismic survey. The shot is at 38m depth.

seismogram may be thought of as a convolution of the source function with the impulse response of the earth. As such, the onset of each arrival corresponds to the traveltime along the raypath (direct or reflected). For the reflected arrivals, it is preferable to produce a section in which the central peak of the arrival waveform corresponds to this traveltime. This may be achieved by converting the effective wavelet in the data to zero-phase.

In order to produce a zero-phase section, a least-squares energy Wiener waveshaping filter (e.g. see Robinson and Treitel, 1985) can be calculated to shape the estimated wavelet into a zero-phase wavelet with a modified amplitude spectrum. This filter may then be convolved with the data to deconvolve the data to zero-phase. An estimated source wavelet is obtained by assuming that it is minimum phase (a common assumption when the source used is an explosive type). The autocorrelation function of the wavelet is taken to be the average autocorrelation of all the traces in the common-shot gather, over a window from 10-60ms. The minimum-phase assumption is then used to obtain a minimum-phase wavelet (Robinson and Treitel, 1985).

Figs. 4.3-4.5 illustrate this method as applied to a raw common-shot gather. Raw data from survey 1 (see Chapter V) are shown in Fig. 4.2, normalized to RMS energy over a window from 10-60ms. Figure 4.3 consists of five waveforms; the first is the estimate of the source wavelet obtained by the method described above, the second is the desired output, a zero-phase Butterworth wavelet, the third is the calculated filter coefficients, and the fourth is the desired output shifted by the optimum lag. The bottom trace is a convolution of the filter with the input wavelet. The respective amplitude spectra of these traces are shown in Fig. 4.4. Figure 4.5 shows the same common-shot gather after application of the waveshaping filter to all traces. It can be seen, by comparison with the raw data, that some of the lower frequencies have been suppressed and that the direct arrivals in Fig. 4.2 now correspond to the trough in Fig. 4.5. The filter length in this example was 3.2ms, and the Butterworth wavelet has a bandwidth from 200-800 Hz. Deconvolution trials were carried out as described below.

4.3.2.1 Deconvolution trials

Deconvolution trials were performed using the common-shot gather shown in Fig. 4.2. Figure 4.6 shows the raw data, with no waveshaping deconvolution

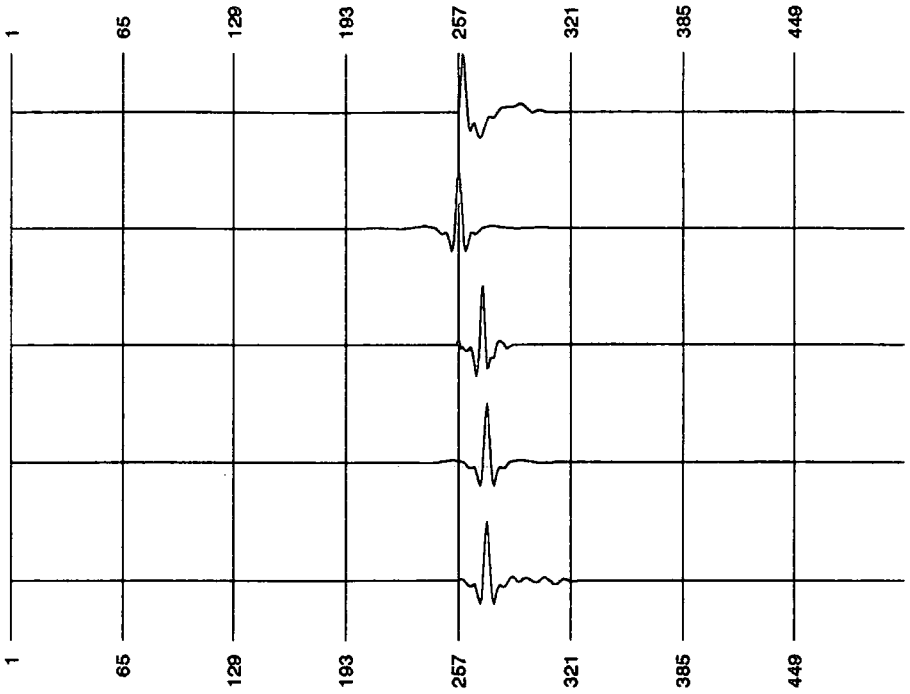

Figure 4.3 Waveshaping deconvolution; traces are, from top, input wavelet, desired output, waveshaping filter, lagged desired output, convolution of input wavelet and filter.

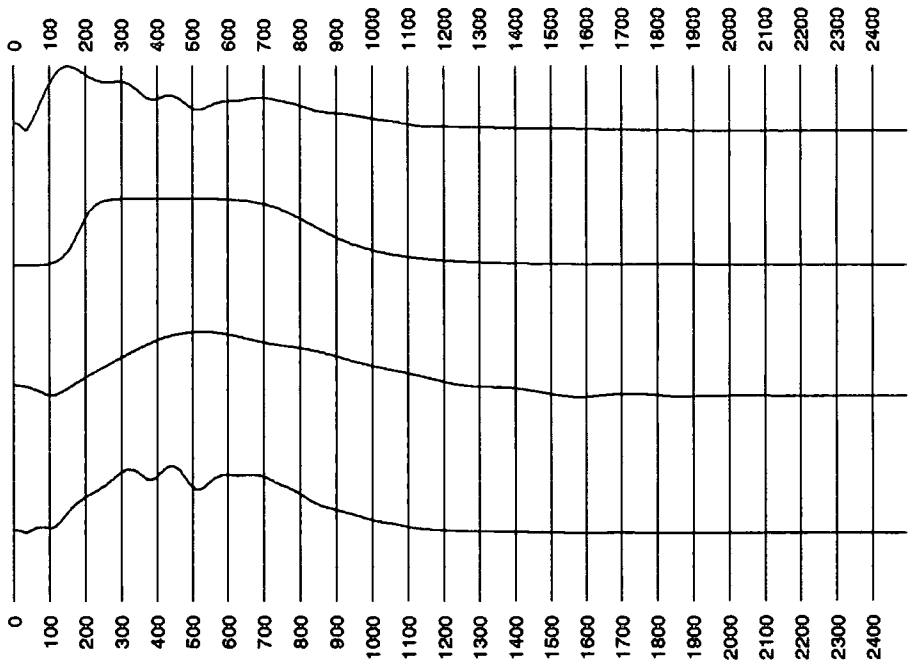

Figure 4.4 Waveshaping deconvolution amplitude spectra, from top, input, desired output, filter, filtered input.

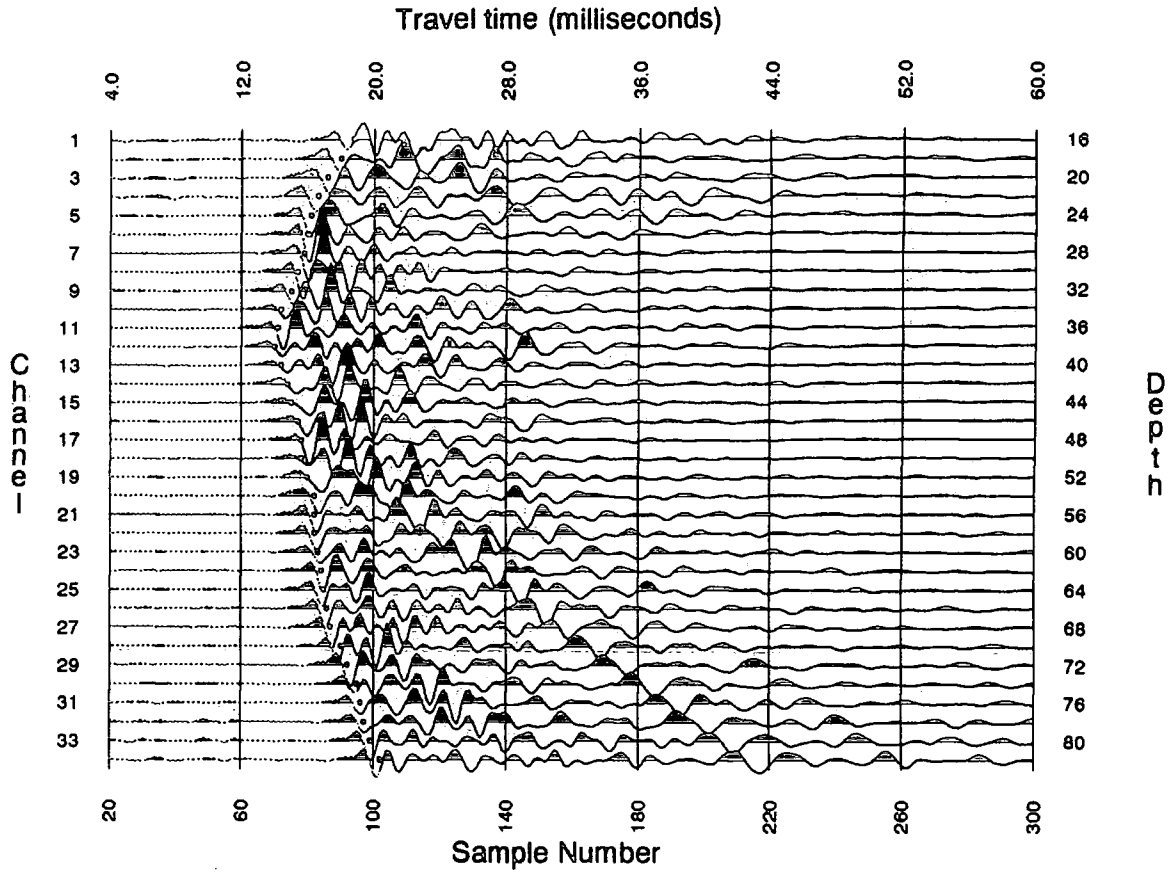

Figure 4.5 Common-shot gather of Figure 4.2 following waveshaping deconvolution.

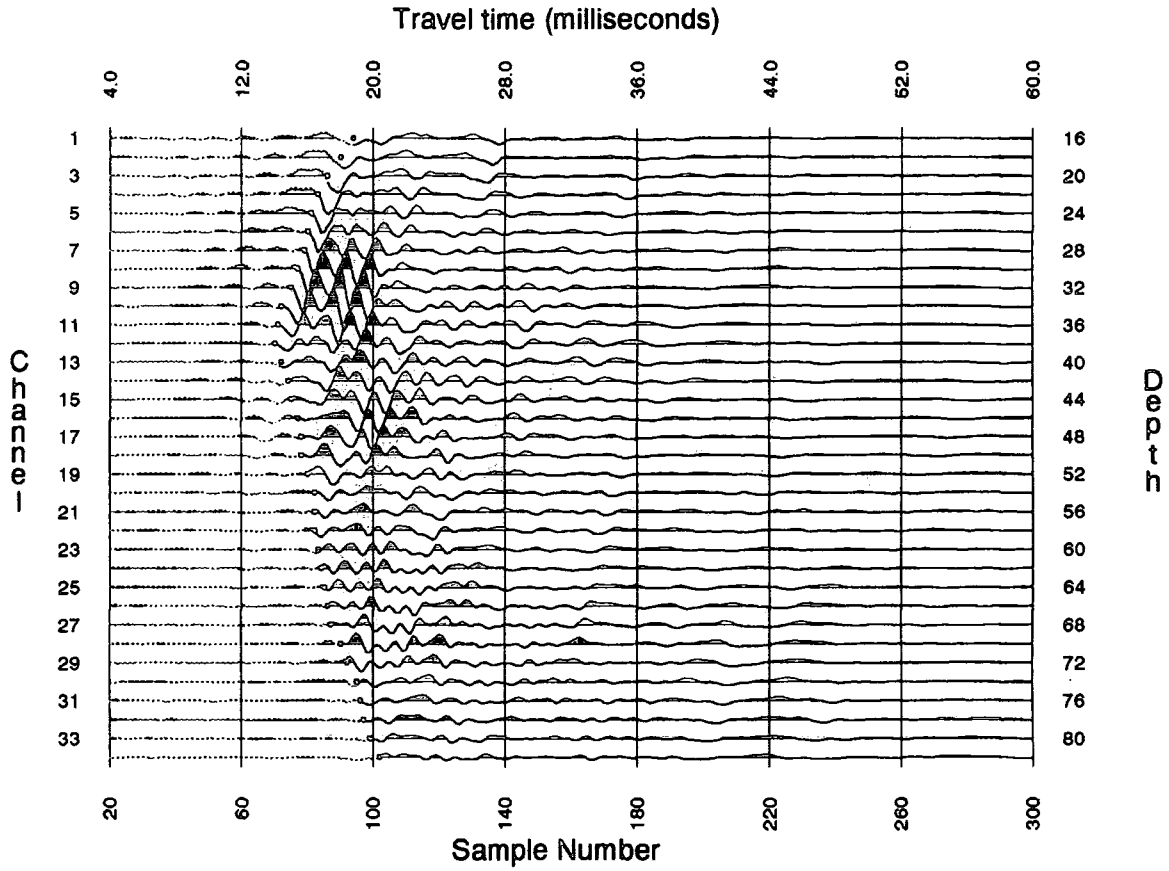

Figure 4.6 Common-shot gather after wavefield separation, with no waveshaping deconvolution applied.

applied, after separating the upgoing wavefield in *f-k* space. On application of a waveshaping deconvolution filter of length 3.2ms, the same record is shown in Fig. 4.7. The peaks of the reflected arrivals in Fig. 4.7 correspond to the onset of the arrivals in Fig. 4.6. The desired output wavelet was a Butterworth with bandwidth 200-800 Hz. There is energy up to 1000 Hz in these data, but the spectrum is dominated by the tube-wave energy from 300-450 Hz. Raising the high-cut frequency of the desired Butterworth output wavelet results in some aliasing of the data. For comparison, a filter length of 6.4ms was used in the deconvolution process, and the results from this are shown in Fig. 4.8.

A trace-by-trace deconvolution method was also tried, with the autocorrelation function of each trace being taken over the same window, 10-60ms. The filter length used was 3.2ms and the desired output was a Butterworth wavelet having the same amplitude spectrum as before. The results from this, shown in Fig. 4.9, are not significantly different from those in Fig. 4.7, although the reflected arrivals in the data are not resolved as easily as those in Fig. 4.7. It is better to average out the autocorrelation functions over all traces because the reflected arrivals in the data cover a range of angles on each trace.

4.3.3 Wavefield separation

Each recorded common-shot gather contains both upgoing and downgoing reflected energy, i.e. waves which travel upwards or downwards, respectively, across the receiver array. These have to be imaged independently since, for any reflecting horizon, the polarity of the reflection coefficient reverses according to whether the incident wave approaches from above or below. These different wavefields are readily separable using velocity filters since the apparent velocities of upgoing and downgoing waves are of opposite sign.

The moveout of the reflected events in crosshole reflection data is non-linear, so a filter that is able to pass or reject a large range of apparent velocities has to be used. The filter that is used in this case is the pie-slice filter which is applied to the data after a two-dimensional Fourier transform into the frequency-wavenumber (*f-k*) domain.

To perform a two-dimensional Fourier transform on a common-shot gather, a Fast Fourier Transform or FFT (see Cooley and Tukey, 1965) is applied first

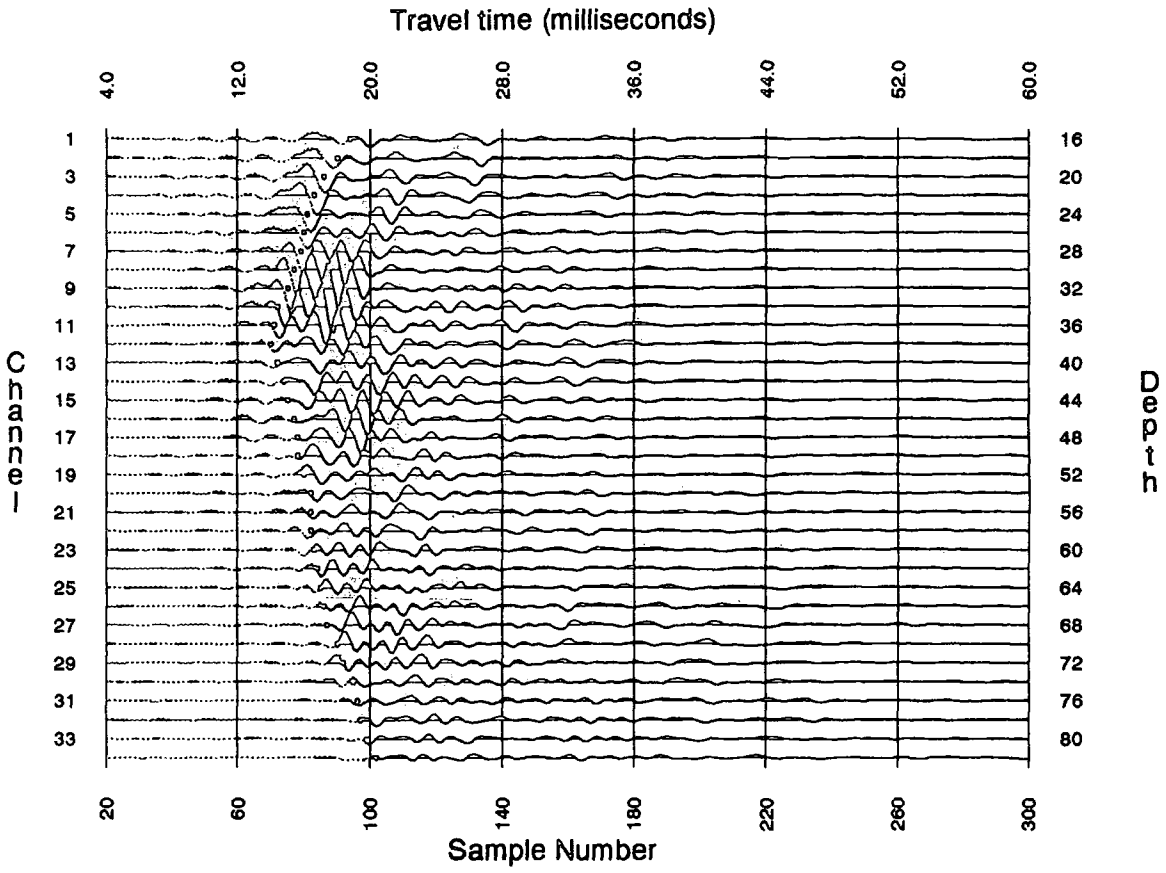

Figure 4.7 Common-shot gather after wavefield separation, with waveshaping deconvolution applied using a filter of 3.2ms length.

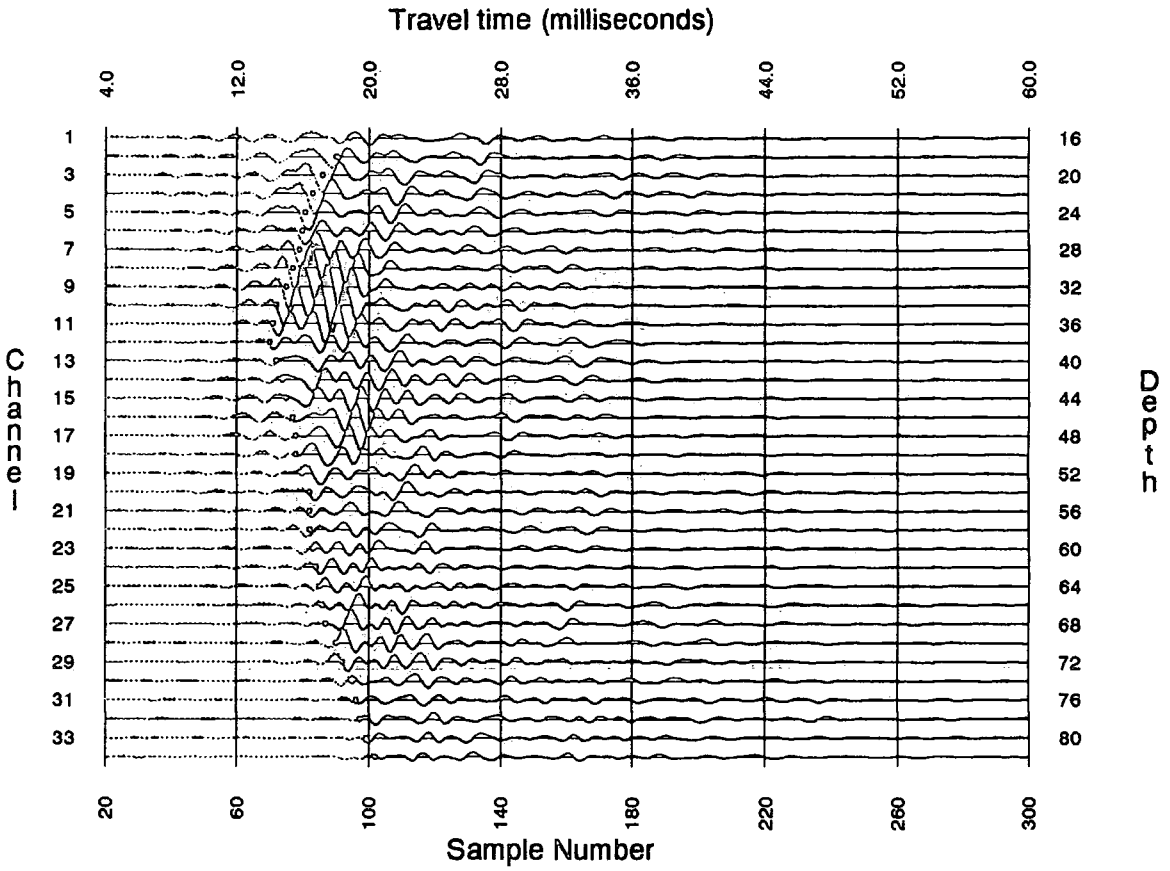

Figure 4.8 Common-shot gather after wavefield separation, with waveshaping deconvolution applied using a filter of 6.4ms length.

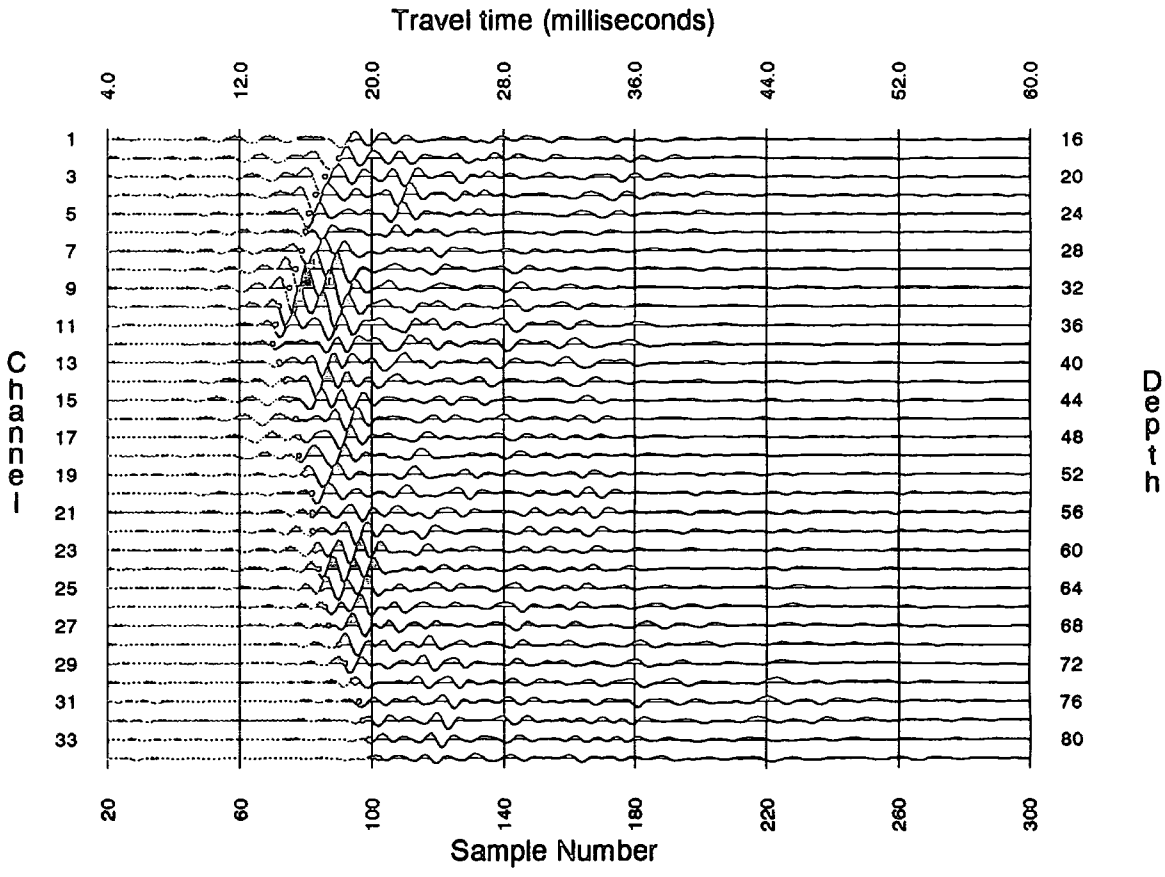

Figure 4.9 Common-shot gather after wavefield separation, with a trace-by-trace waveshaping deconvolution applied.

in the time-direction on all traces, and then in the spatial (depth) direction at all frequencies. This algorithm requires the digital data to consist of $2^m x 2^n$ samples, where m and n are integers.

The impulse response of an *f-k* pass filter is shown in Fig. 4.10. A spike on trace 17, at sample 150, was transformed into the *f-k* domain, and a filter applied to pass all upgoing energy between 2000m/s and 8000m/s, with cosine tapers down to 1500m/s and up to 16000m/s. After transformation back to *z-t* space, it can be seen that the energy has been smeared out over the surrounding traces. This is one reason for very careful design of the two-dimensional filter - the narrower the pie-slice, the more the impulse response is smeared out across adjacent traces. A review of two-dimensional filters is given by March and Bailey (1983).

4.3.4 Two-dimensional filter design

In order to separate the upgoing and downgoing events in crosshole seismic reflection data, it is usually necessary to design the *f-k* filter with steep slopes, so that very little of the reflected P-wave energy is rejected. Before transforming the data into the *f-k* domain, it is necessary to apply a taper to the outermost traces on the common-shot gather, to avoid ringing (Gibb's phenomenon) in the frequency domain caused by discontinuities in the time domain. A simple cosine taper over the outer three traces is sufficient. To keep ringing in the *z-t* domain to a minimum (induced by the steep cutoff slopes), the filter edges are selected to lie along lower amplitude valleys in the data, and a smooth cosine taper is also applied (Fig. 4.11). For an overview of velocity filtering in the *f-k* domain see Christie et al. (1983).

4.3.5 Spatially aliased tube waves in crosshole data

Tube waves are coherent noise events which are very common in crosshole datasets. Tube waves generally have a larger amplitude and lower frequency than body waves and can be thought of as a sort of surface wave (the Stoneley wave) which travels along the interface between the borehole wall and the borehole fluid with an elliptical particle motion. One such tube wave is shown in Fig. 4.12. This tube wave is spatially aliased and so will wrap around in the *f-k* domain due to the periodicity of the discrete Fourier transform. To remove

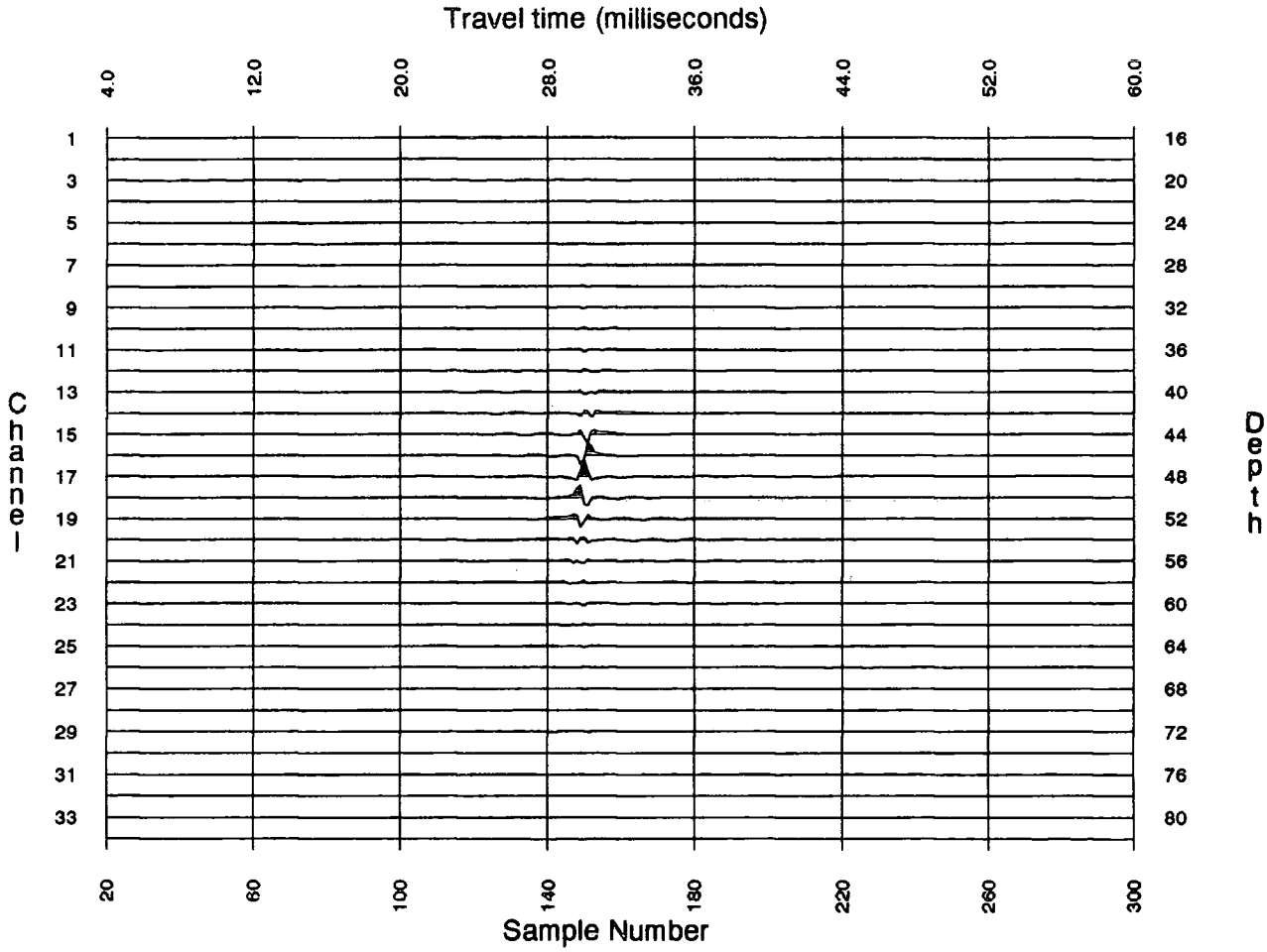

Figure 4.10 Response of an f-k pass filter applied to a record containing only a spike at sample number 150 on trace 17.

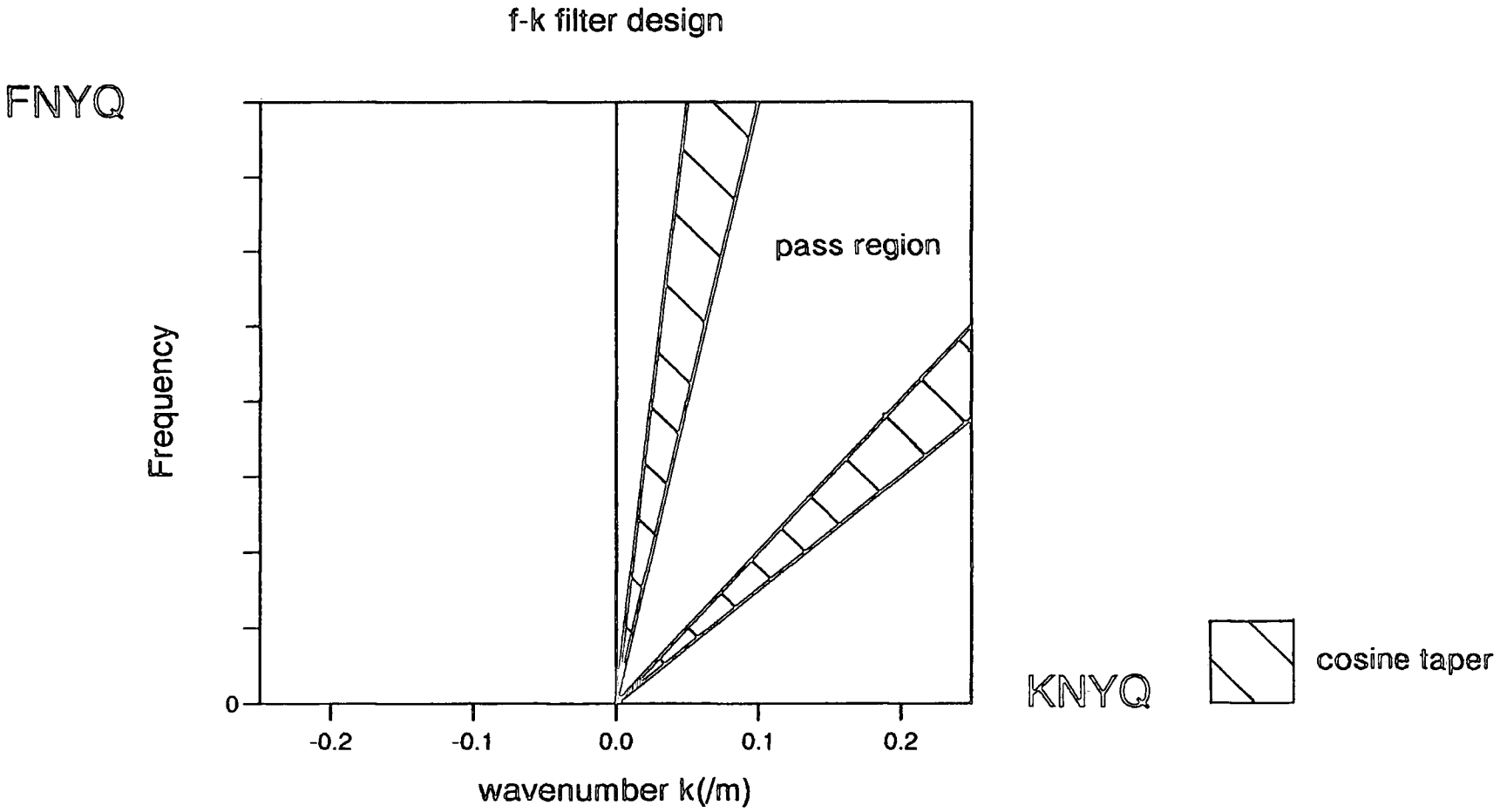

Figure 4.11 Two-dimensional f-k filter implementation.

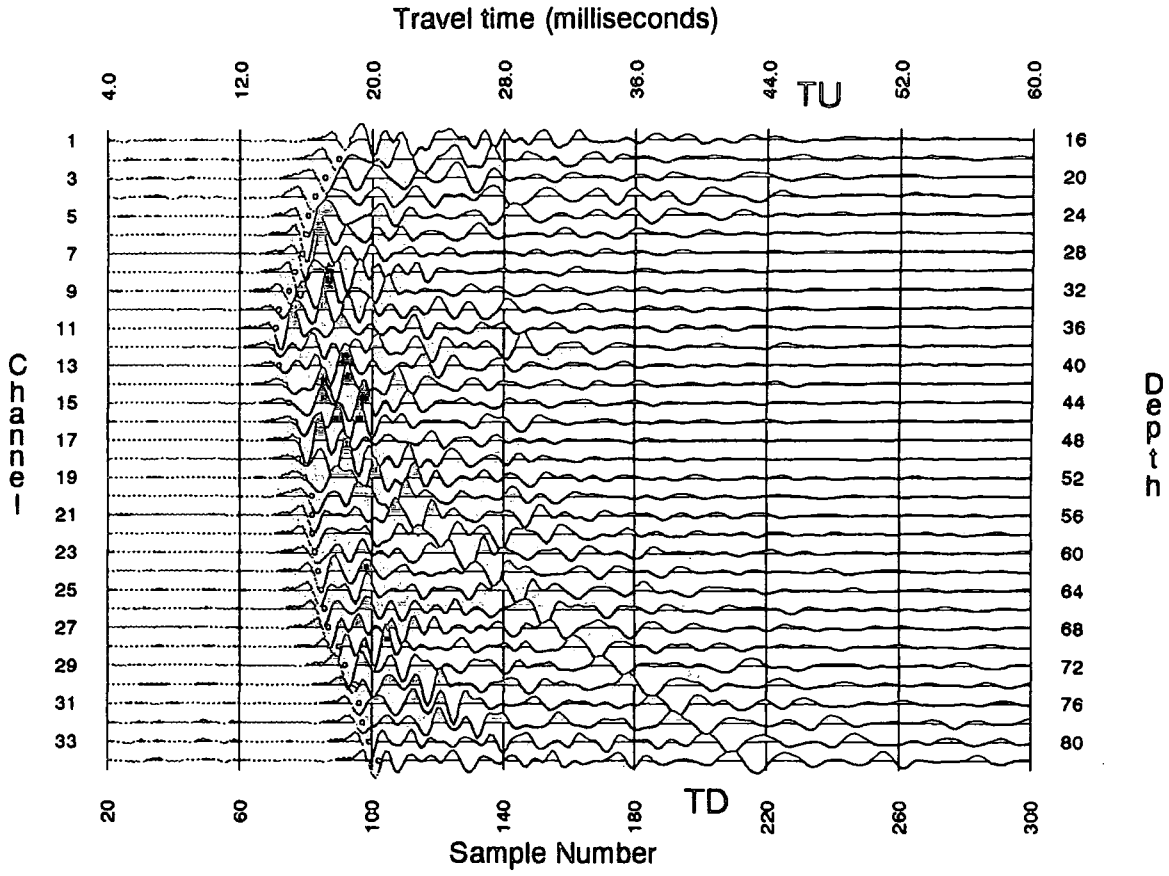

Figure 4.12 An example of tube-waves in crosshole data; upgoing and downgoing tube-wave events are labelled TU and TD respectively.

this it is necessary to apply a rejection filter which will itself wrap around in the *f-k* domain. This type of filter will also remove reflected P-wave energy from the data in the quadrant in *f-k* space into which it wraps round, which may lead to a reduction in the amount of information in the data. Fortunately this was not found to be a serious problem.

4.3.6 Examples of wavefield separation in the f-k domain

The common-shot record shown in Fig. 4.12 contains severely aliased tube waves, upgoing and downgoing reflected energy and direct arrivals. The *f-k* amplitude spectrum of these data is shown in Fig. 4.13. Dominant features of this spectrum include: large amplitude direct wave arrival amplitudes either side of the *k=0* axis and the large amplitude aliased tube wave energy which wraps around the whole of the spectrum.

To reject the tube wave energy, a filter is applied with parallel edges that wraps around from one quadrant to the other, as shown in Fig. 4.14. The tube wave has an apparent velocity of between 1200m/s and 1400m/s. Fig 4.15 shows this data after filtering and transformation back from *f-k* space to *z-t* space. Most of the aliased tube wave has been removed by the application of this filter.

After further filtering to pass all upgoing events that travel with an apparent velocity of between 2000m/s and 8000m/s across the receiver array, the *f-k* spectrum is shown in Fig. 4.16. After transformation back to *z-t* space, it can be seen that the upgoing energy has been enhanced, and most of the downgoing energy has been removed (Fig. 4.17). Similarly, a filter can be applied in the negative *k*-space to separate the downgoing energy. The *f-k* amplitude spectrum after application of this filter is shown in Fig. 4.18, with the results after transformation back to *z-t* space in Fig. 4.19. Any remaining direct wave arrival energy can be muted out in *z-t* space after filtering in *f-k* space, if required.

4.4 Velocity field estimation for migration of the data

To estimate the velocity field for an efficient migration, one can use tomographic methods, traveltime information from uphole shots or velocities obtained from the traveltimes of horizontal raypaths. At Lostrigg, uphole

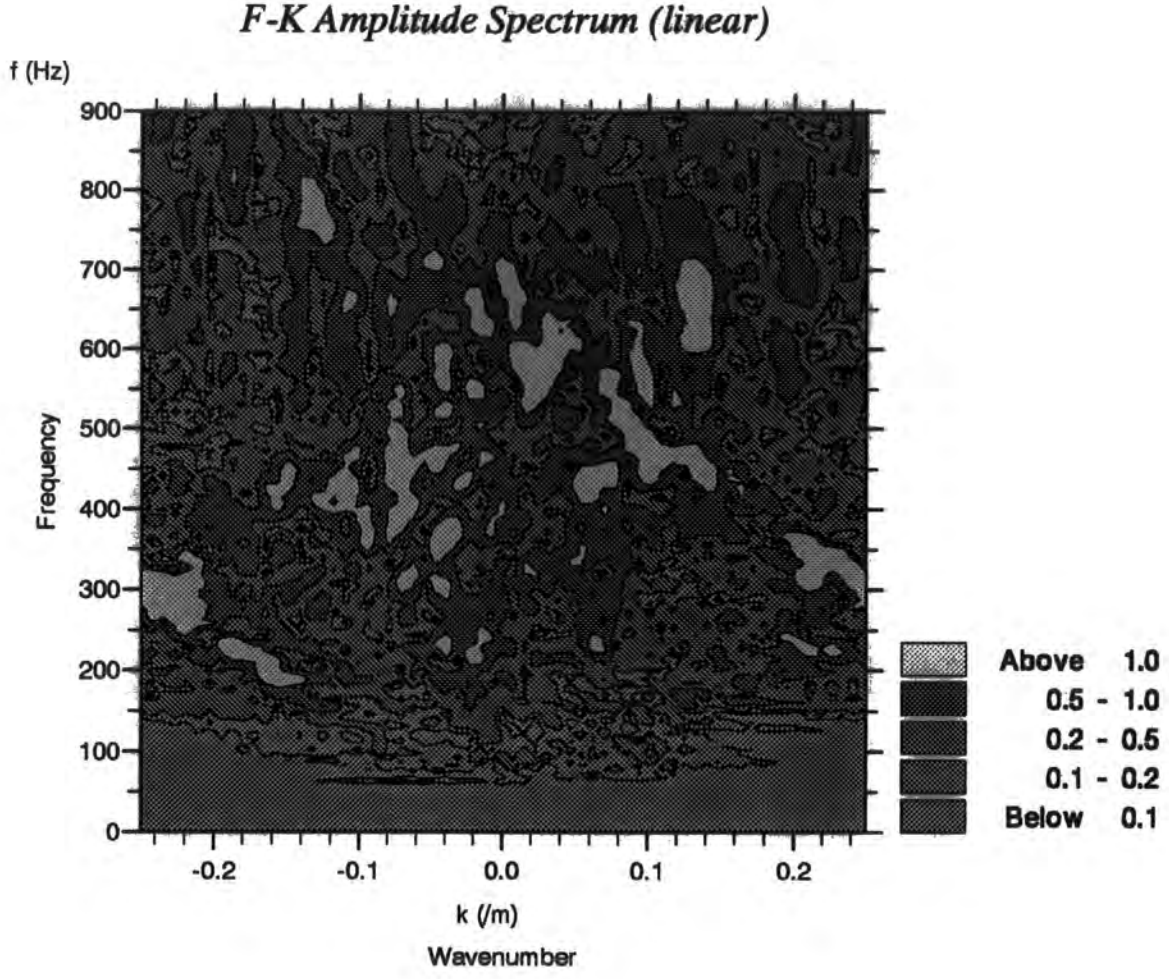

Figure 4.13 Amplitude spectrum of the data shown in Fig. 4.12.

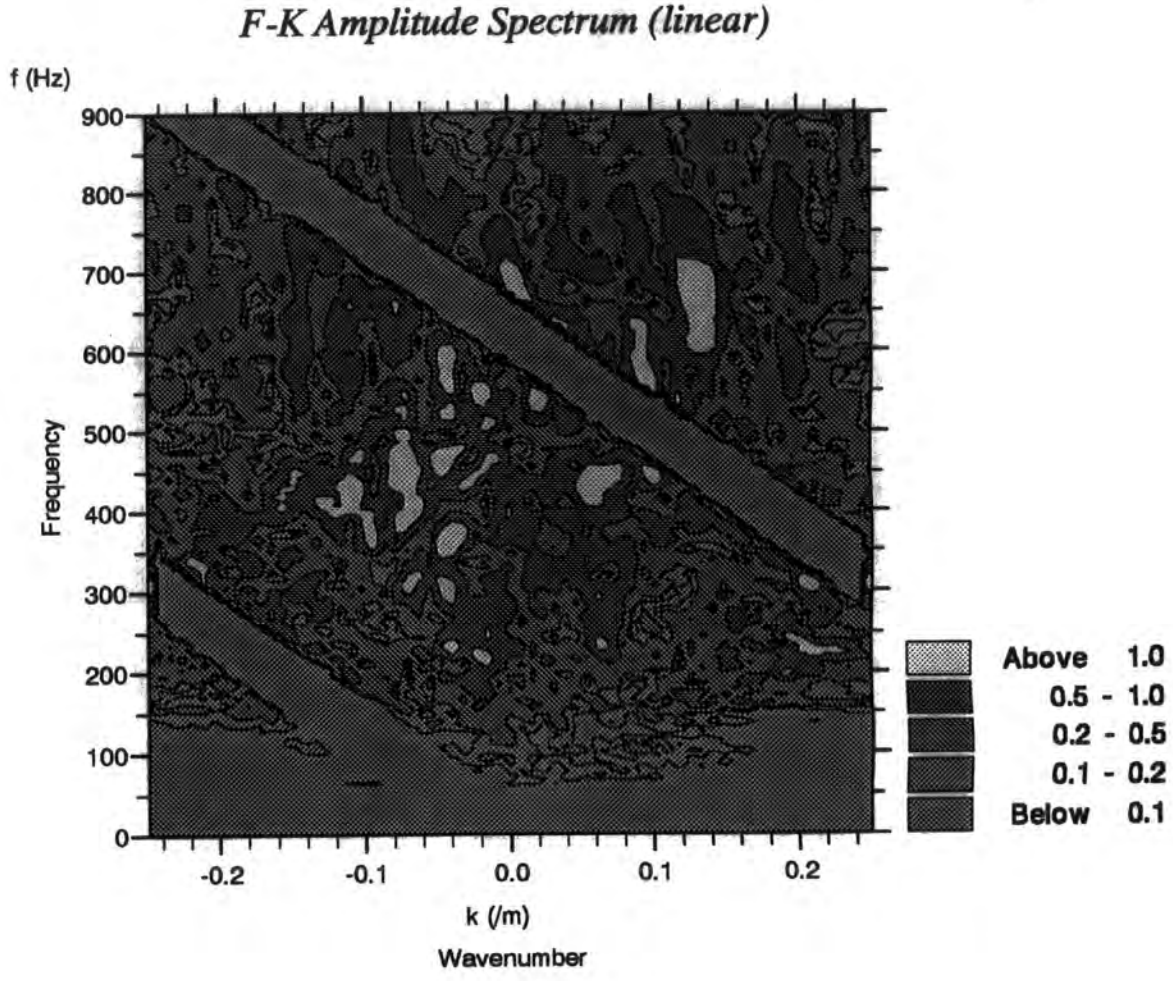

Figure 4.14 Application of an f-k filter to remove tube-wave energy.

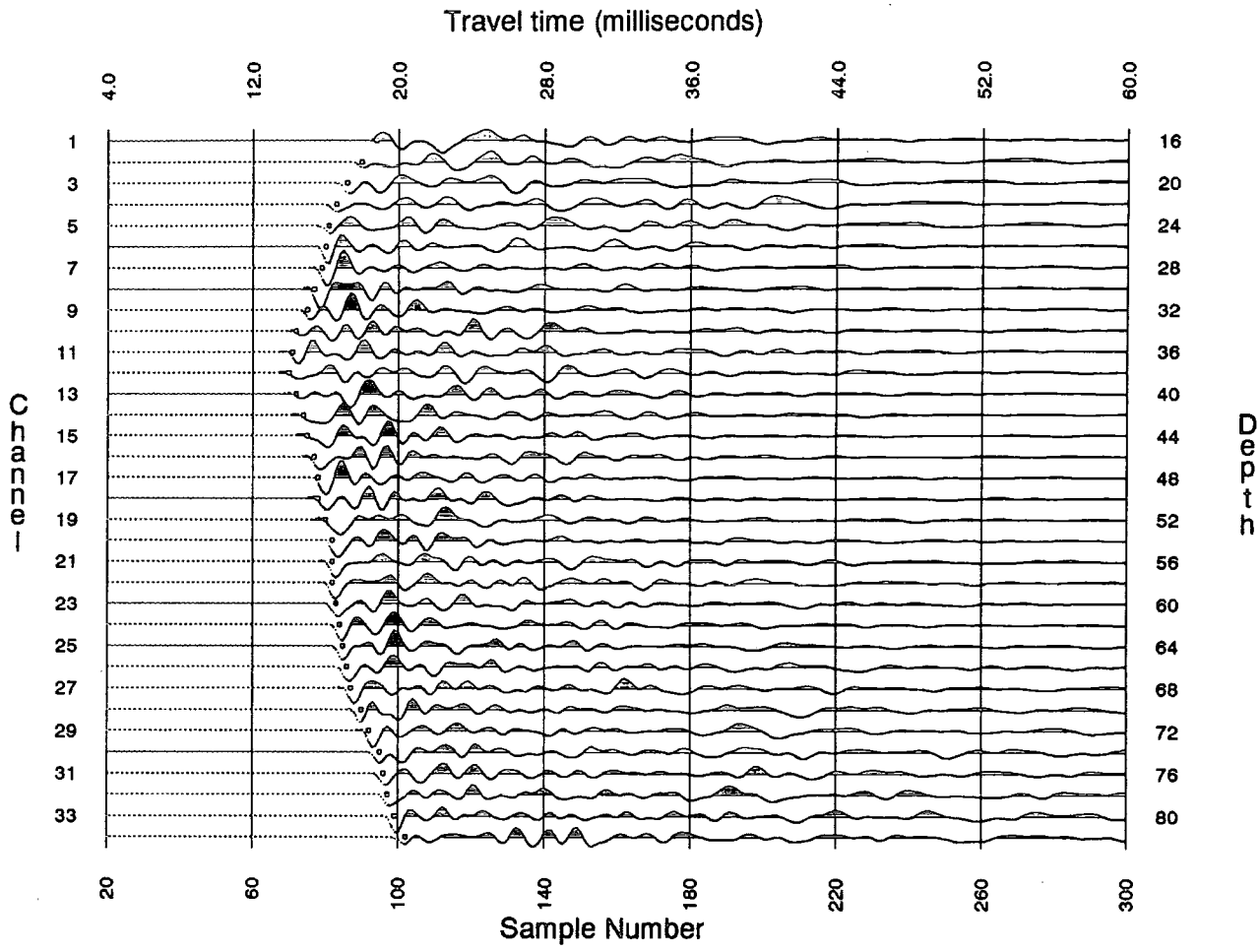

Figure 4.15 Common-shot gather after the application of a reject filter to remove tube-wave energy.

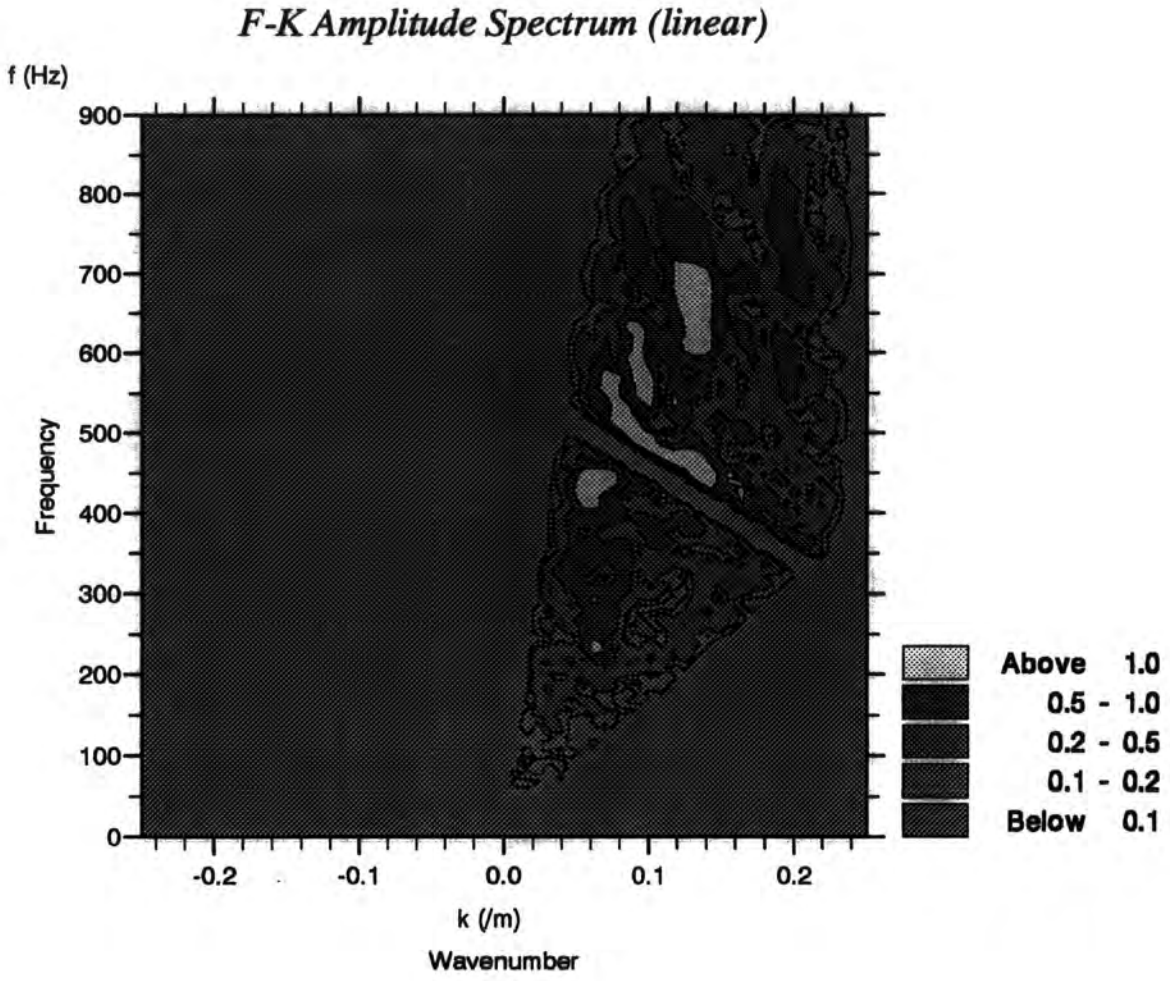

Figure 4.16 Application of an f-k filter to extract the upgoing wavefield from the data.

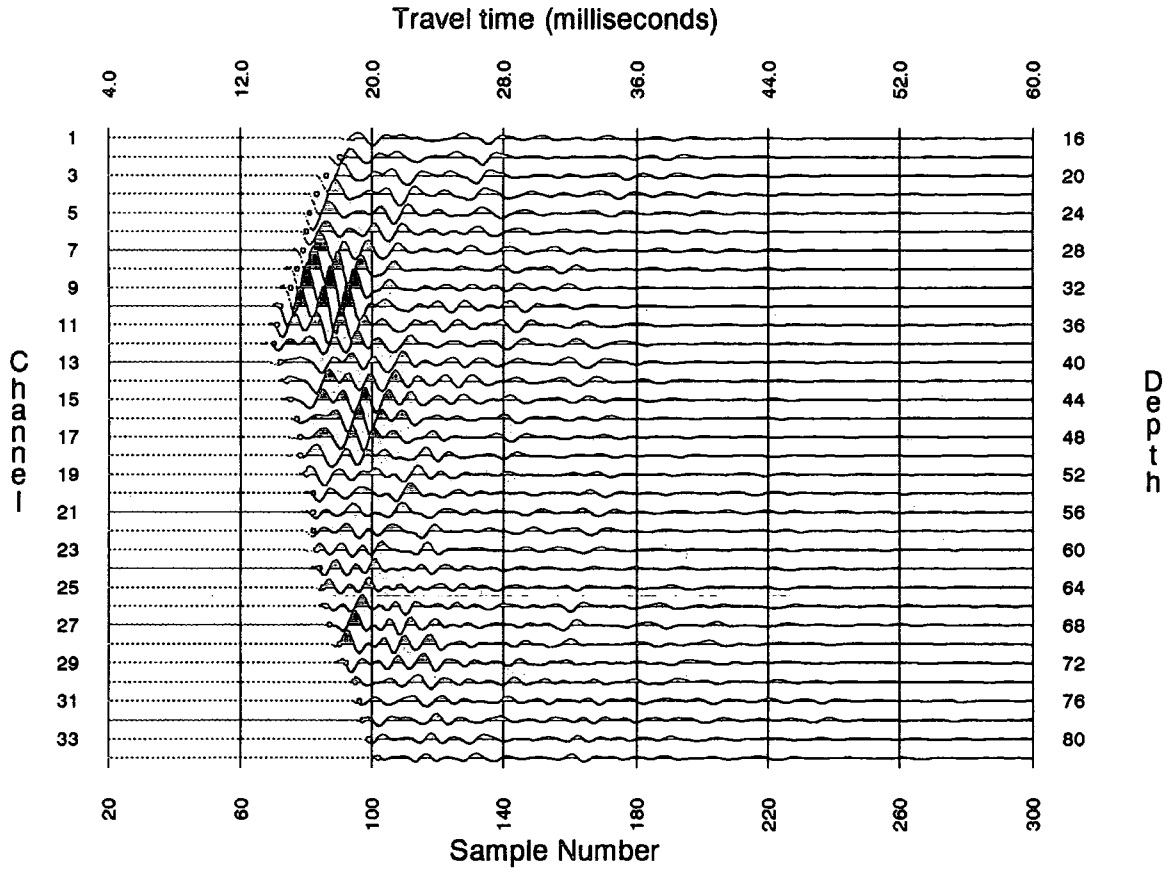

Figure 4.17 Common-shot gather after application of an f-k filter to separate the upgoing wavefield.

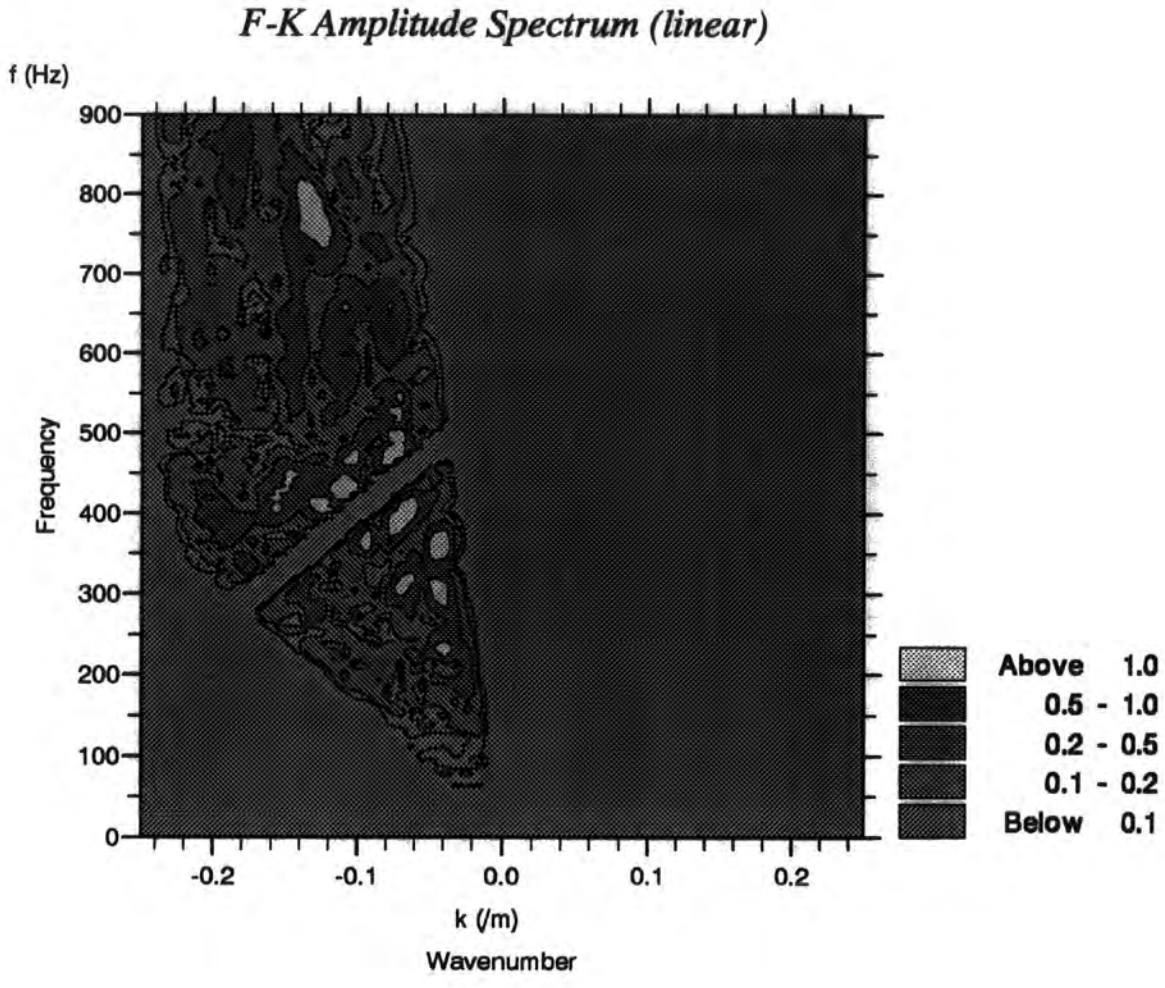

Figure 4.18 Application of an f-k filter to extract the downgoing wavefield from the data.

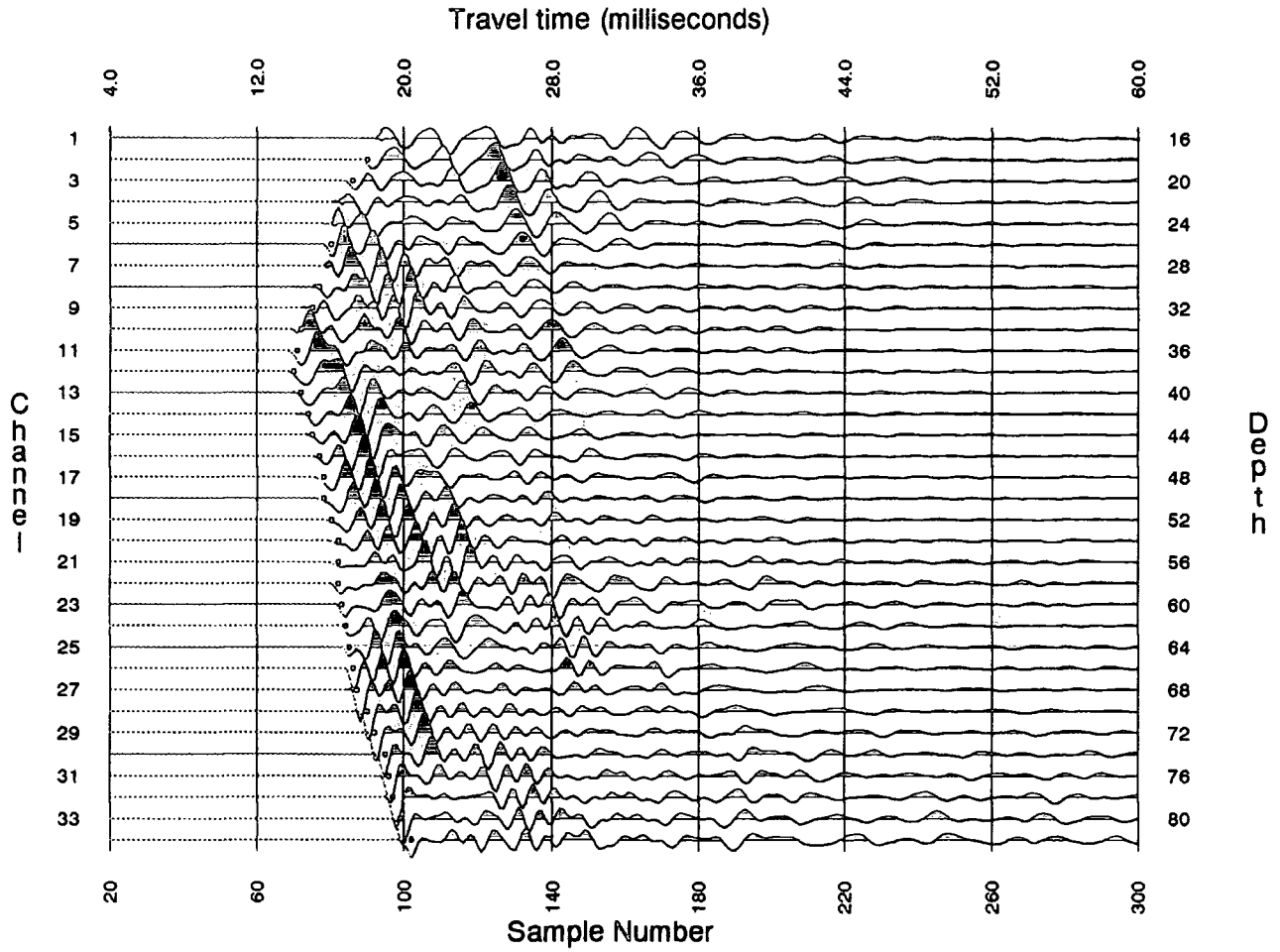

Figure 4.19 Common-shot gather after application of an f-k filter to separate the downgoing wavefield.

surveys were shot by placing the receiver array at different levels in one borehole and firing a shot placed 2m below the bottom hydrophone; this was repeated until the whole available length of the borehole up to the water table had been covered. A sampling interval of 100μsec was used to enable more accurate picking of direct wave traveltimes. From the direct arrival information, the velocities up the borehole can be determined. The tomographic method is severely limited by the lack of vertical raypaths in a typical crosshole reflection survey, and artifacts in the final images produce large errors in velocity estimation. Velocity models were obtained from uphole surveys and by using the near-horizontal raypath traveltimes. No lateral velocity variations were assumed, because of the evenly bedded nature of the Coal Measures strata, and also because no data were available to justify including them. Investigation of the arrival times of reflection events and times actually imaged in the migration, for different shots, revealed anisotropy of 10-15% in the velocity field. This is discussed fully in Chapter V.

4.5 Migration of the crosshole data

On migration of seismic data, reflection events are relocated to their true subsurface positions and diffraction events are collapsed toward a point. Surface seismic data are generally migrated post-stack, with stacked data assumed to be the equivalent of a zero-offset (i.e. coincident sources and receivers) section. Pre-stack migration may be used to improve imaging where there are lateral velocity variations. Computationally, this is an expensive procedure because the data volume is much greater before stacking than after stacking, and the amount of CPU time used will therefore be much larger. With crosshole surveys it is impossible to perform the equivalent operations of velocity analysis, NMO correction and stack to unmigrated data, as for surface seismic reflection surveys, because the source and receiver arrays are not collinear. Fortunately, the data volume is relatively small and so pre-stack depth migration methods can be more readily applied. The two-dimensional migration scheme used in this work is based on the Kirchhoff integral. The implementation used here is specifically for crosshole geometries, but the method is able to cope with VSP and surface seismic data. In fact the operations of prestack migration and stack are carried out in the same pass, although it is possible to obtain migrated images of single common-shot, or common-receiver, gathers, if required.

4.6 Kirchhoff migration

This method is an extension of the diffraction stack migration approach. The algorithm was coded up and tested extensively by Findlay (1991), as was the finite-difference approach. The Generalized Kirchhoff algorithm was adopted on the criterion that it is faster than the other, finite difference, method and there is also more control over final image quality by the use of imaging apertures.

4.6.1 Diffraction stack migration

The diffraction stack migration method was one of the first types of migration to be applied to seismic data. It follows simple ray and wavefront theory. For zero-offset (or post-stack) surface seismic data, diffraction stack migration is implemented by summing along hyperbolic trajectories and placing the results at the apices of the hyperbolas. However, for crosshole data, the summation operator takes on a more complicated form. If we consider a particular source-receiver combination with a single impulsive arrival recorded at time *Ts* and assume that the velocity of the medium is uniform and isotropic, then, for a particular traveltime, the locus of possible reflection points (the isochron) must be an ellipse in image space as shown in Fig. 4.20, with the source and receiver at the focal points. The data may be migrated if the recorded amplitudes in each trace are distributed along the appropriate ellipses for each digital time sample.

Another way of approaching this problem is to consider each image point in turn. If raytracing is performed between the source position and the image point and between the receiver position and the image point, then the amplitude corresponding to the total traveltime from source to image point to receiver is may be assigned to that image point together with similar contributions from other source-receiver pairings.

4.6.2 The Kirchhoff operator

Kirchhoff wave equation migration is an extension of the diffraction stack imaging concept based upon Kirchhoff's integral (French, 1975; Schneider,

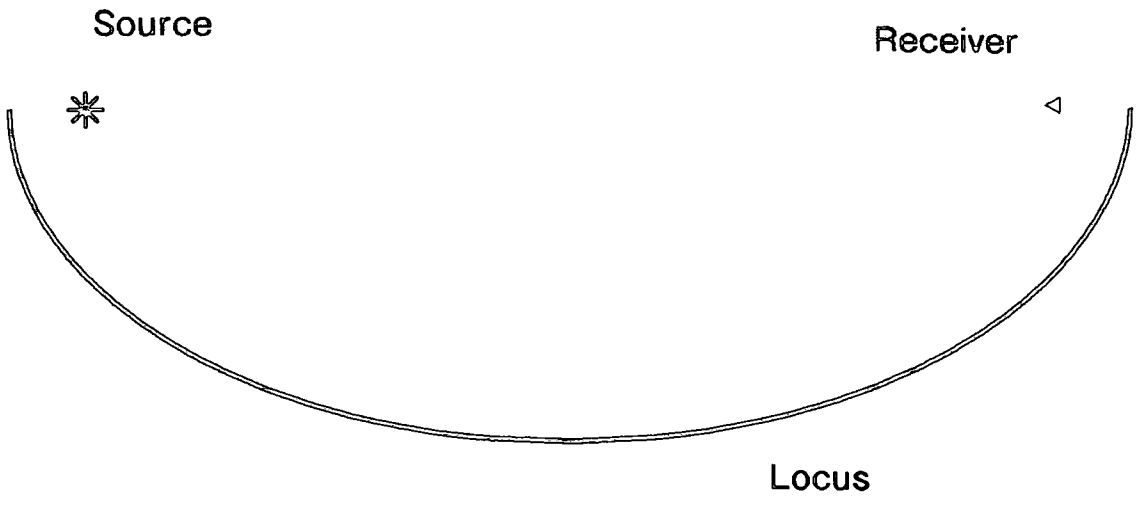

Figure 4.20 Locus of possible reflection point locations for an impulsive arrival at time T for a particular source and receiver combination.

1978). If we consider a wave incident on a scattering interface, then $U(\mathbb{r},\mathbb{s},t)$ is the wavefield recorded at $\mathbb{r}$ due to energy from an impulsive source $\delta(t)$ at $\mathbb{s}$ being scattered from the surface S_x, given by Dillon(1990 equation (1)):

$$U(\mathbb{r},\mathbb{s},t) = \int_{S_x} dS_x \frac{C(x,\phi_x)}{4\pi V} \frac{cos(\phi_s) + cos(\phi_r)}{R_s R_r} \delta'(t - (R_s + R_r)/V) \qquad (4.1)$$

The angles of incidence and scattering, ϕ_s and ϕ_r respectively, and raypath lengths R_s and R_r are illustrated in Fig. 4.21. The reflectivity $C(x,\phi_s)$ is angle-dependent. Equation (4.1) is the three-dimensional response recorded at a receiver. If one assumes that the geological structure is invariant perpendicular to the plane of the survey, then by integrating along one direction, the equivalent 2.5D formula is obtained. Dillon (1990) has derived a 2.5D migration integral, for data acquired with a point source and with compensation for spherical divergence included, which yields the reflectivity $C(\mathbb{x})$

$$C(\mathbb{x}) = \frac{1}{\pi} \int_{L_r} dL_r \sqrt{\frac{R_s(R_s + R_r)}{2VR_r}} cos(\theta_r)\, M(\mathbb{r},(R_s + R_r)/V) \qquad (4.2)$$

where $M(\mathbb{r},T)$ is the source wavefield $U(\mathbb{r},T)$ cross-correlated with a half-differentiator. This filter has a spectrum with a $\pi/4$ phase shift and a high frequency amplitude boost of $f^{1/2}$ and is implemented in the frequency domain. For sampled data, equation (4.2) may be approximated by a summation over the receiver array L_r, giving

$$C(\mathbb{x}) = \sum \Delta L_r \sqrt{\frac{R_s}{R_r}} cos(\theta_r) \sqrt{R_s + R_r}\, M(\mathbb{r},(R_s + R_r)/V)$$

(4.3)

where ΔL_r is the geophone separation and scalar factors have been omitted.

This equation (4.3) is similar to a diffraction stack with the amplitude and phase corrections making the migration consistent with the wave equation

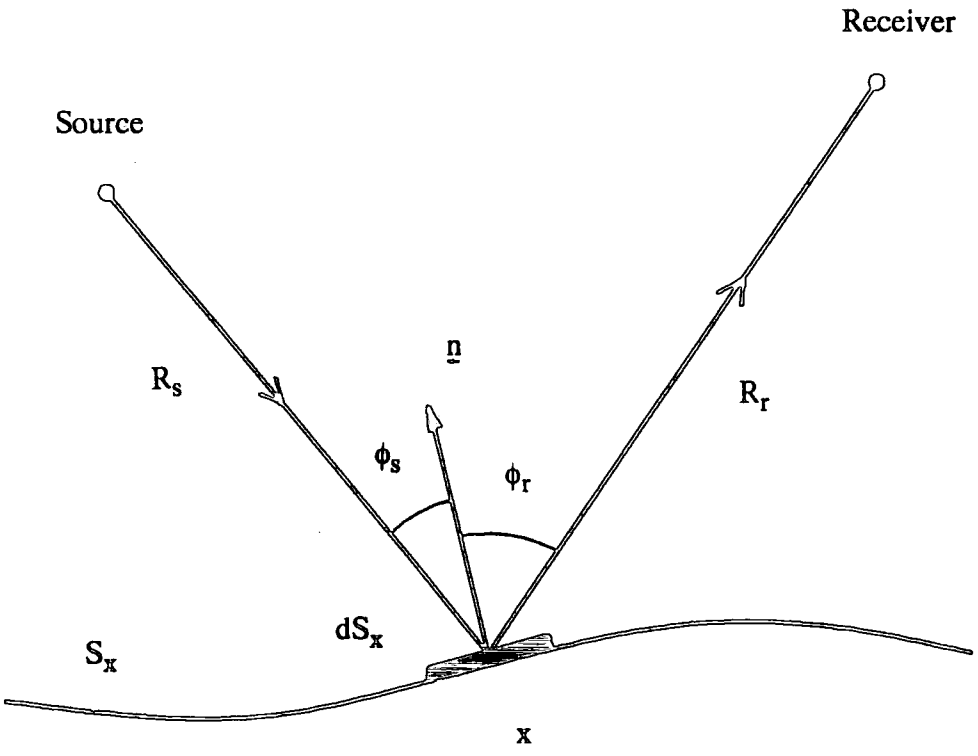

Figure 4.21 Angles and raypaths for equation 4.1.

(Newman, 1990; Larner & Hatton, 1990) and a wavefront spreading correction term being incorporated. The Kirchhoff algorithm considers just one array, in this case the receiver array, which is not in agreement with reciprocity. For crosshole geometries we should obtain similar reflectivity responses across the survey, whereas using equation (4.3) the reflectivity image amplitudes will be larger nearer the receiver borehole, as $R_s > R_r$. Dillon (1990) conducted tests with synthetic data and showed this to be the case in the migrated images. However, the principle of Kirchhoff migration can be extended to handle both arrays (Dillon, 1990 Appendix A) and is referred to as generalized Kirchhoff migration. This is closely related to the Generalised Radon Transform (GRT) migration integral presented by Miller et al. (1987). The 2D Generalized-Kirchhoff migration operator is given by

$$C(\mathbb{x}) = \sum \left[\Delta L_r \sqrt{\frac{R_s}{R_r}} cos(\theta_r) + \Delta L_s \sqrt{\frac{R_r}{R_s}} cos(\theta_s) \right] x M(\mathbb{r}, (R_s + R_r)/V) \qquad (4.4)$$

Migration is performed by summation over source and geophone arrays simultaneously. There is an additional small error term associated with $C(\mathbb{x})$, which is proportional to ($cos(\theta_s)$ - $cos(\theta_r)$), which is small if the zone of illumination extends beyond a few wavelengths from $\mathbb{x}$ and the source and receiver array are extensive enough to capture most of the scattered energy. Therefore a well illuminated part of the subsurface should be correctly imaged.

This algorithm was implemented by Findlay (1991), and used for the migration of all the crosshole seismic data from the Coal Measures. Some options available include restricting the summation locus spatially to realistic geological dips, and restricting the maximum angle raypaths can make with the vertical at each image point. The algorithm was tested extensively by Findlay (1991) and various migration operators were also examined.

Chapter V

Crosshole seismic reflection data in shallow Coal Measures strata

5.1 Introduction

Two surveys were acquired at a British Coal opencast exploration site at Lostrigg, Cumbria (see Fig. 5.1 for location). The results from processing these using the methods detailed in Chapter IV are discussed in this chapter. The boreholes used for the acquisition of the data were four of a long line of boreholes spaced at approximately 15m intervals, running SW-NE. The aim of these surveys was to image and accurately locate the position of the site boundary fault.

5.2 Survey 1; boreholes H and L

The two boreholes, H and L in Fig. 5.2, were open to over 100m depth, and 29 source positions were used, at 2m intervals, from 16m to 72m depth in borehole H (see Fig. 5.3). Single electrical detonators were used as sources. The water table was at a depth of 13m. Three levels of the 12-channel hydrophone string were used to give 34 receivers at 2m intervals from 16m to 82m depth in borehole L. Not all of the shots were fired into the total length of the hydrophone string; the first 11 shots (16-36m) were fired into the 23 uppermost hydrophones; shots 12 to 23 (38-60m) were fired into all 34 hydrophones; and shots 24 to 29 (62-72m) were fired into the lower 23 hydrophones. The Close End Fault, with a throw of 220m to the west, crosses the upper half of the survey. The total borehole separation was 57.28m. The principal coal seams in the area are the Harrington at 72m depth, 1.4m thick, and the Udale at about 91m depth, 0.3m thick. There are other coal seams present, most of them between 0.1 and 0.3m thick (see Fig.

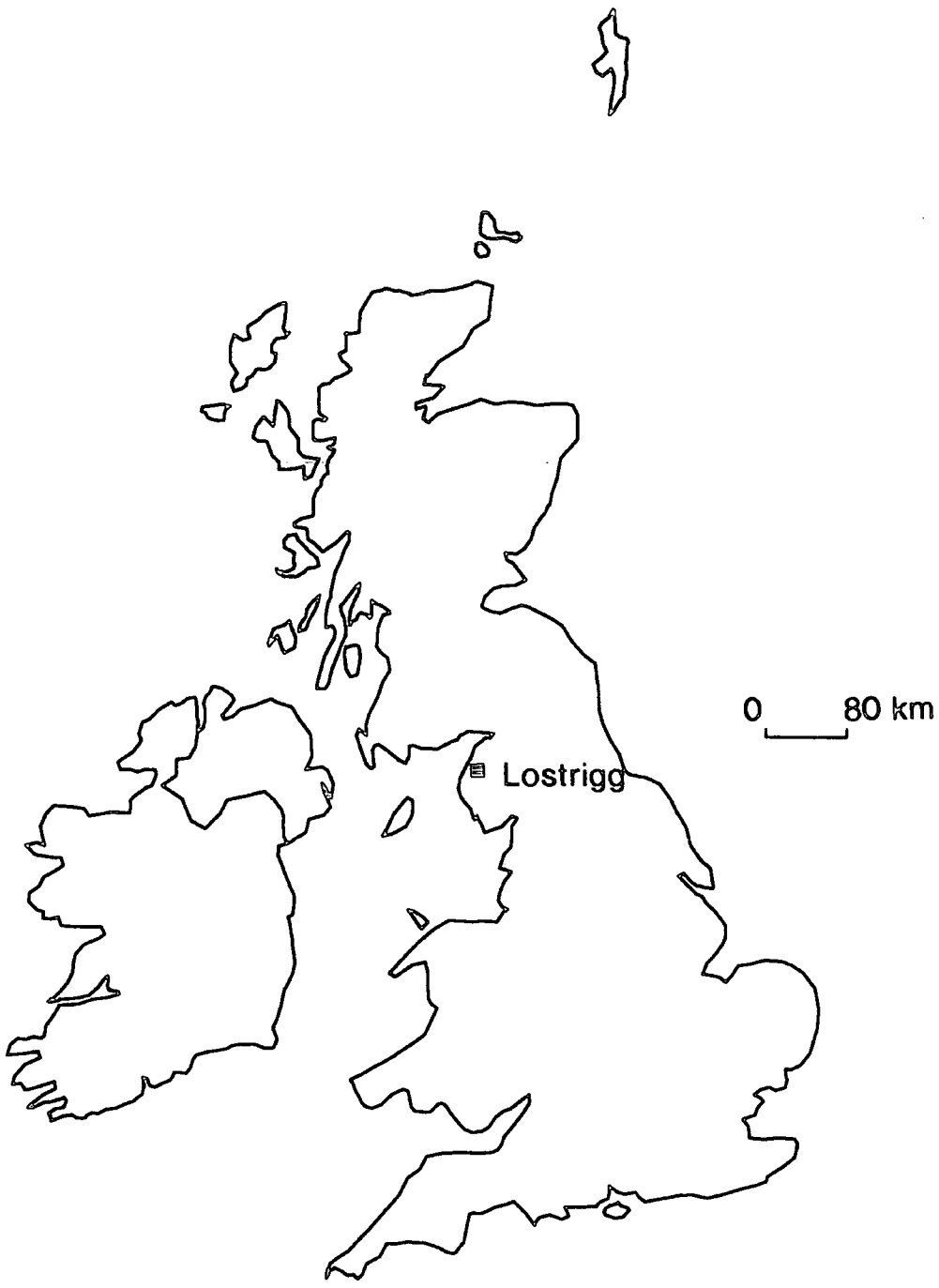

Figure 5.1 Sketch map of the United Kingdom showing the site at which the surveys were obtained.

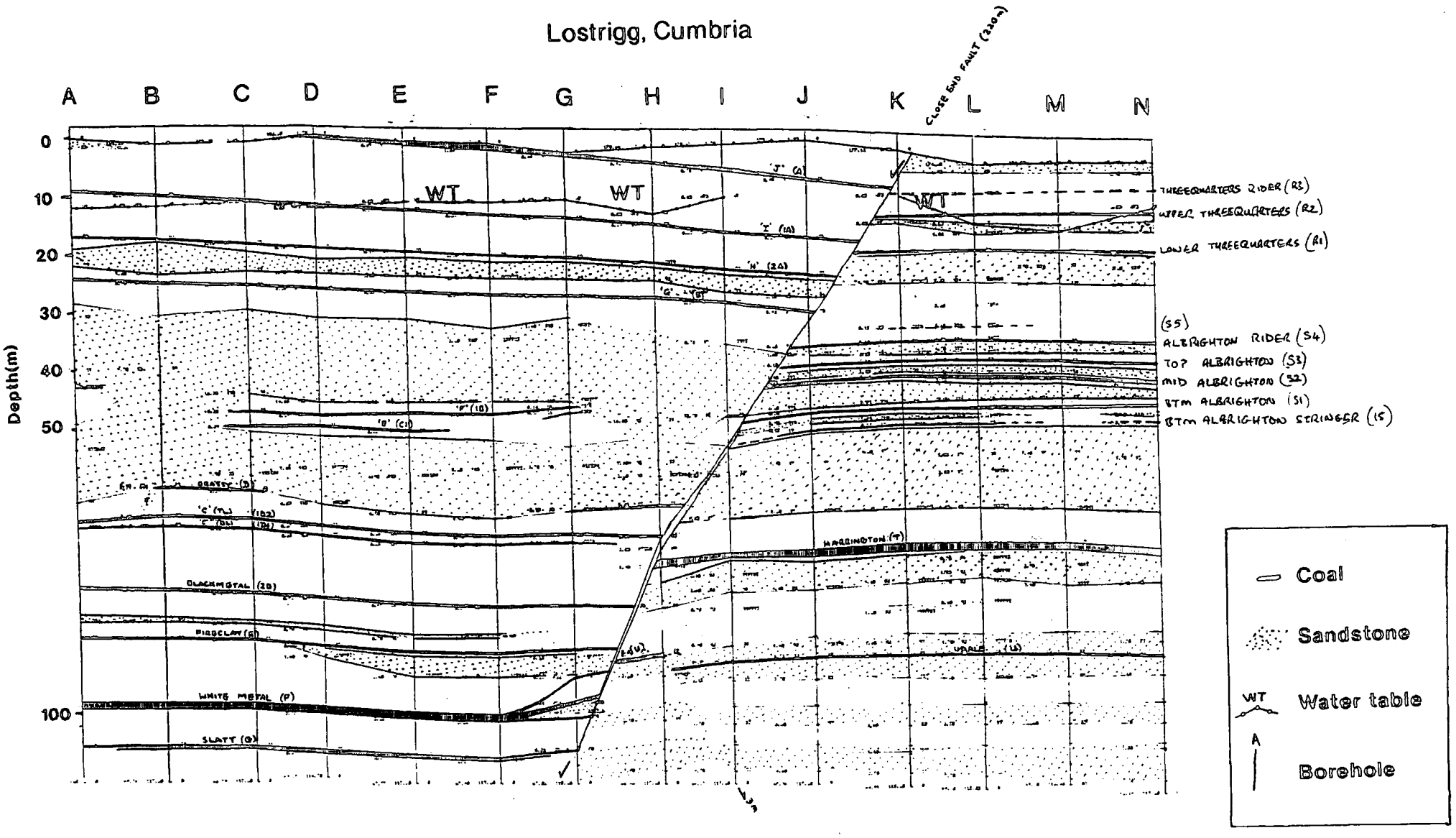

Figure 5.2 Interpreted cross-section using the borehole information from all boreholes A to N at Lostrigg.

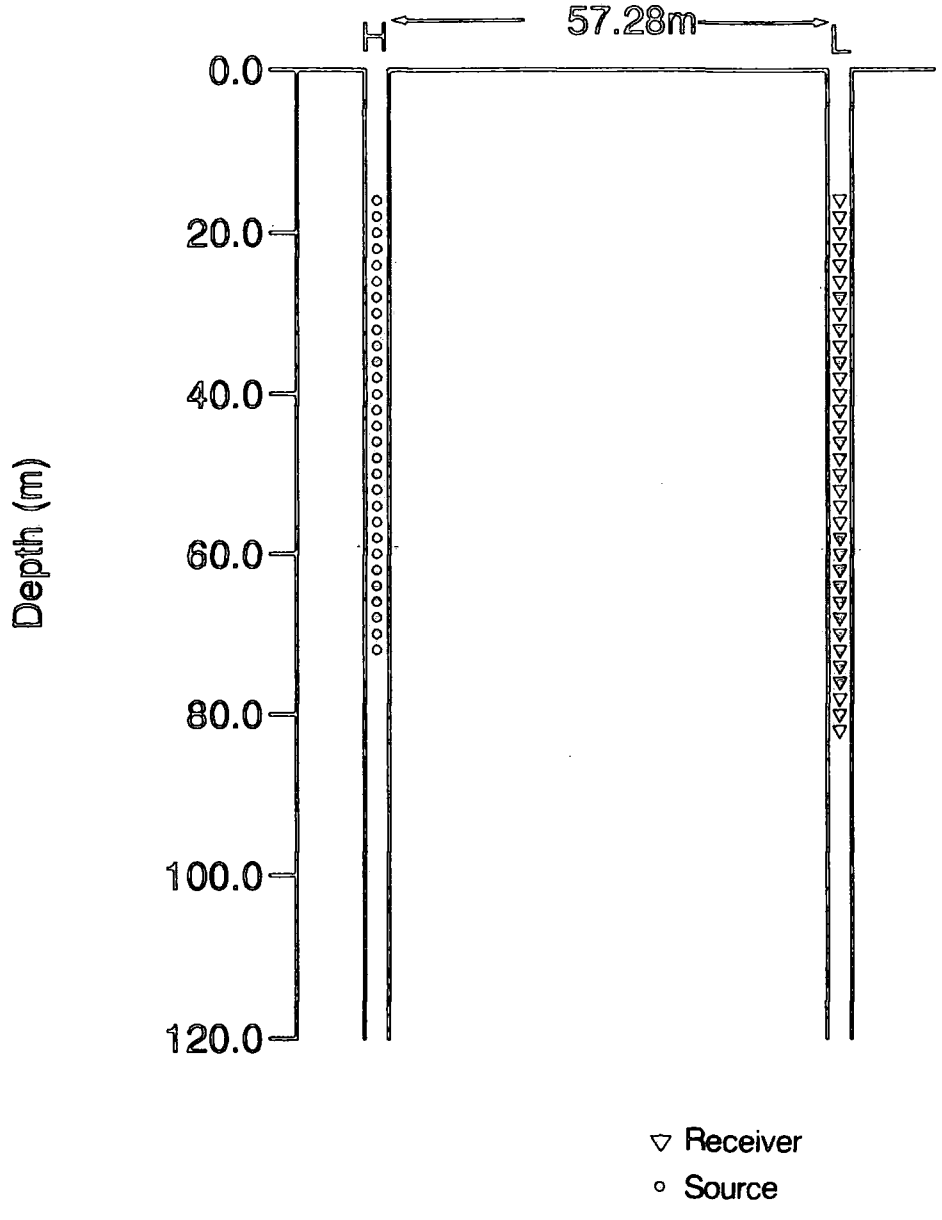

Figure 5.3 Source and receiver positions for the boreholes used in survey 1.

5.2). The strata dip toward the fault from borehole L to borehole H, but at a very shallow angle (less than 2°).

5.2.1 Borehole verticality analysis

Verticality data were available for both boreholes used in this survey, provided by British Coal and acquired when the boreholes were geophysically logged by the logging contractor. These were used to calculate borehole deviations so that the true spatial distribution of source and receivers could be calculated, which is essential for the migration of the data. All deviations were calculated to lie in the plane of the two boreholes.

Borehole deviations in the plane of the survey were small for survey 1 (up to 1.84m for receiver positions in borehole L, towards borehole H; negligible for the sources in borehole H), but included for completeness. Borehole deviation charts are shown in Fig 5.4 for boreholes H and L. The solid circles on the deviation tracks mark every 20m logged, and logging commenced at 10m depth.

5.2.2 Data processing

The full processing sequence used in this survey is as detailed below:

- Normalization to RMS energy over a window 60-100ms
- Waveshaping deconvolution
- *f-k* wavefield separation
- Muting up to the first break, and muting of residual direct wave energy

The data also contained both upgoing and downgoing tube wave energy, which was heavily aliased (spatially). This required careful muting out using a reject filter in the *f-k* domain, although some remnants of the tube wave energy remain in the data after processing. These data were migrated using the Generalized-Kirchhoff algorithm, with a dip aperture of ±22.5°. The velocity field used for the migration, obtained from uphole measurements and examination of the traveltimes of horizontal raypaths, is shown in Table 5.1. The velocities used were also adjusted by examining

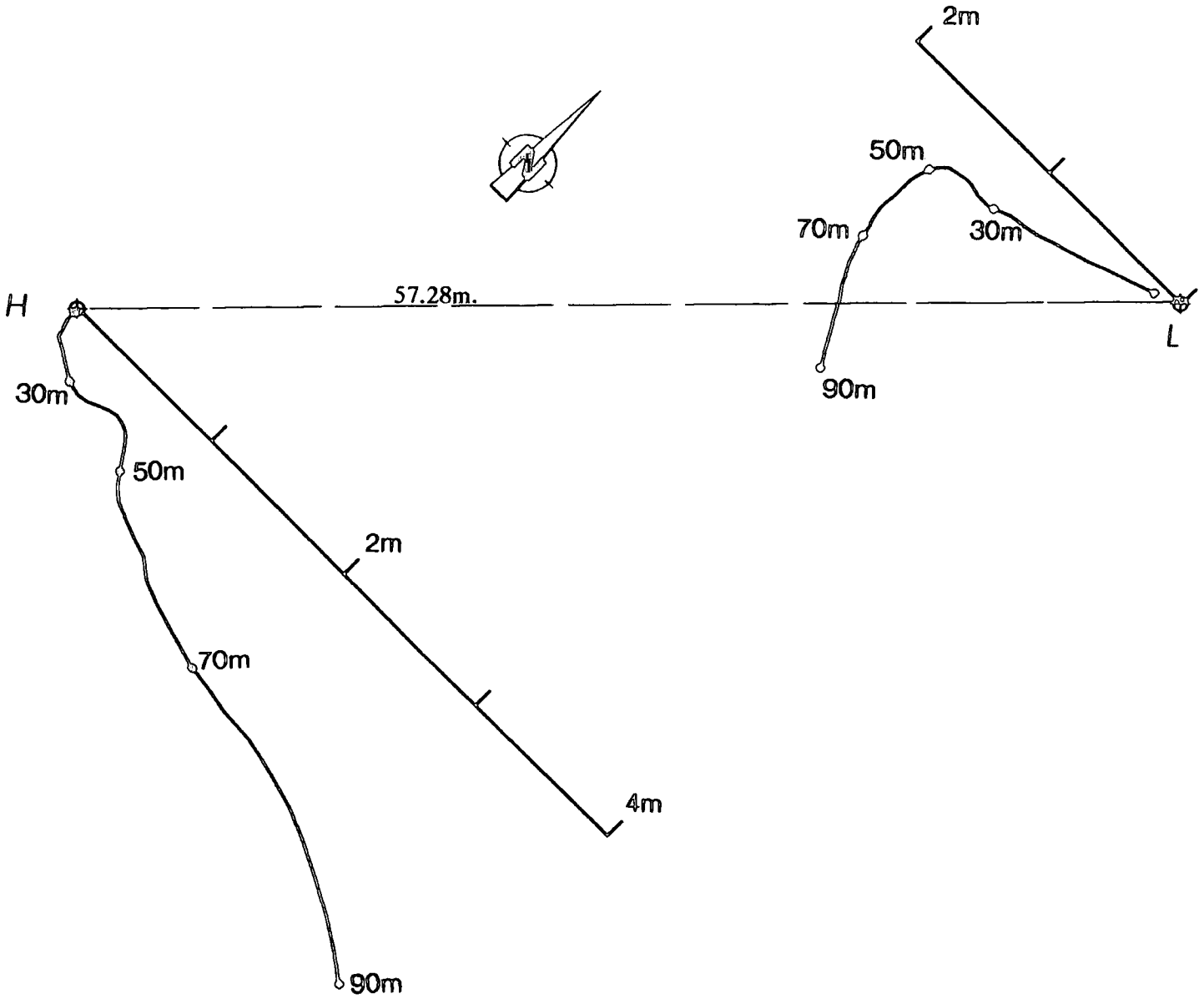

Figure 5.4 Borehole deviation for the boreholes H and L at Lostrigg. The dots mark every 20m of logged depth. Scale bars indicate lateral deviations of the borehole. Borehole separations and track plots have been drawn to different scales.

the traveltimes of the reflected events that could be identified in the data, and the actual portion of each trace that contributed to each image point.

On examination of the values obtained for the horizontal and vertical velocity (Fig. 5.5), it can be seen that there is some degree of anisotropy present in these rocks (in the region of 10-15%). This can be accounted for by adjusting the migration velocities to lie in between the values calculated for the horizontal and vertical velocity fields. Use of an anisotropic velocity field for ray-tracing in the migration made no appreciable improvement on the migrated common-shot gathers.

2200 m/s	0-16m
2480 m/s	16-24m
2700 m/s	24-36m
3020 m/s	36-48m
3350 m/s	48-58m
3740 m/s	58-80m
3800 m/s	80-120m

Table 5.1 Migration velocities for survey 1

5.2.3 Results from Survey 1

Figure 5.2 is the interpreted cross-section using the borehole information in all boreholes at Lostrigg. The major feature on the cross-section is the large fault which surfaces between boreholes K and L, and cuts borehole H at around 74m depth. This fault has a throw of 220m down to the left of the section. A small fault of 3m throw has been interpreted below the Harrington seam, cutting the Udale seam near borehole H at 90m depth. The migrated upgoing wavefield from survey 1 is shown in Fig. 5.6. It is zero-phase and an automatic gain control of 40m has been applied. The traces at the boreholes have been killed because the G-K migration does not image well at the borehole. This depth section, and all subsequent ones, have been plotted with normal SEG polarity (i.e. white troughs correspond to a compressional arrival and black peaks to a dilatational).

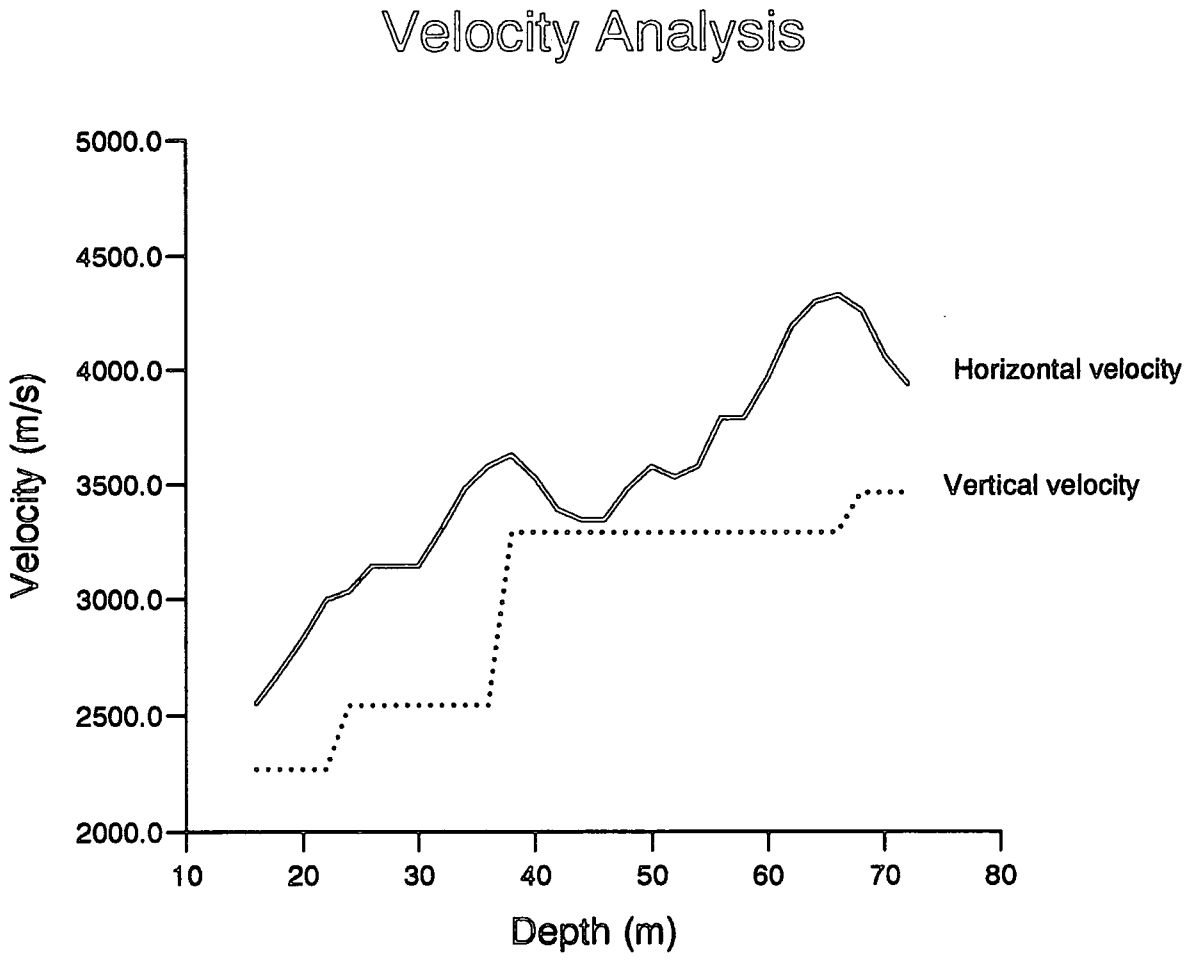

Figure 5.5 Velocities obtained from the uphole survey (vertical) and by estimation from the horizontal direct wave traveltimes (horizontal).

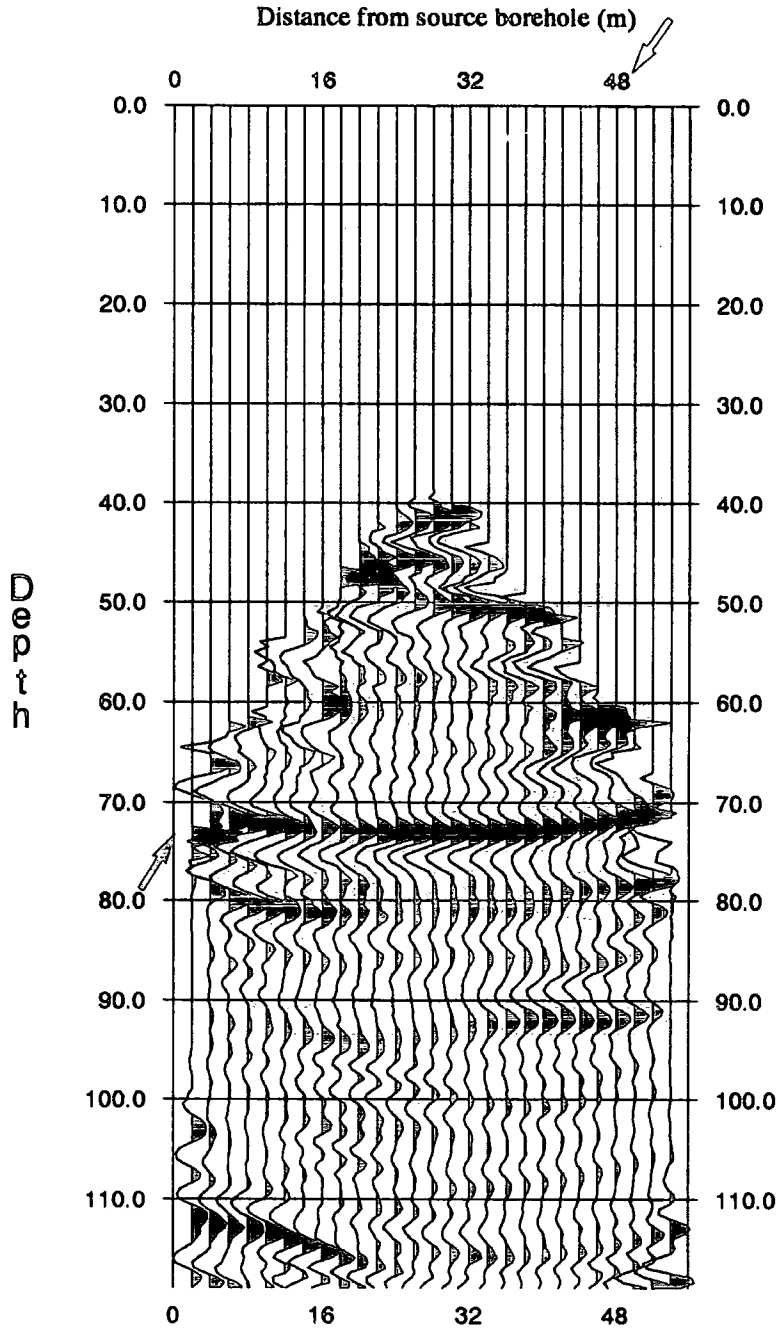

Figure 5.6 Upgoing Generalised-Kirchhoff migrated section for survey 1. An agc of 40m has been applied to this section, and the traces have been tapered off at their onset. The position of the Close End Fault is marked with arrows.

The main feature on this depth section is the Harrington seam at 72m, and a portion of the Udale seam near borehole L. There is some indication of some of the thinner seams between 40m and 54m depth being imaged, but confidence in these is not high. From this section it is impossible to confirm the position of the Close End Fault. There are other events which cannot be tied into the stratigraphy at all, and the origin of these is not clear.

The migrated downgoing wavefield is more disappointing, with nothing being imaged which was interpretable in this survey (Fig. 5.7). The various events observed cannot be correlated with the known stratigraphy. None of the events cross the Close End Fault zone, so they may represent primary reflected energy, but the fault position could not have been located accurately from this section, even knowing the depth value where it cuts borehole H.

An example of common-shot gathers from this dataset is shown in Figure 5.8, after processing. The source depths for these is at (a) 16m and 30m, (b) 46m and 62m. The dots mark the first breaks as picked in the raw data. No muting of direct wave energy has been carried out. As can clearly be seen, there are reflected events in these data, most of which have energy comparable to that of the direct wave, from various depths (the termination of the reflection at the line of first breaks gives an approximate depth of the reflector). But many of these "reflections" have no apparent source from the stratigraphy. One problem that is apparent is that many of these common-shot gathers are very close to being aliased, which may cause some problems in the wavefield separation.

5.2.4 Velocity analysis using CDP gathers

To test that the migration process was stacking up the correct events from each common-shot gather, and common-receiver gather, for the upgoing wavefield, I migrated each one independently. Figure 5.9 shows common depth point (CDP) traces for distances of (a) 8m, (b) 30m and (c) 48m from borehole H. The CDP gathers from migration of the common-shot gathers are shown on the left, and from common-receiver gathers on the right. The depth of the common-shot, or receiver, increases from right to left on each gather, as indicated. The left-hand trace on each panel is the stack of all traces from that gather. From these it can be seen that the event

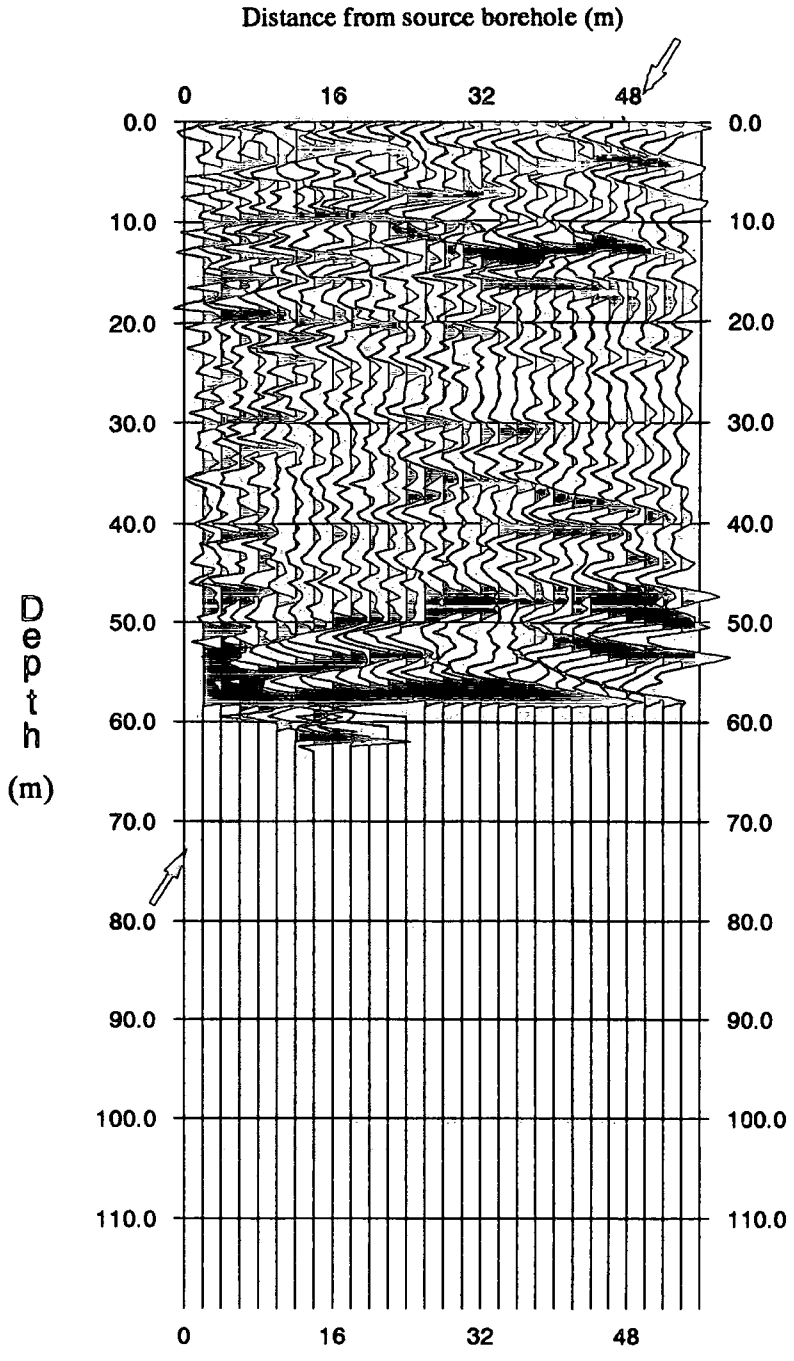

Figure 5.7 Downgoing Generalised-Kirchhoff migrated section for survey 1. An agc of 40m has been applied to this section, and the traces have been tapered off at their onset. The position of the Close End Fault is marked with arrows.

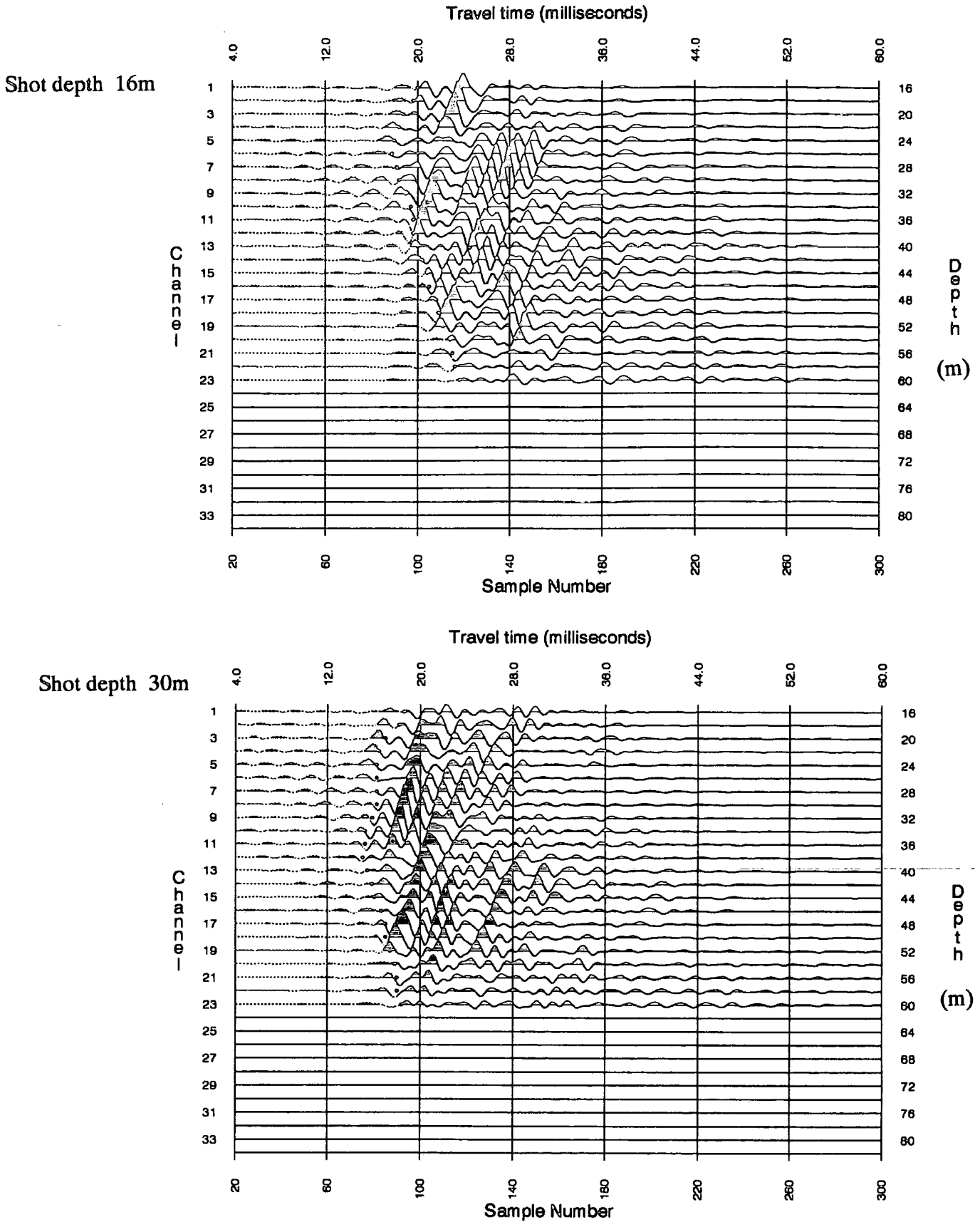

Figure 5.8 (a) Common-shot gathers with shot depths at 16m and 30m.

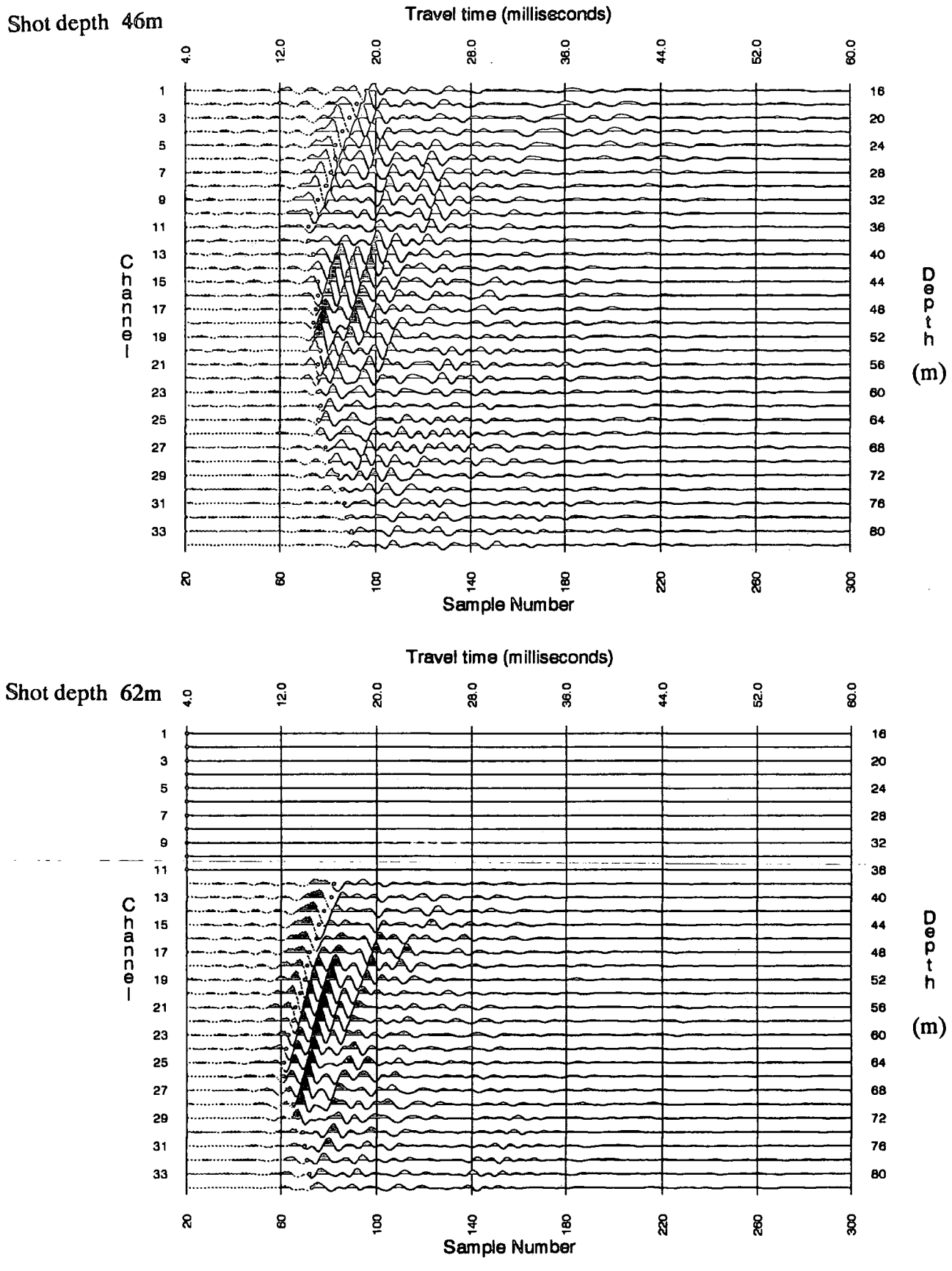

Figure 5.8 (b) Common-shot gathers with shot depths at 46m and 62m.

(a)

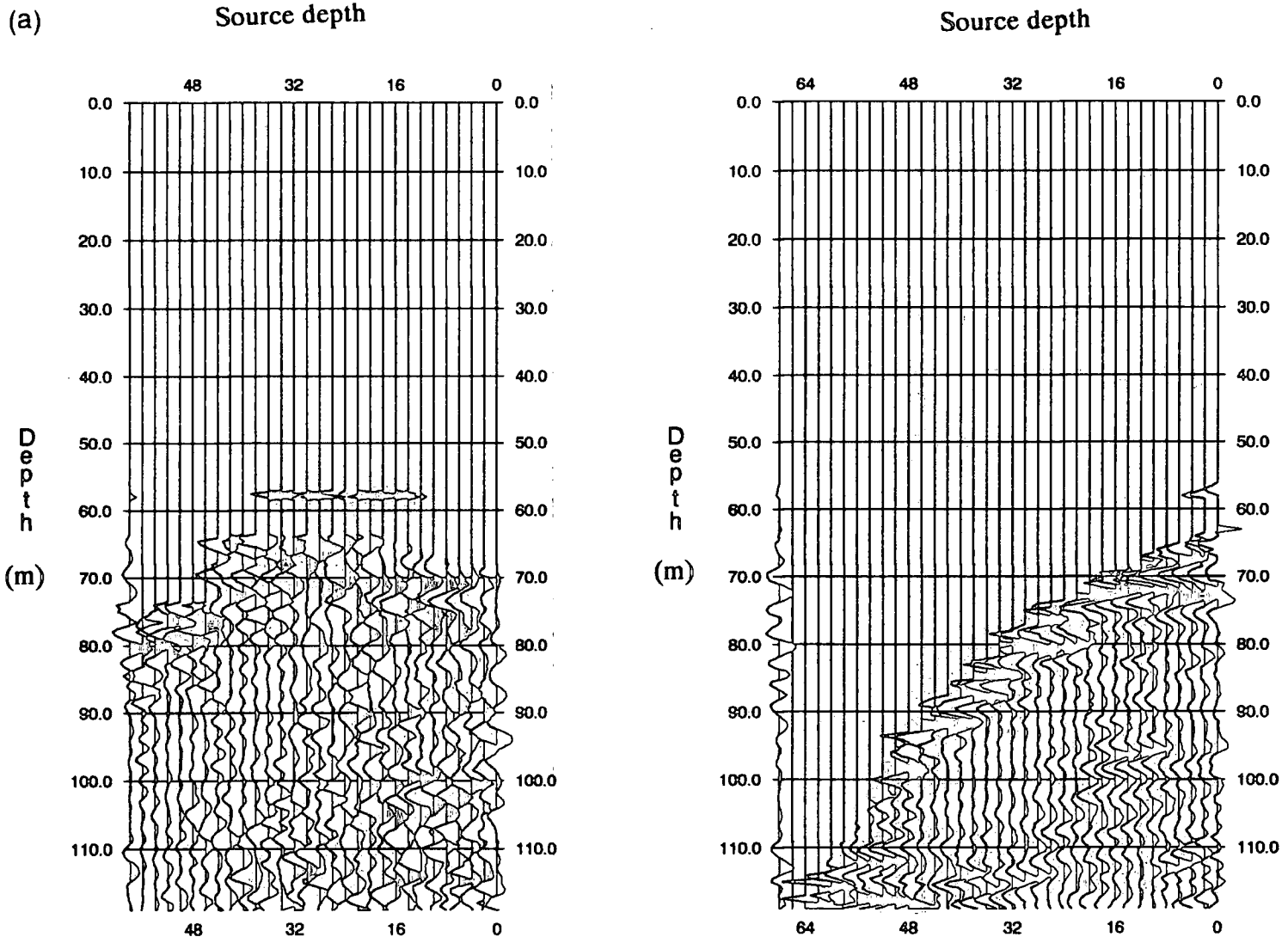

Figure 5.9(a) Common-depth trace gathers from independent migration of common-shot and common-receiver gathers at a distance of 8m from borehole H.

(b)

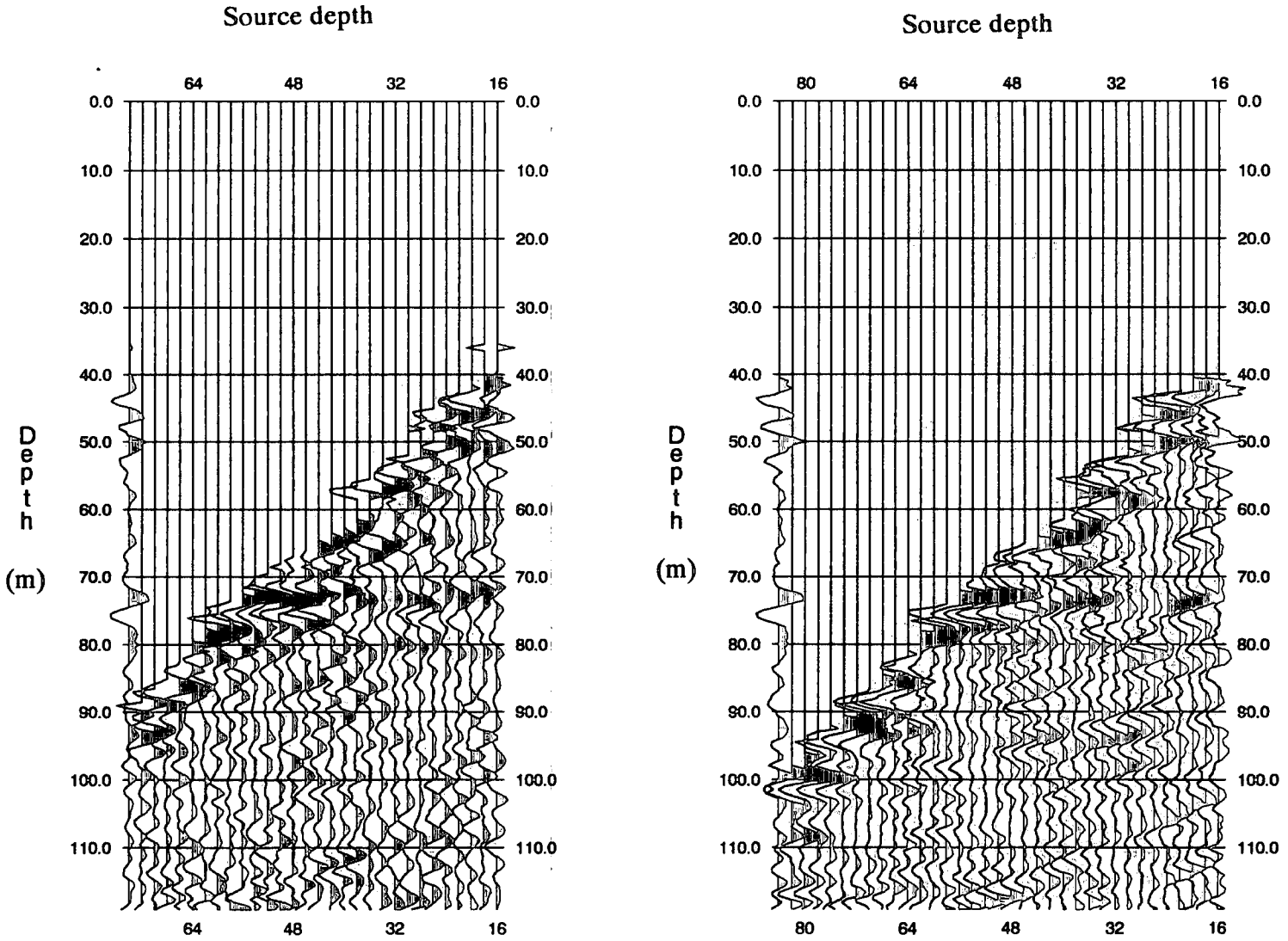

Figure 5.9(b) Common-depth trace gathers from independent migration of common-shot and common-receiver gathers at a distance of 30m from borehole H.

(c)

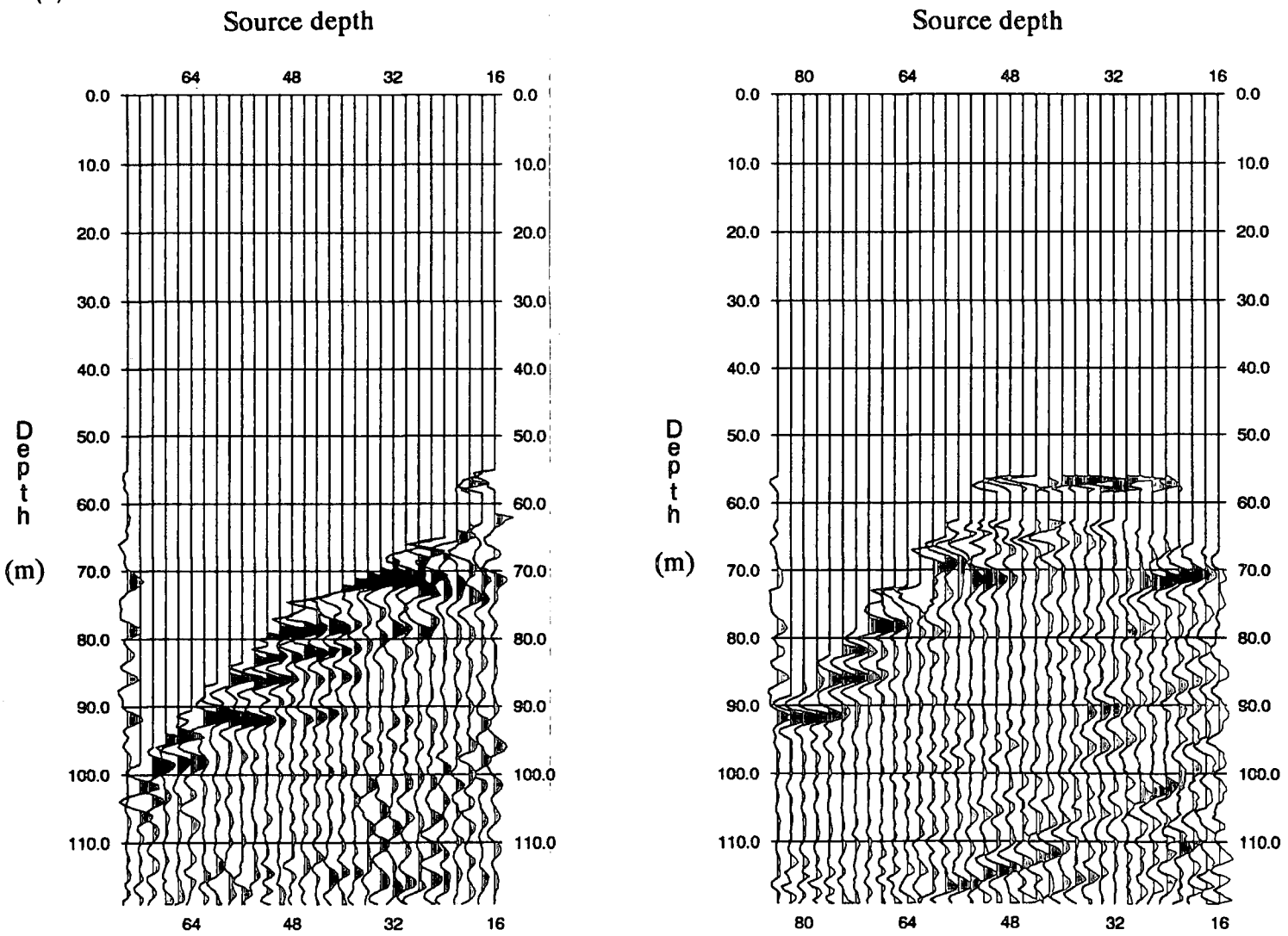

Figure 5.9(c) Common-depth trace gathers from independent migration of common-shot and common-receiver gathers at a distance of 48m from borehole H.

at 72m depth is showing a reasonable stack in places, as is the reflection at just over 90m depth. But in some places there appears to be destructive interference occurring, and the character of the waveforms contributing to the stack is very variable.

In Fig. 5.9 it can be seen that the CDP gathers from the migrated common-receiver gathers look more coherent than those from migration of the common-shot gathers. This may be an indication that shot-to-shot coupling variations are greater than receiver-to-receiver variations. The effects of the borehole at the different source locations (e.g. the diameter, elastic properties and densities of the borehole wall) could lead to variations in the radiation patterns of each shot. As some shots are also repeated at the same depth, the borehole wall could suffer some damage, which may lead to a different response from the explosive source for each shot. It is possible that differing amounts of energy can be radiated into the formation in different directions for each shot.

In the final migrated image, the Harrington has been imaged at the correct depth, as has a portion of the Udale seam just below 90m, but in looking at the CDP gathers, some of the traces contributing to the stack are not very convincing. The character of the reflection from the Harrington also shows some variation from shot to shot.

5.3 Survey 2; Boreholes E and I

The boreholes E and I were again open to over 100m, and 9 source positions were used at 11m intervals in borehole E, using approximately 12.5g of dynamite. The hydrophone string was positioned at 4 intervals in borehole I to give hydrophone depth levels at 2m intervals ranging from 14m to 102m depth. Figure 5.10 shows source and receiver positions for this survey. As in the previous survey, not all shots were fired into the total length of the hydrophone coverage. The survey setup is summarised below.

Shots at 16m and 25m fired into hydrophones from 14m to 58m.

Shots at 36m and 47m fired into hydrophones from 14m to 80m.

Shot at 58m fired into hydrophones from 14m to 102m.

Shots at 69m and 80m fired into hydrophones from 36m to 102m.

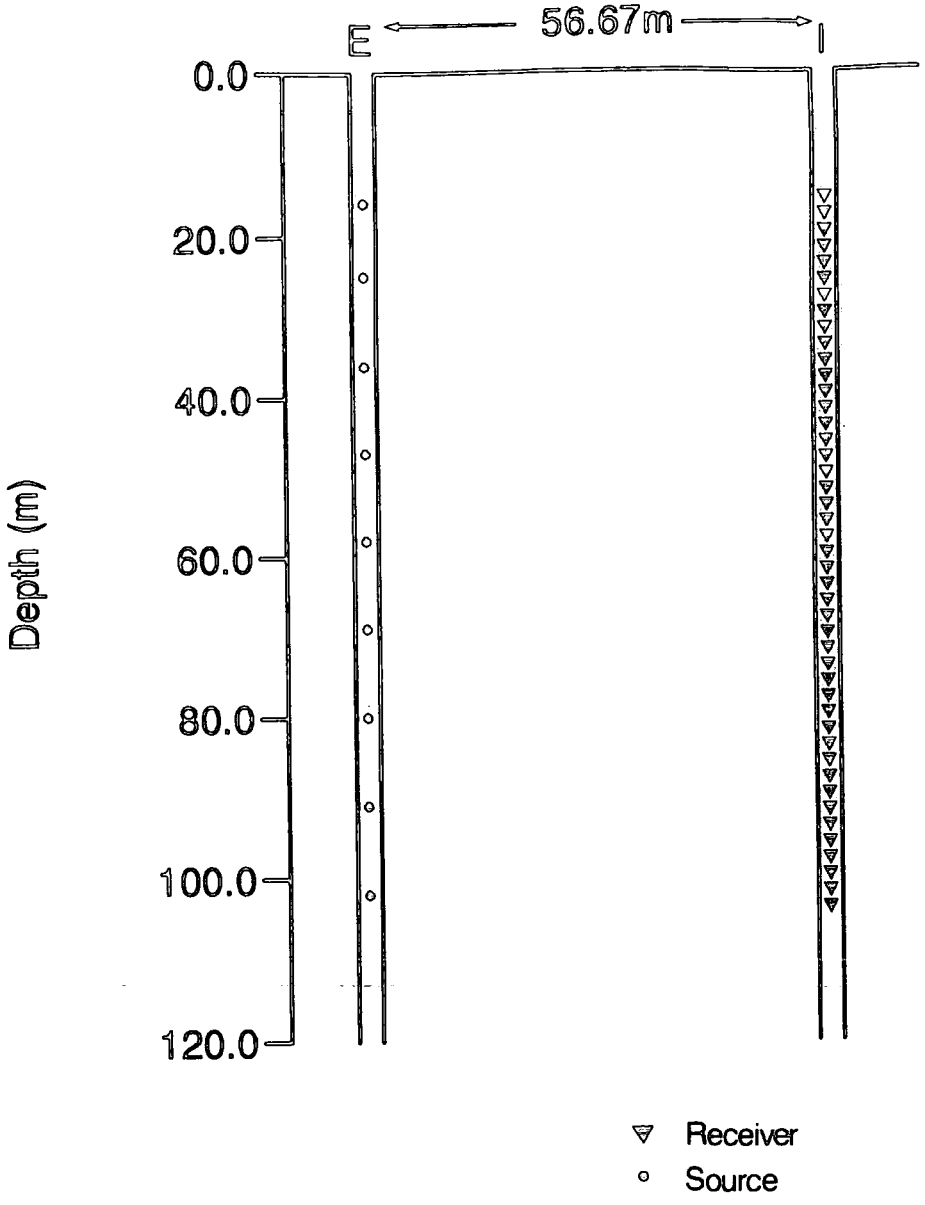

Figure 5.10 Source and receiver positions for the boreholes used in survey 2. In the second half of the survey, sources were placed in borehole I and receivers in borehole E.

Shots at 91m and 102m fired into hydrophones from 58m to 102m.

The survey was then repeated with sources in borehole I from 14m to 102m depth, at 11m intervals, and using the same arrangement of the hydrophone string. This survey was designed to be a time-saving experiment, but this also led to some problems with the coverage of the section. Unfortunately, there was no borehole verticality data available for the boreholes in this survey, so I had to assume that the boreholes were vertical and parallel.

The Close End Fault crosses the lower half of this survey, cutting borehole I at 61m and truncating the Harrington seam 12.73m away from borehole I. The other main seams present are the Black Metal at 83.93m (0.49m thick), the Fireclay at 92.3m (0.38m thick) and the White Metal at 103.52m (0.93m thick).

This survey was beset with the same problems of high amplitude aliased tube waves in the data, which again proved very difficult to remove. The processing sequence was the same as for survey 1, but using a desired Butterworth output wavelet of 100-700Hz bandwidth in the waveshaping deconvolution. These lower frequencies were used because the raw data have a slightly lower bandwidth than in survey 1. The migration velocities used are shown in Table 5.2. These are quite different from those used for survey 1, which is surprising and hard to explain.

2200 m/s	0-16m
2950 m/s	16-24m
3000 m/s	24-36m
3150 m/s	36-48m
3220 m/s	48-110m
3200 m/s	110-120m

Table 5.2 Migration velocities for survey 2

5.3.1 Results from Survey 2

This results from this survey are again inconclusive. There is no real evidence in the migrated data to pin-point the Close End Fault accurately. All nine shots from the first half of this survey were migrated independently and the results shown in Fig. 5.11. It was hoped that reflections could be obtained from the Harrington seam to enable the position of the Close End Fault to be identified. There is some indication of a reflection from the Harrington, but it is unfortunately very weak and variable in character.

Processed common-shot gathers from shots at 36m, 47m, 58m and 69m depth are shown in Fig. 5.12 and Fig. 5.13, with shots in borehole E. Any reflection from the Harrington seam at around 78m depth would only be seen on a few receivers (approximately between 62m and 78m depth). In the common-shot gathers from 36m, 47m and 58m in Fig. 5.12 and Fig. 5.13, there is an event on these receivers which terminates at the right depth on the line of first breaks, but this is very weak and also possesses a quite different character on each gather. It is not surprising, therefore, that this is not very well imaged in the migration. There are other, stronger, events but some of these again have no source in the subsurface. A good example is the high-amplitude event which appears to be a reflection from an interface at about 38m depth. This reflection also varies remarkably in character from shot to shot. There is nothing from the borehole logs to suggest a reflecting horizon at this depth.

A final stack of all 18 shots migrated together is shown in Fig. 5.14. There is no evidence of the Close End Fault in this image, and many of the reflectors imaged have no relation to the stratigraphy. For completeness, I have migrated shots for the downgoing wavefield, and this is shown in Fig. 5.15. This result is disappointing, but two thin seams at about 75m and 79m have been imaged, and there is a hint of a reflection from a coal seam at 29m. But, as most of the events appear to be noise, confidence in identifying any reflectors is low.

The CDP method for checking the velocity field and examining the coherence between individually migrated common-shot and common-receiver gathers could have been used in this survey but there seems little point when the data show so much variation from shot-to-shot.

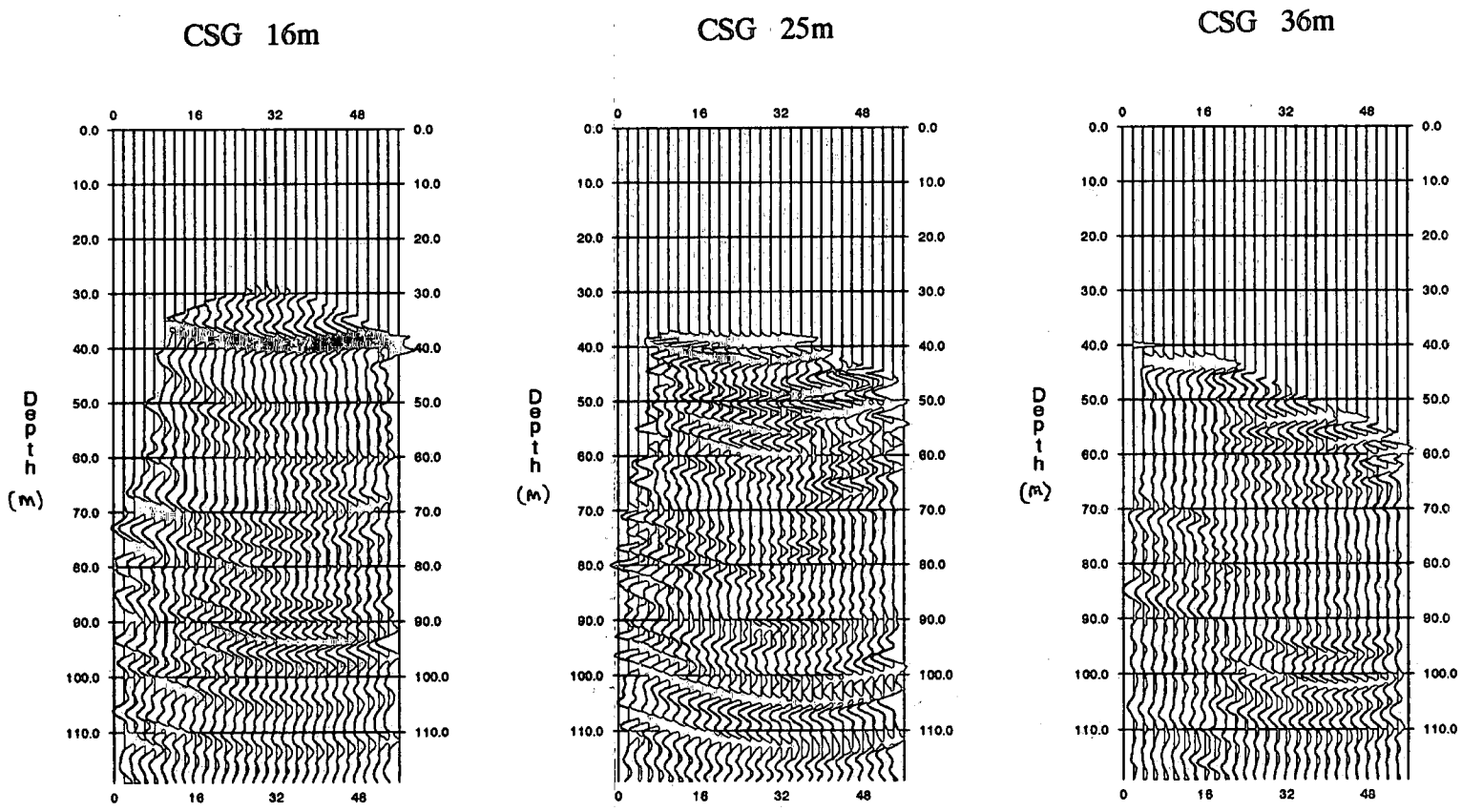

Figure 5.11 (a) Migrated images of common-shot gathers at 16m, 25m and 36m depth.

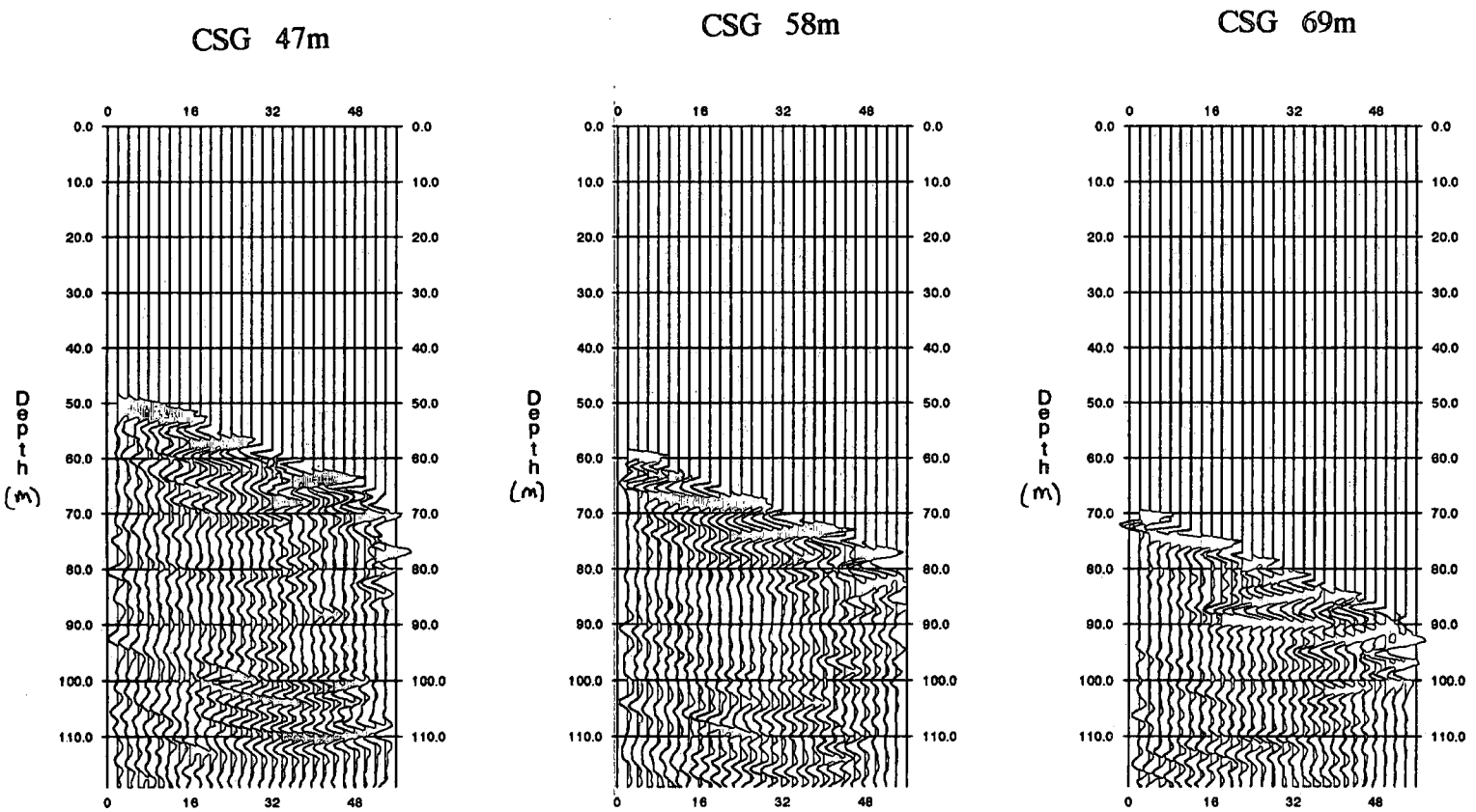

Figure 5.11 (b) Migrated images of common-shot gathers at 47m, 58m and 69m depth.

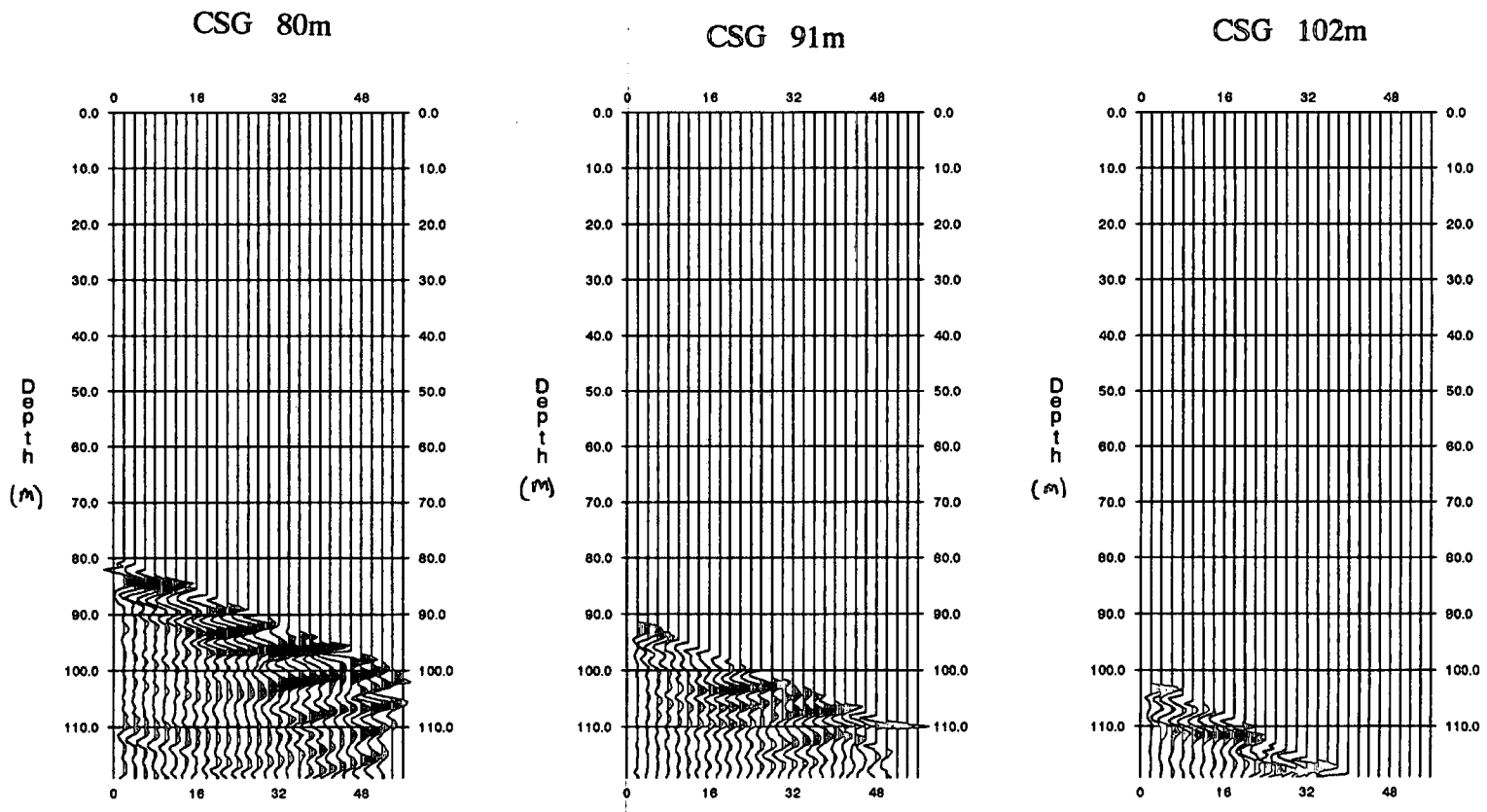

Figure 5.11 (c) Migrated images of common-shot gathers at 80m, 91m and 102m depth.

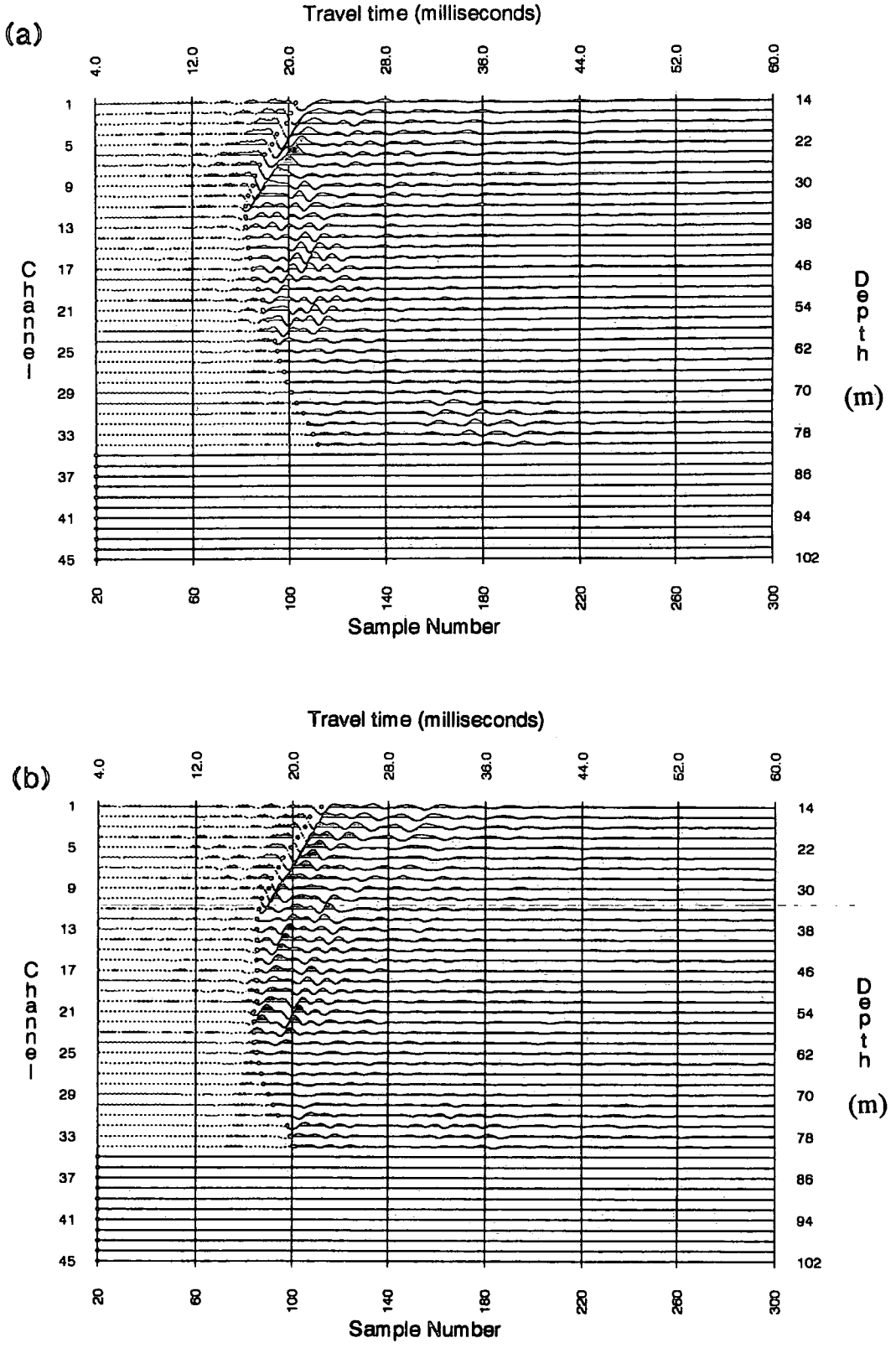

Figure 5.12 Common-shot gathers from survey 2. Depth of shot is (a) 36m and (b) 47m.

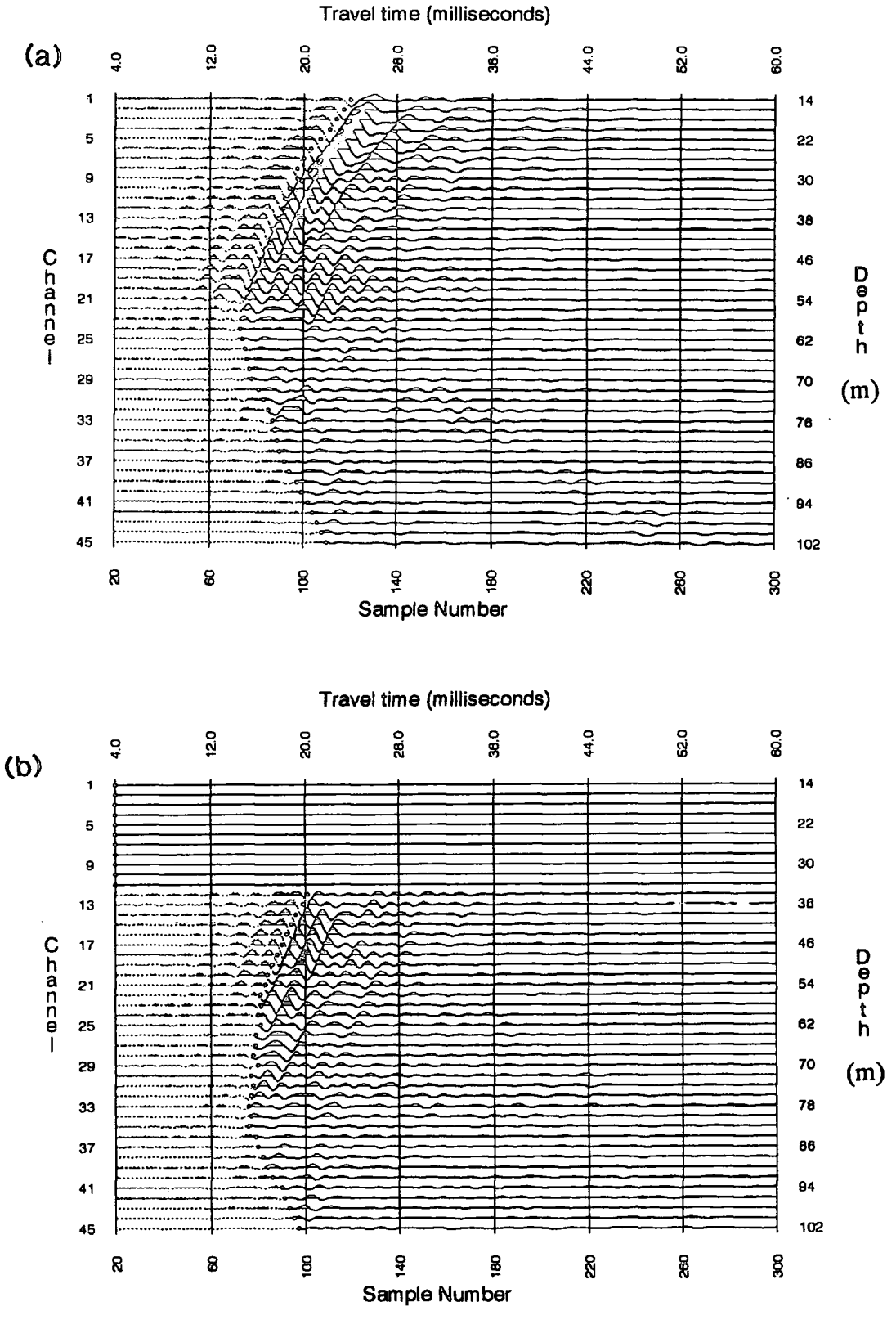

Figure 5.13 Common-shot gathers from survey 2. Depth of shot is (a) 58m and (b) 69m.

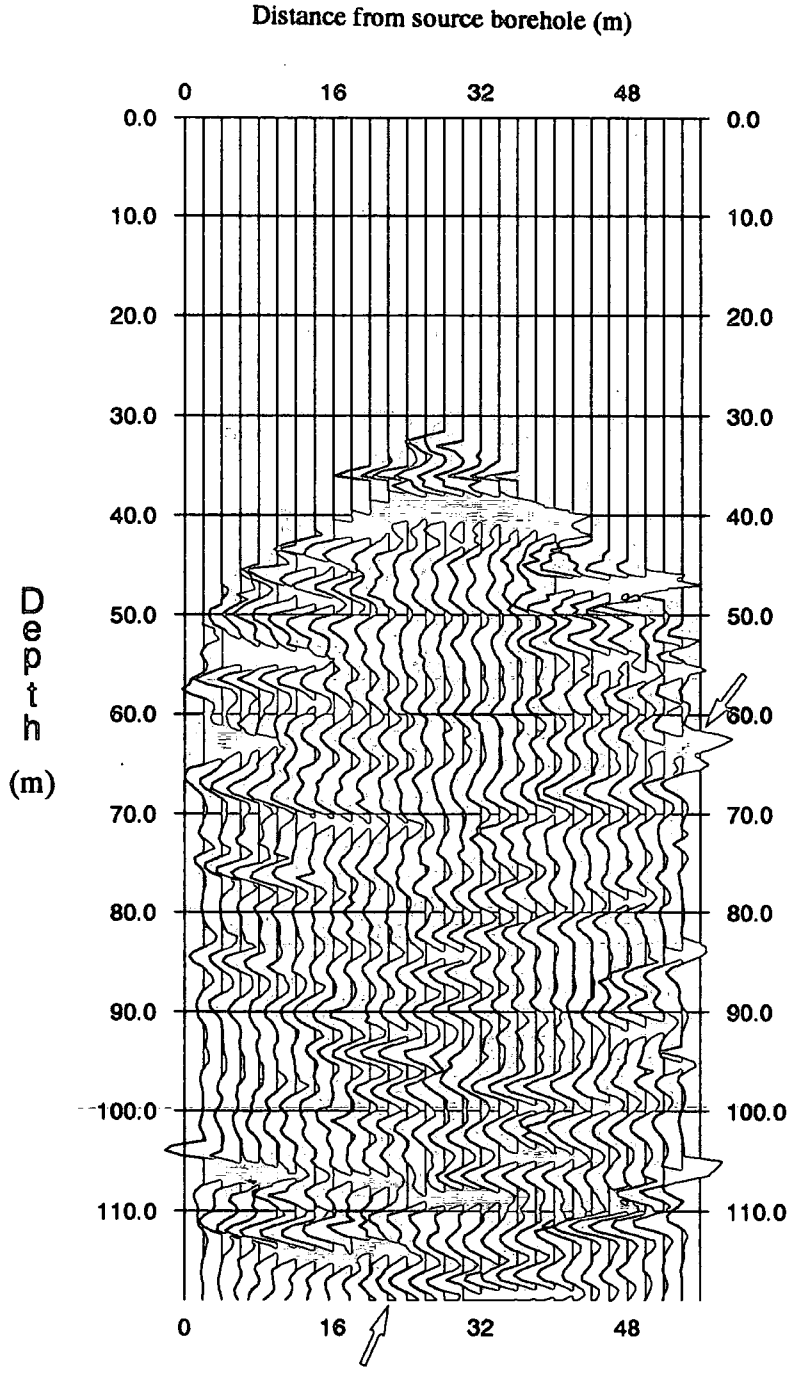

Figure 5.14 Upgoing Generalised-Kirchhoff migrated section for survey 2. An agc of 40m has been applied to this section, and the traces have been tapered off at their onset. The position of the Close End Fault is marked with arrows.

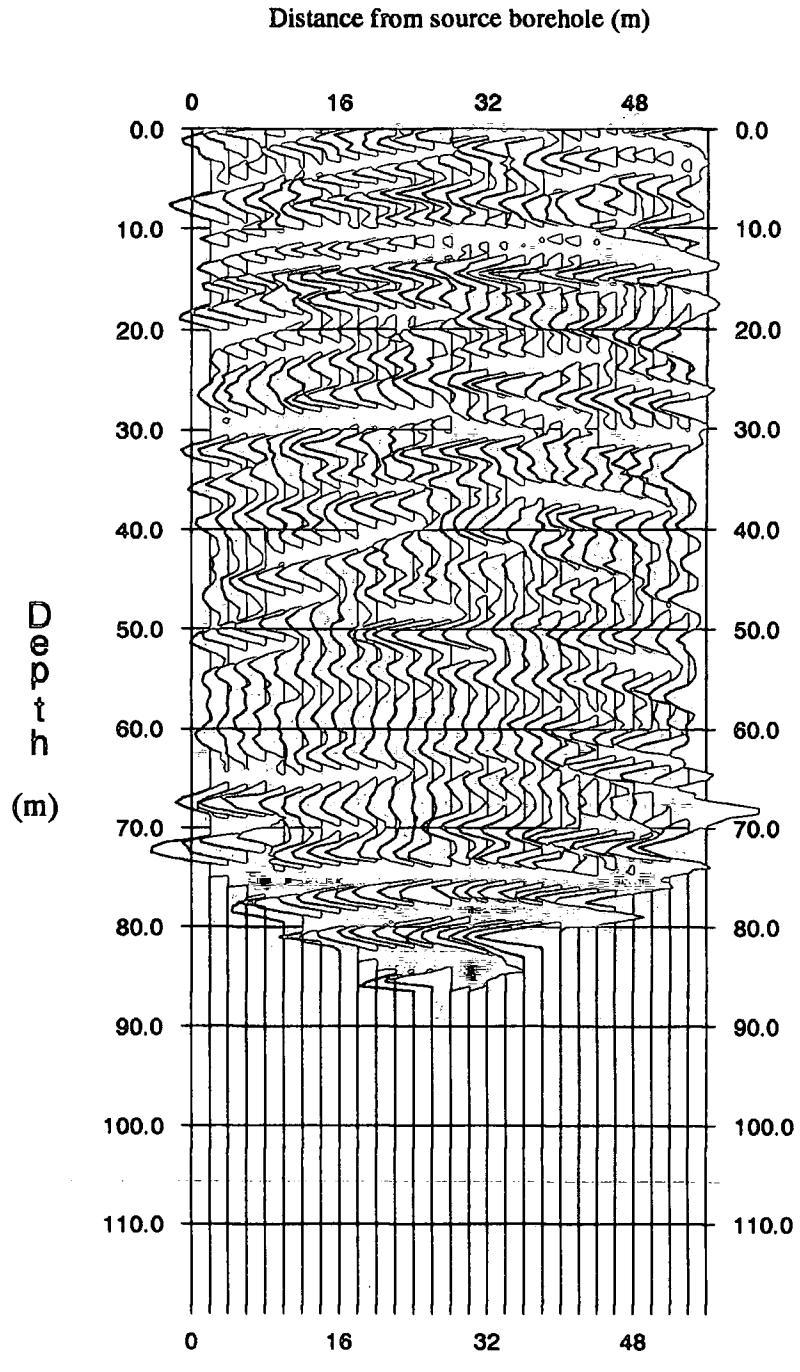

Figure 5.15 Downgoing Generalised-Kirchhoff migrated section for survey 2. An agc of 40m has been applied to this section, and the traces have been tapered off at their onset.

This survey, designed to image the large fault and locate accurately its position in the subsurface, has failed to produce an accurate depth section. One failing in this survey is the lack of coverage of the Harrington and the White Metal coal seams. It may be that a superior image could have been produced if the coverage had been better.

5.4 Discussion and conclusions

These two results from the processing and migration of crosshole seismic reflection data have proved disappointing. It has proved possible to only image one coal seam with any accuracy, and this only with marginal success. These data contain many apparent reflections from the subsurface, but the origin of these is not certain.

The crosshole seismic technique has proved successful in imaging a small fault in Coal Measures rocks (Findlay et al., 1991), but the method appears to be very dependent upon various factors, including the site, source/receiver configurations and borehole separation.

The problems in producing any significant result from survey 2 probably stem from the reduced coverage in that survey (by only having shots at 11m intervals) and the loss of energy to tube wave noise. The wavelengths obtained in the final migrated images for both surveys (around 4m) are very small in comparison to surface seismic, so makes this technique particularly viable where small faults are to be imaged. But the confidence of actually identifying reflections in these data as being real is not high.

The rocks at Lostrigg are much harder, and have a much higher velocity, than at other sites where this technique has been tested. This leads to a decrease in the ratio of P-wave energy to tube wave energy (Chen et al., 1990). In these data the tube waves are of very high amplitude and also have quite a high frequency content (up to 350-450Hz in some records). In the raw data, no reflected events are visible and the records are dominated by the high amplitude direct wave and tube wave energy. Another conclusion reached by Chen et al. is that tube wave amplitude varies only slightly with charge size, whereas the P-wave amplitude is approximately linearly proportional. Any increase in charge size could lead to more damage to the borehole, but would be beneficial to obtaining higher energy P-wave reflections.

With the presence of many thin coal seams, it is also highly likely that there will be lots of interference reflections resulting from short-lag or intra-bed multiples, as well as primary reflections from closely spaced coal seams (e.g. see Gochioco, 1992). These types of interference can lead to complex reflection characters which are hard to interpret. It has been shown (White and Sengbush, 1963) that pressure pulses in the shot-hole fluid also contribute substantially to the waves radiated, which may lead to a rise in the complexity of signals actually received by the hydrophones.

Some other points are worth considering in the crosshole seismic reflection technique. The Generalised-Kirchhoff method of migration is very sensitive to changes in the velocity field between the boreholes, and it is essential to obtain a good estimate before migration of the data. The use of uphole surveys and traveltime tomography go some way to aiding the design of the velocity field. If real reflections can be identified in the data as coming from, e.g., coal seams, then it is possible to invert the reflected traveltimes to give a much better estimate of the velocity field. But this would only be of use where reflections can be positively identified.

Tube waves, which are very common in crosshole surveys, are a big problem and a solution needs to be found to combat this. One possibility is to have some method of clamping baffles in-between the hydrophones so that the tube wave is not allowed to travel up and down the well, or will at least be reduced in amplitude.

This technique is also applicable to the oil industry, in producing high resolution images of reservoir horizons, but there are few examples of this at present. It could prove a valuable complement to existing techniques (VSPs and 3-D surface seismic), to enable much better understanding of reservoir properties, especially in monitoring EOR projects and location of small scale faulting, which are becoming increasingly important in the oil industry.

One other advantage of the technique is that coverage can be obtained below buildings, rivers, dams etc where surface sources and receivers cannot be deployed. The use of tomographic techniques has already proved its worth in these fields, where it is necessary to monitor changes in the rocks in the subsurface. Also, coverage is obtained both above and below the depths of the top and bottom source/receiver locations. This could prove to be valuable in the high resolution imaging of reservoirs where wells do not

extend below the reservoir horizon. To enable this to be done, however, it would be necessary to use a repeatable downhole source (e.g. sparker, air-gun).

The limiting factor in the frequency content of the data in crosshole seismic reflection is the borehole separation. A larger borehole separation will also produce a deterioration in image quality because reflection raypaths become more horizontal, leading to the need for a more accurate velocity model. A large borehole separation results in small errors in velocity producing stack errors to a greater than acceptable level.

The crosshole seismic reflection technique has the potential to image small faults (down to 2m throw with the wavelengths produced in the migrated depth section). However, there are still many mysteries as to why in some cases there are no reflections seen from coal seams that appear good candidates (thickness, depth, etc), but there are reflections that seem to emanate from positions where there are no obvious coal seams or impedance contrasts.

More tests need to be carried out evaluate the viability of the method in Coal Measures rocks, and efforts made to reduce the problems introduced by the amplitude tube waves and the need to produce a highly accurate velocity model before migration. The possibility of using some sort of casing (e.g. a plastic sleeve) in the borehole to prevent collapse at old workings and faults needs to be investigated. Collapse of the borehole wall can cause the hole to be blocked, and then the survey has to be abandoned. Any casing used would have to be lightweight and low-cost as sections would invariably be lost in the borehole. It would also have to have a low impedance contrast with water so that source/receiver coupling is not affected by its presence.

Acquisition time could be reduced by the use of a hydrophone array with 24 channels and a repeatable source such as a downhole airgun or borehole sparker. Explosives are good impulsive sources but tend to be slow to use.

For a viable exploration technique, the crosshole seismic reflection method should be used in conjuction with VSPs (or hole-to-surface surveys, e.g. see Kragh et al., 1991 and Kragh et al., 1992) as the areas of reflector coverage are complementary (see Fig. 5.16). The crosshole method provides better imaging between the boreholes, but image quality is poor near to the boreholes.

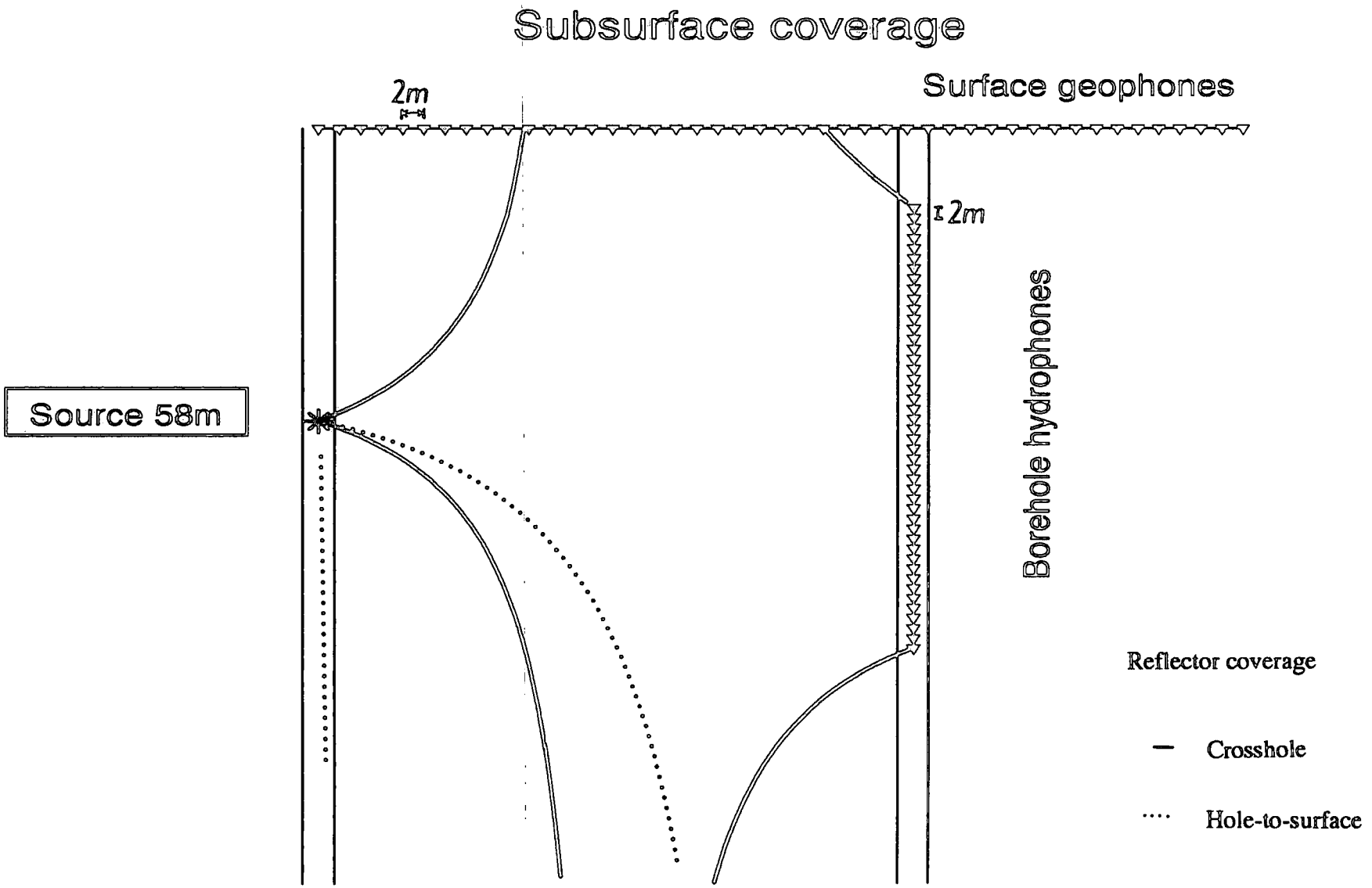

Figure 5.16 Zones of coverage for crosshole and hole-to-surface reflection surveys.

PART 3

Chapter VI

Seismic reflection test on the granite of the Skye Tertiary igneous complex

6.1 Introduction

In June 1991 I took part in a seismic experiment over a short profile on the granite of the Skye Tertiary central intrusive complex (see Goulty et al., 1992). My role in the experiment was originally to help with the data acquisition on Skye, but early in 1992 I processed the data as described below. The aim of the work was to investigate the base of a granitic intrusion, overlying basic igneous rocks. This chapter deals with the geology of the area, data acquisition and processing, and the interpretation of the results.

Previous gravity modelling work suggested that the base of the granite lies at approximately 1.5km and overlies basic rocks. The seismic data indicate that the granite is at least 2km thick at the test location, and provides information about the structure at depth.

6.2 Geology and gravity modelling

The Skye Tertiary central intrusive complex consists of gabbros and ultrabasic rocks, which form the Cuillin hills on the west, and granites which form the Eastern and Western Red Hills on the east (Fig. 6.1). Bott & Tuson (1973) inferred from their gravity work that the granite is approximately 1.5km thick and overlies basic rocks, but that the granite forms less than 8% of the total volume. The bulk of the intrusion may consist of basic rocks to a depth of 14km. The sequence of events in the Skye Palaeocene central igneous complex can be summarised as follows, after Bell (1976) and Emeleus (1992):

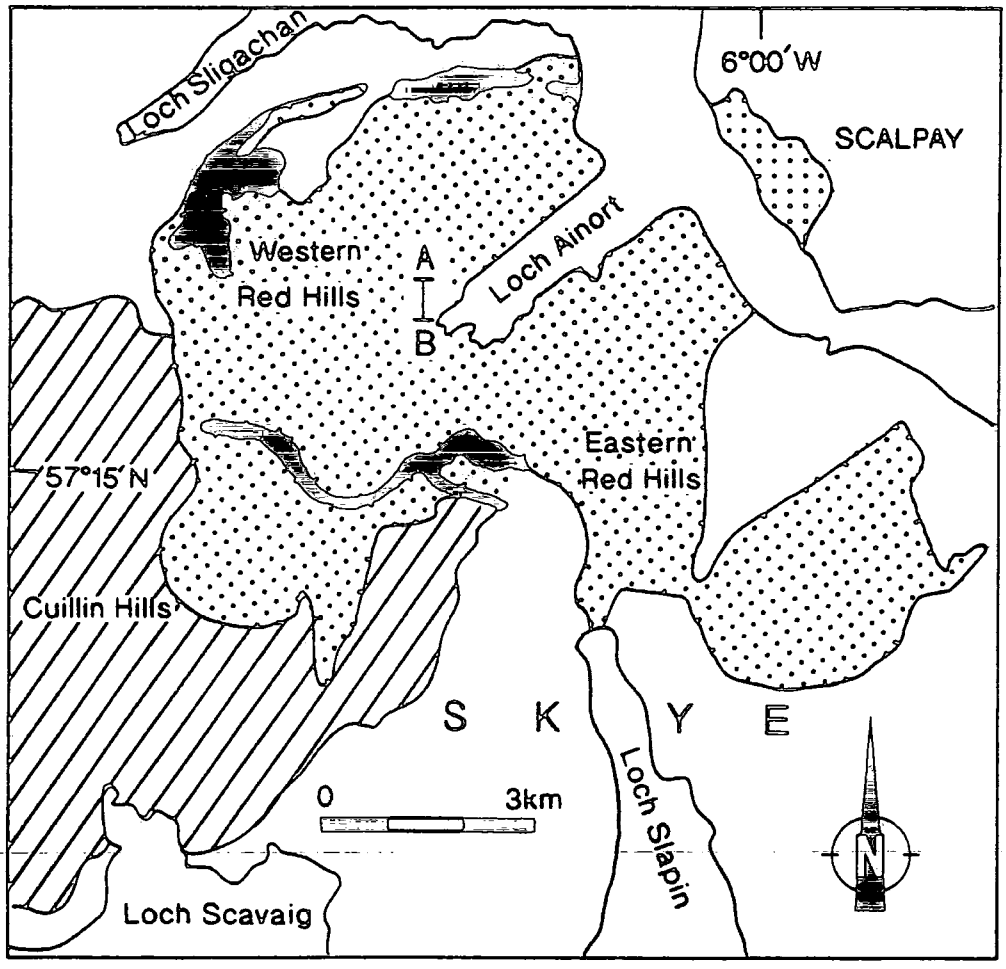

Figure 6.1 Sketch map showing the location of the seismic line AB. The Cuillin complex is indicated by diagonal lines, that of the granites by stippling, and that of the Marscoite suite by solid black. The Strath na Creatheach Centre forms the lobe of Granite on the southern flank of the Western Red Hills.

(1) Eruption of plateau basalt lavas and intrusion of NW-SE basic dykes. In he vicinity of the central complex this was succeeded by acid and intermediate pyroclastic rocks.

(2) Intrusion of gabbros, ultrabasic rocks and basic cone-sheets of the Cuillin Hills. Injection of NW-SE dyke swarms continued.

(3) Granites intruded at three centres. Initially at the Strath na Creatheach Centre in the SW, followed by the Western Red Hills and the Marscoite suite, and finally at the Eastern Red Hills. Intrusion of NW-SE basic dykes continued during and after granite emplacement.

(4) Lavas and volcaniclastics eroded until the granites and gabbros unroofed and exposed at the surface.

Although the granites intrude the Cuillin Hills, mafic magmas continued to be intruded throughout granite emplacement, as shown by the ferrodiorites and hybrids of the Marscoite suite ring-dyke and small amounts of gabbro in the Western Red Hills (Thompson, 1969), and the post-granite basic dykes.

6.3 Data acquisition

In the survey area the granite is overlain by a layer of drift and peat, of varying thickness. A shot-hole was drilled 9m deep into a surface outcrop of granite along the survey line. This was carried out by a a drilling-rig hired from a quarry at Sconser, which was unfortunately only able to drill usable holes at the centre of line AB shown in Fig. 6.1, because of the lack of good access roads and being unable to have boreholes cased down to rockhead. Two shots, each consisting of 1.5kg of gelamex and tamped with water, were fired sequentially into a 24-channel geophone spread, which was laid out on either side of the shot point along the line AB. The receivers used were single 30 Hz geophones spaced at 10m intervals. There was no geophone at the shot position, at the centre of the spread. These data were recorded with a 1ms sample interval and a total of 2048 samples were recorded per trace.

Figure 6.2 shows the two raw common-shot gathers combined into a 48-channel gather, with an automatic gain control (agc) of 200ms applied to the plot. Data are shown to 1s only as there are no features of interest later in the data. Ambient noise in the data is due mainly to wind and rain, with some 50

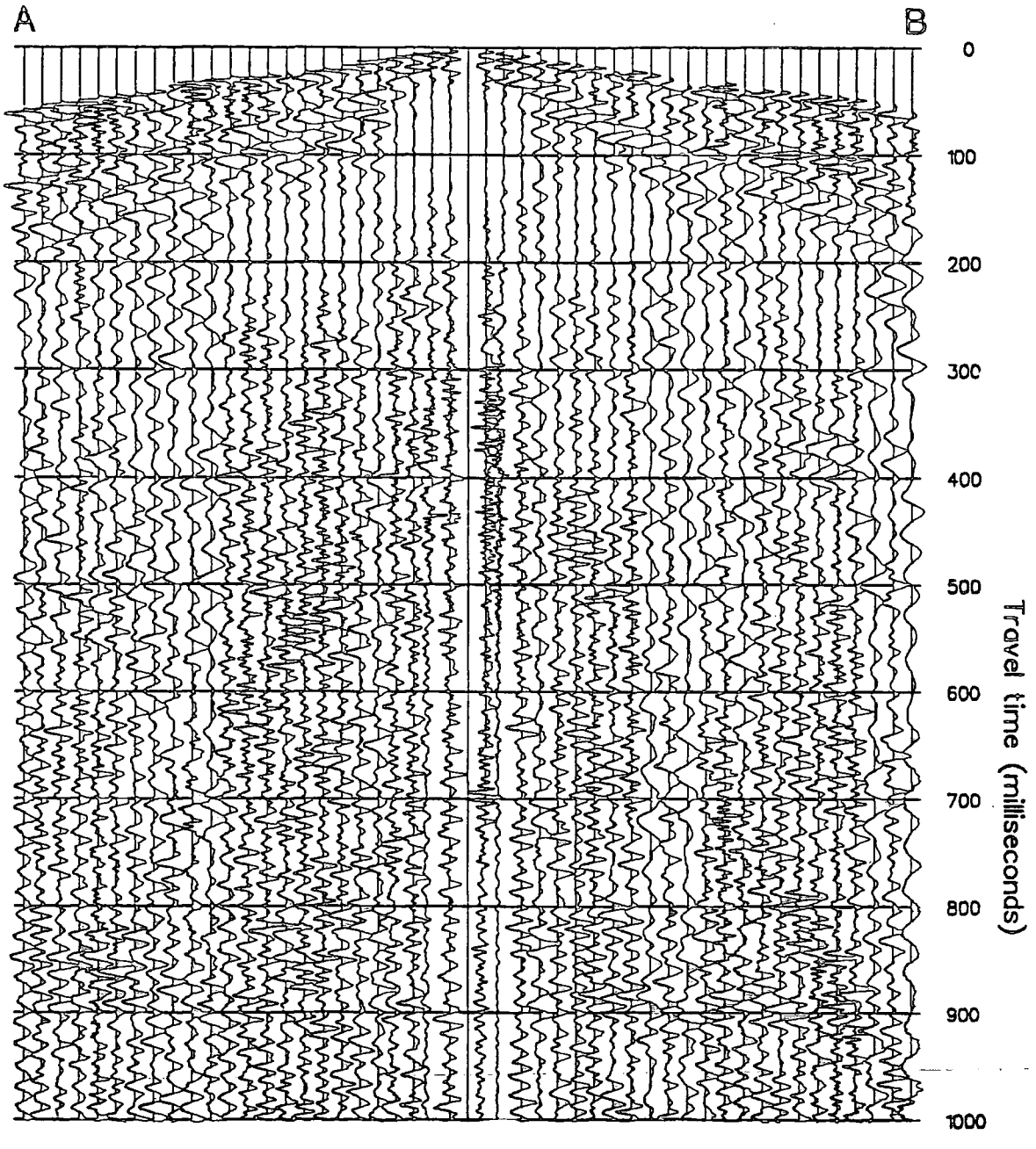

Figure 6.2 Raw data from two shots recorded using a 24-channel geophone spread on either side of the shot-point. An agc of 200ms has been applied.

Hz pick-up from nearby power lines also present. A band of coherent events is apparent between 800 and 900ms.

Near point B on Fig. 6.1 a shallow shot was fired into 24 geophones to obtain a reversed refraction profile. From the minus graph, the velocity for the top of the granite was estimated to be approximately 5.0kms^{-1}. This should give the lower limit for the velocity of the granite as a whole as the top surface is liable to be weathered and fractured, leading to a reduction in the seismic velocity.

6.4 Data processing

All traces had static corrections applied by first aligning all first breaks along a line corresponding to a velocity of 5.0kms^{-1} from the shot point. This brings all the geophones to (approximately) the same datum as the shot, at 100m above mean sea level. Spiking deconvolution was applied to these data with a filter length of 32ms with the autocorrelation function of each trace calculated over the window 700-1100ms. Following this, a bandpass filter was applied to each trace to pass all frequencies between 40 and 100 Hz (with tapers down to 20 Hz and up to 150 Hz). Figure 6.3a shows this data after normalization to equal energy over the window 700-1100ms, and application of residual statics (of up to 2ms) to align the events further. No agc has been applied to this plot.

The band of coherent events between 800 and 900ms is more evident than on the raw common-shot record (Fig. 6.2). The total length of the geophone spread used was 480m, which means that only 240m of the reflector will be imaged. The area of the interface contributing to the reflected signal corresponds approximately to the first Fresnel zone, given by $\sqrt{2d\lambda}$, where d is the depth of the reflector and λ is the wavelength. For the observed reflections, the diameter of the first Fresnel zone is around 600m. Consequently, it is a valid step to sum all the traces to yield the brute stacked trace in Fig. 6.3b. The trace in Fig. 6.3c is the zero-phase wavelet corresponding to the deconvolution process described above.

A comparison of Figs. 6.3b and 6.3c shows that the largest events in Fig. 6.3b correspond to (a) positive reflection events (coefficients) at 812 and 874ms and, (b) negative reflection coefficients at 839 and 890ms (shown by the solid arrows). The first three events all appear to be similar in amplitude, but the

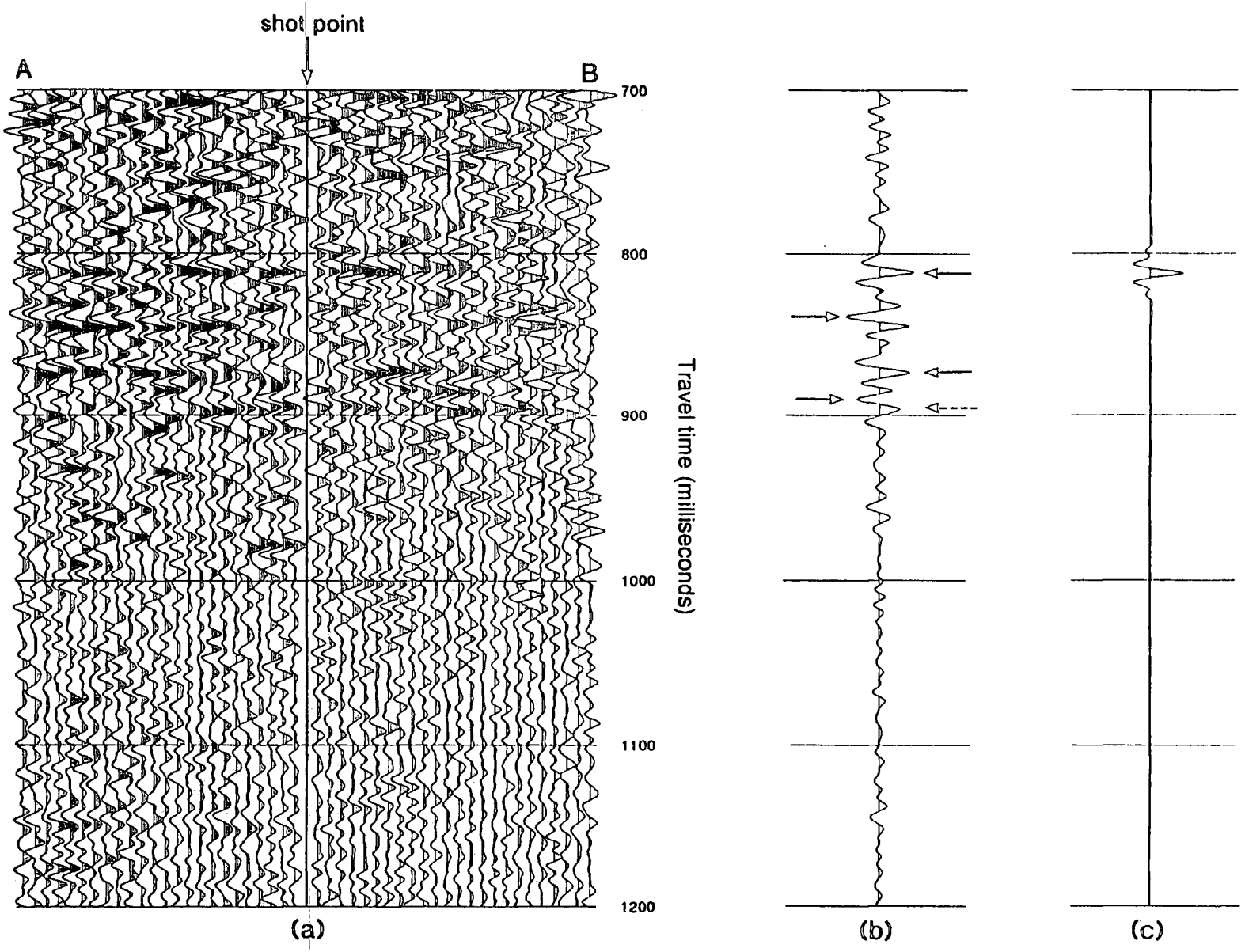

Figure 6.3 (a) Common-shot gather after the application of statics and deconvolution, displayed at fixed gain. (b) Stacked trace from the summation of all 48 filtered traces. (c) Zero-phase wavelet of the same bandwidth as the filtered traces. The seismic datum is 100m above mean sea level.

fourth is somewhat weaker and not so symmetrical in character. A possible reason for this is that there appears to be another positive reflection event at 897ms (indicated by the broken arrow), although this is unfortunately not very clear.

6.5 Interpretation

The value of 5.0kms^{-1} obtained for the velocity of the granite, from the reversed refraction spread, is likely to be too low for the bulk of the granite body. Velocities observed in granite are commonly in the range 5.2 - 5.8kms^{-1}. A velocity of 5.5kms^{-1} is almost certainly within 5% of the true value, so can be used for estimating approximate depths.

Using this velocity, a depth of just over 2.1km below mean sea level is obtained for the observed reflection event at 812ms two-way traveltime. A rock of basic composition would produce a positive reflection coefficient, which is observed in the first event. A typical velocity for gabbro is around 6.7kms^{-1} which can be used to estimate the depth intervals between reflecting interfaces. The negative polarity event at 839ms is similar in amplitude to the first event, which would correspond to gabbro overlying granite. These reflectors seem to bound a basic sheet approximately 90m thick. Using the same velocities, the events at 874 and 890ms may show another basic sheet approximately 54m thick, lying about 96m deeper. Bott and Tuson (1973) showed in their gravity modelling work that the base of the granite is unlikely to be deeper than 2.4km. If the granite overlies basic rocks, the last reflection event should be positive. It is suggested that the lower amplitude reflected event at 897ms (indicated by the broken arrow) represents the base of the granite, although confidence in identifying the actual base of the granite from these results is not high. Figure 6.4 is a one-dimensional depth profile inferred from these results.

The layering described is similar to that inferred at Slieve Gullion, NE Ireland, where flat-lying doleritic and granitic sheets are interlayered within a Tertiary central complex (see Bailey & McCallien, 1956, Fig. 3).

It is possible that the observed reflection events could represent the base of the granite (uppermost event) overlying alternating layers of olivine-rich and feldspar-rich gabbro within an underlying basic intrusion. The similar amplitudes of the first three reflections, and the fact that no deeper reflections can be seen at all in these data, suggest that this not the case.

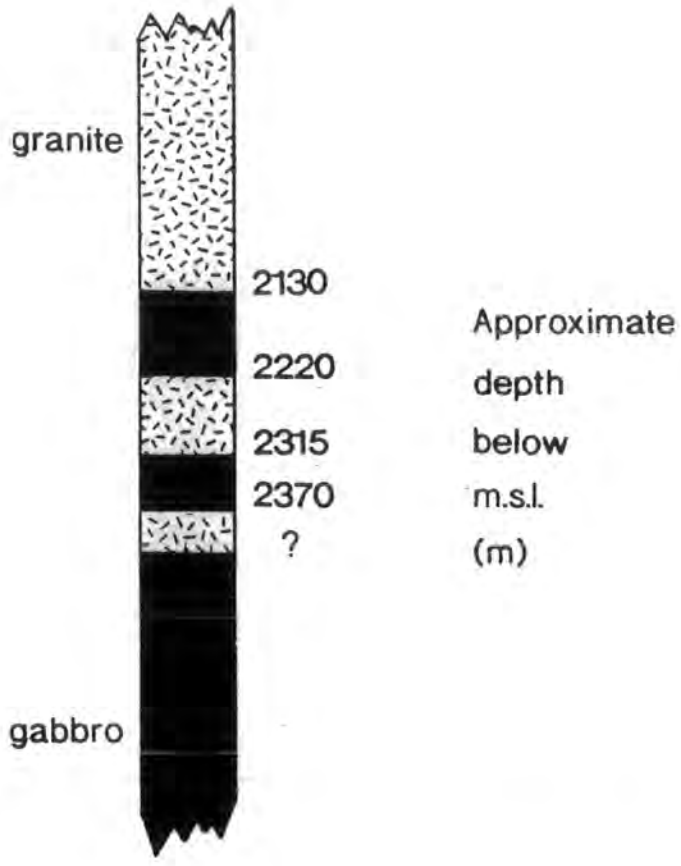

Figure 6.4 One-dimensional interpretation of the seismic reflection test indicating interlayered basic and acidic sheets at the base of the granite.

6.6 Conclusions

The results from this small pilot survey on Skye indicate that a more extensive seismic survey would provide further information about the structural development of this Tertiary igneous complex. The quality of the data could be much enhanced by using multi-fold coverage and groups of geophones to improve the signal-to-noise ratio. It would also be advantageous to extend the seismic survey to cover the edges of the granite mass.

In conclusion, the transition from granite into (presumably) basic rocks is not marked by a simple interface, but is more likely to consist of interlayering between basic and igneous rocks.

Chapter VII
Overview and conclusions

7.1 Introduction

The work presented in this thesis comprises three different seismic processing methods - tomographic, crosshole reflection and surface seismic. The bulk of the work is crosshole seismic processing, using two different methods. The work shows the contrast between the complexity of crosshole seismic data compared to surface seismic data, in the processing and interpretation.

7.2 Tomography and crosshole seismic reflection methods

It has been shown, using physical model data, that seismic tomography (traveltime and amplitude) can be used for monitoring EOR processes in a reservoir. This is important because the extent of flooding (and shape of the flood front) has to be known in order to prevent problems with the recovery process, e.g. gas or water breakthrough to the production well. Unfortunately, the amplitude tomography proved unable to image the flood zone as well as the traveltime tomography, mainly due to being unable to correct for diffraction effects and multipathing in the survey. These effects are large in the physical model because of the sharp corners and large velocity difference in the flood zone. These effects are likely to be less in a real, heterogeneous reservoir because there will not be such sharp discontinuities in structure and velocity.

Even so, it has been proved that amplitude tomography is a viable technique and should be used in conjunction with traveltime tomography to enable a more detailed interpretation of the progress of the flood front through the reservoir. There are still some problems to overcome in amplitude tomography. A better method of inverting the amplitudes, involving wave-equation-based forward modelling, would be advantageous as the ray-based method cannot correct for diffraction effects. Traveltimes are not so drastically affected by variations in rock structure (other than head waves, for which there was no evidence in these data).

Tomography is essentially a low-resolution technique, whereas crosshole reflection surveys can produce high resolution images between the two boreholes. In opencast coal exploration, it is necessary to resolve small faults and the detailed structure of fault zones; hence crosshole reflection surveys are much more suitable. Traveltime tomography can help in making an initial estimate of the velocity field between the boreholes, combined with the uphole information. In using the Generalized Kirchhoff algorithm for depth migration of the data, an accurate estimate of the velocity field is required, but the more complex the model, the greater the computational effort.

The results from the surveys carried out at Lostrigg, Cumbria in the Coal Measures rocks failed to image any reflectors with any great confidence (see Chapter V). Only one coal seam was imaged at the correct depth, in Survey 1. After processing the data as described in Chapter IV, there seemed to be many reflected arrivals present, but their origin is not clear and has no correlation with the information obtained from the well log data. Although previous results from the crosshole seismic reflection method show that faults can be imaged with some accuracy (Findlay et al. 1991), the results obtained here were disappointing.

All records were heavily contaminated with fairly high frequency and high energy (relative to reflected signals and direct wave arrivals) tube waves. It is possible that the use of a larger charge size could have resulted in a gain in amplitude of the reflected P-wave energy relative to the tube waves (Chen et al. 1990). Another effect that can give rise to a higher complexity in the signal received at the hydrophones is tube waves in the source borehole which act as secondary sources where they interact with discontinuities in the borehole walls.

From the borehole logs and geological cross section drawn up by the BCO geologist, it can be seen that there are numerous thin coal seams (predominantly between 0.2-0.3m thick) with thin layers of shale/sandstone between them. The tuning thickness is given by $\lambda/4$ where λ is the wavelength. Using an average velocity of 2200ms^{-1} for the coal seams in this survey, the tuning thickness is calculated to lie in the range 2.75m to 0.55m for frequencies of 200-1000Hz.

It is impossible to state categorically how much these factors influenced the results from Surveys 1 and 2 in Chapter V. It is likely that they all had some effect but the main reason is probably the weak generation of body waves in these relatively hard rocks. However, thin beds can still give an appreciable reflection amplitude at thickness below $\lambda/20$ (Widess 1973). The positioning of baffles between receivers, and above and below the source, may go some way to reducing the effect of the tube waves in the data.

Crosshole seismic reflection surveys also need good coverage to be able to image the area between the boreholes well, and should be planned using some a-priori knowledge (from well log information) so that the required targets are successfully imaged.

7.3 Skye seismic experiment

In contrast to the crosshole seismic processing methods, the pilot seismic experiment on the Isle of Skye (Chapter VI) is a surface seismic survey, designed to determine the depth of the granite mass in the Western Red Hills. Compared to the crosshole seismic reflection work, this is very low resolution and the frequency content much reduced. The results from this experiment, after suitable processing, are encouraging, and suggest that a large-scale seismic survey over the region will image the true extent of the granite body. The stacked trace from all traces in the common-shot gather recorded shows that at the base of the granite (approximately 2.1km below mean sea level) there are alternating layers of basic (gabbro) and acidic (granite) layers. The results also agree closely with previous gravity work by Bott & Tuson (1973).

7.4 Conclusions

In overall conclusion, it is clear that the tomography work has great potential for monitoring work, e.g. enhanced oil recovery processes and that both traveltime and amplitude tomographic inversion should be performed as the results are complementary. The crosshole seismic reflection technique has great potential for obtaining high-resolution seismic sections of the subsurface, and could also be used for monitoring purposes. It has much higher resolution than tomography, but there is less certainty about obtaining a meaningful image. Key factors are the generation of compressional body wave energy, which is more difficult in harder rocks, and the reflectivity.

References

Bailey, E.B. & McCallien, W.J. 1956. Composite minor intrusions and the Slieve Gullion complex, Ireland. *Liverpool and Manchester Geological Journal* 1, 466-501.

Balch, A.H., Lee, M.W., Miller, J.J. & Taylor, R.T. 1982. The use of vertical seismic profiles in seismic investigations of the earth. *Geophysics* 47, 906-818.

Bell, J.D. 1976. The Tertiary intrusive complex on the Isle of Skye. *Proceedings of the Geologists' Association* 87, 242-71.

Bois, P., La Porte, M., Lavergne, M. & Thomas, G. 1972. Well to well seismic measurements. *Geophysics* 47, 471-480.

Bott, M.H.P. & Tuson, J. 1973. Deep structure beneath the Tertiary volcanic regions of Skye, Mull and Ardnamurchan, north-west Scotland. *Nature Physical Science* 242, 114-6.

Bortfeld, R. 1962. Reflection and refraction of spherical compressional waves at arbitrary plane interfaces. *Geophysical Prospecting* 10, 517-538.

Bredewout, J.W. & Goulty, N.R. 1986. Some shallow seismic reflections. *First Break* 4(12), 15-23.

Bregman, N.D., Chapman, C.H. & Bailey, R.C. 1989a. Traveltime and amplitude analysis in seismic tomography. *Journal of Geophysical Research* 94, 7577-7587.

Bregman, N.D., Hurley, P.A. & West, G.F. 1989b. Seismic tomography at a fire-flood site. *Geophysics* 54, 1082-1090.

Brooks, R.A. & di Chiro, G. 1976. Principles of computer assisted tomography (CAT) in radiographic and radioisotopic imaging. *Physics in Medicine and Biology* 21, 689-732.

Carabelli, E. 1988. Sonic velocity tomography in concrete and earth dams evaluation. 58th Annual Meeting, Society of Exploration Geophysicists, Expanded Abstracts, 629-632.

Cassel, B.R. 1982. Seismograms in laterally varying media. *Geophysical J. R. astr. Soc.* 69, 339-354.

Cervený, V., Molotkov, I.A. & Psencik, I. 1977. *Ray method in seismology.* Univerzita Karlova Praha.

Chen, S.T., Eriksen, A. & Miller, M.A. 1990. Experimental studies on downhole seismic sources. *Geophysics* 55, 1645-1651.

Christie, P.A.F, Hughes, V.J. & Kennett, B.L.N. 1983. Velocity filtering of seismic reflection data. *First Break* 1(3), 9-24.

Cooley, J.W. & Tukey, J.W. 1965. An algorithm for the machine calculation of complex Fourier series. *Maths computations* 19, 297-301.

Devaney, A.J. 1984. Geophysical diffraction tomography. *IEEE Transactions on Geoscience and Remote Sensing* GE-22, 3-13.

Dillon, P.B. 1990. A comparison between Kirchhoff and GRT migration in two and three dimensions. *Geophysical Prospecting* 38, 757-777.

Dines, K.A. & Lytle, R.J. 1979. Computerized geophysical tomography. *Proceedings of the IEEE* 67, 1067-1078.

Domenico, S.N. 1976. Effect of brine-gas mixture on velocity in an unconsolidated sand reservoir. *Geophysics* 41, 882-894.

Dyer, B. 1988. *Seismic reflection and transmission tomography.* Ph.D. dissertation, University of London.

Dyer, B. & Worthington, M.H. 1988. Some sources of distortion in tomographic velocity images. *Geophysical Prospecting* 36, 209-222.

Emeleus, C.H. 1992. Tertiary igneous activity. In *Geology of Scotland* (G.Y. Craig ed.). 3rd edition, The Geological Society, London, 455-502.

Findlay, M.J. 1987. *A curved ray iterative technique for tomographic inversion of cross-borehole data.* M.Sc. dissertation, University of Durham.

Findlay, M.J. 1991. *Cross-hole seismic reflection surveying in Coal Measures.* Unpublished Ph.D. dissertation, University of Durham.

Findlay, M.J., Goulty, N.R. & Kragh, J.E. 1991. The crosshole seismic reflection method in opencast coal exploration. *First Break* 9, 509-514.

Fitch, A.A. 1984. Interpretation of vertical seismic profiles. *First Break* 2(6), 19-23.

French, W.S. 1975. Computer migration of oblique seismic reflection profiles, *Geophysics* 40, 961-980.

Gilbert, P. 1972. Iterative methods for three-dimensional reconstruction of an object from projections. *Journal of Theoretical Biology* 36, 105-117.

Gochioco, L.M. 1992. Modeling studies of interference reflections in thin-layered media bounded by coal seams. *Geophysics* 57, 1209-1216.

Goulty, N.R., Thatcher, J.S., Findlay, M.J., Kragh, J.E. & Jackson, P.D. 1990. Experimental investigation of crosshole seismic techniques for shallow coal exploration. *Quarterly Journal of Engineering Geology* 23, 217-228.

Goulty, N.R., Leggett, M., Douglas, T. & Emeleus, C.H. 1992. Seismic reflection test on the granite of the Skye Tertiary igneous centre. *Geological Magazine* 129(3), 633-636.

Gustavsson, M., Ivansson, S., Moren, P. & Pihl, J. 1986. Borehole tomography - measurement system and field studies. *Proceedings of the IEEE* 74, 339-346.

Hardage, B.A. 1992. *Crosswell seismology and reverse VSP. (Seismic Applications Series, Vol. 1).* Geophysical Press, London.

Harris, J.M. 1988. Cross-well seismic measurements in sedimentary rocks. 58th Meeting, Society of Exploration Geophysicists, Expanded Abstracts, 147-150.

Ivansson, S. 1987. Crosshole transmission tomography. In *Seismic Tomography*, G.Nolet (ed.), 159-188. D. Reidel, Hingham, Mass.

Jackson, P.J. 1985. Horizontal seismic in coal seams: Its use in the U.K. coal industry. *First Break* 3(11), 15-24.

Justice, J.H., Vassilou, A.A., Singh, S., Logel, J.D., Hansen, P.A., Hall, B.R., Hutt, P.R. & Solanki, J.J. 1989. Acoustic tomography for monitoring enhanced oil recovery. *The Leading Edge* 8(2), 12-19.

Kaye, G.W.C & Laby, T.H. 1973. *Tables of Physical and Chemical constants and some Mathematical Functions.* Longman, London.

Körmendi, A., Bodoky, T., Hermann, L., Dianiska, L. & Kalman, T. 1986. Seismic measurements for safety in mines - case histories. *Geophysical Prospecting* 34, 1022-1037.

Kragh, J.E., Goulty, N.R. & Findlay, M.J. 1991. Hole-to-surface seismic reflection surveys for shallow coal exploration. *First Break* 9, 335-344.

Kragh, J.E., Goulty, N.R. & Brabham, P.J. 1992. Surface and hole-to-surface seismic reflection profiles in shallow Coal Measures. *Quarterly Journal of Engineering Geology* 25, 217-266.

Krajewski, C., Dresen, L. & Gelbke, C. 1989. Iterative tomographic methods. *Geophysical Prospecting* 37, 717-751.

Larner, K. & Hatton, L. 1990. Wave equation migration: two approaches. *First Break* 8(12), 433-448.

Leggett, M., Goulty, N.R. & Kragh, J.E. (In press). Study of traveltime and amplitude time-lapse tomography using physical model data. *Geophysical Prospecting.*

Lendzionowski, V. 1986. *Tomographic inversion of cross-borehole seismic data.* Unpublished M.Sc. dissertation, University of Durham.

Macrides, G.G., Kanasewich, E.R. & Bharatha, S. 1988. Multiborehole seismic imaging in steam injection heavy oil recovery projects. *Geophysics* 53, 65-75.

March, D.W. & Bailey, A.D. 1983. A review of the two dimensional transform and its use in signal processing. *First Break* 1(1), 9-21.

Marion, D. & Nur, A. 1991. Pore-filling material and its effect on velocity in rocks. *Geophysics* 56, 225-230.

Miller, D., Oristaglio, M. & Beylkin, G. 1987. A new slant on seismic imaging: migration and integral geometry. *Geophysics* **52**, 943-964.

Murphy, W.F. 1982. Effects of partial water saturation on attenuation in Massilon sandstone and Vycor porous glass. *Journal of the Acoustical Society of America* **71**, 1458-1468.

Murphy, W.F. 1984. Acoustic measures of partial gas saturation in tight sandstones. *Journal of Geophysical Research* **89**, 11549-11559.

Newman, P. 1990. Amplitude and phase properties of a digital migration process. *First Break* **8**(11), 397-403.

Nur, A. 1987. Seismic rock properties for reservoir descriptions and monitoring. in *Seismic Tomography*, G.Nolet (ed.), 203-237. D. Reidel, Hingham, Mass.

Pratt, R.G., Li Quan, Dyer, B.C., Goulty, N.R. & Worthington, M.H. 1991. Algorithms for EOR imaging: an experiment with scale model data. *Geoexploration* **28**, 193-220

Pratt, R.G. & Goulty, N.R. 1991. Combining wave-equation imaging with traveltime tomography to form high-resolution images from cross-hole data. *Geophysics* **56**, 208-224.

Pratt, R.G. & Worthington, M.H. 1988. The application of diffraction tomography to crosshole seismic data. *Geophysics* **53**, 1284-1294.

Radcliff, R.P., Balanis, C.A. & Hill, H.W. 1984. A stable geotomography technique for refractive media. *IEEE Transactions on Geoscience and Remote Sensing* **22**, 698-703.

Robinson, E.A., Treitel, S. 1985. *Geophysical Signal Analysis.* Prentice-Hall, New Jersey.

Schneider, W.A. 1978. Integral formulation for migration in two and three dimensions. *Geophysics* **43**(1), 49-76.

Sharp, R.J., Peacock, J.H. & Goulty, N.R. 1985. *Ultrasonic seismic modelling system.* Presented at the 47th EAEG Meeting, Budapest.

Taner, M.T., Koehler, F. & Sheriff, R.E. 1979. Complex seismic trace analysis. *Geophysics* 44, 1041-1063.

Thompson, R.N. 1969. Tertiary granites and associated rocks of the Marsco area, Isle of Skye. *Quarterly Journal of the Geological Society of London* 124, 349-385.

White, J.E. & Sengbush, R.L. 1963. Shear waves from explosive sources. *Geophysics* 28, 1001-1019.

Widess, M.B. 1973. How thin is a thin bed? *Geophysics* 38, 1176-1180.

Winbow, G.A. 1991. Seismic sources in open and cased boreholes. *Geophysics* 56, 1040-1050.

Winkler, K. & Nur, A. 1982. Seismic attenuation : effects of pore fluids and frictional gliding. *Geophysics* 47, 1-15.

Wong, J., Hurley, P. & West, G.F. 1983. Cross-hole seismology and seismic imaging in crystalline rock. *Geophysics Research Letters* 10, 686-689.

Worthington, M.H. 1984. An introduction to geophysical tomography. *First Break* 2(11), 20-26.

Wye, R. 1986. *An investigation into the accuracy of algebraic reconstruction techniques for tomographic inversion.* Unpublished M.Sc. dissertation, University of Durham.

Ziolkowski, A. 1979. Seismic profiling for coal on land. in *Developments in geophysical exploration methods.* A.A. Fitch (ed), Vol. 1, 271-306. Applied Science Publishers Ltd., London.

Appendix A

SIRT inversion scheme and computer software

This appendix gives a brief outline of how to perform a SIRT inversion using the program available in the Department of Geological Sciences, and also lists the few programs and subroutines that I have written. Programs that have merely been altered by me for use with my data are not listed here. External subroutines include the UNIRAS (version 6v2a) plotting library, a library of time-series analysis subroutines from various sources (tsasub.f in user-id dgl3ml on the unix system in the Department). All programs are written in Fortran77 to run on a Sun4. There are some c-shell scripts also written to make life easier when compiling and linking programs.

Other subroutines that have been used are all on public domain on the computer system in the Department of Geological Sciences. These are all from various sources, including some in-house software. All software on user-identifier dgl3ml is commented and has README files to explain how to run the programs, and which versions to use. Parameter statements at the head of each program should be checked and altered to suit the needs of the user.

Appendix A.1

SIRT inversion scheme

The SIRT inversion programs prompt for input as it is run and has various options, including use of gradient fields, back-projection for an initial velocity field, weighting schemes and fixing of velocities in cells. Plotting of velocity tomograms requires a different program, shade1.f for tank data or contour.f which is a general contouring routine. An outline of a SIRT inversion scheme, data formats, etc is given.

SIRT inversion .... or how it all works!!!!

Miles Leggett 31/3/92 - 9/92

Data format :
~~~~~~~~~~~~

THE SUBROUTINE READD READS DATA FOR TOMOGRAPHIC INVERSION
it allows for up to 5 lines of header of up to 60 characters
input files should have header, followed by 2 labels for
number of shots & receivers, on the same line; with the no.s
below, on the next line, followed by no dead times (edited!)-if any.
on the next line input files should have 5 labels, for the
x,z coords of source & receiver, and for the travel times.
below these labels put columns of the appropriate data.
All data can be in unformatted form with commas in-between
or spaces, or even formatted!

e.g.
Lostrigg first breaks

```
~~~~~~~~~~~~~~~~~~~~~~~~~~~~~~~~~~~~~~~~~~~~~~~~~~~~~~~~
No. of shots            No. of receivers    no. edited shots
 29.0                   34.0          0
XSHOT   ZSHOT   XREC   ZREC    TTIME
 0.0    16.0   47.00   1.0   0.02020000    101
 0.0    16.0   47.00   0.0   0.01980000     99
 0.0    16.0   47.00   0.0   0.01900000     95
 0.0    16.0   47.00   0.0   0.01860000     93
```

Velocity file format :
~~~~~~~~~~~~~~~~~~~~~

Two lines of header, followed by a label for number of cells
in total, number of cells in x, no cells in z ; nos on next line
(integers) ; next line has labels for box size, min/max x/z ; nos
on next line (real) ; next line is a line of text showing variances.
Velocities are one to a line, free format (or format f10.2,',')

e.g

```
Travel time inversion
Reconstructed velocity field after 3 iterations
   ICELLS    ICELLX    ICELLZ
   1196,       23,        52,
 BOXX    BOXZ    XMIN    ZMIN
  2.50,   2.50,   0.00,   0.00,
OPT VARS : 0.100000E+01 0.868816E-03 0.000000E+00 0.000000E+00
0.000000E+00
  1477.00,
  1477.00,
  2335.00,
  2335.00,
  2335.00,
  2335.00,
  2335.00,
  2335.00,
  2335.00,
  2335.00,
  2335.00,
  2335.00,
```

Raypath information :
~~~~~~~~~~~~~~~~~~~~~

At present this is written to /ts/kanga/miles/PATHS, in format :
first line is no cells where ray length is not zero ; then followed
by this number of lines - cell no, length. Done for all rays.

1/4/92
No longer!!!! You have to input the name of the file to the
program, at the prompt

Inputs to CSIRT :
~~~~~~~~~~~~~~~~

.... an example below!!!!!!!!

```
2                 lraytrace for all iterations??
```
```

```
/ts/kanga/miles/PATHS   !file for raypath information
2.0                     !constraint for smoothing
0.0                     !angle for shallow ray arc in radians if gt 0.0 get grads in
boxes
0.00332349              !ray search angle
500                     !max no. trials in each search
0.5                     !required accuracy of receiver points
tom.9                   !file to read
2                       !no. lines of header
0. 0.                   !Origin shift   will shift the origin by dx dz
Y                       !coord shift? answer is YES !!!
2.5 2.5                 !cell dimension
F                       !initial velocity  Gradient/File/Bpv (BPV dummy dummy)
modelv1                 !velocity file name or dummy
2                       !no. lines header or dummy
N                       !smoothing between iterations
Y                       !window part of field
1                       !input from screen
0,57.5                  !window size in x
0,130                   ! in z
2                       !no. bodies to fix
1477                    !velocity
0,5                     !x coords
0,130                   !z coords
1477                    !velocity
52.5,57.5               !x coords
0,130                   !z coords
10                      !exit to main program
N                       !raylength weighting option
Y                       !raylength weighting for length of path in box
'outvel'                !BASIC filename for output vel fields
Travel time inversion   !Velocity file header
2220022.                !Max velocity allowed for inversion
100.                    !Min vel for solution
1.                      !damp factor 1.=none 0.= opt damp
10                      !total no. of iterations
1                       !1=SIRT 2=ART 0=SVD (if hds Y .02 1.0 )
```

```
0                       !Zero rays in cell - vels not known
N                       !No further inversions requ'd
```

To compile & link ..... use fsirt (just type and respond to prompts) .... this is an executable c-shell script.

Option to raytrace just once through a known model (1) or raytrace for each iteration (2).

If use gradient option, also have options for homogeneous field, back-projection field (set VOFLAG = 1 , 3 respectively in csirt2.f)

vel_create.f ..... compile & run .... this creates a velocity file for input to SIRT inversion programs. Velocity field is flat i.e. same value over whole field.

contour.f ..... plotting routine, contours traveltime or amplitude tomographic data from same format file as above. Uses UNIRAS. compile using ..... unilink contour.f

30/9/92

Velocity output files ..... with basic filename (input to csirt), this routine will handle up to 60 iterations (i.e. will put the right numbers onto the files etc). Filenames will be 'basic filename' concatenated with the iteration number.

Appendix A.2

Selective smoothing subroutine

The subroutine SUBSM is the selective smoothing routine as described previously in Chapter II. The input velocity field is returned smoothed to the main program on exit.

```
C-----------------------------------------------------------
C  Program to smooth a velocity field by using selective smoothing
C  algorithm of Radcliff,Balanis and Hill (1984) combinsd with
C  weighting factors suggested by Dines and Lytle  (1979).....this
C  helps suppress statistical pseudo-anomalies without blurring contours
C  of the actual anomalies. From Christina Krajewski et al , Geophys
C  Prosp. , 37 , Oct 1989 , pp 717-751
C
C  CONSTR  is the constraint value ( % DIFFERENCE )
C  WT1 , WT2(4) are weighting factors
C
C  At the edge of the grid , the "neighbouring cell outside"
C  ( a fictitious cell ), is assumed to have the same slowness
C  value as the cell itself.
C-----------------------------------------------------------
      SUBROUTINE SMOOTH(VEL,ICELLS,ICELLX,ICELLZ,CONSTR)
C-----------------------------------------------------------
      REAL  VEL(1600 ),VEL1(1600)
      REAL  CONSTR,VDIFF
      INTEGER  ICELLS,WT1,WT2(4)
      INTEGER  ICELLX,ICELLZ
      INTEGER  I,J
      INTEGER  ICELL
      INTEGER  ICOL,IROW
C
C
C
      ICELXZ = ICELLX*ICELLZ
C
C
C     CONSTR = 2.0
      ICELL=1
      DO 123 J=1,ICELXZ
      IF(VEL(J).EQ.0.0) VEL(J)=0.00001
  123 CONTINUE
C
C  SMOOTH THE CELL VELOCITIES
C
      DO 100 , IROW=1,ICELLZ
       DO 200, ICOL=1,ICELLX
C
       DO 700 I=1,4
       WT2(I) = 1
  700  CONTINUE
C
C  SMOOTH THE MAIN BODY OF THE DATA
C
       IF((IROW.GT.1).AND.(IROW.LT.ICELLZ).AND.
     K    (ICOL.GT.1).AND.(ICOL.LT.ICELLX)) THEN
C
        WT1=4
        VDIFF = ABS((VEL(ICELL)-VEL(ICELL+1))*100/VEL(ICELL))
        IF(VDIFF.GT.CONSTR)THEN
         WT1 = WT1 + 1
         WT2(1)=0
        ENDIF
        VDIFF = ABS((VEL(ICELL)-VEL(ICELL-1))*100/VEL(ICELL))
        IF(VDIFF.GT.CONSTR)THEN
         WT1 = WT1 + 1
         WT2(2)=0
        ENDIF
        VDIFF = ABS((VEL(ICELL)-VEL(ICELL+ICELLX))*100/VEL(ICELL))
        IF(VDIFF.GT.CONSTR)THEN
         WT1 = WT1 + 1
         WT2(3)=0
        ENDIF
        VDIFF = ABS((VEL(ICELL)-VEL(ICELL-ICELLX))*100/VEL(ICELL))
        IF(VDIFF.GT.CONSTR)THEN
         WT1 = WT1 + 1
         WT2(4)=0
        ENDIF
           VEL1(ICELL)=( WT1*VEL(ICELL) + WT2(1)*VEL(ICELL+1)
     K        +WT2(2)*VEL(ICELL-1) + WT2(3)*VEL(ICELL+ICELLX)
     K        +WT2(4)*VEL(ICELL-ICELLX) )/
     K        (WT1 + WT2(1) + WT2(2) + WT2(3) + WT2(4) )
C
        ENDIF
C
       DO 701 J=1,4
       WT2(J) = 1
  701  CONTINUE
C
C  SMOOTH THE TOP ROW
C
       IF((IROW.EQ.1).AND.(ICOL.GT.1).AND.(ICOL.LT.ICELLX)) THEN
        WT1 = 5
        WT2(1) = 0
        VDIFF = ABS((VEL(ICELL)-VEL(ICELL+1))*100/VEL(ICELL))
        IF(VDIFF.GT.CONSTR) THEN
         WT1 = WT1 + 1
         WT2(2) = 0
        ENDIF
        VDIFF = ABS((VEL(ICELL)-VEL(ICELL-1))*100/VEL(ICELL))
        IF(VDIFF.GT.CONSTR) THEN
         WT1 = WT1 + 1
         WT2(3) = 0
        ENDIF
        VDIFF = ABS((VEL(ICELL)-VEL(ICELL+ICELLX))*100/VEL(ICELL))
        IF(VDIFF.GT.CONSTR) THEN
         WT1 = WT1 + 1
         WT2(4) = 0
        ENDIF
C
           VEL1(ICELL)=( WT1*VEL(ICELL) + WT2(1)*VEL(ICELL)
     K        + WT2(2)*VEL(ICELL+1) +WT2(3)*VEL(ICELL-1)
     K           +WT2(4)*VEL(ICELL+ICELLX)) /
     K        ( WT1 + WT2(1) + WT2(2) + WT2(3) + WT2(4) )
C
        ENDIF
C
       DO 702 I=1,4
       WT2(I) = 1
  702  CONTINUE
C
C  SMOOTH THE BOTTOM ROW
C
       IF((IROW.EQ.ICELLZ).AND.(ICOL.GT.1).AND.(ICOL.LT.ICELLX)) THEN
        WT1 = 5
        WT2(1) = 0
        VDIFF = ABS((VEL(ICELL)-VEL(ICELL+1))*100/VEL(ICELL))
        IF(VDIFF.GT.CONSTR) THEN
         WT1 = WT1 + 1
         WT2(2) = 0
        ENDIF
        VDIFF = ABS((VEL(ICELL)-VEL(ICELL-1))*100/VEL(ICELL))
        IF(VDIFF.GT.CONSTR) THEN
         WT1 = WT1 + 1
         WT2(3) = 0
        ENDIF
        VDIFF = ABS((VEL(ICELL)-VEL(ICELL+ICELLX))*100/VEL(ICELL))
        IF(VDIFF.GT.CONSTR) THEN
         WT1 = WT1 + 1
         WT2(4) = 0
        ENDIF
C
           VEL1(ICELL)=( WT1*VEL(ICELL) + WT2(1)*VEL(ICELL)
     K        + WT2(2)*VEL(ICELL+1) +WT2(3)*VEL(ICELL-1)
     K           +WT2(4)*VEL(ICELL+ICELLX))/
     K        ( WT1 + WT2(1) + WT2(2) + WT2(3) + WT2(4) )
C
        ENDIF
C
       DO 703 I=1,4
       WT2(I) = 1
  703  CONTINUE
C
C  SMOOTH THE LEFT HAND COLUMN
C
       IF((ICOL.EQ.1).AND.(IROW.GT.1).AND.(IROW.LT.ICELLZ)) THEN
C
        WT1 = 5
        WT2(1) = 0
        VDIFF = ABS((VEL(ICELL)-VEL(ICELL+1))*100/VEL(ICELL))
        IF(VDIFF.GT.CONSTR) THEN
         WT1 = WT1 + 1
         WT2(2) = 0
        ENDIF
        VDIFF = ABS((VEL(ICELL)-VEL(ICELL-ICELLX))*100/VEL(ICELL))
        IF(VDIFF.GT.CONSTR) THEN
         WT1 = WT1 + 1
         WT2(3) = 0
        ENDIF
        VDIFF = ABS((VEL(ICELL)-VEL(ICELL+ICELLX))*100/VEL(ICELL))
        IF(VDIFF.GT.CONSTR) THEN
         WT1 = WT1 + 1
         WT2(4) = 0
        ENDIF
C
           VEL1(ICELL)=( WT1*VEL(ICELL) + WT2(1)*VEL(ICELL)
     K        + WT2(2)*VEL(ICELL+1) +WT2(3)*VEL(ICELL-ICELLX)
     K           +WT2(4)*VEL(ICELL+ICELLX))/
     K        ( WT1 + WT2(1) + WT2(2) + WT2(3) + WT2(4) )
C
        ENDIF
C
       DO 704 I=1,4
       WT2(I) = 1
  704  CONTINUE
C
C  SMOOTH THE RIGHT HAND COLUMN
C
       IF((ICOL.EQ.ICELLX).AND.(IROW.GT.1).AND.(IROW.LT.ICELLZ)) THEN
C
        WT1 = 5
        WT2(1) = 0
        VDIFF = ABS((VEL(ICELL)-VEL(ICELL-1))*100/VEL(ICELL))
        IF(VDIFF.GT.CONSTR) THEN
         WT1 = WT1 + 1
```

```
      WT2(2) = 0
      ENDIF
      VDIFF = ABS((VEL(ICELL)-VEL(ICELL-ICELLX))*100/VEL(ICELL))
      IF(VDIFF.GT.CONSTR) THEN
      WT1 = WT1 + 1
      WT2(3) = 0
      ENDIF
      VDIFF = ABS((VEL(ICELL)-VEL(ICELL+ICELLX))*100/VEL(ICELL))
      IF(VDIFF.GT.CONSTR) THEN
      WT1 = WT1 + 1
      WT2(4) = 0
      ENDIF
C
        VEL1(ICELL)=( WT1*VEL(ICELL) + WT2(1)*VEL(ICELL)
     K       + WT2(2)*VEL(ICELL-1) +WT2(3)*VEL(ICELL-ICELLX)
     K            +WT2(4)*VEL(ICELL+ICELLX))/
     K       ( WT1 + WT2(1) + WT2(2) + WT2(3) + WT2(4) )
      ENDIF
C
      DO 705 I=1,4
      WT2(I) = 1
  705 CONTINUE
C
C  DO THE CORNERS
C
C     TOP LEFT CORNER
C
C
      IF((IROW.EQ.1).AND.(ICOL.EQ.1)) THEN
C
      WT1 = 6
      VDIFF=ABS((VEL(ICELL)-VEL(ICELL+ICELLX))*100/VEL(ICELL))
      IF(VDIFF.GT.CONSTR) THEN
      WT1 = WT1 + 1
      WT2(1) = 0
      ENDIF
      VDIFF=ABS((VEL(ICELL)-VEL(ICELL+1))*100/VEL(ICELL))
      IF(VDIFF.GT.CONSTR) THEN
      WT1 = WT1 + 1
      WT2(2) = 0
      ENDIF
        VEL1(ICELL)=(WT1*VEL(ICELL)+WT2(2)*VEL(ICELL+1)
     K          +WT2(1)*VEL(ICELL+ICELLX))/
     K     ( WT1 + WT2(1) + WT2(2) )
C
      ENDIF
C
      DO 706 I=1,4
      WT2(I) = 1
  706 CONTINUE
C
C     TOP RIGHT CORNER
C
      IF((IROW.EQ.1).AND.(ICOL.EQ.ICELLX)) THEN
C
      WT1 = 6
      VDIFF=ABS((VEL(ICELL)-VEL(ICELL+ICELLX))*100/VEL(ICELL))
      IF(VDIFF.GT.CONSTR) THEN
      WT1 = WT1 + 1
      WT2(1) = 0
      ENDIF
      VDIFF=ABS((VEL(ICELL)-VEL(ICELL-1))*100/VEL(ICELL))
      IF(VDIFF.GT.CONSTR) THEN
      WT1 = WT1 + 1
      WT2(2) = 0
      ENDIF
        VEL1(ICELL)=(WT1*VEL(ICELL)+WT2(2)*VEL(ICELL-1)
     K          +WT2(1)*VEL(ICELL+ICELLX))/
     K     ( WT1 + WT2(1) + WT2(2) )
C
      ENDIF
C
      DO 707 I=1,4
      WT2(I) = 1
  707 CONTINUE
C
C     BOTTOM LEFT CORNER
C
      IF((IROW.EQ.ICELLZ).AND.(ICOL.EQ.1)) THEN
C
      WT1 = 6
      VDIFF=ABS((VEL(ICELL)-VEL(ICELL-ICELLX))*100/VEL(ICELL))
      IF(VDIFF.GT.CONSTR) THEN
      WT1 = WT1 + 1
      WT2(1) = 0
      ENDIF
      VDIFF=ABS((VEL(ICELL)-VEL(ICELL+1))*100/VEL(ICELL))
      IF(VDIFF.GT.CONSTR) THEN
      WT1 = WT1 + 1
      WT2(2) = 0
      ENDIF
        VEL1(ICELL)=(WT1*VEL(ICELL)+WT2(2)*VEL(ICELL+1)
     K          +WT2(1)*VEL(ICELL-ICELLX))/
     K     ( WT1 + WT2(1) + WT2(2) )
C
      ENDIF
C
      DO 708 I=1,4
      WT2(I) = 1
  708 CONTINUE
C
C     BOTTOM RIGHT CORNER
C
      IF((IROW.EQ.ICELLZ).AND.(ICOL.EQ.ICELLX)) THEN
C
      WT1 = 6
      VDIFF=ABS((VEL(ICELL)-VEL(ICELL-ICELLX))*100/VEL(ICELL))
      IF(VDIFF.GT.CONSTR) THEN
      WT1 = WT1 + 1
      WT2(1) = 0
      ENDIF
      VDIFF=ABS((VEL(ICELL)-VEL(ICELL-1))*100/VEL(ICELL))
      IF(VDIFF.GT.CONSTR) THEN
      WT1 = WT1 + 1
      WT2(2) = 0
      ENDIF
        VEL1(ICELL)=(WT1*VEL(ICELL)+WT2(2)*VEL(ICELL-1)
     K          +WT2(1)*VEL(ICELL-ICELLX))/
     K     ( WT1 + WT2(1) + WT2(2) )
C
      ENDIF
C
      DO 709 I=1,4
      WT2(I) = 1
  709 CONTINUE
C
C  INCREMENT THE CELL NUMBER
C
       ICELL=ICELL+1
C
      DO 710 I=1,4
      WT2(I) = 1
  710 CONTINUE
C
  200  CONTINUE
  100 CONTINUE
C
C
      DO 124 J=1,ICELXZ
      IF(VEL1(J).EQ.0.00001) VEL1(J) = 0.0
      VEL(J) = VEL1(J)
  124 CONTINUE
      RETURN
      END
```

Appendix A.3

Contouring/shading software

There are two contouring and shading routines, the first for the data from the tank, shade1.f, which takes into account the cells for the water layer. The second, contour.f, is a general contouring, shading program for output from a SIRT inversion. Both use UNIRAS subroutines and are menu-driven. Hardcopy output can be obtained in colour, greyscale or a white-black scheme.

```
      program shade1

c nx,ny : dimensions of grid.
c ncl   : number of contouring levels.
c Program to contour/shade velocity or attenuation values
c from a SIRT inversion scheme....for tank data at present.
c

      parameter (m=5,iundef=9999,icelk=1196)
      parameter (rundef=999.999)

      real zcl(2),vel(19,50),smth,vel1(19,50)
      real scax(7),scay(7)
      integer lenar1(4),lenar2(3),kol(m),coli(6)
      integer nx,ny,mode,iorn
      character*1 txtar1(4),aval
      character*12 txtar2(3)
      character*40 disc
      character*72 dummy
      character acolr*6,aorn*8,acont*6,aplot*6,strin*24
c
c  set up default values.....
c
      txtar2(1) = 'metres/sec'
      txtar2(2) = 'velocity'
      txtar2(3) = ''
      disc = '      '
      acolr = 'Color'
      mode = 1
      iorn = 1
      icon = 0
      aval = 'v'
      ncl = 5
      aplot='screen'
      acont='off'
      aorn='portrait'
      acolr='colour'

  999 continue

      write(6,1)
      write(6,10)
      write(6,2)
      write(6,3)disc
      write(6,4)acolr
      write(6,5)aplot
      write(6,6)aorn
      write(6,7)acont
      write(6,8)aval
      write(6,9)ncl

    1 format(/,'  Shading / contour plot menu       : 0 = stop')
   10  format(/,'  ~~~~~~~~~~~~~~~~~~~~~~~~~~~~~~~~  ')
    2 format(/,'1 Plot data                        ')
    3 format(/,'2 File to read                     : ',a20)
    4 format(/,'3 Colour/greyscale/defined plot    : ',a6)
    5 format(/,'4 Plot (1) or metafile (2) ?       : ',a6)
    6 format(/,'5 Orientation 1=port, 2=landscape  : ',a8)
    7 format(/,'6 Contours on or off ?             : ',a6)
    8 format(/,'7 Velocity or attenuation ???(v or a): ',a1)
    9 format(/,'8 Number of contour levels required? : ',i2)
      read(5,*) iopt
      if(iopt.eq.1)goto 1033
      if(iopt.eq.2)then
      print*,'enter file containing data'
      read(5,113) disc
  113 format(a40)
 1999 open(unit=2,file=disc,status='old',form='formatted',
     &     iostat=k2,err=92)
   92   if (k2.ne.0) then
          print*,'file does not exist'
          print *, 'enter a new filename'
          print *, 'filename = exit goes back to main menu'
          read (5,113) disc
          if(disc.eq.'exit')goto 999
          goto 1999
        endif
c read data
      do 114 i=1,3
      read(2,115) dummy
  115 format(a72)
  114 continue

      read(2,*)xdum,icellx,icellz
      read(2,115) dummy
      read(2,*) boxx
      read(2,115) dummy

      ny = 50
      nx = 19

      icells = icellx*icellz
      print*,icellx,icellz,icells
c
c read & flip order round in y
c
       do 310 i=1,icellz-2

        read(2,*)dwm
        read(2,*)dwm

        do 311 j=1,nx
          read(2,*) vel1(j,i)
  311   continue

        if(icellx.eq.23)then
        read(2,*)dwm
        read(2,*)dwm
        elseif(icellx.eq.22)then
        read(2,*)dwm
        endif

  310 continue

      vmin = vel1(12,12)
      vmax = vel1(12,12)

      do 116 i=1,icellz-2

        do 117 j=1,nx
          inck = ny - i + 1
          vel(j,i) = vel1(j,inck)
          if(vel(j,i).lt.vmin)vmin = vel(j,i)
          if(vel(j,i).gt.vmax)vmax = vel(j,i)
  117   continue

  116 continue
      close(unit=2)

      endif
      if(iopt.eq.3)then
      print*,'Enter 1 for a colour plot, 2 for pre-defined '
      print*,' white-black and 3 for greyscale  '
      read(5,*) icolr
      if(icolr.eq.1)acolr = 'Colour'
      if(icolr.eq.3)acolr = 'Greysc'
      if(icolr.eq.2)then
      acolr = 'Wh-Bl'
      if(ncl.gt.5)print*,' Only five contour levels allowed!'
      data coli /33,31,30,29,28,32/
c     data coli /33,31,15,30,29,14,28,32/
      ncl = 5
      endif
      endif
      if(iopt.eq.4)then
      read(5,346) mode
  346 format(i1)
      if(mode.eq.1)aplot='screen'
      if(mode.eq.2)aplot='plfile'
      endif
      if(iopt.eq.5)then
      read(5,*) iorn
      if(iorn.eq.1)aorn='portrait'
      if(iorn.eq.2)aorn='lndscape'
      endif
      if(iopt.eq.6)then
      print*,'  Enter 1=on , 0=off '
      read(5,*) icon
      if(icon.eq.1)acont='on'
      if(icon.eq.0)acont='off'
      endif
      if(iopt.eq.7) then
      print*,'v for vel, a for attn, s for slowness, q for Q'
      read(5,164) aval
  164 format(a1)
      if(aval.eq.'a')then
      txtar2(2) = 'absorption'
      txtar2(1) = 'nepers / m'
      txtar2(3) = ''
      elseif(aval.eq.'v')then
      txtar2(1) = 'metres/sec'
      txtar2(2) = 'velocity'
      txtar2(3) = ''
      elseif(aval.eq.'q')then
      txtar2(2) = 'Quality'
      txtar2(1) = 'factor (Q)'
      txtar2(3) = ''
      elseif(aval.eq.'s')then
      txtar2(1) = ' '
      txtar2(2) = 'slowness'
      txtar2(3) = ''
      endif
      endif
      if(iopt.eq.8)read(5,*)ncl
      if(iopt.eq.0)then
      stop
      else
```

```
      goto 999
      endif

 1033 continue

c  data read.....plotting begins!
c user coordinate limits.

      data   xmin,xmax,ymin,ymax,zmin,zmax
     .    / 0.0,46.5,0.0,125.0,0.0,0.0/
c smallest contouring level and distance between levels.


c contour line widths and colors.
c
      data wi /-0.1 /
      data kol / m*1 /
c
c character string lengths of axis texts and axis
c text strings. no axis texts are to be plotted.
c
      data lenar1 /4*0/
      data txtar1 /4*' '/
c
cc character string lengths and character strings
c for color scale.
c
      data lenar2 /12,10,0/
c
c open uniras.
      print*,'Starting plotting....'
c
      if(mode.eq.1) then
      call gbegin('Select mx11;exit',' '
     . ,'tomo.pic')
      else
      call groute('LIST')
      call gopen
      endif
c set limits and viewport.
c
      call glimit(xmin,xmax,ymax,ymin,zmin,zmax)
      call gvport(20.0,20.0,70.,220.)
c set contour levels.
      zcl(1) = vmin
      zcl(2) = vmax
      print*,'min value =  ',vmin
      print*,'max value =  ',vmax
      print*,'Enter 1 if you want to set up your own limits'
      read(5,*)ilim
c
      if(ilim.eq.1)then
       print*,'Enter lowest limit, step'
       read(5,*) rlim,cstep
      if(cstep.eq.0.0)then
       iplpt = 3
       zcl(1) = 0.0
       zcl(2) = vmax
       else
       zcl(1) = rlim
       zcl(2) = cstep
       iplpt = 5
      endif
       call rclass(zcl,ncl,iplpt)
      else
       call rclass(zcl,ncl,3)
      endif
c
c select a grey scale suitable for the plots in
c this manual.
       call rcsird
       if(icolr.eq.2) then
       call rfdcol(33)
       call rshade(coli,6)
       else
       call rshade(icolr,0)
       endif
c
c do the  shaded contour plot.
c
      smth = 5.
      call gconsm(smth)
      call gcnr2s(vel,nx,ny)
c
c contour lines are plotted on top of the shaded map
c by gcnr2v. set contour line widths and colors.
c
      call gconwi(-1.0,1)
      call gconco(kol,1)
      height = 0.015*min(70.0,220.0)
c
c
      if(icon.eq.1) then
      call gconsm(smth)
      call gcnr2v(vel,nx,ny)
      endif
c
c plot four axes. to make room for a
c color scale, the y-axis to the right is
c plotted without numeric labels.
c
      call gscale
      call raxlas(2)
      call raxdis(2,1,0)
      call raxdis(3,0,0)
      call raxdis(4,0,0)
      call raxdis(5,0,0)
      call raxdis(6,0,0)
      call raxdis(8,0,0)
      call raxis2(ymin,xmin,height,lenar1,txtar1)
      call raxis(1,ymax,height,1)
      call raxis(2,xmax,height,2)
c
c
c
c plot a color scale.
c
      call rbfont('swil',1)
      call rbspf(0.15)
      if(aval.eq.'a')then
      idec = 5
      elseif(aval.eq.'v')then
      idec = 1
      else
      idec = 1
      endif
      call gclopt(lenar2,txtar2,4.0*height,idec,0.0,1)
      call gcoscl(xmax+0.1*(xmax-xmin),ymax)
c
c give the plot a title.
c
      tpy = ymax-0.05*(ymin-ymax)
      tpx = 0.5*(xmin+xmax)
      call rbjus(1,3)
      call rbhei(5.0)
      scax(1)=xmax+11.
      scay(1)=ymax-34.
      scax(2)=xmax+11.
      scay(2)=ymax-33.
      scax(3)=xmax+21.
      scay(3)=ymax-33.
      scax(4)=xmax+21.
      scay(4)=ymax-34.
      scax(5)=xmax+21.
      scay(5)=ymax-33.
      scax(6)=xmax+31.
      scay(6)=ymax-33.
      scax(7)=xmax+31.
      scay(7)=ymax-34.
      call gvect(scax,scay,7)
      call rbhei(3.0)
      call rbx(-1,'0',xmax+11.,ymax-37.)
      call rbx(-1,'10',xmax+21.,ymax-37.)
      call rbx(-1,' 20 m',xmax+31.,ymax-37.)
      if(mode.eq.2) then
      call gend
      else
      call gclose
      endif
      if(iopt.ne.0)goto 999
      stop
      end
```

```
      program contour

c icellx,icellz : dimensions of grid.
c ncl   : number of contouring levels.
c Program to contour/shade velocity or attenuation values
c from a SIRT inversion scheme.....general case!!
c Miles Leggett 1992
c
c     parameter (m=5,iundef=9999,rundef=999.999)
      real vel(2000),coord(6),vpl(100,100),vel1(100,100)
      integer lenar1(4),lenar2(3)
      integer icellx,icellz,mode,iorn
      character*1 txtar1(4),aval
      character*12 txtar2(3)
      character*40 disc
      character*72 dummy
      character acolr*6,aorn*8,acont*6,aplot*6
c
c  set up default values.....
c
      disc = '         '
      acolr = 'Color'
      mode = 1
      iorn = 1
      icon = 0
      aval = 'v'
      ncl = 5
      aplot='screen'
      acont='off'
      aorn='portrait'
      acolr='colour'

 999  continue

      write(6,1)
      write(6,10)
      write(6,2)
      write(6,3)disc
      write(6,4)acolr
      write(6,5)aplot
      write(6,6)aorn
      write(6,7)acont
      write(6,8)aval
      write(6,9)ncl

 1    format(/,'   Shading / contour plot menu        : 0 = stop')
 10    format(/,'   ------------------------------------     ')
 2    format(/,'1  Plot data                       ')
 3    format(/,'2  File to read                       : ',a20)
 4    format(/,'3  Colour/greyscale/defined plot      : ',a6)
 5    format(/,'4  Screen (1) or metafile (2)        : ',a6)
 6    format(/,'5  Orientation 1=port, 2=landscape    : ',a8)
 7    format(/,'6  Contours on or off ?               : ',a6)
 8    format(/,'7  Velocity or attenuation ???(v or a): ',a1)
 9    format(/,'8  Number of contour levels required? : ',i2)

      read(5,*) iopt
      if(iopt.eq.1)goto 1033
      if(iopt.eq.2)then
      print*,'enter file containing data'
      read(5,113) disc
 113  format(a40)
```

```
 1999 open(unit=222,file=disc,status='old',form='formatted',
   &     iostat=k2,err=92)
  92   if (k2.ne.0) then
       print*,'file does not exist'
       print *, 'enter a new filename'
       print *, 'filename = exit goes back to main menu'
       read (5,113) disc
       if(disc.eq.'exit')goto 999
       goto 1999
      endif
c  read data
      do 114 i=1,3
      read(222,115) dummy
 115  format(a72)
 114  continue

      read(222,*)xdum,icellx,icellz
      read(222,115) dummy
      read(222,*) boxx,boxz
      read(222,115) dummy


      icells = icellx*icellz
      print*,icells,boxx,boxz
      do 1233 j = 1 , icells
      read(222,*) vel(j)
 1233 continue

      close(unit=222)

      endif
      if(iopt.eq.3)then
      print*,'Enter 1 for a colour plot, 2 for pre-defined '
      print*,' white-black and 3 for greyscale   '
      read(5,*) icolr
      if(icolr.eq.1)acolr = 'Colour'
      if(icolr.eq.3)acolr = 'Greysc'
      if(icolr.eq.2)then
      acolr = 'Wh-Bl'
      if(ncl.gt.5)print*,' Only five contour levels allowed!'
      ncl = 5
      endif
      endif
      if(iopt.eq.4)then
      read(5,346)mode
 346  format(i1)
      if(mode.eq.1)aplot='screen'
      if(mode.eq.2)aplot='plfile'
      endif
      if(iopt.eq.5)then
      read(5,*) iorn
      if(iorn.eq.1)aorn='portrait'
      if(iorn.eq.2)aorn='lndscape'
      endif
      if(iopt.eq.6)then
      print*,'  Enter 1=on , 0=off '
      read(5,*) icon
      if(icon.eq.1)acont='on'
      if(icon.eq.0)acont='off'
      endif
      if(iopt.eq.7) then
      print*,'v for vel, a for attn, s for slowness, q for Q'
      read(5,164) aval
```

```
 164  format(a1)
      if(aval.eq.'a')then
      txtar2(2) = 'absorption'
      txtar2(1) = 'napers / m'
      txtar2(3) = ''
      elseif(aval.eq.'v')then
      txtar2(1) = 'metres/sec'
      txtar2(2) = 'velocity'
      txtar2(3) = ''
      elseif(aval.eq.'q')then
      txtar2(2) = 'Quality'
      txtar2(1) = 'factor (Q)'
      txtar2(3) = ''
      elseif(aval.eq.'s')then
      txtar2(1) = ' '
      txtar2(2) = 'slowness'
      txtar2(3) = ''
      endif
      endif
      if(iopt.eq.8)read(5,*)ncl
      if(iopt.eq.0)then
      stop
      else
      goto 999
      endif

 1033 continue

c user coordinate limits.
        xmin = 0.0
        xmax = boxx * icellx
        ymin = 0.0
        ymax = boxz * icellz
        zmin = 0.0
        zmax = 0.0
        coord(1)=xmin
        coord(2)=xmax
        coord(3)=ymin
        coord(4)=ymax
        coord(5)=zmin
        coord(6)=zmax
c smallest contouring level and distance between levels.


c
c character string lengths of axis texts and axis
c text strings. no axis texts are to be plotted.
c
      data lenar1 /4*0/
      data txtar1 /4*' '/
c
cc character string lengths and character strings
c for color scale.
c
       data lenar2 /12,10,0/
c
      call subcont(coord,mode,ncl,lenar1,lenar2,txtar1,txtar2,
     1     icon,iorn,icolr,vel,icells,icellx,icellz,aval,vpl,vel1)

      if(iopt.ne.0)goto 999
      stop
      end
```

```
      subroutine subcont(coords,mode,ncl,lenar1,lenar2,txtar1,txtar2,
     1       icon,iorn,icolr,vel,lclls,icelx,icelz,aval,vpl,vel1)
c
c plotting subroutine
c
      parameter (m=5,lundef=9999,rundef=999.999)
      real scax(7),scay(7),zcl(2),vel1(icelx,icelz)
      real coords(6),vpl(icelx,icelz),vel(lclls)
      integer lenar1(4),lenar2(3)
      integer iorn,icolr,ncl,mode,coli(6),kol(m)
      character aval*1,txtar1(4)
      character*12 txtar2(3)

      xmin = coords(1)
      xmax = coords(2)
      ymin = coords(3)
      ymax = coords(4)
      zmin = coords(5)
      zmax = coords(6)

c
c read & flip order round in y
c
       itz = 0
       vmin = vel(1)
       vmax = vel(1)


       do 310 j=1,icelz

         do 311 i=1,icelx
           itz = i + (icelx)*(j-1)
           vpl(i,j) = vel(itz)
           if(vpl(i,j).lt.vmin)vmin = vpl(i,j)
           if(vpl(i,j).gt.vmax)vmax = vpl(i,j)

 311     continue

 310   continue

       do 116 i=1,icelz

         do 117 j=1,icelx
           inck = icelz - i + 1
           vel1(j,i) = vpl(j,inck)
 117     continue

 116   continue

c open unitas.
      print*,'Starting plotting....'
c contour line widths and colors.
c
      data kol / m*1 /
      data coli /33,31,30,29,28,32/
c     data coli /33,31,15,30,29,14,28,32/
c
      if(mode.eq.1) then
      call groute('Select mx11;exit')
      call gopen
      elseif(mode.eq.2) then
      call gbegin('Select mx11;exit',' '
     . ,'tomo.plc')
      else
      call groute('LIST')
      call gopen
      endif
c set limits and viewport.
c
      call glimit(xmin,xmax,ymax,ymin,zmin,zmax)
      call gvport(60.0,20.0,70.,220.)
c set contour levels.
      zcl(1) = vmin
      zcl(2) = vmax
      print*,'min value =  ',vmin
      print*,'max value =  ',vmax
      print*,'Enter 1 if you want to set up your own limits'
      read(5,*)ilim
c
      if(ilim.eq.1)then
       print*,'Enter lowest limit, step'
       read(5,*) rlim,cstep
      if(cstep.eq.0.0)then
       iplpt = 3
       zcl(1) = 0.0
       zcl(2) = vmax
       else
       zcl(1) = rlim
       zcl(2) = cstep
       iplpt = 5
      endif
       call rclass(zcl,ncl,iplpt)
      else
       call rclass(zcl,ncl,3)
      endif
c
c select a grey scale suitable for the plots in
c this manual.
       call rcsini
       if(icolr.eq.2) then
       call ridcol(33)
       call rshade(coli,6)
       else
       call rshade(icolr,0)
       endif
c
c do the  shaded contour plot.
c
       smth = 5.
       call gconsm(smth)
       call gcnr2s(vel1,icelx,icelz)
c
c contour lines are plotted on top of the shaded map
c by gcnr2v. set contour line widths and colors.
c
       call gconwi(-1.0,1)
       call gconco(kol,1)
       height = 0.015*min(70.0,220.0)
c
c
       if(icon.eq.1) then
       call gconsm(smth)
       call gcnr2v(vel1,icelx,icelz)
       endif
c
c plot four axes. to make room for a
c color scale, the y-axis to the right is
c plotted without numeric labels.
c
       call gscale
       call raxlas(2)
       call raxdis(2,1,0)
       call raxdis(3,0,0)
       call raxdis(4,0,0)
       call raxdis(5,0,0)
       call raxdis(6,0,0)
       call raxdis(8,0,0)
       call raxis2(ymin,xmin,height,lenar1,txtar1)
       call raxis(1,ymax,height,1)
       call raxis(2,xmax,height,2)
c
c
c
c plot a color scale.
c
       call rtxfon('swil',1)
       call rtxspf(0.15)
       if(aval.eq.'a')then
       idec = 5
       elseif(aval.eq.'v')then
       idec = 1
       else
       idec = 1
       endif
       call gclopt(lenar2,txtar2,3.50*height,idec,0.0,1)
       call gcoscl(xmax+0.1*(xmax-xmin),ymax)
c
c give the plot a title.
c
c      call fdate(strin)
       tpy = ymax-0.05*(ymin-ymax)
       tpx = 0.5*(xmin+xmax)
       call rtxjus(1,3)
       call rtxhsi(5.0)
       if(aval.eq.'a')then
       call rtx(-1,
     .   'Relative attenuation',tpx,tpy)
       elseif(aval.eq.'v')then
       call rtx(-1,
     .   'Travel time inversion',tpx,tpy)
       endif

       scax(1)=xmax+11.
       scay(1)=ymax-34.
       scax(2)=xmax+11.
       scay(2)=ymax-33.
       scax(3)=xmax+21.
       scay(3)=ymax-33.
       scax(4)=xmax+21.
       scay(4)=ymax-34.
       scax(5)=xmax+21.
       scay(5)=ymax-33.
       scax(6)=xmax+31.
       scay(6)=ymax-33.
       scax(7)=xmax+31.
       scay(7)=ymax-34.
       call gvect(scax,scay,7)
       call rtxhsi(3.0)
```

```
call rtx(-1,'0',xmax+11.,ymax-37.)
call rtx(-1,'10',xmax+21.,ymax-37.)
call rtx(-1,'  20 m',xmax+31.,ymax-37.)

if(mode.eq.2) then
call gend
else
call gclose
endif


return
end
```

Appendix A.4

Program for estimation of amplitudes

This program reads in a given seismic record (which has to be zero-phase, and include first-breaks in the headers), and will calculate the amplitude of the direct-wave arrival over a given window, using the scheme described previously in Chapter III. The amplitudes are output in a format ready for input to an amplitude inversion scheme.

```
      program ampest
c ************************************************************
c
c  Calculates envelope amplitude over specified window for
c  data that is zero-phase ..... must have first-breaks in
c  the header information, in XHR format.
c
c  Miles Leggett June-July 1992
c
c ************************************************************
c subroutines called:
c       FFT
c       POLAR      both from tsasub.f
c       QUADT
c       AMPE
      parameter(m=51,n=1024,mr=64)
      real r4dat(n,m), recdep(mr),dbgain(mr),gcmscl(mr),idproc(5,24)
      real sorpos,qutr(n,mr)
      integer nfirst(mr),ncr(2),ishot,ropt
      character*180 a
      character*50 idisc,odisc


c  some defaults
       idisc = '      '
       odisc = '      '
       nrecs = 51
       nsams = 1024
       ishot = 1
       ropt = 1


      print*,'Enter file name to read  '
      read(5,6) idisc
 6    format(a50)

      print*,'Enter file name to write to   '
      read(5,7) odisc
 7    format(a50)

      print*,'Enter shot number             '
      read(5,*) ishot

      print*,'Enter no of channels          '
      read(5,*) nrecs

      print*,'Enter no of samples           '
      read(5,*) nsams

      print*,'Enter samples in window for amplitude calculation'
      read*,iwin3

      print*,'Enter XREC '
      read(5,*)xrec



      idcode = (ishot - 1)*(nrecs+1) + 1
      len = (nsams + 2)*4
      open(unit=10,file=idisc,status='old',access='direct',recl=len)

      do 20 i=1,nrecs
        do 30 j=1,nsams
         r4dat(j,i) = 0.
 30     continue
 20   continue

      do 98 j=1,nrecs
       do 97 i=1,4
        idproc(i,j) = 0.
 97    continue
 98   continue
      print*,' reading headers.....'
      read(10,rec=idcode)a,sorpos,nreci,recdep,dbgain,gcmscl,nfirst,
     &     ncr,nprocs,idproc,dt
      print*,' reading data .....'
      do 345 j=1,nrecs
       nrec = idcode + j
       read(10,rec=nrec)(r4dat(i,j),i=1,nsams)
 345  continue
      rewind(unit=10)
 1234 continue
      close(10)
      call quadt(nsams,nrecs,r4dat,qutr)
      print*,'amplitude calculation'
       do 9999 jk = 1 , nrecs
       write(6,*)qutr(100,jk),qutr(512,jk)
 9999  continue

      call ampe(nsams,nrecs,r4dat,qutr,nfirst,odisc,adum,iwin3
     &  ,recdep,sorpos,xrec)
      stop
      end

      subroutine quadt(nx,nz,r4dat,rdat)

c     subroutine to compute quadrature trace by fft then shifting
c     all frequencies by pi/2, nx should be a power of two.

      real rdat(nx,nz),phz(4096),amp(4096),r4dat(nx,nz)
      complex cdat(4096)

      pi = acos(-1.0)
      do 3000 ik = 1 , nz

c1    call fft
      do 5 i = 1,nx
        cdat(i) = cmplx(r4dat(i,ik),0.0)
 5    continue

      call fft(nx,cdat,-1.0)

c2    compute phase and add pi/2
      call polar(nx,cdat,amp,phz)
      do 10 i = 1,nx/2+1
        phz(i) = phz(i) + (pi/2.0)
 10   continue

c3    reform complex fft
      do 20 i = 1,nx/2+1
        rea = amp(i) * cos(phz(i))
        rim = amp(i) * sin(phz(i))
        cdat(i) = cmplx(rea,rim)
 20   continue

      k=2
      do 21 i = nx,nx/2+2,-1
        cdat(i) = conjg(cdat(k))
      k = k+1
 21   continue


c4    transform back to time series
      call fft(nx,cdat,1.0)

      do 15 i = 1,nx
        rdat(i,ik) = real(cdat(i))
 15   continue
 3000 continue

      return
      end
      subroutine ampe(n,ntrs,r4dat,qutr,nfrst,odisc,ampl1,iwin3,
     &      recdep,sorpos,xrec)

c ---------------------------------------
c  average amplitude calculation
c  .....using envelope amplitude method.....
c  ....qutr is quadrature trace
c  ....r4dat is real trace
c ---------------------------------------

        real  r4dat(n,ntrs),ampl1(ntrs),qutr(n,ntrs)
        real  rdep1,delrec,recx,sdep1,shotx
        real  recdep(ntrs),sorpos
        integer iwin3,nfrst(ntrs)
        character*50 odisc

c ---------------------------------
c     open output file
c ---------------------------------

        open(unit=27,file=odisc,status='unknown')

        do 1345 k=1,ntrs

         x2 = 0.
        iwint = int(iwin3/2) + 1

        do 1347 j=nfrst(k)-iwint,nfrst(k)+iwint

        ampl1(k) = ampl1(k) + ( r4dat(j,k)**2 + qutr(j,k)**2 )

        x2 = x2 + 1.
 1347   continue

 9372   continue

        ampl1(k) = sqrt( ampl1(k)/( x2 ))

        if(k.eq.1) then
        write(27,*) 'xshot   zshot   xrec   zrec   amplitude'
c       write(27,*) '   amplitude'
        endif

 1345   continue

        rdep1 = 0.0
```

```
      delrec = 10.0
      recx = 0.0
      sdep1 = 0.0
      shotx = 0.0

      do 4700 k=1,ntrs
       write(27,788) shotx,sorpos,xrec,recdep(k),ampl1(k)
 788   format(f8.4,2x,f8.4,2x,f8.4,2x,f8.4,2x,f13.4)
c       write(27,*) ampl1(k)
 4700  continue

 766   return
       end
```

Appendix A.5

Subroutine to calculate geometrical-spreading corrections for amplitude inversion

This subroutine is adapted from the raytracing scheme used in the traveltime inversions to calculate parameters for the in-plane and out-of-plane geometrical spreading corrections for use in the amplitude inversion. It requires the SIRT subroutine libraries to run. Three output files are produced; TIMES, which contains angle information for a single raytrace through the velocity model; TIMES2, which contains the parameters for calculating the in-plane correction; and TIMES3 which has the out-of-plane correction calculated and written to the last column in the file.

```
c now the raytracing subroutine
c  this raytracing only applicable to tank data set (water in 1st 2,last 1 cell)
ccthe subroutine is divided into two major sections:
c            1)raytracing of rays from source cells,as there may not
c             be on exact grid positions.
c 00         2)the main raytracing loop for all other cells.
c
c this second main loop is divided into the following:
c            2i)check for direction of rays...if ray going to left
c             it will try next angle increment.for rays travelling
c             downwards isn is flagged as +1 and for rays travelling
c             upwards isn is flagged -1.
c            2ii)if rays are horizontal ..simple update of path,time etc.
c            2iii)if dynamic source on horizontal mesh line or corner:
c               a)check if arc of circle raytracing required
c               b)routine for rays travelling through the horizontal
c                 base of box
c               c)routine for rays travelling through the vertical
c                 side of a box
c            2iv)if dynamic source on a vertical mesh line:
c               a)check if arc of circle raytracing required
c               b)routine for rays travelling through the horizontal
c                 base of box
c               c)routine for rays travelling through the vertical
c                 side of a box
c            3)check where the ray ends and if captured.
c            4)update the take off angle
c                 there are two methods of ray search for updating
c               the take off angle.the original method,for which the
c               flag lost is set as 0,is an iterative technique using
c               the previous distance and final angle for calculation
c               of the new angle.this converges very fast (5-10 its')
c               on the required angle but can get caught in loops and
c               generally 5-30% of rays are lost.the second method which
c               is only used when the first method loses a ray(lost is
c               now set to 1)uses a simple step search method.this
c               generally finds an extra 80-90% of the lost rays.
c  ------------------------------------------------------------------------------
c
      SUBROUTINE RAYT(COORDS,TIMES,SL,TK,RAYLEN,NORAYS,BOXX,BOXZ,ICELLS,
     1NIT,ICELXZ,ICELLX,ICELLZ,IRAYS,XMAX,ZMAX,ASD,ASTEP,ACC,NTRY,ANARR)
      REAL COORDS(6,3000),TIMES(1,3000),RAYLEN(1,3000),OPHI(200)
      REAL BOXX,BOXZ,TK(1600),SL(1600),XMAX,ZMAX,ANARR(3000),RAL(200)
      INTEGER ICELLS,ICELXZ,NORAYS(1600),WRITE,IRANG,ITCH
      CHARACTER*40 STORE
      CHARACTER*72 BALLS
      CHARACTER*1  ESS
      PI=ACOS(-1.)
      PI2=PI/2.
      ICIR=1
      DO 105,I=1,ICELXZ
         NORAYS(I)=0
  105 CONTINUE
C
C NOW PREPARE STORAGE FILES  ------------------------------------
C
      STORE='TIMES'
      OPEN(UNIT=2,FILE=STORE,STATUS='UNKNOWN')
      STORE='XTIMES1'
      OPEN(UNIT=4,FILE=STORE,STATUS='UNKNOWN')
      STORE='TIMES2'
      OPEN(UNIT=11,FILE=STORE,STATUS='UNKNOWN')
      STORE='TIMES3'
      OPEN(UNIT=12,FILE=STORE,STATUS='UNKNOWN')
      STORE='ANGS'
      OPEN(UNIT=3,FILE=STORE,STATUS='UNKNOWN')
      REWIND(UNIT=2)
      REWIND(UNIT=4)
      REWIND(UNIT=11)
      REWIND(UNIT=12)
      REWIND(UNIT=3)
C -------------------------------------------------------------
      WRITE(2,110)'IRAY','TTOT','TOTR','AINT','AIN','DIF'
      WRITE(11,110)'IRAY','TTOT','TOTR','AINI','AIN','DIF'
      WRITE(12,110)'IRAY','TTOT','TOTR','AINI','AIN','DIF'
  110 FORMAT(A4,6X,5(A4,7X))
C -------------------------------------------------------------
C NOW FOR SEARCH LOOP FOR SOURCE CELLS....AND DETERMINING WHICH SEARCH
C METHOD WILL BE USED
C SET UP FLAGS AND INITIALIZE ANY VARIABLES
C
        READ(4,696) BALLS
  696   FORMAT(A72)
C SET PARMS FOR ITERATIVE SEARCH
      ASTEP1 = 0.009973
      ACCZ = ACC
C NOW MAIN LOOP .. PER RAYPATH
      DO 200,IRAY=1,IRAYS
           WRITE = 0
C READ IN INITIAL ANGLE FROM STRAIGHT RAYSEARCH FILE
           IF(WRITE.EQ.0) THEN
            READ(4,697) IAY,ESS,TOT,TOR,BAA1
  697    FORMAT(I4,1X,A1,1X,F8.6,3X,F8.4,3X,F8.4)
           AINI = BAA1
           ISTRT = 0
          ENDIF
         IF(ESS.EQ.'S') THEN
          ISTRT = 1
          AINI = ATAN((ZREC - ZSOR)/(XREC - XSOR))
         ENDIF
         IF(ESS.EQ.' ') AINT=AINI
           ITCH = 0
C           IF ISTRT = 1 THEN STRAIGHT RAYS
          A2 = AINI
          ACC = ACCZ
          INCH = 0
          WRITE =0
          IRFLAG=0
          LOST=0
C          (LOST FLAG = 0 FOR ORIG' SEARCH , 1 FOR NEW SEARCH)
          KFLAG=0
   55      XSOR=COORDS(1,IRAY)
          ZSOR=COORDS(3,IRAY)
          XREC=COORDS(4,IRAY)
          ZREC=COORDS(6,IRAY)
          IREC=INT(XREC/BOXX)+1
          XPO = XSOR
          ZPO = ZSOR
          IF(WRITE .EQ. 1) THEN
                  NPT = 1
          ENDIF
          ITRY=0
          LTRY=0
          ITRY2=0
          INX = 0
          D1=0.0
          PHI1=0.0
          ANGLE=0.0
          IADD = 0
          IRFLAG = 0
          REWIND(UNIT=3)
  120      CONTINUE
          ITRY=ITRY+1
C
C  ANGLE INCREMENT.....FOR DIVERGENCE
C
          IF(INCH.EQ.1)THEN
          AINI=AINI+0.02
          WRITE=1
          ITRY=0
          ENDIF
C
C
          AIN=AINI
          IRFLAG=0
          IF(LOST.EQ.1)ITRY2=ITRY2+1
          DO 122,I=1,ICELXZ
             TK(I)=0.0
  122     CONTINUE
          IF(ITRY.EQ.NTRY.AND.LOST.EQ.0) THEN
            TTOT=0.0
            TOTR=0.0
            PRINT*,'RAY ',IRAY,' LOST'
C-------------------------------------------------------------
C             NOW TRY NEW RAY SEARCH
C             BASED ON HALVING OF ANGLES
C
            AINI = A2
            LOST=1
C             LOST = 1 MEANS NEW RAY SEARCH!
            AINSAV = PI/2.
C             AINSAV IS THE VALUE OF AINI ON THE PREVIOUS ITERATION
            ITRY2 = 1
            D1 = -999
          ENDIF
C
C          NOW SET UP CONDITION IF RAY STILL NOT FOUND
C
          IF(ITRY2.EQ.NTRY.AND.LOST.EQ.1)THEN
            TTOT=0.0
            TOTR=0.0
            PRINT*,'RAY ',IRAY,' LOST STEP '
            DO 444 I=1,ICELXZ
             TK(I) = 0.0
  444        CONTINUE
            NPT = 0
C             USE A STRAIGHT RAY FOR THIS RAYPATH
            LOST = 0
            ITCH = ITCH + 1
         IF(ITCH.EQ.2) THEN
            ISTRT = 1
            WRITE = 1
            AINI=ATAN((ZREC-ZSOR)/(XREC-XSOR))
            REWIND(UNIT=3)
c            ITRY = 0
            ITRY2 = 0
            INX = 0
            D1 = 0.0
```

```
            PHI1 = 0.0
            ANGLE = 0.0
            IADD = 0
            IRFLAG = 0
            ACC = 5.0
            GOTO 1993
         ELSEIF(ITCH.EQ.1) THEN
            ISTRT = 0
            WRITE = 0
            AINI = BAA1 -  0.334*SIGN(1.0,BAA1)
            GOTO 55
         ENDIF
            ENDIF
C ---------------------------------------------------------
         IF(AINI.LT.0.0.AND.ZSOR.EQ.0.0) AINI=0.005
         IF(ABS(AINI).GE.PI2) GOTO 126
         GOTO 128
126        WRITE(6,127) AINI,IRAY
127        FORMAT(/1X,'SHOOTING OUT OF FRAME - ABORT!'/1X,
   1          'AINI= ',E10.4,' IRAY= ',I5/)
         IF(AINI.GE.PI2)AINI=PI2-.4
         IF(AINI.LE.-PI2)AINI=-PI2+.4
2345       CONTINUE
1993       CONTINUE
128        XPO=XSOR
         ZPO=ZSOR
         IX=INT(XPO/BOXX+0.0001)+1
         IZ=INT(ZPO/BOXZ+0.0001)+1
         IF(ZPO-FLOAT(IZ-1)*BOXZ.LT.0.0001.AND.AINI.LT.
   1      -0.0005) IZ=IZ-1
         ICELL=(IZ-1)*ICELLX+IX
         DZ=ZSOR-(FLOAT(IZ-1))*BOXZ
         DX=FLOAT(IX)*BOXX-XSOR
         K=0
         IF(AINI.LT.0.0) K=1
         ALPHA=ATAN(DZ/DX)
         BETA=ATAN((BOXZ-DZ)/DX)
         IEXIT=1
         IF(AINI.LE.BETA) IEXIT=0
         IF(AINI.LT.-ALPHA) IEXIT=-1
         IF(IEXIT) 130,140,130
130        TOTR=ABS((DZ-BOXZ*((IEXIT+1)/2))/SIN(AINI))
         TTOT=TOTR*SL(ICELL)
         IZ=IZ+IEXIT
         NCELL=(IZ-1)*ICELLX+IX
         IF(NCELL.LT.1) THEN
           AINI=0.0
           GOTO 120
         ENDIF
         VL=1.0/SL(ICELL)
         VELI=1.0/SL(NCELL)
         IF(VL.GE.VELI) GO TO 131
         CRIT=ACOS(VL/VELI)
         IF(ABS(AINI).GT.ABS(CRIT)) GOTO 131
         IF(ISTRT.EQ.0)GO TO 1800
131        IF(ISTRT.EQ.0)
   &       AIN=ACOS(VELI*COS(AINI)/VL)*SIGN(1.0,AINI)
         IF(ISTRT.EQ.1)AIN = AINI
C
C O-P DIVERGENCE
C
         IF(WRITE.EQ.1.OR.ISTRT.EQ.1) THEN
      IF(ABS(AINI).GT.0.0000)THEN
         AZN = PI2 - ABS( AINI)
         AZN1 = PI2 - ABS( AIN)
         OPQ = TAN( ABS(AZN) )/TAN( ABS(AZN1) )
         WRITE(3,*) OPQ,TOTR
      ELSE
         WRITE(3,*)VL,TOTR
      ENDIF
         INX = INX + 1
         ENDIF
         ZPO=FLOAT(IZ-1)*BOXZ
         IF(IEXIT.EQ.-1) ZPO=FLOAT(IZ)*BOXZ
135        XPO=XPO+TOTR*COS(AINI)
         GOTO 150
140        TOTR=ABS(DX/COS(AINI))
         TTOT=TOTR*SL(ICELL)
         IX=IX+1
         NCELL=(IZ-1)*ICELLX+IX
         IF(ISTRT.EQ.0) THEN
         AIN=ASIN(SIN(AINI)*SL(ICELL)/SL(NCELL))
         ENDIF
         IF(ISTRT.EQ.1)AIN = AINI
C
C O-P DIVERGENCE
C
         IF(WRITE.EQ.1.OR.ISTRT.EQ.1) THEN
      IF(ABS(AINI).GT.0.0000)THEN
         AZN = ABS( AINI)
         AZN1 = ABS( AIN)
         OPQ = TAN( AZN1 )/TAN( AZN )
         WRITE(3,*) OPQ,TOTR
      ELSE
         WRITE(3,*)VL,TOTR
      ENDIF
         INX = INX + 1
         ENDIF
         XPO=FLOAT(IX-1)*BOXX
         ZPO=ZPO+TOTR*SIN(AINI)
150        TK(ICELL)=TOTR
         ICELL=NCELL
         IF(ICELL.LE.0) THEN
           AINI=AINI+ASTEP
           GOTO 120
         ENDIF
C
C----------------------------------------------------------
C NOW FOR MAIN LOOP - I.E. CELLS EXCLUDING SOURCE
C
C ISN = SIGN OF AIN IE: +VE = RAY TRAVELLING DOWN
C
C
155  ISN=1
     K=0
     ICELL=(IZ-1)*ICELLX+IX
     IF(ABS(AIN).GE.PI2) GO TO 1610
C RAY GOING TO LEFT TRY NEXT ANGLE INCREMENT
     IF(AIN.GE.0.0) GO TO 1450
     ISN=-1
     K=1
C RAY GOING UP
1450  VL=1.0/SL(ICELL)
     AIN1 = ABS(AIN)
C
C
C IF ROUTINE FOR STRAIGHT THROUGH RAYS ----------------------
C
C
     IF(AIN1.LE.0.00001)THEN
         RLEN=BOXX
         TD=BOXX/VL
         XPO=XPO+RLEN
            IF(WRITE.EQ.1.OR.ISTRT.EQ.1) THEN
            WRITE(3,*) VL,RLEN
            INX = INX + 1
            ENDIF
         IX=IX+1
         GOTO 1220
     ENDIF
C  ---------------------------------------------------------
C
C
C
     AAA = AIN
     IF (ABS(FLOAT(IZ - 1 + K)*BOXZ - ZPO) .GT. 0.001 ) GO TO 1530
C
C
C
C** DYN. SOURCE EITHER ON HOR. MESH LINE OR CORNER
C**********************************************************************
C
C ---------------------------------------------------------
C RAY SEGMENT AS AN ARC OF A CIRCLE?
C
         IF (ABS(AAA) .GT. ASD) GO TO 1470
         NSUB = NSUB + 1
         IF (ICIR .EQ. 1) GO TO 1460
 1460    ISW = 0
     CALL CIRCLE(XPO, ZPO, ISW, ISN, AIN, IX, IZ, SL, RLEN, TD,ICELLX,
    1    ICELXZ,BOXX,BOXZ, GRAD, APR, AINI,NIT,IRAY)
         IF (ISW .EQ. 0) GO TO 1220
         IF(ISW.EQ. 10) GO TO 1800
 9122            CONTINUE
 1470    GRAD = 0.0
C----------------------------------------------------------
         DIS = FLOAT(IX) * BOXX - XPO
C
C
C* DIS IS DISTANCE FROM DYNAMIC SOURCE TO NEXT VERTICAL MESH LINE.
C
C
C     BOXX
     BX = DIS * TAN(AIN) * FLOAT(ISN)
C* BX IS VERTICAL DISTANCE FROM DYN.SOURCE TO EXIT POINT ON VERTICAL MESI
     IF (BX .EQ. BOXZ) BX = BX + 0.0001
     IF (BX .LT. BOXZ) GO TO 1500
C
C
C* RAY THROUGH HOR. SIDE OF BOX  ------------------------------------
C
C
C
     RLEN = ABS(BOXZ/SIN(AIN))
     TD = RLEN / VL
     IF(IZ+ISN.GT.ICELLZ+1.OR.IZ+ISN.LT.1)THEN
         VELI=VL
         DIF=ZPO-ZREC+(XREC-XPO)*TAN(AIN)
         IF(DIF*ISN.GT.0.0) GOTO 1800
         KFLAG=1
```

```
      GOTO 1699
   ENDIF
   VELI = 1.0/SL((IZ+ISN-1)*ICELLX +DX)
   IF (VL .GE. VELI) GO TO 1480
   CRIT = ACOS(VL/VELI)
   IF (ABS(AAA) .GT. ABS(CRIT)) GO TO 1480
   D1 = -DIF
   IF(ISTRT.EQ.0)GO TO 1800
1480 IF(ISTRT.EQ.0) AIN = ACOS(VELI*COS(AAA)/VL) * FLOAT(ISN)
        IF(WRITE.EQ.1.OR.ISTRT.EQ.1) THEN
        AZN = PI2 - ABS( AAA )
        AZN1 = PI2 - ABS( AIN )
        OPQ = TAN( ABS(AZN) )/TAN( ABS(AZN1) )
        WRITE(3,*) OPQ,RLEN
        INX = INX + 1
        ENDIF
   ZPO = FLOAT(IZ - K) * BOXZ
   IZ = IZ + ISN
1490 XPO = XPO + (SQRT((RLEN*RLEN) - (BOXZ*BOXZ)))
   GO TO 1220
C
C
C
C* RAY THROUGH VERT. SIDE OF BOX ----------------------------------
C
C
C
 1500 RLEN = ABS(DIS/COS(AIN))
   TD = RLEN / VL
   IF(IX+1.GT.ICELLX)THEN
      VELI=VL
      GOTO 1502
   ENDIF
   VELI = 1.0/SL((IZ-1)*ICELLX+IX+1)
1502 IF (VL .GE. VELI) GO TO 1510
   CRIT = ASIN(VL/VELI)
   IF (ABS(AAA) .LT. ABS(CRIT)) GO TO 1510
4628 D1 = -DIF
   IF(ISTRT.EQ.0)GO TO 1800
1510 IF(ISTRT.EQ.0) AIN = ASIN(VELI*SIN(AAA)/VL)
        IF(WRITE.EQ.1.OR.ISTRT.EQ.1) THEN
        OPQ = TAN( ABS(AIN) )/TAN( ABS(AAA) )
        WRITE(3,*) OPQ,RLEN
        INX = INX + 1
        ENDIF
   XPO = FLOAT(IX) * BOXX
   IX = IX + 1
1520 ZPO = ZPO + (BX*FLOAT(ISN))
   GO TO 1220
C
C
C ***********************************************************************
C** DYN. SOURCE ON VERTICAL MESH LINE
C ***********************************************************************
C
C
C
C ---------------------------------------------------------
C RAY SEGMENT AS AN ARC OF A CIRCLE ?
C
1530 IF (ABS(AAA) .GT. ASD) GO TO 1550
   NSUB = NSUB + 1
   IF (ICIR .EQ. 1) GO TO 1540
1540 ISW = 0
   CALL CIRCLE(XPO, ZPO, ISW, ISN, AIN, IX, IZ, SL, RLEN, TD,ICELLX,
  1   ICELXZ,BOXX,BOXZ, GRAD, APR, AINI,NIT,IRAY)
   IF (ISW .EQ. 0) GO TO 1220
   IF(ISW.EQ. 10)  GO TO 1800
1550 GRAD = 0.0
C ---------------------------------------------------------
C
C
C
C
   DEP = FLOAT(IZ) * BOXZ - ZPO
C DEP IS DEPTH THAT RAY SOURCE IS FROM NEXT HORIZONTAL MESH LINE.
   IF (AIN .LT. 0.0) DEP = BOXZ - DEP
   BX = DEP / TAN(AIN)
C BX IS HORIZONTAL DISTANCE TRAVELLED BY RAY TO NEXT HOR. MESH LINE.
   IF (ABS(BX) .EQ. BOXX) BX = ABS(BX + 0.0001)
   IF (ABS(BX) .LT. BOXX) GO TO 1580
C
C
C* RAY THROUGH VERT. SIDE OF BOX ----------------------------------
C
C
C
   RLEN = ABS(BOXX/COS(AIN))
   TD = RLEN / VL
   IF(IX+1.GT.ICELLX)THEN
      VELI=VL
      GOTO 1552
   ENDIF
   VELI = 1.0/SL((IZ-1)*ICELLX+IX+1)
1552 IF (VL .GE. VELI) GO TO 1560
   CRIT = ASIN(VL/VELI)
   IF (ABS(AAA) .LT. ABS(CRIT)) GO TO 1560
2637 D1 = -DIF
   IF(ISTRT.EQ.0)GO TO 1800
1560 IF(ISTRT.EQ.0) AIN = ASIN(VELI*SIN(AAA)/VL)
        IF(WRITE.EQ.1.OR.ISTRT.EQ.1) THEN
        OPQ = TAN( ABS(AIN) )/TAN( ABS(AAA) )
        WRITE(3,*) OPQ,RLEN
        INX = INX + 1
        ENDIF
   XPO = FLOAT(IX) * BOXX
   IX = IX + 1
1570 ZPO = ZPO + ((SQRT((RLEN*RLEN) - (BOXX*BOXX)))*FLOAT(ISN))
   GO TO 1220
C
C
C
C* RAY THROUGH HOR. SIDE OF BOX ----------------------------------
C
C
C
 1580 RLEN = ABS(DEP/SIN(AIN))
   TD = RLEN / VL
   IF(IZ+ISN.GT.ICELLZ.OR.IZ+ISN.LT.1)THEN
      VELI=VL
      DIF=ZPO-ZREC+(XREC-XPO)*TAN(AIN)
      IF(DIF*ISN.GT.0.0) GOTO 1800
      KFLAG=1
      GOTO 1699
   ENDIF
1581 VELI = 1.0/SL((IZ+ISN-1)*ICELLX+IX)
1582 IF (VL .GE. VELI) GO TO 1590
   CRIT = ACOS(VL/VELI)
   IF (ABS(AAA) .GT. ABS(CRIT)) GO TO 1590
   D1 = -DIF
   IF(ISTRT.EQ.0)GO TO 1800
1590 IF(ISTRT.EQ.0) AIN = ACOS(VELI*COS(AAA)/VL) * FLOAT(ISN)
        IF(WRITE.EQ.1.OR.ISTRT.EQ.1) THEN
        AZN = PI2 - ABS( AAA )
        AZN1 = PI2 - ABS( AIN )
        OPQ = TAN( ABS(AZN) )/TAN( ABS(AZN1) )
        WRITE(3,*) OPQ,RLEN
        INX = INX + 1
        ENDIF
   ZPO = FLOAT(IZ - K) * BOXZ
   IZ = IZ + ISN
 1600 XPO = XPO + ABS(BX)
   GO TO 1220
C**********************************************************************
C
C* * * * * * * * * * * * * * * * * * * * * * * * * * * * * * * * * *
C
C
C* CHECK WHERE RAY ENDS
C
 1220          IF(WRITE.EQ.1)THEN
                  NPT = NPT + 1
            ENDIF
   IF(XPO.GE.XREC) GOTO 1690
   TTOT=TTOT+TD
   TOTR=TOTR+RLEN
   TK(ICELL)=RLEN + TK(ICELL) * IADD
   IF(IADD.EQ.1) IADD = 0
   IF(IRFLAG.EQ.1) IADD = 1
   IRFLAG = 0
C
C RAY ENTERING SAME COLUMN IN GRID AS RECEIVER POSITION.
C
   IPP = 1
   IF(ZPO.LE.0.0.AND.ISN.EQ.-1) THEN
      DIF=ZPO-ZREC+(XREC-XPO)*TAN(AIN)
      IF(IX.EQ.ICELLX) GO TO 1700
      GOTO 1800
   ENDIF
C RAY EXITING THROUGH SURFACE
C ---------------------------------------------------------
   IF (ZPO .GE. ZMAX+BOXZ) THEN
      DIF=ZPO-ZREC+(XREC-XPO)*TAN(AIN)
      GOTO 1800
   ENDIF
C RAY LEAVING VELOCITY FIELD THRO' BOTTOM.
C---------------------------------------------------------
 1300 CONTINUE
   GO TO 155
1610 DIF=ZPO-ZREC+(XREC-XPO)*TAN(AIN)
   GOTO 1699
1690     XPO=XPO-RLEN*COS(AIN)
      ZPO=ZPO-RLEN*SIN(AIN)
      RLEN=ABS((XREC-XPO)/COS(AIN))
   TD=RLEN/VL
   TOTR=TOTR+RLEN
   TTOT=TTOT+TD
   TK(ICELL)=RLEN
   ZPO=(XREC-XPO)*TAN(AIN)+ZPO
```

```
      DIF=ZPO-ZREC
 1699 IF(KFLAG.EQ.1.AND.IZ.LE.1)THEN
         RLEN=ABS((ZREC-ZPO)/SIN(AIN))
         TK(ICELL)=RLEN
         TD=RLEN/VL
         TOTR=TOTR+RLEN
         TTOT=TTOT+TD
      ENDIF
C
C
C     ----------------------------------------------------------
C     NOW CHECK WHERE RAY ENDS
C
      IF(INCH.EQ.1)GOTO 2067
 1700 IF(ABS(DIF).LE.ABS(ACC))THEN
                LOST=0
C                (RESET LOST FLAG)
                IF(ISTRT.EQ.1)GO TO 2000
                IF(WRITE .EQ. 0)THEN
                        WRITE = 1
                        GO TO 55
                ENDIF
                GOTO 2000
      ENDIF
C
C * RAY HAS BEEN FOUND.  ===> GOTO 2000
C     ----------------------------------------------------------
C
 1800 ANGLE=AINI
C
C
C     ----------------------------------------------------------
C     NOW DO THE RAY SEARCH TO UPDATE THE "TAKE OFF" ANGLE
C     THIS THE ORIGINAL ITERATIVE SEARCH ...WHEN LOST = 0
C
      IF(INCH.EQ.1) GOTO 2067
      IF(LOST.EQ.1) GOTO 1777
      IF(D1.EQ.0.0) THEN
         AINI= AINI-ASTEP1*SIGN(1.0,DIF)
         GOTO 1805
      ENDIF
      IF(DIF.EQ.D1) GOTO 1801
      IF(SIGN(1.0,DIF).EQ.SIGN(1.0,D1)) THEN
         AINI= AINI-ASTEP1*SIGN(1.0,DIF)
         GOTO 1805
      ENDIF
      AINI= AINI-(DIF/(DIF-D1))*(AINI-PHI1)
 1801 IF(AINI.EQ.ANGLE) AINI=ANGLE+ASTEP1
 1805 D1=DIF
      PHI1=ANGLE
      GOTO 120
C     ----------------------------------------------------------
C     NOW NEW SEARCH METHOD
C
 1777 IF(LOST.EQ.1) THEN
         IF(ITRY2.EQ.1)THEN
            IF(DIF.GT.0.0)AAAI = AINI - (PI/2. + ABS(AINI))/2.
            IF(DIF.LT.0.0)AAAI = AINI + (PI/2. - ABS(AINI))/2.
         ELSE

        AAAI = AINI - SIGN(1.0,DIF)*((PI/2 - ABS(AINI)))/33.
         ENDIF
 1778    D1=DIF
         AINSAV = AINI
         AINI = AAAI
         GOTO 120
      ENDIF
C     ----------------------------------------------------------
C
C
 2000 CONTINUE
      AA11 = AINI
      RAYLEN(1,IRAY)=TOTR
      ANARR(IRAY)=AINI
      IRANG=0
  357 CONTINUE
C  Calculate out-of-plane divergence correction.....
C
C  ..for horizontal raypaths this is the Newman divergence correction
C  for normal incidence ( approximates to the raylength in a homogeneous
C  medium ).
C
      AL = 0.0
      DL = 0.0
      POPH = 1.0
      REWIND(UNIT=3)
      IF(INX.GT.200)INX = 72
      IF(ABS(AINI).GT.0.0) THEN
      DO 713 I=1,INX
      READ(3,*) OPHI(I),RAL(I)
  713 CONTINUE
C
C
      DO 715 I = 1 , INX
        POPH = OPHI(I)
        DL = DL + POPH * RAL(I)
  715 CONTINUE
C
      ELSE
      DO 714 I=1,INX
      READ(3,*) VX,RALL
      AL = AL + VX*RALL
  714 CONTINUE
      DL = AL*SL(1)
      ENDIF
      IF(ISTRT.EQ.0)PREDIV = DL
      IF(ISTRT.EQ.1)THEN
      DL = PREDIV * 1.057367874
      PREDIV = DL
      ENDIF
 2067 CONTINUE
      IF(INCH.EQ.0)THEN
      IF(ISTRT.EQ.0) WRITE(2,2011) IRAY,TTOT,TOTR,AINI,AIN,DIF
      IF(ISTRT.EQ.1) WRITE(2,2211) IRAY,TTOT,TOTR,AINI,AIN,DIF
      IF(ISTRT.EQ.0) WRITE(12,2012) IRAY,TTOT,TOTR,AINI,AIN,DIF,DL
      IF(ISTRT.EQ.1) WRITE(12,2212) IRAY,TTOT,TOTR,AINI,AIN,DIF,DL
      ELSEIF(INCH.EQ.1)THEN
      IF(ABS(DIF).LT.50.)DIFV=DIF
      IF(ABS(DIF).GT.50.)DIF=DIFV
      IF(ISTRT.EQ.0) WRITE(11,2013) IRAY,TTOT,TOTR,AINI,AIN,DIF
      IF(ISTRT.EQ.1) WRITE(11,2213) IRAY,TTOT,TOTR,AINI,AIN,DIF
      ENDIF
      NC = 0
      DO 2005 I=1,ICELXZ
         IF(TK(I).NE.0.0) NORAYS(I)=NORAYS(I)+1
         IF(TK(I).NE.0.0) NC = NC + 1
 2005 CONTINUE
 2009 FORMAT(I4)
 2010 FORMAT(6(I4,F8.4))
 2011 FORMAT(I4,3X,F8.6,3X,F8.4,3X,F8.4,3X,F8.4,3X,F8.4)
 2211 FORMAT(I4,1X,'S',1X,F8.6,3X,F8.4,3X,F8.4,3X,F8.4,3X,F8.4)
 2012 FORMAT(I4,3X,F8.6,3X,F8.4,3X,F8.4,3X,F8.4,3X,F8.4,1X,F13.4)
 2212 FORMAT(I4,1X,'S',1X,F8.6,3X,F8.4,3X,F8.4,3X,F8.4,3X,F8.4,1X,F13.4)
 2013 FORMAT(I4,3X,F8.6,3X,F8.4,3X,F8.4,3X,F8.4,3X,F8.4,1X,F13.2)
 2213 FORMAT(I4,1X,'S',1X,F8.6,3X,F8.4,3X,F8.4,3X,F8.4,3X,F8.4,1X,F13.2)
      IF(INCH.EQ.0)THEN
       INCH = 1
       WRITE = 1
       GOTO 120
      ELSE
       CONTINUE
      ENDIF
C  ADD INITIAL TAKEOFF ANGLE TO ANOTHER O/P FILE
 200  CONTINUE
      CLOSE(UNIT=2)
      CLOSE(UNIT=3)
      CLOSE(UNIT=11)
      CLOSE(UNIT=12)
      CLOSE(UNIT=4)
      RETURN
      END
```

Appendix A.6

Program to apply corrections to amplitude data

This program is only applicable to the physical model data, and the files for input are the three files that are output from the previous subroutine and the velocity field used for the raytracing. Other inputs are the recorded amplitudes and the directivity of the amplitude.

```
      PROGRAM AMPCOR
C  Sorts velocities from inversions for calculating Zoeppritz
C  coefficients at the edge of the model ( water/model interface )
C
      REAL VEL(2000),BOXX,BOXZ,XMIN,ZMIN,VEL1,VEL2
      REAL V1(51),V2(51)
      CHARACTER*72  HEAD(5),DUMMY
      INTEGER ICELLS,ICELLX,ICELLZ
      CHARACTER*30  IDISC,ODISC1,ODISC2
      CHARACTER*30  TFILE,TFILE1,TFILE2
      CHARACTER*30  AFILE1,AFILE2,AFILE3
C Files for divergence correction
      PRINT*, 'Enter file containing velocity values'
      READ(5,1) IDISC
      PRINT*,' Enter output file from tomography'
      READ(5,1) TFILE
      PRINT*,' Enter output file from ray increment'
      READ(5,1) TFILE1
      PRINT*,' Enter file containing divergence factors'
      READ(5,1) TFILE2

C     TFILE3='ZCOF'
C Files for amplitude onformation
      PRINT*,' Enter file containing measured amplitude values'
      READ(5,1) AFILE1
      PRINT*,' Enter file to write ampiltudes corrected by'
      PRINT*,' Zoeppritz coefficients'
      READ(5,1) AFILE2
      PRINT*,' Enter file to write out divergence corrected Aref'
      READ(5,1) AFILE3
    1 FORMAT(A30)

      OPEN(UNIT=1,FILE=IDISC,STATUS='UNKNOWN')
      ODISC1='TVEL'
      ODISC2='TVEL1'
      OPEN(UNIT=2,FILE=ODISC1,STATUS='UNKNOWN')
      OPEN(UNIT=3,FILE=ODISC2,STATUS='UNKNOWN')

      DO 10 I=1,3
      READ(1,2) HEAD(I)
    2 FORMAT(A72)
   10 CONTINUE

      READ(1,*) ICELLS,ICELLX,ICELLZ
      READ(1,2) DUMMY
      READ(1,*) BOXX,BOXZ,XMIN,ZMIN
      READ(1,2) DUMMY

      DO 100 I=1,ICELLZ - 1
      READ(1,*) VELW
      READ(1,*) VELW
      READ(1,*)  VEL1
      WRITE(2,*) VEL1
      DO 300 K=1,ICELLX-6
      READ(1,*) VEL(K)
  300 CONTINUE
      READ(1,*) VEL2
      WRITE(3,*) VEL2
      READ(1,*) VELW
      READ(1,*) VELW
  100 CONTINUE
      REWIND(UNIT=2)
      REWIND(UNIT=3)
      DO 1000 I=1,51
      READ(2,*) V1(I)
      READ(3,*) V2(I)
 1000 CONTINUE
      REWIND(UNIT=2)
      REWIND(UNIT=3)
      DO 2000 I=51,1,-1
      WRITE(2,*) V1(I)
      WRITE(3,*) V2(I)
 2000 CONTINUE
      REWIND(UNIT=2)
      REWIND(UNIT=3)
      DO 1001 I=1,51
      READ(2,*) V1(I)
      READ(3,*) V2(I)
 1001 CONTINUE
      CLOSE(1)
      CLOSE(2)
      CLOSE(3)

      CALL ZOEP(TFILE,AFILE1,AFILE2,V1,V2)

      PRINT*,' Enter angle increment used for I-P divergence'
      READ(5,*)RINCR

      CALL GEOM(AFILE1,TFILE,TFILE1,TFILE2,AFILE3,RINCR)

      STOP
      END


      SUBROUTINE ZOEP(IDISC,IPDISC,OPDISC,VEL,VEL1)
C
C  THIS SUBROUTINE CALCULATES ZOEPPRITZ'S DISPLACEMENT AMPLITUDE
C  COEFFICIENTS FOR PLANE HARMONIC ELASTIC P-WAVES INCIDENT ON A
C  PLANE INTERFACE BETWEEN TWO ISOTROPIC, HOMOGENEOUS HALF-SPACES.
C  THE EXPRESSIONS USED TO CALCULATE THE COEFFICIENTS HAVE BEEN
C  TAKEN FROM CERVENY & RAVINDRA,1971 (THEORY OF SEISMIC HEAD WAVES)
C  AND INCLUDE FREE SURFACE REFLECTIONS AND SURFACE CONVERSION
C  COEFFICIENTS .
C  (FOR THE COMPUTATION OF AMPLITUDE COEFFICIENTS FOR INCIDENT
C  SV-WAVES ETC., SEE YOUNG & BRAILE,1976 (BSSA,66,1881-1885) .)
C
C  IRT = 1 FOR REFLECTION,
C      = 2 FOR TRANSMISSION,
C      = 3 FOR FREE SURFACE REFLECTION,
C      = 4 FOR SURFACE CONVERSION COEFF. (Z-COMPONENT),
C      = 5 FOR SURFACE CONVERSION COEFF. (X-COMPONENT).
C  AIN - INCIDENT ANGLE TO THE INTERFACE
C  RR  - RETURNS COMPLEX COEFFICIENT
C  VP1 -INCOMING , VP2 -OUTGOING P VELOCITY.
C
      PARAMETER(LR=2601)
      COMPLEX RZ1,RZ2, RR
      CHARACTER*30  IDISC,IPDISC,OPDISC
      CHARACTER  DUMMY*72, ESS*1
      REAL VEL(51),VEL1(51),AIN1,AIN2
      REAL RUB2,RUB3,ZCA,ZCOF(LR)
      INTEGER RUB1

      PRINT*,' Enter vel water'
      READ(5,*) VW
      OPEN(UNIT=1,FILE=IDISC,STATUS='UNKNOWN')
      REWIND(1)

      READ(1,111)  DUMMY
  111 FORMAT(A72)


      ZCB = 0.6544

      DO 300  L=1,51


      DO 200  I=1,51

       READ(1,201) RUB1,ESS,RUB2,RUB3,AIN1,AIN2
  201  FORMAT(I4,1X,A1,1X,F8.6,3X,F8.4,3X,F8.4,3X,F8.4)
C  SETTING UP DENSITIES AND SHEAR WAVE VELOCITIES
C  FIRST DO RECEIVER POSITION
      AIN = ABS(AIN1)
      IF(ESS.EQ.'S')AIN = AIN * 0.4100444343
      VP1 = VW
      VP2 = VEL(L)/1000.
      CALL RZOEP(AIN,VP1,VP2,RZ1)
C  NOW DO FOR SOURCE POSITION
      VP2 = VW
      VP1 = VEL1(I)/1000.
      IF(ESS.EQ.'S')AIN2= AIN2 * 0.4100444343
      ASN = ABS(SIN(AIN2)*VPA/VW)
      IF(ASN.GT.1.)ASN=0.9
      AIN = ASIN( ASN )
      CALL SZOEP(AIN,VP1,VP2,RZ2)
C
C NOW WORK OUT TOTAL ZOEPPRITZ COEFF
C
      IF(CABS(RZ1).EQ.0.0)THEN
      ZCA = CABS(RZ2)
      ELSEIF(CABS(RZ2).EQ.0.0)THEN
      ZCA=CABS(RZ1)
      ELSE
      RR = RZ1 * RZ2
      ZCA = CABS(RR)
      ENDIF
      IF(ZCA.EQ.0.0)ZCA=ZCB
      IF(ZCA.LT.0.090)ZCA=ZCB
      IF(ESS.NE.'S') THEN
      ZCB = ZCA
      ENDIF
      IF(ESS.EQ.'S')THEN
      ZCA = ZCB
      ENDIF
      IZCF = ( L - 1 )*51 + I
      ZCOF(IZCF) = ZCA
  200 CONTINUE
  300 CONTINUE
      CLOSE(1)
      CLOSE(4)
      CALL ZCOR(IPDISC,OPDISC,ZCOF)
      RETURN
      END
```

```
      SUBROUTINE RZOEP(AIN,VP1,VP2,R13)
C
C CALCULATES ZOEPPRITZ COEFF FOR REC POSN
C
      COMPLEX P1, P2, P3, P4, R13, D
      AIN = AIN
      RZ1 = (0.0,0.0)
      IF(VP2.GE.2.000) THEN
      SIGM = 0.391
      VS2 = VP2*SQRT( (2*SIGM-1)/(2*SIGM-2) )
      RHO2 = 1.4
      ENDIF
      IF(VP2.GE.2.65) THEN
      SIGM = 1.0/3.0
      VS2 = VP2*SQRT( (2*SIGM-1)/(2*SIGM-2) )
      RHO2 = 1.48
      ENDIF
      IF(VP2.GE.2.900) THEN
      SIGM = 0.3559
      VS2 = VP2*SQRT( (2*SIGM-1)/(2*SIGM-2) )
      RHO2 = 1.55
      ENDIF
      IF(VP2.GE.3.009) THEN
      SIGM = 0.2865
      VS2 = VP2*SQRT( (2*SIGM-1)/(2*SIGM-2) )
      RHO2 = 1.55
      ENDIF
C     LIQUID LAYER
      VS1 = 0.000001
      RHO1 = 1.0

      THETA = SIN(AIN) / VP1
      THSQ = THETA * THETA
      QA = 2.0 * (RHO2*VS2*VS2 - RHO1*VS1*VS1)
      T1 = VP1 * VP1 * THSQ
      T2 = VS1 * VS1 * THSQ
      T3 = VP2 * VP2 * THSQ
      T4 = VS2 * VS2 * THSQ
C     TEST FOR CRITICAL P REFLECTION
      IF (THETA .GT. 1.0/VP1) GO TO 60
      A1 = SQRT(1.0 - T1)
      B1 = 0.0
C     TEST FOR CRITICAL S REFLECTION
   30 IF (THETA .GT. 1.0/VS1) GO TO 70
      A2 = SQRT(1.0 - T2)
      B2 = 0.0
C     TEST FOR CRITICAL P REFRACTION
   40 IF (THETA .GT. 1.0/VP2) GO TO 80
      A3 = SQRT(1.0 - T3)
      B3 = 0.0
C     TEST FOR CRITICAL S REFRACTION
   50 IF (THETA .GT. 1.0/VS2) GO TO 90
      A4 = SQRT(1.0 - T4)
      B4 = 0.0
      GO TO 101
   60 B1 = -SQRT(T1 - 1.0)
      A1 = 0.0
      GO TO 30
   70 B2 = -SQRT(T2 - 1.0)
      A2 = 0.0
      GO TO 40
   80 B3 = -SQRT(T3 - 1.0)
      A3 = 0.0
      GO TO 50
   90 B4 = -SQRT(T4 - 1.0)
      A4 = 0.0
  101 X = RHO2 - QA * THSQ
      Y = RHO1 + QA * THSQ
      Z = RHO2 - RHO1 - QA * THSQ
      P1 = CMPLX(A1,B1)
      P2 = CMPLX(A2,B2)
      P3 = CMPLX(A3,B3)
      P4 = CMPLX(A4,B4)
      VS1 = 0.000
      D = VP1 * VP2 * VS1 * VS2 * THSQ * Z * Z + VP2 * VS2 * P1 * P2 *
     1X * X + VP1 * VS1 * P3 * P4 * Y * Y + RHO1 * RHO2 * (VS1*VP2*P1*
     2P4 + VP1*VS2*P2*P3) + QA * QA * THSQ * P1 * P2 * P3 * P4

C
C  COMPUTE THE COEFFICIENTS
C
       IF(ABS(AIN) .LT. 0.00001) P1 = CMPLX(1.,0.)
      R13 = 2.0 * VP1 * RHO1 * P1 * (VS2*P2*X + VS1*P4*Y) / D

      RETURN
      END
      SUBROUTINE SZOEP(AIN,VP1,VP2,R13)
C
C CALCULATES ZOEPPRITZ COEFF FOR SOURCE POSN
C
      COMPLEX P1, P2, P3, P4, R13, D
      AIN = AIN
      IF(VP1.GE.2.000) THEN
      SIGM = 0.391
      VS1 = VP1*SQRT( (2*SIGM-1)/(2*SIGM-2) )
      RHO1 = 1.4
      ENDIF
      IF(VP1.GE.2.65) THEN
      SIGM = 1.0/3.0
      VS1 = VP1*SQRT( (2*SIGM-1)/(2*SIGM-2) )
      RHO1 = 1.48
      ENDIF
      IF(VP1.GE.2.900) THEN
      SIGM = 0.3559
      VS1 = VP1*SQRT( (2*SIGM-1)/(2*SIGM-2) )
      RHO1 = 1.55
      ENDIF
      IF(VP1.GE.3.009) THEN
      SIGM = 0.2865
      VS1 = VP1*SQRT( (2*SIGM-1)/(2*SIGM-2) )
      RHO1 = 1.55
      ENDIF
C     LIQUID LAYER
      VS2 = 0.000001
      RHO2 = 1.0

      THETA = SIN(AIN) / VP1
      THSQ = THETA * THETA
      QA = 2.0 * (RHO2*VS2*VS2 - RHO1*VS1*VS1)
      T1 = VP1 * VP1 * THSQ
      T2 = VS1 * VS1 * THSQ
      T3 = VP2 * VP2 * THSQ
      T4 = VS2 * VS2 * THSQ
C     TEST FOR CRITICAL P REFLECTION
      IF (THETA .GT. 1.0/VP1) GO TO 60
      A1 = SQRT(1.0 - T1)
      B1 = 0.0
C     TEST FOR CRITICAL S REFLECTION
   30 IF (THETA .GT. 1.0/VS1) GO TO 70
      A2 = SQRT(1.0 - T2)
      B2 = 0.0
C     TEST FOR CRITICAL P REFRACTION
   40 IF (THETA .GT. 1.0/VP2) GO TO 80
      A3 = SQRT(1.0 - T3)
      B3 = 0.0
C     TEST FOR CRITICAL S REFRACTION
   50 IF (THETA .GT. 1.0/VS2) GO TO 90
      A4 = SQRT(1.0 - T4)
      B4 = 0.0
      GO TO 101
   60 B1 = -SQRT(T1 - 1.0)
      A1 = 0.0
      GO TO 30
   70 B2 = -SQRT(T2 - 1.0)
      A2 = 0.0
      GO TO 40
   80 B3 = -SQRT(T3 - 1.0)
      A3 = 0.0
      GO TO 50
   90 B4 = -SQRT(T4 - 1.0)
      A4 = 0.0
  101 X = RHO2 - QA * THSQ
      Y = RHO1 + QA * THSQ
      Z = RHO2 - RHO1 - QA * THSQ
      P1 = CMPLX(A1,B1)
      P2 = CMPLX(A2,B2)
      P3 = CMPLX(A3,B3)
      P4 = CMPLX(A4,B4)
      VS2 = 0.000
      D = VP1 * VP2 * VS1 * VS2 * THSQ * Z * Z + VP2 * VS2 * P1 * P2 *
     1X * X + VP1 * VS1 * P3 * P4 * Y * Y + RHO1 * RHO2 * (VS1*VP2*P1*
     2P4 + VP1*VS2*P2*P3) + QA * QA * THSQ * P1 * P2 * P3 * P4

C
C  COMPUTE THE COEFFICIENTS
C
       IF(ABS(AIN) .LT. 0.00001) P1 = CMPLX(1.,0.)
      R13 = 2.0 * VP1 * RHO1 * P1 * (VS2*P2*X + VS1*P4*Y) / D

      RETURN
      END

      SUBROUTINE ZCOR(IPDISC,OPDISC,COF)
C     This program carries out a transmission coeffs  corr n
C     to amplitudes using trans Zoeppritz cofs  derived
C
      PARAMETER(LRAY=2601)
      REAL RUB1(LRAY),RUB2(LRAY),RUB3(LRAY),RUB4(LRAY)
      REAL AMP(LRAY),COF(LRAY),CAMP(LRAY)
      CHARACTER*30  OPDISC,IPDISC
      CHARACTER*72  DUMMY(5)

C OPEN FILES
      OPEN(UNIT=1,FILE=IPDISC,STATUS='UNKNOWN')
      OPEN(UNIT=3,FILE=OPDISC,STATUS='UNKNOWN')
      REWIND(1)
      REWIND(3)
C  READ HEADER LINE
      DO 999 J=1,5
```

```
      READ(1,2) DUMMY(J)
      WRITE(3,2) DUMMY(J)
2     FORMAT(A72)
999   CONTINUE

C NOW READ IN AMPLITUDES AND TRANSMISSION COEFFS
      DO 100 I=1,LRAY
      READ(1,3) RUB1(I),RUB2(I),RUB3(I),RUB4(I),AMP(I)
3     FORMAT(F8.4,2X,F8.4,2X,F8.4,2X,F8.4,2X,F8.4)

C NOW CALCULATE NEW CORRECTED AMPLITUDES
      CAMP(I) = AMP(I) / COF(I)
C NOW WRITE ALL TO FILE

      WRITE(3,5) RUB1(I),RUB2(I),RUB3(I),RUB4(I),CAMP(I)
5     FORMAT(F8.4,2X,F8.4,2X,F8.4,2X,F8.4,2X,F10.4)
100   CONTINUE
      CLOSE(1)
      CLOSE(2)
      CLOSE(3)
      RETURN
      END

      SUBROUTINE GEOM(IPDISC,DISC,DISC1,DISC2,OPDISC,RINCR)
C
C     This program carries out a divergence correction
C     to amplitudes using incremented angle path differences
C     and out-of-plane divergence of the raypath
C
      PARAMETER(LRAY=2601)
      REAL RUB1(LRAY),RUB2(LRAY),RUB3(LRAY),RUB4(LRAY)
      REAL AMP(LRAY),DIV(LRAY),CAMP(LRAY),DIV1(LRAY)
      REAL RIB2(LRAY),RIB3(LRAY),RIB4(LRAY),RIB5(LRAY),RIB6(LRAY)
      REAL RB2(LRAY),RB3(LRAY),RB4(LRAY),RB5(LRAY),RB6(LRAY)
      REAL R2,R3,R4,R5,R6,RAVE(LRAY)
      REAL SORFAC(51),SORANG(51),DIVKL(LRAY),A0(LRAY)
      INTEGER RIB1(LRAY),RB1(LRAY),R1
      CHARACTER*30 OPDISC,IPDISC,DISC,DISC1,DISC2,SORD
      CHARACTER DUMMY(5)*72 , ESS*1

C OPEN FILES
      SORD='sor_difac'
      OPEN(UNIT=1,FILE=IPDISC,STATUS='UNKNOWN')
C AMPLITUDE INFO
      OPEN(UNIT=2,FILE=DISC,STATUS='UNKNOWN')
C FROM TTIME INVERSION
      OPEN(UNIT=4,FILE=DISC1,STATUS='UNKNOWN')
C  DIVERGENCE FACTORS...OUT OF PLANE
      OPEN(UNIT=13,FILE=DISC2,STATUS='UNKNOWN')

      OPEN(UNIT=3,FILE=OPDISC,STATUS='UNKNOWN')
C
      OPEN(UNIT=43,FILE=SORD,STATUS='UNKNOWN')

      REWIND(1)
      REWIND(2)
      REWIND(3)
      REWIND(4)
      REWIND(13)
      REWIND(43)
      DO 997 I=1,51
       READ(43,*)SORFAC(I),SORANG(I)
997   CONTINUE

C  READ HEADER LINE

      DO 999 J=1,5
      READ(1,2) DUMMY(J)
2     FORMAT(A72)
999   CONTINUE

      DO 998 J=1,5
      WRITE(3,6) DUMMY(J)
6     FORMAT(A72)
998   CONTINUE

      READ(2,2) DUMMY1
      READ(4,2) DUMMY1
      READ(13,2) DUMMY1

C  NOW READ IN AMPLITUDES AND DISTANCE DATA AND ANGLES

      DO 1000 I=1,LRAY
      READ(1,3) RUB1(I),RUB2(I),RUB3(I),RUB4(I),AMP(I)
3     FORMAT(F8.4,2X,F8.4,2X,F8.4,2X,F8.4,2X,F8.4)

      READ(2,4) RIB1(I),ESS,RIB2(I),RIB3(I),RIB4(I),RIB5(I),RIB6(I)
      READ(4,14) RB1(I),RB2(I),RB3(I),RB4(I),RB5(I),RB6(I)
4     FORMAT(I4,1X,A1,1X,F8.6,3X,F8.4,3X,F8.4,3X,F8.4,3X,F8.4)
14    FORMAT(I4,3X,F8.6,3X,F8.4,3X,F8.4,3X,F8.4,3X,F8.4,1X,F13.2)


      READ(13,1004) R1,R2,R3,R4,R5,R6,DIV(I)
1004  FORMAT(I4,3X,F8.6,3X,F8.4,3X,F8.4,3X,F8.4,3X,F8.4,3X,F8.4,1X,F13.4)

C  NOW CALCULATE NEW CORRECTED AMPLITUDES
C  First the in-plane divergence correction
C
      IF(ESS.EQ.'S')RIB4(I)=RIB4(I)*0.409763807
      IF(ESS.EQ.'S')RIB5(I)=RIB5(I)*0.459763807

      IF(RB6(I).EQ.0.0.OR.RIB6(I).EQ.0.0)THEN
       RAVE(I) = ABS ( ABS(RB6(I)) - ABS(RIB6(I)) )
      ELSEIF(RB6(I).LT.0.0.AND.RIB6(I).LT.0.0)THEN
       RAVE(I) = ABS( RB6(I) ) - ABS( RIB6(I) )
      ELSEIF(RB6(I).LT.0.0.AND.RIB6(I).GT.0.0)THEN
       RAVE(I) = ABS( RB6(I) ) + ABS( RIB6(I) )
      ELSEIF(RB6(I).GT.0.0.AND.RIB6(I).LT.0.0)THEN
       RAVE(I) = ABS( RB6(I) ) + ABS( RIB6(I) )
      ELSEIF(RB6(I).GT.0.0.AND.RIB6(I).GT.0.0)THEN
       RAVE(I) = ABS( RB6(I) - RIB6(I) )
      ENDIF
      RAVE(I) = ABS( RAVE(I) )
C
C  If angle increment produces no difference at the receiver.....
C
C     IF(ESS.EQ.'S')RAVE(I) = RAVE(I-1)*1.5
      IF(ABS(RAVE(I)).NE.0.000)RV1=RAVE(I)
      IF(ABS(RAVE(I)).EQ.0.000)RAVE(I)=RV1*0.8922424226

C  Calculate the divergence -- in-plane
C
      DIV1(I) = ABS ( RAVE(I)*COS(RIB5(I)) / RINCR )
C
C Now calculate reference amplitude from angles.....
C ...interpolate between to find the best fit Aref
C

C  Found from shot in water only in centre, symmetrical about
C  the shot axis.
C

       ANG = RIB4(I)

      IF(ABS(ANG).EQ.0.0)THEN
       A0(I) = SORFAC(36)
       GOTO 9972
      ENDIF

      IF(ABS(ANG).GT.ABS(SORANG(1)))THEN
       A0(I) = SORFAC(1)
       GOTO 9972
      ENDIF

      IF(ANG.LT.0.0)THEN

      DO 9971 JL = 2,36

       SANG = SORANG(JL-1)
       SANG1 = SORANG(JL)
      IF(ABS(ANG).LT.ABS(SANG).AND.ABS(ANG).GT.ABS(SANG1))THEN

        GRAD = ABS( SORFAC(JL) - SORFAC(JL-1) )/
     &   ABS( ABS(SANG) - ABS(SANG1) )

        A0(I) = SORFAC(JL) - GRAD*( ABS(ANG) - ABS(SANG1) )
        GOTO 9972
      ENDIF

9971  CONTINUE

      ELSE

      IF(ABS(ANG).LT.ABS(SORANG(37)))THEN
       IF(ABS(ANG).GT.SORANG(36))THEN
       A0(I) = SORFAC(36)
       GOTO 9972
       ENDIF
      ENDIF

      DO 9973 JL = 38,51

       SANG = SORANG(JL-1)
       SANG1 = SORANG(JL)
      IF(ABS(ANG).LT.ABS(SANG1).AND.ABS(ANG).GT.ABS(SANG))THEN

        GRAD = ABS( SORFAC(JL) - SORFAC(JL-1) )/
     &   ABS( ABS(SANG) - ABS(SANG1) )

        A0(I) = SORFAC(JL) - GRAD*( ABS(SANG1) - ABS(ANG) )
        GOTO 9972
      ENDIF

9973  CONTINUE

      ENDIF

9972  CONTINUE

C
C  Now calculate total divergence factor.....
```

```
C
      IF(RIB4(I).EQ.0.000)THEN
      DIVKL(I) = DIV1(I)
      ELSE
      DIVKL(I) = SQRT( DIV1(I)*DIV(I) )
      ENDIF
C
C  Divide reference amplitude by the correction factor calculated above....
C  this corrected amplitude used in amplitude inversion
C


C  NOW WRITE ALL TO FILE

      IF(A0(I).EQ.0.0)THEN
        A0(I) = SORFAC(1)*ABS( SORANG(1) / RIB4(I) )
      ENDIF
        CAMP(I) = A0(I) / DIVKL(I)
      WRITE(3,5)  RUB1(I),RUB2(I),RUB3(I),RUB4(I),CAMP(I)
5     FORMAT(F8.4,2X,F8.4,2X,F8.4,2X,F8.4,2X,F10.4)

1000  CONTINUE

      RETURN
      END
```

Appendix A.7

Amplitude inversion program

The program amp.f reads in the measured and reference amplitudes, and the raypath information from raytracing through the final velocity field obtained from the traveltime inversion. There are options for damping and to fix cells of a known value.

```
      PROGRAM AMPINV

C     This program will read AMPLITUDE data from a tomgraphy survey .. format
C     the same as the FB input files ... and using path length data from
C     a raytrace run will carry out a tomography inversion on the amplitudes.
C       When a straight ray is substituted for curved ray after ray is lost,
C     this program does not use these rays in the inversion.

C                          I hope!!!!!!!!!
C     It does!!!!!

      PARAMETER (LRAY=2601,LCELL=1198)

      REAL EAMP(LRAY),AMP(LRAY),AMPERR(LRAY),RLEN(LRAY)
      REAL CAMP(LRAY),CAMP1(LRAY),CONSTR
      REAL ALPHA(LCELL),DALPHA(LCELL),TK(LCELL),TKWT(LCELL)
      INTEGER NRAYS(LCELL),IFIX(LCELL),IRANG

      CHARACTER*72 DUMMY,DUMMY2
      CHARACTER*30 IFILE,INFILE,IDISC,DISC,DISC1
      CHARACTER*1 IANS



C     AMP(LRAY)    - Measured amp values - corrected for transmission loss
C     CAMP(LRAY)   - Estimated amp from  Reference Amplitude / Divergence
C     CAMP1(LRAY)  - Log ratio of amplitudes - log < measured / initial >
C     EAMP(LRAY)   - Estimated amp from summation of "attenuation" in each cell
C     AMPERR(LRAY) - Error in amp .. AMP-EAMP
C     RLEN(LRAY)   - Length of each raypath
C     ALPHA(LCELL) - "Attenuation" value for each cell
C     DALPHA(LCELL) - "Attenuation" update for each cell
C     TK(LCELL)    - Path length in each cell
C     TKWT(LCELL)  - Sum of path lengths in each cell
C     NRAYS(LCELL) - No. of raypaths crossing a given cell .. interest only!
C     IFIX(LCELL)  - Flag = 0 to fix the value of a given cell , else = 1

      PRINT*,' Enter file containing raypath data '
      READ(5,10)IFILE
   10 FORMAT(A30)

      PRINT*,' Enter comment for output files '
      READ(5,100)DUMMY2
      PRINT*,'Enter constraint required for selective smoothing'
      READ(5,*) CONSTR


C1    First read in the measured amplitudes
C     ------------------------------------
      PRINT*,' File containing the measured amplitude data?'
      READ(5,11)INFILE
   11 FORMAT(A30)
      OPEN(UNIT=1,FILE=INFILE,STATUS='UNKNOWN')
  100 FORMAT(A72)
      READ(1,100) DUMMY
      READ(1,100) DUMMY
      READ(1,100) DUMMY
      READ(1,*)SHOTS,RECS,MISS
      NSHOTS=SHOTS
      NRECS=RECS
      NMISS=MISS
      READ(1,100) DUMMY
      JRAYS = NSHOTS*NRECS-NMISS
      PRINT*,' JRAYS = ',JRAYS
      DO 110 I = 1,JRAYS
         READ(1,105)RUB1,RUB2,RUB3,RUB4,AMP(I)
  105    FORMAT(F8.4,2X,F8.4,2X,F8.4,2X,F8.4,2X,F10.4)
  110 CONTINUE

C     ------------------------------------
C1A   Next read in the corrected amplitudes
C     ------------------------------------

      PRINT*,' File containing the corrected amplitude data?'
      READ(5,19)DISC1
   19 FORMAT(A30)
      OPEN(UNIT=9,FILE=DISC1,STATUS='UNKNOWN')
  900 FORMAT(A72)
      READ(9,900) DUMMY
      READ(9,900) DUMMY
      READ(9,900) DUMMY
      READ(9,*)SHOTS,RECS,MISS
      NSHOTS=SHOTS
      NRECS=RECS
      NMISS=MISS
      READ(9,100) DUMMY
      JRAYS = NSHOTS*NRECS-NMISS

      DO 910 I = 1,JRAYS
         READ(9,915)RB1,RB2,RB3,RB4,CAMP(I)
  915    FORMAT(F8.4,2X,F8.4,2X,F8.4,2X,F8.4,2X,F10.4)
  910 CONTINUE



C     ------------------------------------------------
C     Now work out the log-amplitude ratios
C     ------------------------------------------------

      DO 667 J=1,JRAYS
      CAMP1(J) = -ALOG( AMP(J) / CAMP(J) )
  667 CONTINUE

C     ------------------------------------------------
C2    Now read in the "attenuation" values for each cell
C     ------------------------------------------------

      PRINT*,' File containing the initial attenuation/cell data'
      READ(5,12) IDISC
   12 FORMAT(A30)
      OPEN(UNIT=2,FILE=IDISC,STATUS='UNKNOWN')
      READ(2,100)DUMMY
      READ(2,100)DUMMY
      READ(2,100)DUMMY
      READ(2,*)ICELXZ,ICELLX,ICELLZ
      PRINT*,' ICELXZ = ',ICELXZ
      READ(2,100)DUMMY
      READ(2,*)BOXX,BOXZ,RUB1,RUB2
      READ(2,100)DUMMY

      DO 120 ICELL=1,ICELXZ
         READ(2,*)ALPHA(ICELL)
  120 CONTINUE

C     ------------------------------------------------

C     Now fix the values in required cells
C     ------------------------------------

      PRINT*,' Do you want to fix a given value? Y/N '
      READ(5,5) IANS
    5 FORMAT(A1)
      IF(IANS.EQ.'Y'.OR.IANS.EQ.'y')THEN
         PRINT*,' Enter value to fix '
         READ*,RFIX
         DO 125 ICELL = 1,ICELXZ
            IFIX(ICELL) = 1
            IF(ALPHA(ICELL).EQ.RFIX)IFIX(ICELL) = 0
  125    CONTINUE
      ELSE
         DO 126 ICELL = 1,ICELXZ
            IFIX(ICELL) = 1
  126    CONTINUE
      ENDIF
C     ------------------------------------------------



C     If data is being read in as velocity . ie:travel time inversion
C     then convert the velocity to slowness
C     ------------------------------------------------------------
      PRINT*,' Is data being read in as velocity? y/n '
      READ(5,5)IANS
      IF(IANS.EQ.'Y'.OR.IANS.EQ.'y')THEN
         DO 122 ICELL = 1,ICELXZ
            ALPHA(ICELL) = 1./ALPHA(ICELL)
  122    CONTINUE
      ENDIF
C     ------------------------------------------------------------



C3    Now calculate the total path length from the path length in each cell
C3    Note that if ifix=0 for a given cell this cell is not included
C     ------------------------------------------------------------
      DO 135 IC = 1,ICELXZ
         TK(IC) = 0.0
         TKWT(IC) = 0.0
  135 CONTINUE
C     Open the required file:

      OPEN(UNIT=10,STATUS='UNKNOWN',FILE=IFILE)
      REWIND(10)
      DO 140 IRAY = 1,JRAYS
         READ(10,43)IRANG
   43    FORMAT(I4)
         DO 145 L = 1,IRANG
            READ(10,3333) ICELL,TK(ICELL)
 3333    FORMAT(I4,F8.4)
  145    CONTINUE
         RLEN(IRAY) = 0.0
         DO 150 ICELL = 1,ICELXZ
```

```
        RLEN(IRAY) = RLEN(IRAY) + TK(ICELL)*FLOAT(IFIX(ICELL))
        TK(ICELL) = 0.0
150     CONTINUE
140  CONTINUE
C    ------------------------------------------------------------


C    Damping can speed up convergence slightly .....
C    Less than 1 increases perturbations to amp/velocity
C    Note:  less than .6 is dodgy!
     PRINT*,' Enter damping factor .... 1 = no damping '
     READ*, DAMP



C    Start the loop for each iteration
     PRINT*,' Enter the number of iterations '
     READ*, NIT
     DO 1000 IT = 1,NIT

C    ------------------------------------------------------
C    Now reset tk(icell) , tkwt(icell) to zero
     DO 996 IC = 1,ICELXZ
        TK(IC) = 0.0
        TKWT(IC) = 0.0
 996 CONTINUE
C    ------------------------------------------------------



C4   Now calculate the estimated amplitude by summation of the "attenuation"
C4   factors in each cell .. for each raypath
C    Use the loops to set up tkwt(icell) sum of path lengths in each cell
C    ------------------------------------------------------------
     REWIND(10)
     DO 160 IRAY = 1,JRAYS
        READ(10,44)IRANG
  44    FORMAT(I4)
        DO 146 L = 1,IRANG
         READ(10,3334) ICELL,TK(ICELL)
3334     FORMAT(I4,F8.4)
 146     CONTINUE
         EAMP(IRAY) = 0.0
        DO 170 ICELL = 1,ICELXZ
         IF(TK(ICELL).GT.0.0)THEN
          EAMP(IRAY) = EAMP(IRAY) + (ALPHA(ICELL)*TK(ICELL))
          TKWT(ICELL) = TKWT(ICELL) + TK(ICELL)
          TK(ICELL) = 0.0
         ENDIF
 170     CONTINUE
 160  CONTINUE
C    ------------------------------------------------------------


C    ------------------------------------------------------
C    Now calculate the error in the amplitude .. observed-estimate
C    ------------------------------------------------------
     VAR = 0.0
     DO 180 IRAY = 1,JRAYS
        AMPERR(IRAY) = (CAMP1(IRAY) - EAMP(IRAY))
        VAR = VAR + AMPERR(IRAY)**2
 180  CONTINUE
C    ------------------------------------------------------------


C6   Now do the inversion .... Take the error , divide it by the total
C6   path length to give the error/unit length of ray , multiply this
C6   by the path length in each cell to give the update for that cell
C6   for the given ray path. To get the total error for a cell sum all
C6   the contributions from all raypaths. Then need to normalize this
C6   by dividing by total raypath length for the given cell
C    ------------------------------------------------------------
     REWIND(10)
     DO 200 ICELL = 1,ICELXZ
        TK(ICELL) = 0.0
        DALPHA(ICELL) = 0.0
        NRAYS(ICELL)  = 0
 200  CONTINUE
     DO 210 IRAY = 1,JRAYS
        READ(10,13)IRANG
  13     FORMAT(I4)
        DO 147 L = 1,IRANG
           READ(10,3335) ICELL,TK(ICELL)
3335     FORMAT(I4,F8.4)
 147     CONTINUE
        DO 220 ICELL = 1,ICELXZ
         IF(TK(ICELL).GT.0.0)THEN
           NRAYS(ICELL) = NRAYS(ICELL) + 1
           DALPHA(ICELL) = DALPHA(ICELL) +
     &      (AMPERR(IRAY)*TK(ICELL)*FLOAT(IFIX(ICELL))
     &      /RLEN(IRAY))
          TK(ICELL) = 0.0
          ENDIF
 220     CONTINUE
 711     CONTINUE
 210  CONTINUE

C    now normalize by tkwt(icell)
     DO 230 ICELL = 1,ICELXZ
        IF(TKWT(ICELL).GT.0.0)THEN
        DALPHA(ICELL) = DALPHA(ICELL)/TKWT(ICELL)
        ENDIF
 230  CONTINUE
C    ------------------------------------------------------------


C    CALL SMOOTH(DALPHA,ICELLS,ICELLX,ICELLZ,CONSTR)


C7   Now update the "attenuation" factors in each cell
C    ------------------------------------------------------
     DO 240 ICELL = 1,ICELXZ
        IF(ALPHA(ICELL).LT.0.0.AND.DALPHA(ICELL).LT.0.0)THEN
         ALPHA(ICELL) = ALPHA(ICELL) - DALPHA(ICELL)/DAMP
        ELSE
         ALPHA(ICELL) = ALPHA(ICELL) + DALPHA(ICELL)/DAMP
        ENDIF
 240  CONTINUE
C    ------------------------------------------------------


C now call smooth to smooth out the field before the next iteration
C    ------------------------------------
     CALL SMOOTH(ALPHA,ICELLS,ICELLX,ICELLZ,CONSTR)
C    ------------------------------------


C9   Now write out the new "attenuation" factors
C    ----------------------------------------
     PRINT*,'ENTER OUTPUT FILE FOR ATTENUATION FACTORS'
     READ(5,14) DISC
  14 FORMAT(A30)
     OPEN(UNIT=3,FILE=DISC,STATUS='UNKNOWN')
     WRITE(3,100)DUMMY2
     WRITE(3,*) 'Iteration number ',NIT
     WRITE(3,*)' No cells ICELLX  ICELLZ '
     WRITE(3,*)ICELXZ,ICELLX,ICELLZ
     WRITE(3,*)' BOXX BOXZ '
     WRITE(3,*)BOXX,BOXZ,RUB1,RUB2
     WRITE(3,*)VAR
     IF(IANS.EQ.'Y'.OR.IANS.EQ.'y')THEN
     DO 620 ICELL=1,ICELXZ
        WRITE(3,*)1./ ALPHA(ICELL)
 620 CONTINUE
     ELSE
     DO 630 ICELL=1,ICELXZ
        WRITE(3,*)ALPHA(ICELL)
 630 CONTINUE
     ENDIF
     CLOSE(UNIT=3)
C    ----------------------------------------


1000 CONTINUE
C    end of loop for one iteration
     PRINT*,' Iteration  ',NIT, ' finished'


     STOP
     END
```